Papers presented to the

TWELFTH SYMPOSIUM

ON ANTARCTIC METEORITES

8–10, June 1987

NATIONAL INSTITUTE OF POLAR RESEARCH, 国立極地研究所
TOKYO

Papers presented to the

TWELFTH SYMPOSIUM

ON ANTARCTIC METEORITES

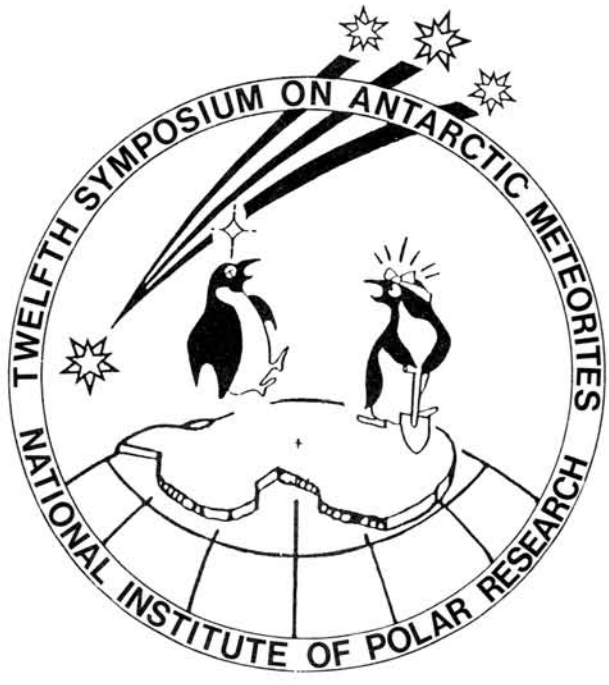

8–10, June 1987

NATIONAL INSTITUTE OF POLAR RESEARCH, 国立極地研究所
TOKYO

NOTICE

Manuscripts Deadline: September 1, 1987

The publication of the full papers, which are here presented as abstracts, will be in the Proceedings of the NIPR Symposium on Antarctic Meteorites, the Memoirs of the National Institute of Polar Research. For inclusion in this publication the full text and illustrations of a paper must be received by the organizing secretary (Dr. K. Yanai) by September 1, 1987.

Please send manuscripts to:

Dr. K. Yanai
Curator of meteorites
National Institute of Polar Research
9-10 Kaga 1-chome, Itabashi-ku
Tokyo 173
Japan

Telephone: Tokyo (03) 962-4711
Cable Address: POLARESEARCH TOKYO
Telex: 2723515 POLRSC J

Monday, June 8, 1987

0830-1200 Registration Auditorium (6th Floor)

0930 - 0935 Opening Address Takao Hoshiai
Chief Research Officer
National Institute of
Polar Research

* Speaker

Chairmen: Yasunori Miura and Akira Shimoyama

1 0935 - 0950 Nishio F.*, Ohmae H., Mori K., Osada K. and Urazuka S.
Collection of Yamato and Sor Rondane meteorites in the 1986-87 field season, Antarctica

2 0950 - 1005 Yanai K.* and Kojima H.
Preliminary identification of new Antarctic meteorites collected by Japanese party in 1986-87 season

3 1005 - 1030 Annexstad J. O.
Mechanisms of meteorite concentrations in Antarctica - A review

4 1030 - 1045 Yanai K.* and members of ANSMET US
Report of ANSMET US (Antarctic Search for Meteorites U.S.) 1986-87

5 1045 - 1100 Koeberl C.*, Yanai K., Cassidy W. A. and Schutt J. W.
Investigation of dust components from dust bands from blue ice fields in the Lewis Cliff (Beardmore) area, Antarctica.

6 1100 - 1115 Naraoka H.*, Shimoyama A., Komiya M., Yamamoto H. and Harada K.
Carboxylic acids and hydrocarbons in Antarctic carbonaceous chondrite

7 1115 - 1130 Miura Y.*, Abe K. and Kojima H.
Compositional variation of phyllosilicates and formation processes in CV and CM carbonaceous chondrites

8 1130 - 1145 Kojima H.* and Yanai K.
Yamato-82162; Possible first C1 carbonaceous chondrite from Antarctica

1145 - 1245 Lunch Time

- Special session: Lunar meteorites and Yamato-691 E3 chondrite -

Chairmen: Yukio Ikeda and Takaaki Fukuoka

9 1245 - 1300 Yanai K.* and Kojima H.
New lunar meteorite: Yamato-793274

10 1300 - 1320 Lindstrom M.*, Korotev R., Lindstrom D. and Haskin L.
Lunar meteorites Y-82192 and Y-82193: Geochemical and petrologic comparisons to other lunar breccias

11 1320 - 1340 Warren P.H. and Kallemeyn G.W.*
New data for the bulk compositions of four lunar meteorites, and for Anfe-rich basaltic clast of probable Vlt-mare affinity from Y-791197

12 1340 - 1400 Koeberl C.
Trace elements in lunar meteorites Y-791197 and Y-82192

13 1400 - 1420 Eugster O.
Cosmogenic and trapped noble gas isotopes, exposure age and terrestrial age of lunar meteorites Yamato-82192 and -82193

14 1420 - 1440 Ikeda Y.
Major element chemical compositions of chondrules in Y-691

15 1440 - 1500 Kitamura M.*, Watanabe S. and Isobe H.
Relict pyroxene and olivine in chondrules of Y-691 (EH3)

16 1500 - 1520 Ebihara M.
Distribution of trace elements in unequilibrated enstatite chondrites

1520 - 1550 Tea Time

17 1550 - 1605 Yabushita S. and Inagaki T.
Ultraviolet spectroscopic measurement of organic extracts from carbonaceous chondrites

18 1605 - 1620 Matsunami S.
On the formation of matrix materials of unequilibrated ordinary chondrites in turbulent solar nebula. --- Constraints from reaction kinetics between enstatite and metallic iron

19 1620 - 1635 Sato H.*, Mori H. and Takeda, H.
Mineralogical study on the matrices of Yamato-790448 and a few chondrites by transmission electron microscope

20 1635 - 1650 Watanabe S.* and Morimoto N.
A subsilicic aluminian pyroxene pair in a fragment of Y-82038 (H3)

21 1650 - 1705 Kimura M.
Petrology of unique Antarctic chondrites, Y-74025 and Y-74063

22 1705 - 1720 Noguchi T.
Texture and chemical composition of pyroxenes in ordinary chondrites

1730 - 1930 Reception

Tuesday, June 9, 1987

Chairmen: Kosuke Onuma and Masao Kitamura

23 0900 - 0915 Tsuchiyama A.*, Fujita T. and Morimoto N.
Fe-Mg homogenization of pyroxenes in ordinary chondrites

24 0915 - 0930 Miura Y.
Compositional characteristics of plagioclase feldspar in various chondritic meteorites

25 0930 - 0945 Graham A. L.
The composition of spinels in the Julesburg (L3) meteorite

26 0945 - 1000 Nishida T.
Studies on metallic minerals in ALH-77231 by X-ray diffraction and S.E.M.

27 1000 - 1015 Yanai K.* and Kojima H.
Yamato-8451; Newly identified pyroxene bearing pallasite

28 1015 - 1035 Prinz M.*, Weisberg M. K., Nehru C. E. and Delaney J. S.
Mineral and lithic clasts in the EET 83309 polymict ureilite: Evidence for primitive origins

29 1035 - 1050 Takeda H.* and Ogata H.
On the pairing of Antarctic ureilites with reference to their parent body

30 1050 - 1105 Aoyama T.* and Takeda H.
Mineralogy of Yamato-79 and -82 achondrites and their parent body

31 1105 - 1120 Kushiro I.* and Mysen B. O.
Experimental studies on vaporization and condensation in the system Mg_2SiO_4-SiO_2-H_2 at low pressures: Application to the solar nebula processes

32 1120 - 1135 Tsuchiyama A.*, Kushiro I. and Morimoto N.
An electron microscopic study of gas condensates in the system Mg-Si-O-H

33 1135 - 1150 Nagahara H.*, Kushiro I., Mysen B. O. and Mori H.
Vaporization and condensation experiments on olivine solid solution system

1150 - 1300 Lunch Time

Chairmen: Noboru Nakamura and Mitsuru Ebihara

34 1300 - 1315 Okada A.*, Ito T., Kobayashi K. and Sakurai T.
Crystal structure of perryite

35 1315 - 1330 Takahashi E.* and Ito E.
Melting of peridotite under very high pressure -II: A laboratory simulation for early evolution of the earth

36 1330 - 1350 Kallemeyn G. W.
Compositional comparisons of some CO, CV and metamorphosed carbonaceous chondrites from Allan Hills

37 1350 - 1405 Tazawa Y.* and Sasaki T.
Chemical composition of fusion crusts on Antarctic chondrites

38 1405 - 1420 Nagamoto H., Nakamura N.*, Nishikawa Y., Misawa K. and Noda S.
Distribution of trace elements in the rim-core of Tieschitz (H3) chondrules and the matrix

39 1420 - 1435 Fukuoka T.*, Tazawa Y. and Nagasawa H.
Meteoritic components in sediments collected from impact crater, Arizona

40 1435 - 1450 Misawa K.* and Nakamura N.
Rare earth elements in chondrules from the Felix (CO3) chondrite: Comparison with the Allende (CV3) chondrules

41 1450 - 1505 Uyeda C.*, Suzuki M. and Okano J.
The correlation of chondrule texture and magnesium isotope abundance

1505 - 1535 Tea Time

42 1535 - 1550 Takahashi K.*, Shimizu H. and Masuda A.
The Rb-Sr systematics for diogenites

43 1550 - 1605 Honda M.*, Nagai H., Takahashi M. and Akizawa S.
Scandium 45 in Antarctic iron meteorites.

-- Special Lecture --

44 1605 - 1705 Koeberl C. (University of Vienna, Austria)
The origin of tektites: A geochemical discussion

Wednesday, June 10, 1987

Chairmen: Kunihiko Kigoshi and Jun-ich Matsuda

45 0900 - 0915 Nagai H., Imamura M., Kobayashi K., Kobayashi T. and Honda M.
Aluminum 26 and beryllium 10 in meteoritic irons

46 0915 - 0930 Kaneoka I.*, Takaoka, N. and Yanai K.
40Ar-39Ar age of a L7 clast-bearing chondrite Y-75097(L6) and the effect of collision on degassing

47 0930 - 0945 Beukens R. P.*, Rucklidge J. C. and Miura Y.
14C ages of Yamato and Allan Hills meteorites

48 0945 - 1000 Matsubara K.*, Nagao K. and Matsuda J.
Noble gases in Belgica-7904 carbonaceous chondrite

49 1000 - 1015 Nagao K.
Rare gas isotopic composition of achondrites from Antarctica

50 1015 - 1030 Takaoka N.
Noble gas analysis of Yamato-74013 (Di)

51 1030 - 1045 Igarashi G.* and Ozima M.
Comparison between terrestrial Xe and Xe in carbonaceous meteorites; constraints on the early history of the earth

52 1045 - 1100 Fukunaga K.*, Matsuda J., Nagao K., Miyamoto M. and Ito K.
Noble gas enrichment in vapor growth diamonds and the origin of diamonds in meteorites

53 1100 - 1115 Ozima M.* and Zashu S.
Solar type He and Ne in diamonds

54 1115 - 1130 Amari S.*, Ozima M. and Hamano Y.
3He/4He ratios in a sedimentary rock from K-T boundary, Hokkaido and in Fig Tree shales

55 1130 - 1145 Wu S. and Zhang S.*
Significance of the geoscience in the Duolun crater impact event

56 1145 - 1200 Miyamoto M.
Hydration bands around 3 m and weathering of meteorites

1200 - 1300 Lunch Time

Chairmen: Naoji Sugiura and Nobuo Takaoka

57 1300 -1315 Matsui T. and Tajika E.
Orbit of the Allende meteorite -- Is the Allende meteorite an extinct cometary nucleus? --

58 1315 - Sugiura N.* and Sneyd D.
Magnetic susceptibility anisotropy and porosity of chondrites; A review

59 - 1340 Sugiura N.* and Strangway D. W.
Hysteresis and NRM properties of meteorites

60 1340 - 1355 Funaki M.*, Taguchi I., Danon J. and Nagata T.
Magnetic and metallographical studies of Bocaiuva iron meteorite

61 1355 - 1410 Nagata T.
Magnetic analysis of Antarctic stony meteorites on the basis of magnetic coercivity

---

-- Special Lecture --

62 1410 - 1510 Arnold J. R. (Invited Speaker, Professor, University of California, U.S.A.)
Terrestrial ages of Antarctic meteorites and ice

Monday, June 8, 1987

0830 - 1200	*Registration, 6th Floor*
0930 - 0935	*Opening address, Auditorium*
0935 - 1145	*Symposium, Auditorium*
1245 - 1520	*Special session:*
	Lunar meteorites and Yamato-691 E3 chondrite
1550 - 1720	*Symposium*
1730 - 1930	*Reception, Lecture Room, 2nd Floor*

COLLECTION OF YAMATO AND SØR RONDANE METEORITES IN THE 1986-87 FIELD SEASON, ANTARCTICA

Fumihiko NISHIO[1], Hirokazu OHMAE[2], Kazuhiko MORI[3], Kazuo OSADA[4] and Seiho URAZUKA[5]

1.National Institute of Polar Research, 9-10, Kaga 1-chome, Itabashi-ku, Tokyo 173.
2.The Institute of Low Temperature Science, Hokkaido University, Kita-19, Nishi-8, Kita-ku, Sapporo.
3.Electrotechnical Laboratory, 1-1-4, Umezono, Sakura-mura, Niihari-gun, Ibaraki.
4.Water Research Laboratory, Chikusa-ku, Furo-cho, Nagoya.
5.Radio Research Laboratory, Ministry of Posts and Telecommunications, 2-1, Nukui-kitamachi 4-chome, Koganei-shi, Tokyo.

Search and collection of Antarctic meteorites were carried out by the inland traverse party of the 27th Japanese Antarctic Research Expedition in the Meteorite Ice Field near the Yamato Mountains and the bare ice area of the Sør Rondane Mountain region in 1986-87 austral summer.

In the southern part of bare ice area extended from the Minami Yamato Nunataks in the Meteorite Ice Field, the glaciological party stayed about a month, resurveyed the triangulation chain installed in 1983 for measuring ice flow and strain rates, and conducted the radio-echo sounding to depict topographic map of the bare ice area, in which a large number of meteorite were collected in the last two austral summer of 1982-83 and 1986-87. During the glaciological survey, search for meteorites was not systematically organized, but conducted by careful observations of the bare ice surface with the naked eye mostly from the moving oversnow vehicles at all times.

Collected meteorites are about 800 fragments, their total weight is over 30 kg. More than 150 meteorite fragments were found in the limited area of the triangulation chain installed from Kuwagata Nunatak of the Minami-Yamato Nunataks to the above Nunatak.

About 600 fragments of chondrites were collected in the very limited area within 1x1 km in square between Kurakake and Kuwagata Nunatak of the Minami-Yamato Nunataks. It may be inferred these meteorite fragments fell over the Meteorite Ice Field in meteorite shower in a recent event.

On the western part of thebare ice surface, 10 km apart from the C Massif of the Yamato Mountains, one meteorite buried in the bare ice was found and collected with the surrounding ice.

Within the grid, hexagonal in shape, established by the JARE-16, 1975, for measurement of glacier movement, 5 meteorite specimens were found near Motoi Nunatak. Since all the meteorite fragment on the bare ice surface in the grid near Motoi Nunatak had been collected by JARE-16's meteorite search party, it would be expected that there is no more meteorite on the bare ice surface of the grid. It may be considered that 5 meteorite specimens buried in the ice are coming up and have

been exposed on the bare ice surface in the grid installed by JARE-16, 1975.

In region of the Sør Rondane Mountains, bare ice area is widely extended around the exposed rock area. Search for meteorite in this region were carried out by JARE-25 and JARE-26 in the area of down-glacier behind the Sør Rondane Mountains and the outlet glaciers through the mountain range, but no meteorite was discovered. In 1987, 3 chondrites were found and collected on the bare ice surface of the east of Balchen Nunataks located in the eastern part of the Sor Rondane Mountains. A bare ice area widely extends southward up-glacier from the Mountains, and it is a large possibility that many meteorites might be discovered in the unexplored bare ice area.

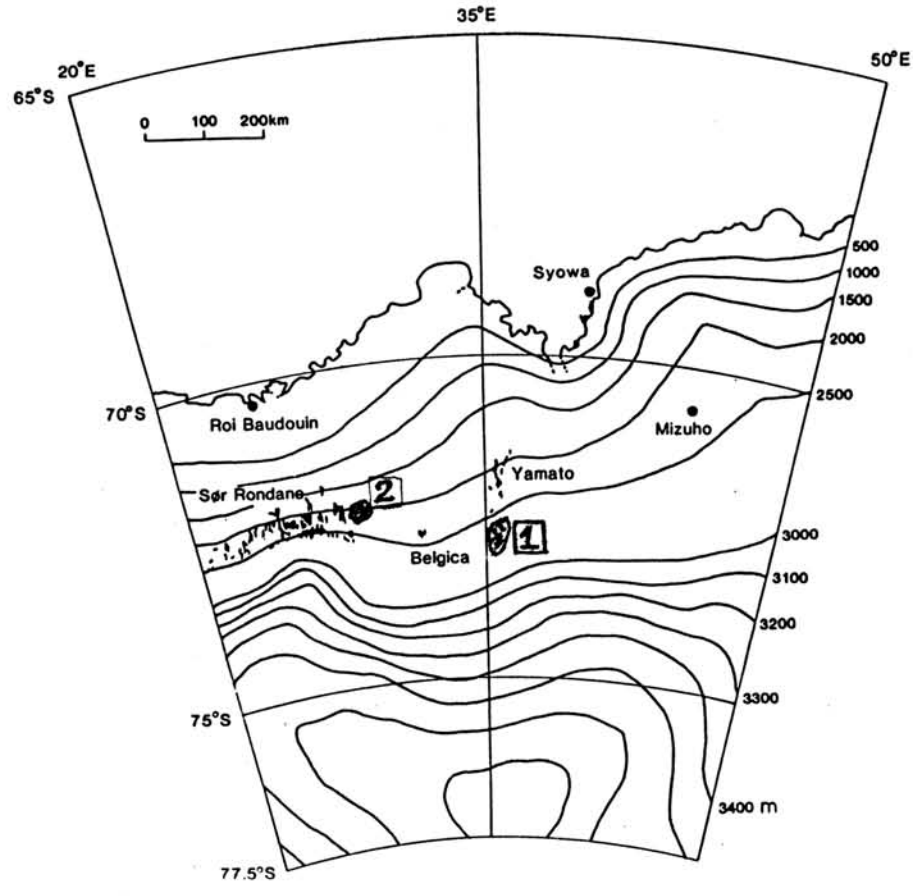

Fig. 1. Location map of the meteorite collection area.

[1] Southern bare ice of the Minami-Yamato Nunataks in the Meteorite Ice Field near the Yamato Mountians.
[2] Eastern bare ice of the Sor Rondane Mountains.

PRELIMINARY IDENTIFICATION OF NEW ANTARCTIC METEORITES COLLECTED BY JAPANESE PARTY IN 1986-87 FIELD SEASON

Keizo Yanai and Hideyasu Kojima, National Institute of Polar Research, 9-10, Kaga 1-chome, Itabashi-ku, Tokyo 173

More than 800 meteorite specimen have been collected as individuals or fragments on the bare ice area around the Yamato Mountains, Antarctica. Three individual specimen had been recovered as for the first time in the Sör Rondane Mountains, Antarctica. These collections were carried to the National Institute of Polar Research (NIPR) in the late April 1987, then the collections have been processed initially and identified briefly in the Antarctic meteorites processing laboratory of NIPR. These collections will be designated Yamato-86(Y-86) meteorites and Sör Rondane-86(S-86) meteorites respectively, but S-86 meteorites is tentative name now.

Meteorite types in the Yamato-86 meteorites are distributed as following result of the preliminary processing and identification; Iron 1(?), Stony-Irons 0, Carbonaceous Chondrites 33, Ordinary Chondrites 770, Diogenite (A) 2, Eucrites-Howardites 4, Lunar Meteorite 1, Unclassified (unique?) 3 and Total 814 specimens.

Preliminary identified lunar meteorite is fairly large specimen about 650 grams and it is very similar to Yamato-82192 and Yamato-82193 collected previously at the same bare ice area in the Yamato Mountains. Carbonaceous chondrites classified briefly are large number and show variety in their features. They may be classified as C1 (possible), C2 (mostly), C3 and C4 (less), and some of them are paired. Number of ordinary chondrites are complete individual stones, however most of ordinary chondrites are fragments, this seems that many are paired. The largest ordinary chondrite is complete stone, about 6.1Kg.

Sör Rondane-86 meteorites were classified to ordinary chondrites and they ranged from 45 grams to 1.5Kg.

MECHANISMS OF METEORITE CONCENTRATIONS IN ANTARCTICA - A REVIEW

Annexstad, John O.

Division of Science & Math, Bemidji State University, Bemidji, MN 56601

The total collection of meteoritic material available for analysis has been immeasurably enhanced by the initial Japanese discovery of specimens in 1969 at the Yamato Mountains. Since 1974 both the Japanese and U.S. search expeditions have been outstandingly successful in finding meteorites in Antarctica. Other nations have reportedly conducted searches (India, South Africa, Australia, USSR, New Zealand, West Germany) and some have also found specimens. Regardless of the numbers of finds, it seems a given that the Antarctic ice sheet acts as a giant collector, transporter, concentrator and and preserver of meteorites. The mechanisms of transportation and concentration by the ice sheet that have been suggested seem to follow a fairly common theme. In general, meteorites fall onto the ice sheet, become incorporated into it, and are transported along flow lines toward coastal areas where the ice flow is retarded or blocked by surface or sub-glacial obstructions. These obstructions cause the ice sheet to upwell and create areas of concentration where specimens are constantly supplied to the surface by the emerging ice and exposed by the ablation process (1).

Nagata (2) refined this hypothesis by utilizing meteorite collection and ice movement data from the Meteorite Ice Field (Yamato). His idea has formed a basis for other models and still seems to adequately explain the process today.

Nishio and Annexstad (3) attempted to quantify the rate of ice movement by establishing a triangulation network in the Allan Hills Icefield, Victoria Land for the purpose of measuring horizontal surface flow and vertical emergence parameters. The network was remeasured in 1979 (4) and again in 1981 (5) with the noted result that ice sheet flow was certainly retarded at the meteorite concentration zone and ice upwelling was probably balanced by ablative processes. The steady state (emergence/ablation) condition was suggested by the data but is considered inconclusive because measurement errors exceeded movement parameters.

Three models of meteorite concentration were proposed and each differed in their estimates of the origin of the ice seen in the Allan Hills meteorite concentration zone. Nishio et al (6) suggested a short path length based upon ice fabric data, Whillans and Cassidy (7) a long path length based on theoretical considerations and Schultz and Annexstad (5) a variable path length based on triangulation data, meteorite residence ages and weathering considerations.

At a workshop conducted in Mainz in July 1985 (8) the question of concentration mechanisms and the glaciological connection was addressed. Drewry suggested that the concentration regions may possibly be insensitive responders to climate fluctuations where ancient ice is preserved. Therefore, the relationship between long terrestrial ages of meteorites and the age of the ice sheet would be a useful indicator of long-term ice sheet stability. Oeschgar suggested a plan for sampling and dating ice cores in the meteorite areas by comparing isotopic, total gas and chemical composition data to that of cores of known depth. Cassidy noted that meteorites are found downstream of blocking mountains and in moraines instead of only on the upstream side of ice fields as originally suspected. The same

situation was reported by Delisle in his report on a find of 42 specimens in the Frontier Mountains region. Cassidy labeled these stranding sites and Drewry suggested that they may be remnants of the uplift of the Trans Antarctic Mountains.

Although a general idea of the mechanism of concentration has evolved, little field work has been done recently to help understand the phenomena. As the searches for meteorites continue and the data base on residence ages, weathering and find locations increases it becomes increasingly more important to recognize the operative glaciological processes. It is suggested that a comprehensive theory of meteorite concentration must address the following points at least.

The origin of the ice in the concentration area.

The size of the catchment basin.

The age of the ice in the concentration area.

Why meteorites appear in downstream locations (stranding sites) and in moraines.

Why some icefields are barren and others yield many specimens.

The relationship of meteorite terrestrial residence ages to surface exposure and encasement.

The relationship between sub-glacial topography and concentration areas.

References

(1) Cassidy, W.A., Olsen, E. and Yanai, K. (1977) Science 198, pp 727-731.

(2) Nagata, T. (1978) Mem. Nat. Inst. Pol. Res. 8, pp 70-92.

(3) Nishio, F. and Annexstad, J.O. (1979) Mem. Nat. Inst. Pol. Res. 15, pp 13-23.

(4) Nishio, F. and Annexstad, J.O. (1980) Mem. Nat. Inst. Pol. Res. 17, pp 1-13.

(5) Schultz, L. and Annexstad, J.O. (1984) Smith Cont. Earth Sci. 26, pp 17-22.

(6) Nishio, F., Azuma, N., Higashi, A., and Annexstad, J.O. (1982) Ann. Glac. 3, pp 222-226.

(7) Whillans, I.M. and Cassidy, W.A. (1983) Science 222, pp 55-57.

(8) Annexstad, J.O., Schultz, L. and Wänke, H. (1986) L.P.I. Tech. Rep. 86-01, 119 pgs.

4—1

REPORT OF ANSMET US (ANTARCTIC SEARCH FOR METEORITES U.S.) 1986-87

Keizo Yanai[1] and members of ANSMET US[2]

1) National Institute of Polar Research, 9-10, Kaga 1-chome, Itabashi-ku, Tokyo 173. 2) U.S.A., Austria, Netherlands and Canada.

The ANSMET US 1986-87 project was organized by National Science Fundation, Division of Polar Program (NSF, DPP) and six meteorite hunters participated with the project in this field season. Professor W. A. Cassidy, University of Pittsburgh conducted the project and led five members; American, Austrian, Dutch, Canadian and Japanese.

The team tried to search for meteorite at the Lewis Cliff Ice Tang (LCIT, 84°17'S; 160°50'E), Transantarctic Mountains, Antarctica for seven weeks supported by C-130 Hercules aircraft. The team members have been carried to the Beardmore South Camp (temporary) by C-130, then the team moved to the campsite which was located just close in the LCIT with six Skidoos and nine sledges. Searching of meteorite have been carried out under very serious weather condition at the LCIT and nearby the several exposed bare ices areas. The bare ice of the LCIT is a very narrow accumlation area of about 25Km^2, although the bare ice has numerous meteorite specimens.

About 600 meteorite specimens have been recovered as completes or fragmental stones on the LCIT and expored few others. According to the field identification, these specimens contain kinds of meteorite type as following; Irons 0, Stony-Irons 0, Carbonaceous Chondrites 4 (mostly small), Eucrites 3 (about 200g, -30g and -5g respectively), unique (possible chondritic) 2 (One is about 2kg, containg large olivine crystal about 1cm accross, seems high petrologic type) and abundant ordinary chondrites include many low petroligic types.

INVESTIGATION OF DUST COMPONENTS FROM DUST BANDS FROM BLUE ICE FIELDS IN THE LEWIS CLIFF (BEARDMORE) AREA, ANTARCTICA.

Christian Koeberl[1], Keizo Yanai[2], William A. Cassidy[3], and John W. Schutt[4]

(1) Institute of Geochemistry,University of Vienna,A-1010 Vienna, Austria.
(2) National Institute of Polar Research, Itabashi ku, Tokyo 173, Japan
(3) Dept. of Geology, University of Pittsburgh, Pittsburgh, PA 15260, USA
(4) P.O.Box 767, Ferndale, WA 98248, USA

An integrated study of dust bands from ice fields in Antarctica is performed in order to reveal the origin and provenance of the dust material. We report here some preliminary results from investigations on recently acquired samples. During the last ANSMET (Antarctic Search for Meteorites) expedition of the U.S. Antarctic Research Program (USARP) in the Austral summer of 1986/87, the authors collected a number of ice samples with dust components. The location of the field party was at the Walcott Nevé, near Beardmore Glacier. The next prominent landmark is the Lewis Cliff, associated with the Lewis Cliff Ice Tongue. Meteorites were found on the Lewis Cliff Ice Tongue and on nearby blue ice fields.

Part of the field studies were devoted to the investigation of dust bands, found to be prominent and abundant on all ice fields investigated. One of the field aspects of this study included mapping of selected dust bands. The bands were found to run predominantly in a 90° angle to the direction of the ice flow, but deviation from that common orientation were recorded very often.In some cases we observed, that dust bands running in one direction curl back 180° and run back in the other direction. Obviously this is in direct connection with ice flows, and it seems that a sometimes very complicated ice movement leads to blurring of the dust bands. The surface expression width of the bands is usually 10-25 cm, with widths larger than 40 cm leading to problems in recognition. The amount of dust per dust band seems to be within some margin, and if the bands get to wide, they are just thinning out.

Mapping was performed using a theodolite situated on some station with well defined coordinates (usually a peak of a nearby mountain or hill), equipped with an infrared distance measuring device. A number of points along a dust band was then mapped in using a retro-reflector. The evaluation of the mapping data is linked to the mapping of meteorite location on the ice fields and at this time still in progress.

Previous investigations of dust bands from the Allan Hills (Fireman 1985, 1986; Marvin 1986, 1987) seem to indicate a major contribution of volcanic glass shards. In that case the ice is of age comparable to the dust. The second possibility of dust band origin is material scraped up from basement rocks by glacial flow, which seems possible in some cases.

Samples from the dust bands discussed here have been taken also for age determination (to be performed by E. Fireman). The ice blocks were cut out using a chainsaw and measure about 60x60x60 cm. Chips of ice taken from nearby have been used in this study. The ice, containing dust particles, was put into clean plastic bags, slowly melted, and the dust was allowed to settle on the bottom of the plastic bag. Then the water was decanted and the dry dust wrapped in another clean bag. Performing these operations in the field ensures no additional, non-Antarctic contamination.

The dust collected this way, in most cases only a few milligrams, was then subjected to petrographic and geochemical studies. We have performed neutron activation analyses of a number of dust band samples. Weights of samples analysed range from 0.860 mg to 263.04 mg. We have to distinguish between two types of dust bands. Gow and Williamson (1971) distinguish between dirt bands and cloudy bands. Here we have used the general term "dust bands". One of the samples investigated was taken from a location very close to a moraine intruding in the Lewis Cliff Lower Ice Tongue. This sample was already optically different from the other samples, because it contained larger particles, like small chunks of rock. Most probably this dust band (dirt band) is associated with the formation of the moraine. The chemistry of that sample is quite different from the chemistry of the other samples investigated.

In most cases the content of the alkalies (K, Na) is rather high, with a Na/K-ratio of larger than one. The rare earth element content of most samples is also rather high (La 50-90 ppm), with La/Lu ratios of approximately 5. Elements like As, Sb, and Ga show rather high abundances. This points to an origin from volcanic debris, probably from some alkaline volcanic eruption. Since the analyses are still in progress at that time, we are not yet able to pinpoint the exact type of volcanism. The one exception is sample No. 86-05, which was mentioned above as having been collected next to a moraine. The sample shows low REE contents and a different major and trace element chemistry.

References:

Fireman, E.L. (1985) Lunar Planet. Sci. 16, 240-241.
Fireman, E.L. (1986) Lunar Planet. Sci. 17, 226-227.
Gow, A.J., and Williamson, T. (1971) Earth Planet. Sci. Lett. 13, 210-218.
Marvin, U.B. (1986) Meteoritics 21, 442-443.
Marvin, U.B. (1987) Lunar Planet. Sci. 18, 597.

Carboxylic acids and hydrocarbons in Antarctic carbonaceous chondrites

Naraoka, H., Shimoyama, A., Komiya, M., Yamamoto, H.*, and Harada, K.

Department of Chemistry, University of Tsukuba, Sakura-mura, Ibaraki 305
*Faculty of Education, Ibaraki University, Mito, Ibaraki 310

Carbonaceous chondrites contain various types of organic compounds. In previous studies, we reported that Y-74662(C2) yielded amino acids[1] and Y-791198(C2) yielded amino acids and carboxylic acids[2,3]. These organic compounds are indigeous to the chondrites and abiotic in origin.

In this work, we analyzed Y-74662 for carboxylic acids, and Y-791198 for aliphatic and aromatic hydrocarbons. Y-793321(C2), which was unusually depleted in amino acids[4], was also analyzed for carboxylic acids and hydrocarbons.

Analytical procedure for carboxylic acids was reported previously[3]. For hydrocarbons a powdered sample was extracted with methanolic potassium hydroxide. Water was added to this methanolic solution which was extracted with benzene. The residue was extracted with benzene and methanol(9:1 by volume). The benzene and the benzene-methanol solutions were combined, concentrated, and eluted with hexane followed by benzene in a silica gel column. The hexane and benzene eluates were concentrated and analyzed for aliphatic and aromatic hydrocarbons, respectively. Organic compounds were analyzed qualitatively and quantitatively by gas chromatography and gas chromatography combined with mass spectrometry.

Monocarboxylic acids obtained from Y-74662(Fig.1) is similar to those from Y-791198 except for 2-ethylhexanoic acid and nonanoic acid. 2-Ethylhexanoic acid was not detected Y-791198 and the quantities of nonanoic acid from Y-74662 was more than

that from Y-791198. The presence of the two compounds were confirmed by duplicated analyses at separate time. Therefore, they are not from contaminants during analysis. The origin of these compounds were not clear. Y-793321 yielded no detectable amounts of carboxylic acids.

Chromatogram of aromatic hydrocarbons from Y-791198 is shown in Fig.2. Although the major components were phenanthrene, fluoranthene and pyrene, low molecular weight compounds, *e.g.* naphthalene, were not detected. The total content of aromatic hydrocarbons was about 10^{-6}g/g. Aliphatic hydrocarbons were also detected, however, at the lower level(about 10^{-8}g/g). Y-793321 yielded no hydrocarbons at the detectable level.

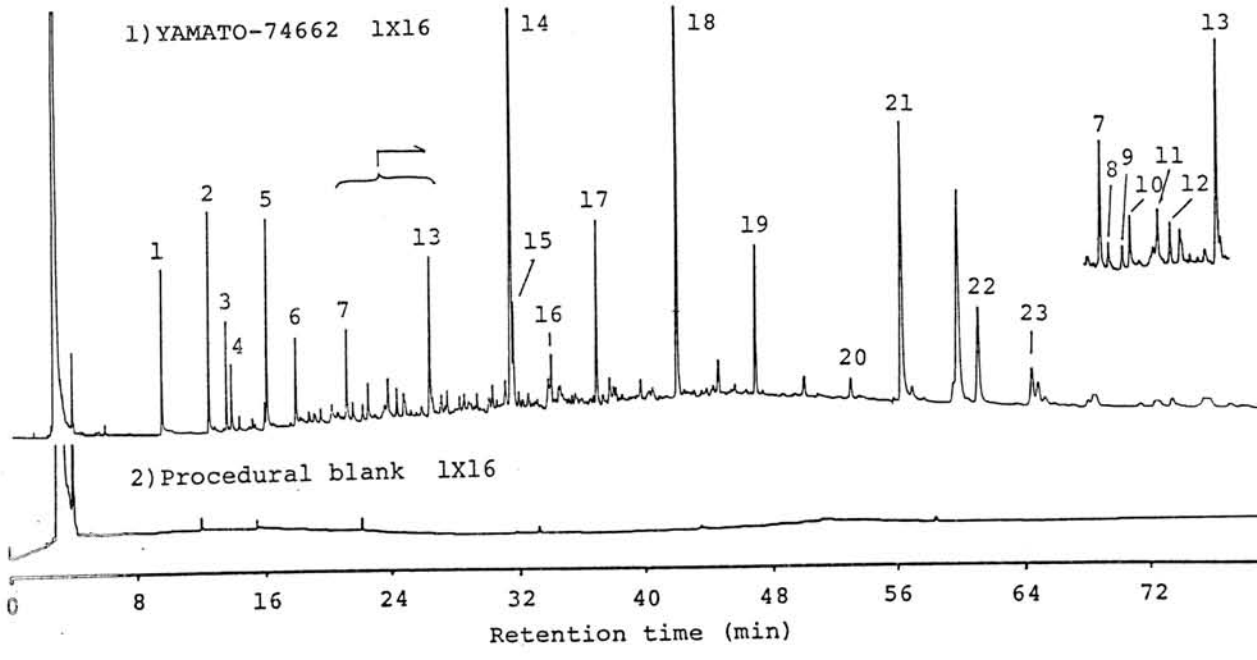

Fig. 1 Gaschromatogram of monocarboxylic acids from YAMATO-74662

Peak No., 1. Acetic acid, 2. Propionic acid, 3. 2-Methylpropionic acid, 4. 2,2-Dimethylpropionic acid, 5. Butanoic acid, 6. 2-Methylbutanoic acid and 3-Methylbutanoic acid, 7. Pentanoic acid, 8. 2,3-Dimethylbutanoic acid, 9. 2-Ethylbutanoic acid, 10. 2-Methylpentanoic acid, 11. 3-Methylpentanoic acid, 12. 4-Methylpentanoic acid, 13. Hexanoic acid, 14. 2-Ethylhexanoic acid, 15. Heptanoic acid, 16. Phenol, 17. Octanoic acid, 18. Nonanoic acid, 19. Decanoic acid, 20. Undecanoic acid, 21. Benzoic acid, 22. Dodecanoic acid, 23. *m*- and *p*-Methylbenzoic acid

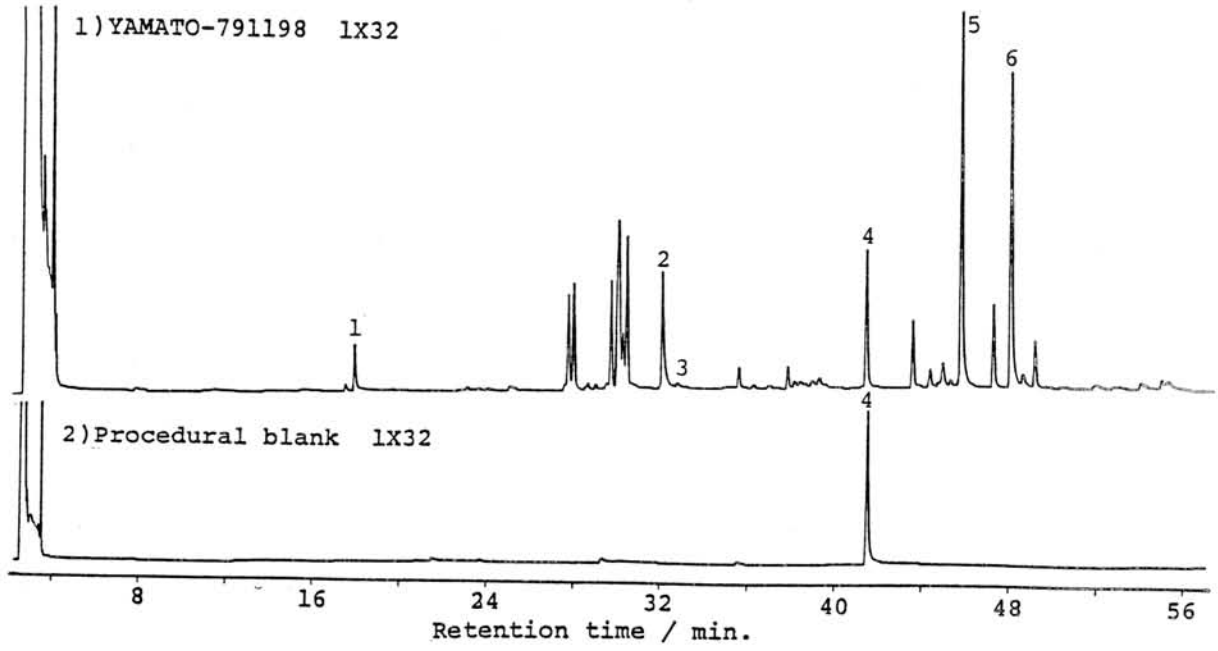

Fig.2 Gaschromatogram of aromatic hydrocarbons from YAMATO-791198

Peak No., 1.Acenaphtene, 2.Phenanthrene, 3.Anthracene, 4.Dibutylphthalate, 5.Fluoranthene, 6.Pyrene.

It is clear that different kinds of C2 chondrites in Antarctic carbonaceous chondrites exist as observed by this and previous studies. The difference has been also noted by other studies of inorganic constituents. Combined studies of organic and inorganic constituents are necessary for the better understanding of the origin and the subsequent history of carbonaceous chondrites.

References

1)A.Shimoyama, C.Ponnamperuma and K.Yanai, Nature,282,394(1979)

2)A.Shimoyama, K.Harada and K.Yanai, Chemistry Letters, 1183(1985)

3)A.Shimoyama, H.Naraoka, H.Yamamoto and K.Harada, Chemistry Letters, 1561(1986)

4)A.Shimoyama and K.Harada, Geochemical J.,18, 281(1984)

7—1

COMPOSITIONAL VARIATION OF PHYLLOSILICATES AND FORMATION PROCESSES IN CV AND CM CARBONACEOUS CHONDRITES

Miúra, Y.[1], Abe, K.[1] and Kojima, H.[2]

1) Department of Mineralogical Sciences and Geology, Faculty of Science, Yamaguchi University, Yamaguchi, 753, Japan.
2) National Institute of Polar Research, Itabashi, Tokyo 173.

Compositional variations of phyllosilicate minerals are discussed in CV3 and CM2 carbonaceous chondrites from microprobe data and heating experiment to elucidate the formation process. The comparative results of the phyllosilicates with terrestrial standards [1, 2] are summarized as follows (Figs. 1 to 3; [1, 2]):

1. The major phyllosilicate minerals in the carbonaceous chondrites are Fe-bearing serpentine and cronstedtite [1-3].

2. Structural substitution and compositional variation in meteoritic phyllosilicates can be discussed by diagram of Si and (Mg+Fe)/(Si+Al), where crystalline state is different with micro-crystalline aggregates of PCP (poorly crystallized phase). Large and closed packing crystals show stoichiometric composition, whereas loose and wavy (or cylindrical) grains have various intermediate compositions containing Fe or Mg ions.

3. Phyllosilicates in the Allende (CV3) chondrite show three closely related reaction lines (oblique), and two octahedral ratios of early and later crystallizations. Various substitutions are also observed in olivine composition, as shown in Fig. 1. This shows that hydro-alteration from olivine in the Allende chondrites is multi-stages under relatively higher P-T condition and closed system remaining early stage of crystallization in the parent body.

4. Phyllosilicates in the Murchison (CM2) chondrite have two oblique lines and four crystallization stages with definite compositions of olivine, as shown in Fig. 2. Formation process of the Murchison is simple hydro-alteration at relatively lower P-T condition, resulting only in various compositions of Fe-bearing serpentine. Stoichiometric composition of phyllosilicates can be obtained after heating experiment (cf. Fig. 2).

5. Compared with the above two data, ALH-77307,85-1 (CV3) chondrite indicates widely-separated oblique lines and three or four crystallization stages, as shown in Fig. 3. This various compositional trends are similar to the Allende (CV3) phyllo-silicates and olivines. Formation condition and process of the ALH-77307,85-1 chondrites might be much higher P-T condition and larger substitution ratios in more fluid and turbulent parent body than those of the Allende (CV3). But the phyllosilicates of early stage direct from olivine could not observed in this Antarctic chondrite (cf. Fig. 3).

6. Compositional pattern of phyllosilicates in Si - (Mg+Fe)/(Si+Al) diagram indicates formation condition and process of carbonaceous chondrites in the parent body.

REFERENCES:
[1] Miúra, Y.(1986): Proc. Symposium on Antarctic Meteorite, pp. 2.
[2] Miúra, Y. et al. (1987): Technical Report of the Fundamental Scientific Research of 1986. p.97 - 101.

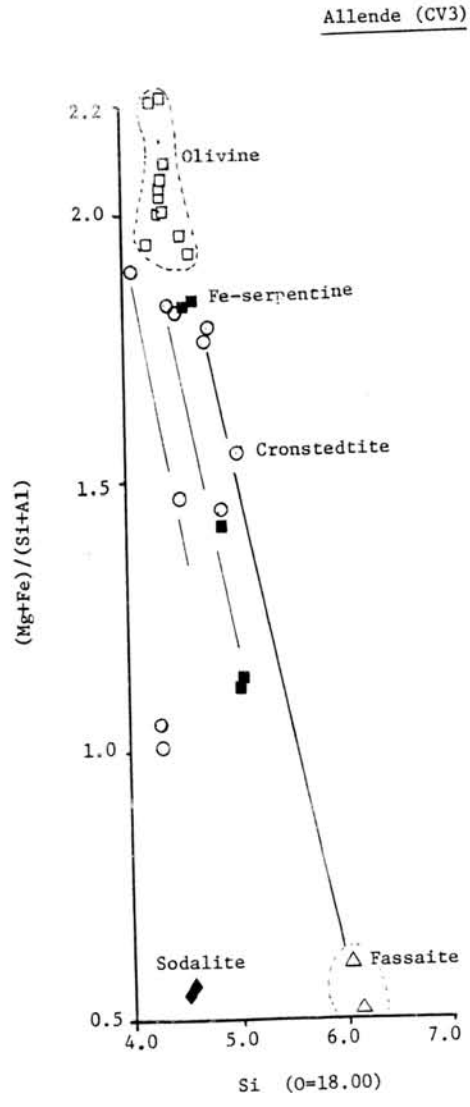

Fig. 1. Various compositional trends of the Allende (CV3) in Si - (Mg+Fe)/(Si+Al) diagram. Three reaction lines and two crystallization stages of phyllosilicates are observed.

ALH-77307,85-1 (CV3)

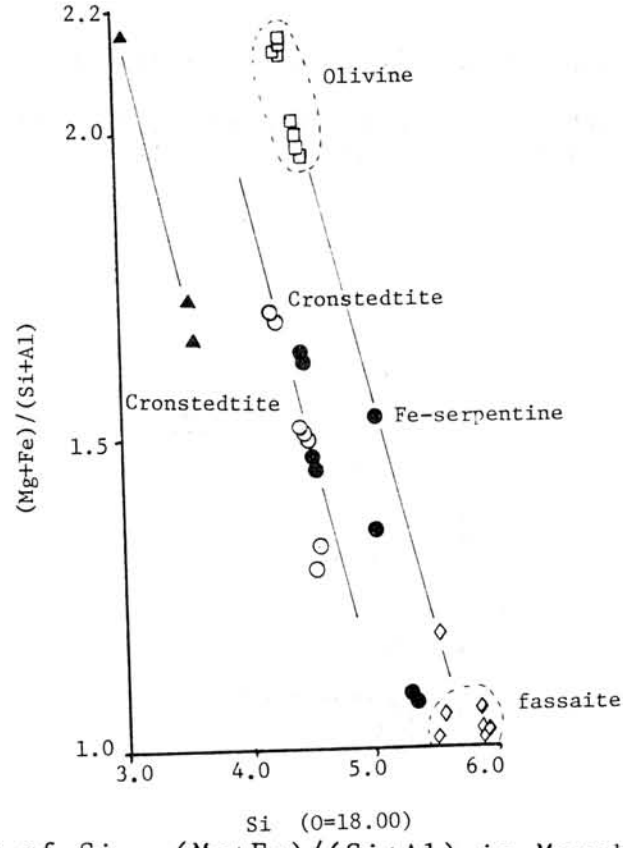

Fig. 2. Diagram of Si - (Mg+Fe)/(Si+Al) in Murchison (CM2) before and after heating experiment. Two reaction lines and three crystallization stages are observed. Reaction line after heating is simple one.

Murchison(CM2)

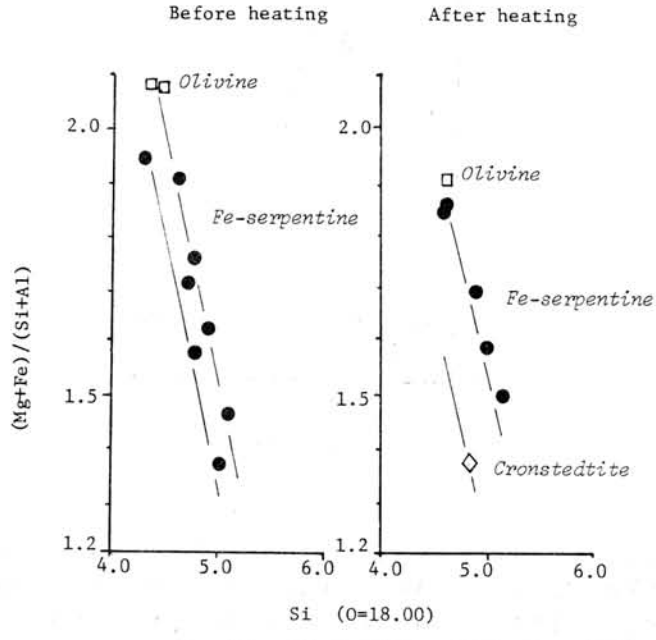

Fig. 3. Diagram of Si and (Mg+Fe)/(Si+Al) in ALH-77307,85-1 (CV3) chondrite showing three reaction lines and three or four crystallization stages.

YAMATO-82162; POSSIBLE FIRST C1 CARBONACEOUS CHONDRITE FROM ANTARCTICA

Hideyasu Kojima and Keizo Yanai, National Institute of Polar Research, 9-10, Kaga 1-chome, Itabashi-ku, Tokyo 173

Yamato-82162(Y-82162) consists of three fragmental pieces, totally 39.5g which was partly covered with polygonal and dull black fusion crust. Interior is black in color and shows breccia like texture. Chondrules and aggregates are extremely rare on the broken surface. Some parts of the surface are coated with thin and powdery efflorescence like materials which are a white to pale gray in color.

In the thin section, this specimen consists mostly of dark matrix inculding very fine transparent phyllosilicate aggregates and sulphide with minor magnetite. Chondrules and inclusions are almost absent, but we found only one olivine grain, up to 30 m across in the dark matrix. Some narrow veins are observed, however these are not so large scale as those in Orgueil CI chondrite (Richardson, 1978). Transparent phyllosilicate aggregates are scattered in the matrix, and most of aggregates are several tens microns in size and are associated with sulphide and magnetite. But some of aggregates consist of only phyllosilicates. Two types of sulphide are observed in the specimen; one is up to 100 m in size and nearly euhedral. The other is under 10 m in average size and anhedral. In sulphides, troilite is much more abundant than pentrandite.

The bulk chemical analyses (Analyst: H. Haramura, Univ. of Tokyo) show following features;

1. Bulk Mg/Si and Al/Si versus Fe/Si weight ratios of Y-82162 are plotted in the area of CI chondrites of McSween (1979).
2. The volatile components (mainly H2O and C) of Y-82162 are obviously lower than those of known CI chondrite.

As described above, petrographic features and the result of bulk chemical analyses except of the volatiles show that Y-82162 is classified as C1 chondrite affinity.

There are two possibilities for the cause of less volatiles about Y-82162; Y-82162 was originally poor in volatiles or Y-82162 was primarily rich in volatiles, but the dehydration took place in the later stage.

Richardson, S. M. (1978) Meteoritics 13, 141-159.
McSween, H. Y. Jr. (1979) Rev. Geophys. Space Phys. 17, 1059-1078.

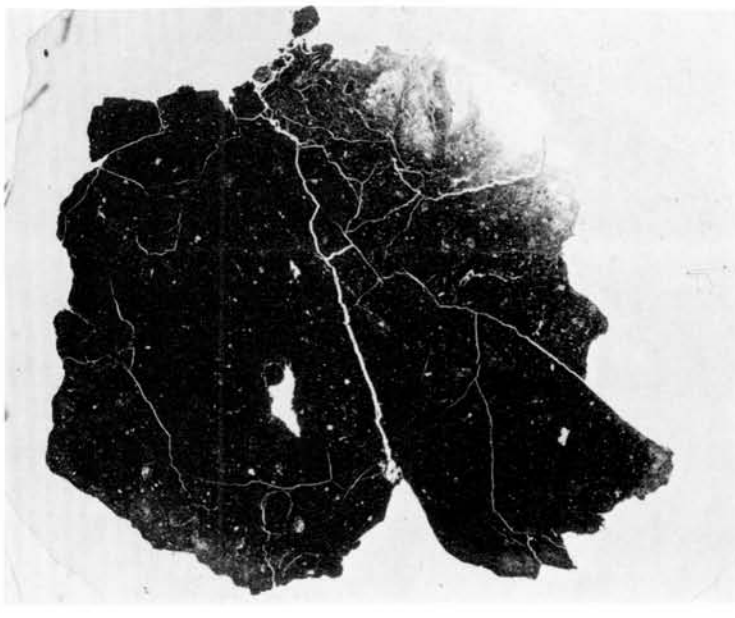

Photomicrograph of the thin section of Y-82162 carbonaceous chondrite.
10mm width.

Special Session: Lunar Meteorites and Yamato-691 E3 Chondrite

Monday, June 8, 1987

1245 - 1520

NEW LUNAR METEORITE: YAMATO-793274

keizo Yanai and Hideyasu Kojima, National Institute of Polar Research, 9-10, Kaga 1-chome, Itabashi-ku, Tokyo 173

Yamato-793274 meteorite has been newly identified as an anorthositic regolith breccia. This specimen was classified as the fifth lunar meteorite originated from the moon surface. Yamato-793274 (Y-793274) was found on the bare ice area between Massif B and the Minami Yamato Nunataks of the Yamato Mountains, Antarctica in January 3, 1980 by the meteorite search party of the 20th Japanese Antarctic Research Expedition 1979-80. In the field Y-793274 was collected as an one of achondrites as same as Yamato-791197 lunar meteorite.

Yamato-793274 is nearly complete and angular shaped small stone with some smooth surface (might original face), 8.66 grams and covered with a thin fusion crust which is brownish to greyish dusty color. A lot of clasts ranging from few to several millimeters across are recognized in dark grey to black matrix. The clasts show mostly angular shape, white and black in color set in the matrix. This specimen measured 2.6 x 1.8 x 1.2 centimeters. The original volume of the specimen is 2.82 cubic centimeter and the specific gravity is 3.07 (g/cm^3).

The thin section of the Y-793274 is a polymict microbreccia containing numerous clasts in brown matrix with green colored fusion crust which contained many fine vesiculars. Clasts in the section show varieties in their texture; anorthositic, troctolitic, gabbroic, melted rockfragments with greenish glass, recrystallized rock fragments and small spherule. Numerous mineral fragments are in the section, as pyroxene (abundant), olivine (intermediate), calcic plagioclase (comparatively little) and gass spherule (rare).

Microproble analyses show that feldspar ranges from An88.3 to An97.4. Pyroxene and olivine are variable in composition, pyroxene En4.2-67.5 Fs16.4-64.3 Wo2.8-40.1 and olivine Fo2.7-82.2 were analyzed. MnO content of the both pyroxene and olivine are remarkably lower than those of the all basaltic achondrites, but they are very similar to the some of lunar rock especially anorthositic regolith breccia.

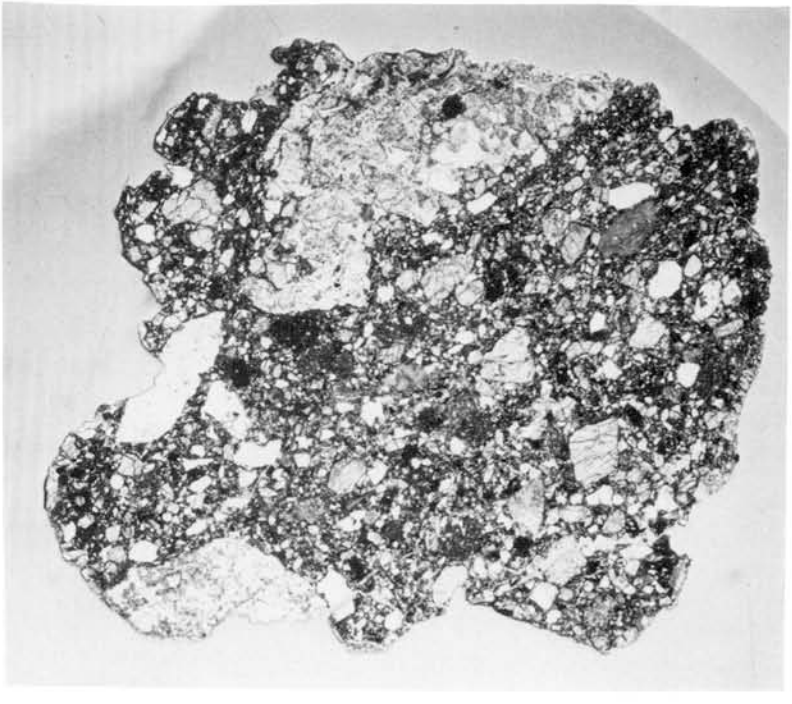

Fig.1. Photomicrograph of the thin section of Y-793274, width 7mm

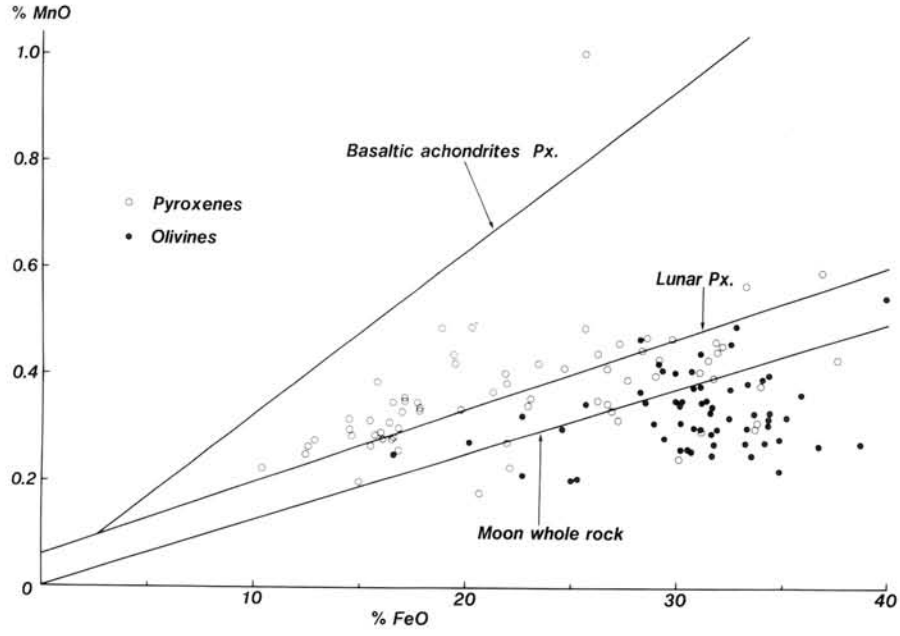

Fig.2. MnO-FeO values of pyroxenes and olivines in Yamato-793274 as compared with those of lunar and achondritic pyroxenes and lunar whole rock analyses.

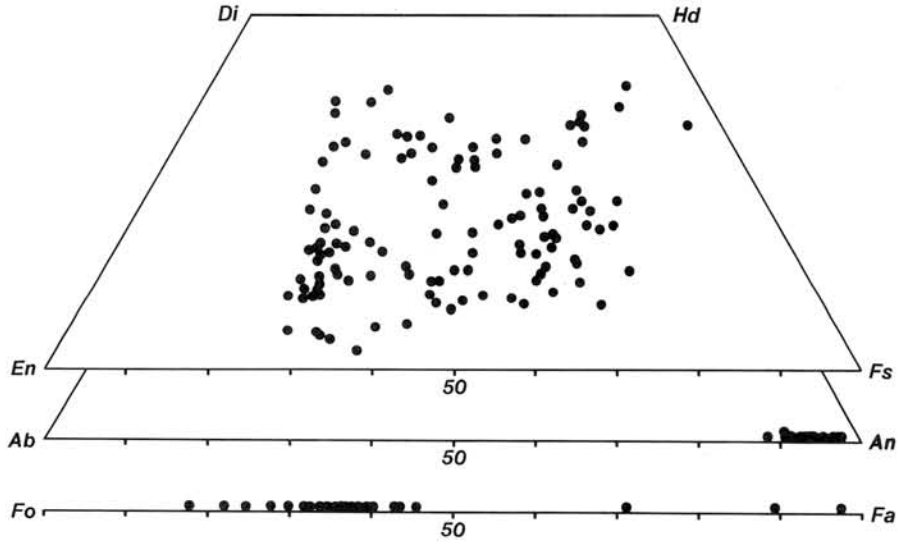

Fig.3. Pyroxene quadrilaterals of pyroxene grains in the matrices and clasts of Yamato-793274. Plagioclases and olivines also plotted.

LUNAR METEORITES Y82192 AND Y82193: GEOCHEMICAL AND PETROLOGIC COMPARISONS TO OTHER LUNAR BRECCIAS

Marilyn Lindstrom(1,2), Randy Korotev(2), David Lindstrom(3,2) and Larry Haskin(2)

1) NASA-Johnson Space Center, Houston, TX; 2) Washington University, St Louis, MO; 3) Lockheed EMSCO, Houston, TX

The lunar meteorites discovered in Antarctica during the last few years are important to our understanding of the Moon. They are random samples of the lunar crust that were sent to Earth by meteorite impact. As random samples they may be more representative of the average lunar crust than the returned samples which were selected to represent specific geologic units on the nearside. In this regard it is essential to determine from geochemical and petrographic studies whether the lunar meteorites represent a single or multiple impacts, and therefore, one or more regions of the lunar crust.

We have analyzed two subsamples of Y82192 by INAA for 22 major and trace elements. Results are presented in Table 1, where they are compared to previous analyses of lunar meteorites (1,2,3). As was noted at the 11th Symposium on Antarctic Meteorites Y82192 and Y82193 are feldspathic breccias with compositions very similar to ALHA81005 and Y791197. They have slightly lower concentrations of REE and other incompatible trace elements than the other lunar meteorites. Their siderophile element concentrations are also lower than the other lunar meteorites, but are within the range of lunar polymict breccias. Previous analyses have also shown that the bulk Mg' [molar Mg/(Mg+Fe) x 100] is in the range of Y791197 and distinctly lower than ALHA81005. All are within the range of lunar polymict breccias. We have also briefly examined a thin section of Y82193. It is a polymict breccia containing abundant monomineralic fragments, scattered irregular patches of dark brown glass and a few large lithic clasts. Lithic clasts are dominated by recrystallized rocks. Some coarse-grained poikilitic clasts were once plutonic rocks, but other fine-grained granulitic clasts have brecciated textures. Most lithic clasts have 20-40% mafic minerals, although some anorthosite clasts are found. All of the petrographic and bulk compositional characteristics of the two new meteorites are consistent with a lunar origin.

Comparison of the lunar meteorites to returned lunar samples has previously shown that they differ from typical lunar polymict breccias in being highly feldspathic and having much lower concentrations of incompatible elements (1,2,3). They are instead similar to both lunar granulites and feldspathic fragmental breccias from North Ray Crater, Apollo 16 (4,5). Granulites are common clasts in the lunar meteorites and in the NRC breccias (6). We showed that although the NRC breccias consist largely of different proportions of the same components, the variation in some components is extreme and leads to major differences in bulk composition, especially Mg'. We concluded that the lunar meteorites might have come from different parts of a heterogeneous target area analagous to that sampled by North Ray Crater (5). This conclusion is not altered by new data on Y82192 and Y82193. More recently Warren (7,8) has

compared the compositional variations among lunar meteorites to those in Apollo 16 regolith breccias. Because Mg' variations are smaller in the Apollo 16 regolith breccias he concluded that the lunar meteorites are unlikely to have resulted from a single site. The question of which rocks are best used for comparison to the lunar meteorites is a difficult one. McKay (9) addresses the relationship betweeen NRC feldspathic fragmental breccias and regolith breccias saying that the fragmental breccias are similar to very immature regolith breccias. They may have been early breccias in the megaregolith which were buried and sheltered from further mixing and homogenization. The lunar meteorites are immature regolith breccias with textures and bulk compositions similar to those of the feldspathic fragmental breccias. Their compositions are distinct from the KREEP-enriched and more mafic Apollo 16 regolith breccias. We still feel that the NRC breccias are the best analogues for the lunar meteorites. This analogy does not prove that the lunar meteorites are from a single site, but does support that hypothesis. The evidence of exposure histories of the lunar meteorites should be reevaluated in light of variations in exposure histories of the NRC breccias. It is not suggested that the lunar meteorites are all paired (only Y82192 and Y82193 are paired), but that they might have been preexisting breccias at a single site on the Moon, and could have been sent Earthward by a single impact.

References:
(1) Various authors, 1983, Geophys. Res. Lett. 10, 773-840.
(2) Various authors, 1986, Proc. 10th Sym. Ant. Met., NIPR.
(3) Various authors, 1986, Abs. 11th Sym. Ant. Met., NIPR.
(4) Korotev et al, 1983, Geophys. Res. Lett. 10, 829-832.
(5) Lindstrom et al, 1986, Proc. 10th Sym. Ant. Met., 58-75.
(6) Lindstrom and Salpas, 1983, PLPSC13, JGR 88, A671-A683.
(7) Warren and Kallemeyn, 1986, Proc. 11th Sym. Ant. Met., NIPR.
(8) Warren and Kallemeyn, 1986, Meteoritics 21, 532.
(9) McKay et al, 1986, PLPSC16, JGR 91, D277-D303.

Fig. 1 REE in Lunar Meteorites

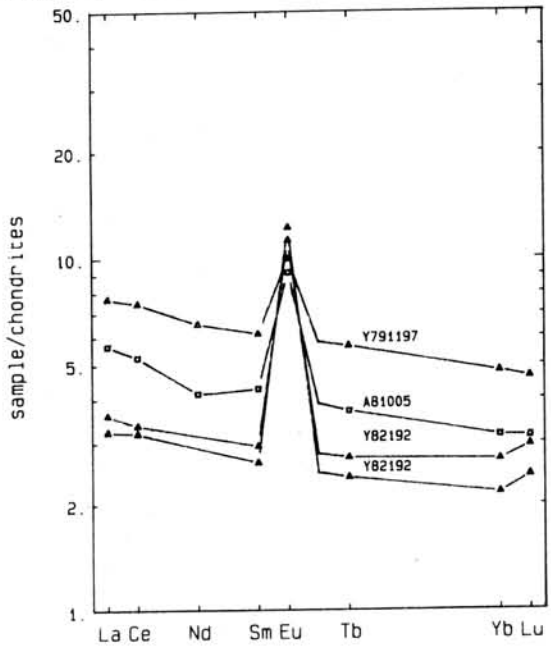

Fig. 2 North Ray Crater Breccias

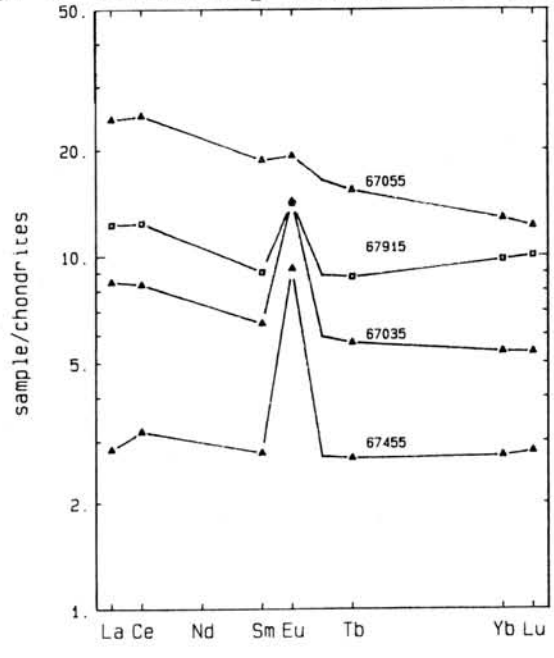

Table 1. Compositions of Lunar Meteorites (INAA).

	Y82192 141A1	Y82192 141A2	Y82192[1] mean	Y82193[1] mean	A81005[2] mean	Y791197[2] mean
TiO2(%)	--	--	0.22	0.27	0.26	0.33
Al2O3	--	--	27.0	25.8	25.7	26.3
FeO	5.05	4.12	4.60	5.64	5.51	6.41
MgO	--	--	4.5	5.1	8.20	5.98
CaO	14.4	15.0	15.1	16.7	15.0	15.3
Na2O	0.411	0.441	0.49	0.41	0.302	0.327
K2O	<.09	<.08	.020	.037	.023	.028
Sc(ppm)	10.9	8.23	8.68	12.2	9.1	13.4
Cr	894	701	753	1055	890	910
Co	15.8	13.0	14.4	19.2	21.0	25.0
Ni	140	110	121	148	198	250
Sr	163	180	190	180	135	137
Ba	29	25	26	28	28.4	33
La	1.18	1.06	1.11	1.27	1.98	2.38
Ce	2.90	2.76	2.7	3.0	5.2	6.0
Nd	<6	<6	1.5	2.0	3.2	4.1
Sm	.596	.534	0.54	0.65	0.95	1.13
Eu	.866	.939	0.94	0.82	0.69	0.79
Tb	.140	.123	0.12	0.14	.214	.256
Yb	.590	.475	0.55	0.73	0.84	1.07
Lu	.100	.082	.082	.117	.124	.157
Zr	37	36	--	--	27	32
Hf	0.46	0.43	0.36	0.45	0.73	0.86
Ta	.060	.058	.043	.034	.093	.103
Th	.133	.100	0.14	0.20	0.29	0.33
U	<.08	<.07	.031	.040	.098	.119
Ir(ppb)	3.2	3.8	2.9	5.7	6.8	6.6
Au	2.5	6.6	0.7	1.3	2.2	6.6

1) Various authors, Abs. 11th Sym. Ant. Met., NIPR.
2) Warren and Kallemeyn, Abs. 11th Sym. Ant. Met., NIPR.

NEW DATA FOR THE BULK COMPOSITIONS OF FOUR LUNAR METEORITES, AND FOR AN FE-RICH BASALTIC CLAST OF PROBABLE VLT-MARE AFFINITY FROM Y791197

PAUL H. WARREN AND GREGORY W. KALLEMEYN

Institute of Geophysics and Planetary Physics, University of California, Los Angeles, CA 90024, USA

We have used our standard fused bead - electron probe technique [1] to obtain new analyses of four lunar meteorites for major elements and Ti. These new data supplement our INAA analyses determined from the same samples [e.g., 2], including a new INAA analysis (this work) of Y82193. We have also applied our RNAA technique [1] to the same four samples, to determine seven trace, mainly siderophile elements: Au, Cd, Ge, Ir, Ni, Os and Re. In addition, we have used INAA to analyze three clasts from lunar meteorites: two from Y82193, and most importantly, the "HPF" clast from Y791197 [3] (we are extremely grateful to Professor H. Takeda for suggesting that this would be an interesting clast for us to study).

For the most part our new major-element data for ALHA81005, Y791197, and Y82192 only confirm earlier analyses. The new data for SiO_2 (44.8, 45.0, and 45.8 wt%, respectively) are far less redundant, however. The only previous analyses of lunar meteorites for Si were by [4] and [5], for ALHA81005 and Y791197, respectively. The normative olivine/pyroxene ratios implied by our analyses are more moderate (more like Apollo-16 soils) than implied by the previous analyses. Our Y82193 sample seems unrepresentative. Presumably Y82192 and Y82193 are paired [6]. However, our data for Y82193 (MgO = 6.0 wt%, FeO = 4.3 wt%; FeO result from fused bead analysis precisely confirmed by INAA) indicate a far higher *mg* ratio (0.712) than we find for Y82192 (0.622) (other Y82192 analyses [7,8] range from 0.613-0.635), and also far higher than indicated by an earlier analysis of Y82193 (0.618) [7]. This huge discrepancy is all the more surprising because compared to previous analyses of Y82192 and Y82193 [2,7-9], there are only a few other significant differences: Heavy REE contents are slightly lower (the most extreme case: Dy = 0.73 μg/g), Al_2O_3 is slightly higher (27.6 wt%), TiO_2 is slightly lower (0.19 wt%), SiO_2 is slightly lower (44.5 wt%), and strongly Fe-correlated elements Sc, Cr, and Mn are all lower (7.7, 690, and 460 μg/g, respectively) in our Y82193 sample. Nor did we notice any obvious difference in macroscopic appearance while preparing the Y82193 sample for analysis. It will be interesting to see if additional analyzed samples of Y82193 tend to resemble our sample, or tend to resemble the Y82193 sample of Fukuoka et al. [7].

Two clasts that we separated from our Y82193 allocation are not greatly different from the bulk sample in composition. However, one of the clasts has an unusually high Na content (0.64 wt%), and a high La/Sm ratio (3.85) by the standards of the lunar meteorites. The Y791197 HPF clast consists of extremely Fe-rich pyroxene (zoned from pigeonite to nearly pure hedenbergite), plagioclase, fayalite, and minor silica mineral and ilmenite [3]. Takeda et al. [3] could not be certain whether this lithology represents an extreme differentiate of highlands affinity, or a modally unrepresentative piece from a low-Ti mare basalt. Clasts of VLT mare basalt have been spotted previously in thin sections from ALHA81005 [10] and from elsewhere in Y791197 [11]; one of the clasts described by [11] is petrographically similar to the HPF clast, with fayalite and extremely low-*mg* pyroxenes, plus considerable troilite.Macroscopically, the HPF clast appeared reddish-brown. We managed to extract nearly all of it, yielding a reasonably pure sample of 0.97 mg. Our INAA data tend to suggest that the clast is of mare affinity. Results (to date) are as follows: in wt%, Na = 0.143, Ca = 5.7±0.7, Fe = 22.3; in μg/g, K = 340±70, Sc = 59, Cr = 980, Mn = 2640, Co = 23, Ga = 4.1±0.7, Ba = 28, La = 3.0, Ce = 7.8±1.5, Sm = 1.57, Eu = 0.55, Tb = 0.49±0.13, Dy = 5.1, Ho = 0.88, Yb = 3.2, Lu = 0.53, and Hf = 1.24±0.16. The REE pattern is remarkably similar to that of Luna-24 very-low-Ti (VLT) mare basalt 24174 [12], except the HPF clast has an even greater enrichment in heavy REE relative to light REE. Like most VLT mare basalts, the HPF clast has a slight negative Eu anomaly. The composition of the HPF clast shows remarkably high Sc/Sm and Mn/Sm ratios. High Sc/Sm and Mn/Sm are also distinctive characteristics of VLT mare basalts (and the Apollo-15 green mare glasses). However, a few pristine nonmare rocks (dunite 72415/7 and gabbronorites 61224,6 and 67667) also feature extremely high Sc/Sm and Mn/Sm. The HPF clast also has a surprisingly high Ca/Na ratio (cf. the plagioclase compositions reported by [3]), which tends to distinguish it from the high-Sc/Sm gabbronoritic nonmare rocks, and its extremely low-*mg* pyroxenes obviously rule out any affinity with the dunite. Considering that the source locale for Y791197 is a completely unexplored region of the Moon, it is difficult to be certain about the relationship of this clast to any of the Apollo or Luna samples. But its composition seems most consistent with an uncommonly ferroan variety of low-Ti, and probably VLT, mare basalt.

Our new RNAA results for Au, Ir, and Ni in the four lunar meteorites generally confirm earlier results reported from several INAA labs, including our own. We find that Y791197 is relatively rich in Ge (400 ng/g, vs. 220 ng/g for ALHA81005, 200 ng/g for Y82192, and 340 ng/g for Y82193), and ALHA81005 is relatively rich in Re (0.68 ng/g, vs. 0.45 ng/g for both Y791197 and Y82192, and 0.61 ng/g for Y82193). Osmium contents are similar in all four meteorites (6.9 ng/g in Y82193, 7.6-8.4 ng/g in the others).

The lunar meteorites are all regolith breccias, and may for many purposes be regarded as lithified, relatively immature soils. Among Apollo soils and polymict rocks, those from Apollo 16 tend to have the highest Au/Ir ratios. Several mature Ap-16 soils have Au/Ir >1, higher than even the highest-Au/Ir type of chondrite (EH chondrites have avg. Au/Ir = 0.6). In contrast, mare soils tend to have Au/Ir between 0.25 and 0.4, like typical chondrites. Soils from another mainly highlands site (Ap-14) tend to have Au/Ir slightly lower than Ap-16 soils, and soils from Ap-15 and Ap-17 that are mixtures of both highland and mare material tend to have intermediate Au/Ir. Wasson et al. [13] inferred that meteoritic material accreted after roughly 3.8 Ga tended to have moderate, CM-chondrite-like Au/Ir, but an earlier, "short-lived" population of projectiles epitomized by the Ap-16 samples had extremely high (by chondritic standards) Au/Ir. Hertogen et al. [14] interpreted the high-Au/Ir matter ("Group 1H") typical of Ap-16 as representative of uncommonly young (though still older than 3.8 Ga) meteoritic debris, similar to but distinct from Group 1L, which they ascribed to Imbrium. According to [14], low-Au/Ir matter accreted early, and high-Au/Ir matter accreted relatively late, because the early projectiles were similar to the bulk Moon in composition, whereas the late projectiles were "complementary" to the bulk Moon (these authors assumed that the bulk Moon has a high Ir/Au, due to a general enrichment in refractory elements). Korotev [15] suggests that the Ap-16 area was hit by a giant iron meteorite with relatively high Au/Ir (and Ni/Ir). Despite representing nearly pure highlands soils, at least two of the lunar meteorites have "low," chondrite-like, Au/Ir: ALHA81005 and Y82192 have Au/Ir = 0.32 and 0.33, respectively. The Au/Ir ratio of Y791197 scatters among literature analyses from 0.09 (this work) to 0.39, but one analysis that did not determine Ir gave extremely high Au [16], which if factored into a mass-weighted mean of all analyses would (ignoring the possibility that Ir was also enriched in the same sample) imply Au/Ir = 0.7. Assuming these meteorites are reasonably representative of regoliths from three separate sites, their compositions tend to indicate that high Au/Ir is not a general feature of highlands soils, as assumed by [13], but rather an anomaly peculiar to the central near side (CNS) region of the Moon. The fact that anomalously high Au/Ir is also found in highlands samples from CNS sites other than Ap-16, especially Ap-14 (a trend reinforced by recent analyses of "exotic" Ap-14 regolith breccias 14315 and especially 14076 [17]), is difficult to reconcile with models attributing the anomalously high Au/Ir to a few (but >1) discrete impacts, as implied by the models of [14] and [15]. We assume that a projectile's composition cannot determine where on the Moon it will strike. We are drawn to the very tentative conclusion that the Au enrichment of the CNS highlands soils may be at least partly due to indigenous lunar Au, presumably transported as a volatile and very roughly correlated with KREEP, which is also anomalously enriched in the CNS area. Speculations along similar lines are at least as old as Hughes et al. [18]. Meteorite-free eucrites, which formed in an environment closely analogous to the lunar crust, generally have greatly hyperchondritic Au/Ir [e.g., 1]. Possibly the chemistry of the Ap-16 site reflects both high indigenous Au and impact of a high-Au/Ir, high Ni/Ir projectile.

The high Ni/Ir ratios of the polymict samples from Ap-16 have been interpreted by Ringwood et al. [19] as evidence for high indigenous Ni, supposedly derived from Mg-rich rocks with Ni and Mg contents remarkably similar to those of terrestrial komatiites, thus confirming that the Moon formed essentially by fission from the Earth's mantle. However, the Ni/Ir ratios of the lunar meteorites (and for that matter other highlands regolith samples) indicate that the high Ni/Ir of the Ap-16 polymict samples is not a general feature of the lunar crust, but a local anomaly, such as might be produced by impact of a relatively high-Ni/Ir projectile [13-15].

References: [1] Warren P. H. & Jerde E. A. (1987) *GCA* **51**, 713-725. [2] Warren P. H. & Kallemeyn G. W. (1987) *Proc. Symp. Ant. Met. 11*, in press. [3] Takeda H. et al. (1986) *Proc. Symp. Ant. Met. 10*, 45-57. [4] Palme H. et al. (1983) *GRL* **10**, 817-820. [5] Yanai K. & Kojima H. (1984) *Proc. Symp. Ant. Met. 9*, 18-34. [6] Nishiizumi K. et al. (1986) *Abstr. Symp. Ant. Met. 11*, 58-59. [7] Fukuoka T. et al. (1986) *Abstr. Symp. Ant. Met. 11*, 40-42. [8] Nakamura N. et al. (1986) *Abstr. Symp. Ant. Met. 11*, 47-48. [9] Bischoff A. et al. (1986) *Abstr. Symp. Ant. Met. 11*, 34-36. [10] Treiman A. H. & Drake M. J. (1983) *GRL* **10**, 783-786. [11] Lindstrom M. M. et al. (1986) *Proc. Symp. Ant. Met. 10*, 58-75. [12] Laul J. C. et al. (1978) in *Mare Crisium: The View From Luna 24*, p. 537-567. [13] Wasson J. T. et al. (1975) *Moon* **13**, 121-141. [14] Hertogen J. et al. (1977) *PLSC 8*, 17-45. [15] Korotev R. (1987) *PLPSC 17*, E491-E512. [16] Kaczaral P. W. et al. (1986) *Proc. Symp. Ant. Met. 10*, 76-83. [17] Warren P. H. et al. (1987) *LPS XVII*, 1060-1061. [18] Hughes T. C. et al. (1973) *Lunar Sci. IV*, 400-401. [19] Ringwood A. E. et al. (1987) *EPSL* **81**, 105-117.

TRACE ELEMENTS IN LUNAR METEORITES Y-791197 AND Y-82192

Christian Koeberl

Institute of Geochemistry, University of Vienna
Dr.-Karl-Lueger-Ring 1, A-1010 Vienna, Austria

The discovery of lunar meteorites in the ice of Antarctica is of great importance for the study of lunar materials, since with almost each new lunar meteorite the number of lunar sites sampled increases. Unfortunately we do not know the exact point of origin on the moon. There are, however, a number of indications that the lunar meteorites known to date are not derived from one single impact (Warren and Kallemeyn, 1986). Among the differences between Apollo and Luna material and the lunar meteorites are lower concentrations of incompatible elements in the latter. An interesting result , which may distinguish Y-791197 from the other lunar meteorites, is an enrichment in volatile elements found in several subsamples of this meteorite. Elements like Se, Te, Bi, In, Zn, Ga, Ag, and Sb (Kaczaral et al., 1986) and the halogens (Koeberl and Kiesl, 1986) show a sometimes considerable enrichment compared to ALHA-81005, Y-82192, or comparable lunar rocks. This has been interpreted as a contamination from lunar volcanism. The study reported here is intended to complement the halogen study of Koeberl and Kiesl (1986), where fine and coarse fractions of Y-791197 and Y-82192 have been investigated.

Here we have performed whole rock analyses, and investigations of coarse and fine fractions along with studies of white clasts separated from the matrix. Clasts analysed have a weight range from 0.58 to 2.89 mg. The results from the whole rock studies are in agreement with other analyses reported in the literature. Ga seems to be distributed very inhomogeneously, since we find a whole range of different Ga contents, which are, however, consistent with published numbers. There seems to be a trend to Ga enrichment in the fine fraction compared to the coarse fraction. The chemistry of the clasts differs in some cases from the whole rock chemistry. Although the REE pattern is rather similar, volatile elements do show a pronounced difference.

It is interesting that clasts in Y-791197 do not show a prominent deviation from the whole rock chemistry, although some volatile enrichment, in agreement with the volcanic contamination proposed, is present. The clasts in Y-82192, however, do show a marked difference in volatile element content if compared to whole rock data. Generally, Y-82192 has a lower content not only of volatiles but also of incompatible elements when compared to Y-791197. Large enrichments in elements like Au, Ga, and Sb have been found, with enrichment factors ranging up to 20 compared to whole rock averages.

This leads to the conclusion that Y-82192 also contains some volatile rich material, which may have the same origin as the volatiles in Y-791197. Since gamma counting of the samples is still in progress at that time, we do expect more results and final data at the time of the Symposium.

Acknowledgements: The work reported here has been supported in part by the Jubiläumsfonds der Österreichischen Nationalbank, project No. 2691 (to C.K.).

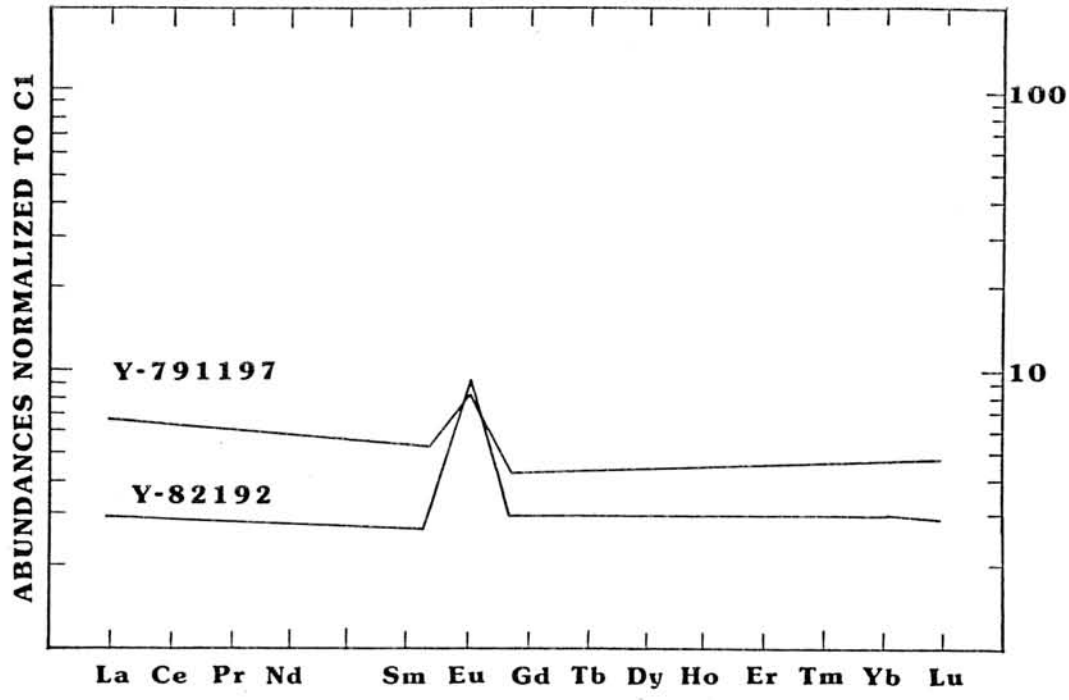

Fig. 1 Chondrite-normalized REE patterns for whole rocks of Y-791197,98 and Y-82192,72.

References:

Kaczaral, P.W., Dennison, J.E., and Lipschutz, M.E. (1986) Mem.Natl.Inst. Polar Res., Spec. Issue, 41, 76-83.
Koeberl, C., and Kiesl, W. (1986) Meteoritics, 21, 420-421.
Warren, P.H., and Kallemeyn, G.W. (1986) Meteoritics, 21, 532.

COSMOGENIC AND TRAPPED NOBLE GAS ISOTOPES, EXPOSURE AGE AND TERRESTRIAL AGE OF LUNAR METEORITES YAMATO 82192 and 82193

Eugster, O.
Physikalisches Institut, University of Bern, 3012 Bern, Switzerland

Samples of about 0.3 g of the lunar meteorites Y82192 and Y82193 were obtained for the investigation of the noble gas isotopic abundances. These anorthositic breccias were recognized to originate from impact ejection from the Moon [cf. 1, 2]. The objective of this study is to derive the cosmic-ray exposure history on the lunar surface and in space and to calculate the terrestrial age of these meteorites. In order to investigate the question whether the trapped noble gases are sited on the breccia grain surfaces, as expected for solar wind implanted particles, two grain size fractions (> 25 μm and ≤ 25 μm) were prepared for each meteorite after crushing the material in a stainless steel mortar. The noble gases were analyzed mass spectrometrically and the data obtained so far for the grain size fractions > 25 μm are given in Tables 1-3.

Table 1. Cosmogenic and trapped He, Ne, and Ar in >25μm grain size fractions of lunar meteorites Yamato 82192 and 82193.

	Cosmogenic				Trapped	
	^{3}He	^{21}Ne	^{38}Ar	$^{22}Ne/^{21}Ne$	^{20}Ne	^{36}Ar
		10^{-8} cm^3 STP/g			10^{-8} cm^3 STP/g	
82192,82	8.1 ±1.0	2.14 ±0.10	2.31 ±0.15	1.252 ±0.050	10.5 ±0.8	8.9 ±0.7
82193,100	7.2 ±1.0	2.18 ±0.10	2.81 ±0.20	1.285 ±0.050	24.2 ±1.3	19.3 ±1.4

Table 2. Cosmogenic and trapped Kr in >25μm grain size fractions of lunar meteorites Yamato 82192 and 82193.

	Cosmogenic							Trapped
	^{83}Kr	^{81}Kr	$^{78}Kr/^{83}Kr$	$^{80}Kr/^{83}Kr$	$^{81}Kr/^{83}Kr$	$^{82}Kr/^{83}Kr$	$^{84}Kr/^{83}Kr$	^{86}Kr
	10^{-12} cm^3 STP/g							10^{-12}cm^{3}STP/g
82192,82	11.8 ±2.5	0.156 ±0.035	0.167 ±0.014	0.544 ±0.030	0.0132 ±0.0014	0.741 ±0.090	0.50 ±0.16	32.6 ±7.0
82193,100	11.9 ±2.5	0.167 0.035	0.166 ±0.013	0.615 ±0.030	0.0140 ±0.0008	0.825 ±0.040	0.45 ±0.15	39.2 ±8.0

Table 3. Cosmogenic and trapped Xe in >25μm grain size fractions of lunar meteorites Yamato 82192 and 82193.

	Cosmogenic						Trapped
	^{126}Xe	$\frac{^{124}Xe}{^{126}Xe}$	$\frac{^{128}Xe}{^{126}Xe}$	$\frac{^{129}Xe}{^{126}Xe}$	$\frac{^{130}Xe}{^{126}Xe}$	$\frac{^{131}Xe}{^{126}Xe}$	^{132}Xe
	10^{-12} cm^3 STP/g						10^{-12} cm^3 STP/g
82192,82	0.49 ±0.10	0.60 ±0.04	1.63 ±0.17	1.6 ±0.8	0.96 ±0.13	3.43 ±0.30	25.1 ±5.0
82193,100	0.50 ±0.10	0.60 ±0.05	1.93 ±0.14	3.3 ±1.4	1.08 ±0.15	2.74 ±0.60	31.6 ±6.0

The total amounts of trapped noble gases are about three orders of magnitude lower than those in the lunar meteorites ALHA 81005 and Y791197. ^4He appears to have been partially lost as the observed amounts are lower than those expected from U and Th decay. The amounts of the trapped gases in Y82193 are up to a factor of ∿2 higher than those in the Y82192 sample. The elemental pattern of the trapped noble gases is similar to that observed for trapped solar wind in lunar surface material.

In order to calculate cosmic-ray exposure ages from the amounts of cosmogenic nuclei, the respective production rates have to be known. Since production rates are depth dependent, the shielding depths of the samples were derived. The depth sensitive cosmogenic ratios $^{22}Ne/^{21}Ne$ and $^{131}Xe/^{126}Xe$ both indicate a shallow shielding. The theoretical depth profile of the $^{131}Xe/^{126}Xe$ ratio was calculated for the chemical abundances of the investigated meteorites [3,4,5] using the data given by Hohenberg et al. [6]. The measured $(^{131}Xe/^{126}Xe)_c$ ratios correspond to a shielding <25 g/cm^2. Average shielding depths during cosmic-ray exposure of 17 g/cm^2 for Y-82192,82 and of 10 g/cm^2 for Y-82193,100 are adopted.

The noble gas production rates were calculated for the adopted shielding, inserting the abundances of the target elements [3,4,5]. The following methods were employed: ^{21}Ne - Hohenberg et al. [6] and Schultz and Freundel [7]; ^{38}Ar - Hohenberg et al. [6] and Freundel et al. [8]; ^{83}Kr - Regnier et al. [9] and Marti et al. [10]; ^{126}Xe - Hohenberg et al. [6] and Marti et al. [10]. For each species the average value obtained from the two methods was adopted. For the 4π-2π geometry conversion a factor of 2 was used.

Table 4. Galactic cosmic-ray exposure ages (10^6 years) and terrestrial ages.

Sample	Apparent ^{81}Kr-Kr age (T^{81})	T^{21}	T^{38}	T^{83}	T^{126}	$T^{av(stable)}$	$T^{av(stable)}$	T_{terr}
		4π geometry					2π geometry	
Y-82192,82	13.9 ±1.5	10.2 ±2.0	12.3 ±2.5	9.0 ±3.0	11.4 ±2.5	10.7 ±1.3	21.4 ±2.6	80'000 y
Y-82193,100	13.9 ±1.0	10.5 ±2.0	13.8 ±2.5	9.0 ±3.0	11.2 ±2.5	11.1 ±2.0	22.2 ±4.0	70'000 y

Galactic cosmic-ray exposure ages were calculated, on the one hand, using ^{81}Kr-Kr dating:

$$T^{81} = \tau^{81} \, (P^{81}/P^{83}) \, (^{83}Kr/^{81}Kr)_c$$

with τ^{81} = 303000 y. P^{81}/P^{83} is the production rate ratio [11].

On the other hand, exposure ages based on the stable nuclei were derived for a 4π- and a 2π-exposure geometry. Table 4 shows that the exposure ages based on stable isotopes agree within experimental errors. For Y-82192 Takaoka [12] and Weber et al. [13] both obtained a 4π- exposure age of about 10 m.y. for a shielding of <40 and 10 g/cm^2, respectively. The data in Tables 1-4 confirm beyond any doubt that the two meteorites represent different splits of the same meteoroid as suggested by several authors [1,3,14].

^{10}Be data given by Nishiizumi et al. [14] show that Y-82192 and Y-82193 experienced a 4π exposure for at least about 5 m.y. of their most recent cosmic-ray exposure history. Therefore, ^{81}Kr was present at the time of fall in equilibrium activity and the terrestrial ages can be calculated from

$$T_{terr} = \tau^{81} \ln[T^{81}/T^{av(stable)}].$$

The resulting terrestrial ages are 70'000 y and 80'000 y, respectively; they are consistent with Nishiizumi et al's estimate of <10^5 y and are typical for meteorites collected in the Yamato mountains [15].

The most probable scenario for the history of the Y-82192/3 meteoroid can be summarized as follows: Excavation on the Moon from a depth completely shielded from cosmic rays occurred 11 m.y. ago. This impact event caused ejection from the Moon's gravitational field. The meteoroid was captured by the Earth about 70'000 y ago. Only if future analyses of the ^{53}Mn activity show that this radioisotope with a half life of 3.7 m.y. is not in equilibrium with respect to a 4π exposure, the above scenario has to be modified in the sense that a pre-exposure occurred on the lunar surface. In such a case two different impacts have to be invoked to excavate and propel the meteoritic material.

Acknowledgements: This work was supported by the Swiss National Science Foundation. I appreciate the generosity of K. Yanai for making available the samples. I thank S. Niedermann, I. Peter, A. Rakovski, A. Schaller, and M. Zuber for their help at various stages of this work.

References: [1] K. Yanai, H. Kojima, and S. Ikadai, Abstr. 11th Symp. Antarctic Meteorites, Tokyo, 10-1 (1986). [2] H. Takeda, A. Mori, and T. Tagai, Abstr. 11th Symp. Antarctic Meteorites, Tokyo, 14-1 (1986). [3] A. Bischoff, H. Palme, B. Spettel, D. Stöffler, H. Wänke, and R. Ostertag, Abstr. 11th Symp. Antarctic Meteorites, Tokyo, 13-1 (1986). [4] T. Fukuoka, J.C. Laul, M.R. Smith, and R.A. Schmitt, Abstr. 11th Symp. Antarctic Meteorites, Tokyo, 15-1 (1986). [5] P.H. Warren and G.W. Kallemeyn, Abstr. 11th Symp. Antarctic Meteorites, Tokyo, 12-1 (1986). [6] C.M. Hohenberg, K. Marti, F.A. Podosek, R.C. Reedy, and J.R. Shirck, Proc. Lunar Planet. Sci. Conf. 9th, p. 2311-2344 (1978). [7] L. Schultz and M. Freundel, in Isotopic Ratios in the Solar System CNES ed., CEPAD, 27 (1985). [8] M. Freundel, L. Schultz, and R.C. Reedy, Geochim. Cosmochim. Acta, 50, 2663-2673 (1986). [9] S. Regnier, C.M. Hohenberg, K. Marti, and R.C. Reedy, Proc. Lunar Planet. Sci. Conf. 10th, p. 1565-1586 (1979). [10] K. Marti, P. Eberhardt, and J. Geiss, Z. Naturforsch. 21a, 398-413 (1966). [11] K. Marti and G.W. Lugmair, Proc. Lunar Sci. Conf. 2nd, p. 1591-1605 (1971). [12] N. Takaoaka, Proc. 11th Symp. Antarctic Meteorites, Tokyo (1986), preprint. [13] H.W. Weber, O. Braun, and F. Begemann, Abstr. 11th Symp. Antarctic Meteorites, Tokyo, 20-1 (1986). [14] K. Nishiizumi, J. Klein, R. Middleton, D. Elmore, P.W. Kubik, and J.R. Arnold, Abstr. 11th Symp. Antarctic Meteorites, Tokyo, 22-1 (1986). [15] K. Nishiizumi and D. Elmore, Abstr. 10th Symp. Antarctic Meteorites, Tokyo, 48-1 (1985).

Major Element Chemical Compositions of Chondrules in Y-691

Ikeda, Y.

Department of Earth Sciences, Ibaraki University, Mito, 310.

Various kinds of chondrules occur in Y-691, the major type being radial-Pyx chondrules. Porphyritic to granular chondrules are common, and minor types include barred-Ol, cryptocrystalline, spherulitic, opaque-massive, and transparent-SiO2 chondrules. In addition to these chondrules, unique types occur rarely in Y-691.

Major element chemical compositions of chondrules were obtained using defocussed beam of an electron-probe microanalyser. Minor types of chondrules in Y-691, barred-Ol, cryptocrystalline, spherulitic and opaque-massive chondrules, tend to show lower Mg/Si and higher Ca/Al ratios in comparison to radial-Pyx chondrules. Porphyritic to granular type shows intermediate values of the ratios between the former minor types and the latter major type. This difference may be explained by the ideas that the precursor materials of the former minor types were higher-temperature condensates and that the fractionation of Mg- and Ca- bearing materials such as niningerite, oldamite, etc. produced Mg- and Ca-poor precursor materials as lower-temperature condensates which result in radial-Pyx chondrules. Transparent-SiO2 chondrules are very small spherules less than about 100 microns in diameter and consist almost of SiO2 which may be a latest-stage condensate.

A unique type of chondrules in Y-691 is a quench-Xal-bearing material which shows a chemical composition similar to fine-grained CAI's in the Allende chondrite. Another unique type is a dark material including small grains of fassaite and calcic plagioclase, and the composition is similar to those of amoeboid olivine inclusions in Allende. These unique substances could be high-temperature condensates.

RELICT PYROXENE AND OLIVINE IN CHONDRULES OF Y-691 (EH3)

Masao Kitamura, Seiko Watanabe and Hiroshi Isobe
Department of Geology and Mineralogy, Faculty of Science, Kyoto University, Sakyo 606, Japan

Relict olivine and pyroxene of Fe-rich composition were found in chondrules and mineral fragments in Y-691 [1,2]. In the present study, relict pyroxene and olivine and their poikilitic texture in the chondrules were studied by EPMA, back scattered electron images, and cathodeluminescence to elucidate the condition before the chondrule formation.

Most of the chondrules do not include relict minerals. They are considered to have melted in highly reduced condition during formation of chondrules.

(1) Two types of relict pyroxene grains are found; (a) simple relict pyroxene with iron blebs, and (b) pyroxene poikilitically including olivine which includes iron blebs.

(a) The simple relict pyroxene was found in one chondrule. This chondrule is porphyritic and resembles to chondrules without relict minerals except for existence of the relict pyroxene. One of enstatite ($Wo_{0.6}Fs_{0.7}$) has a ferrous core as a relict (Wo_1Fs_8) (Fig. 1). Metallic iron inclusions are observed surrounding the core. The analyses including the metal blebs give $Wo_{1.5}Fs_{8-9}$. It is considered that the ferrous pyroxene was once melted during the chondrule formation. The metal blebs precipitated in the melt due to a reducing condition, and then were incorporated during re-growth of pyroxene.

(b) The relict pyroxene which poikilitically includes olivine with metallic iron inclusions was found in two chondrules (Figs. 2 & 3). In one chondrule, the relict is orthopyroxene ($Wo_{3-4}Fs_7$) rimmed by pigeonite, and in the other it is pigeonite ($Wo_{6-8}Fs_{4-7}$). Small enstatite grains ($Wo_{1-3}Fs_{0-3}$ in the case of the former) and mesostasis of glass surround the relict grains. The metallic iron blebs in olivine are considered to have precipitated during the chondrule formation. Chemical composition of the olivine plus the metal, (Fa_{6-8}), gives almost the same Mg/Fe ratio as that of the pyroxene, indicating they were equilibrated before the formation of chondrules.

Formation of the poikilitic pyroxene can be explained either by (i) formation from olivine by a reaction with gas, such as reduction of Fe^{2+} or addition of SiO_2, (ii) a reaction between olivine and melt or (iii) a long annealing of the mixture of olivine and pyroxene. The fact that the relict pyroxene is pigeonite or orthopyroxene rimmed by pigeonite suggests the igneous origin, because the dust origin requires the condensation of large olivine grain followed by the reaction to form pyroxene accompanied by the Mg-Ca exchange by keeping at high temperature.

(2) Two chondrules are characterized by large ferrous pyroxene including tiny metallic iron in the rim (Figs. 4 and 5). Mesostasis also contains small blebs of metallic iron. Althogh these pyroxenes have no direct evidence as relict, their ferrous compositions can not be explained by crystallization during formation of chondrules. Therefore, these are also considered to be relict of pyroxenes which have crystallized before the chondrule formation. The compositional zoning of the pyroxenes is different between the two chondrules; in one, Fe/Mg ratio is constant in pyroxenes (Fig. 5a), and the other shows increase of Fe/Mg with increasing Ca (Fig. 5b). These may suggest variation of conditions, probably oxygen fugacity, before the formation of chondrules.

[Concluding remarks] : Relict pyroxenes were found in some chondrules in Y-691. The relict poikilitic pyroxene are considered to have formed by an igneous process rather than the reaction of olivine in the nebula. Compositional trends of large ferrous pyroxenes may reflect variation in the conditions before the formation of chondrules.

[references]

[1] Nagahara,H. (1985) Abstract in 10th Symposium on Antarctic Meteorites.
[2] Kitamura,M., Watanabe,S., Isobe, H. & Morimoto,N. (1987) Mem. Natl. Inst. Polar Res., Spec. Issue, 46, 113-122.

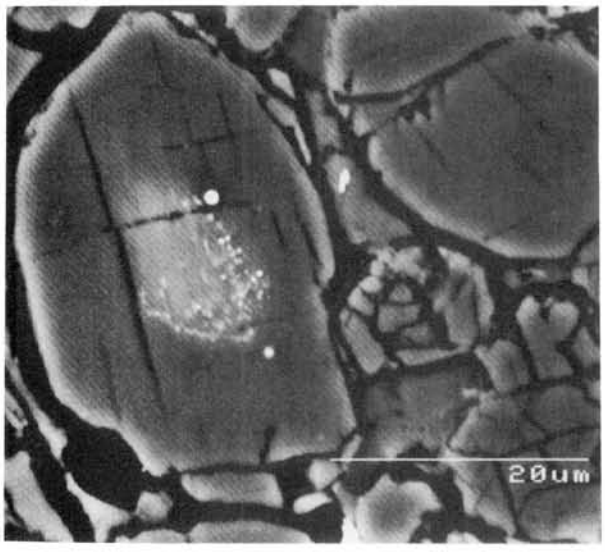

Fig. 1. An enstatite grain in chondrule of enstatite and glass includes fine metal grains and ferrous core.

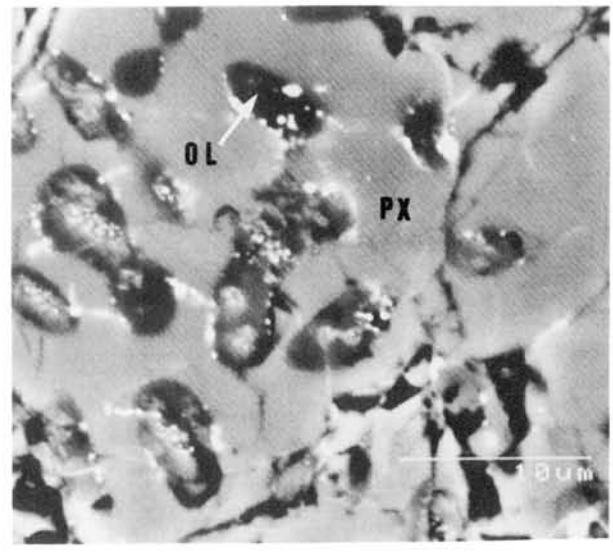

Fig. 2. A chondrule consists mostly of a single crystal of orthopyroxene poikilitically including olivine and Fe-metal.

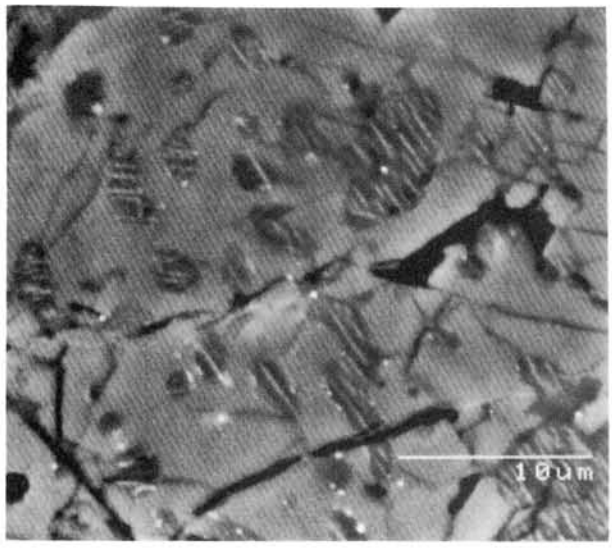

Fig. 3. A large pigeonite grain includes olivine with lamellar Fe-metal. Enstatite and pigeonite are in the mesostasis surrounding large pigeonite.

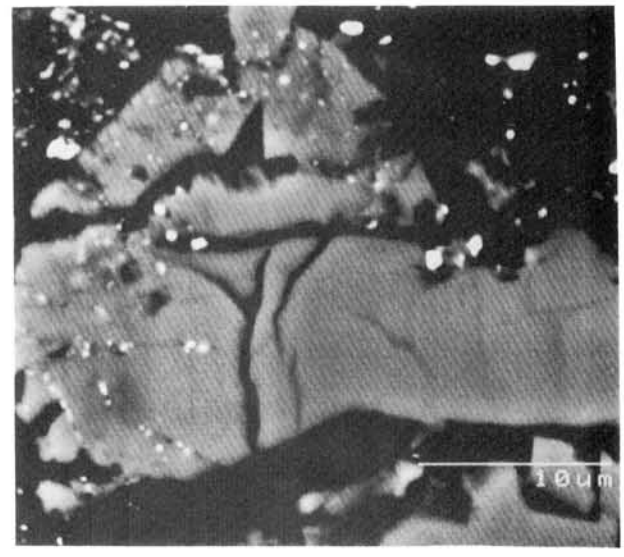

Fig. 4. A chondrule consists of pyroxene and mesostasis. The pyroxne shows the chemical zoning from ferous Opx to less ferrous pigeonite and augite.

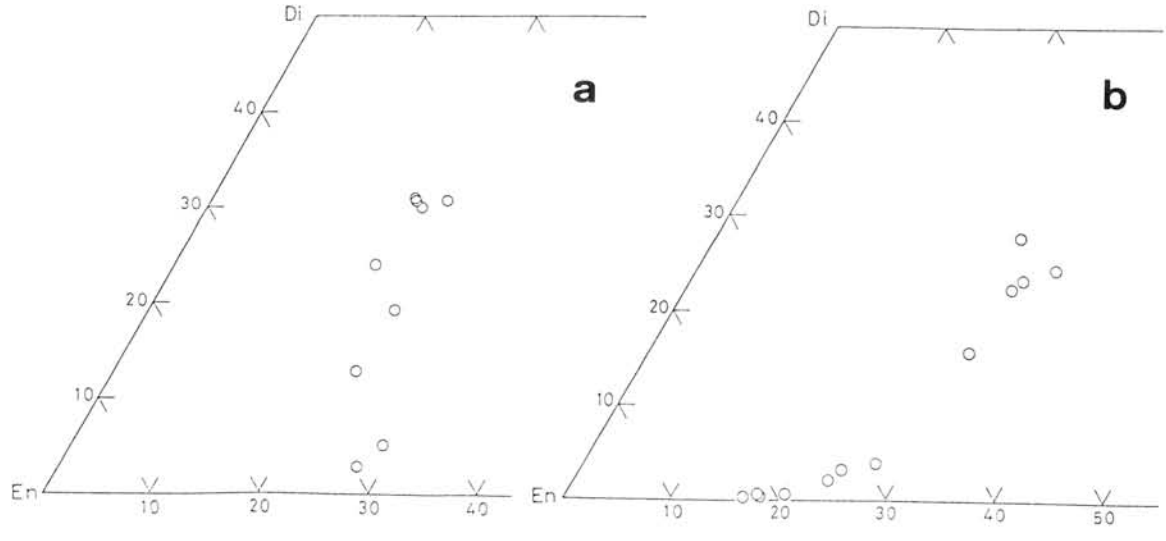

Fig. 5. Compositonal trend of ferrous pyroxenes in the chondrules plotted in the pyroxene quadrilateral. Two trends are different from each other, showing the variation of the condition before the chondrule formation.

Distribution of trace elements in unequilibrated enstatite chondrites

Mitsuru Ebihara

Department of Chemistry, Gunma University, 4-2 Aramaki, Maebashi, Gunma 371

Enstatite chondrites are classified into two groups: high-iron EH, which are petrologic types 3-5, and low-iron EL, which are petrologic type 6. In spite of rather large differences in mineralogical features between EH3 and EH4,5 chondrites (Prinz et al., 1984; McKinly et al., 1984) only a faint difference in chemical compositions has been recognized between them. Weeks and Sears (1985) pointed out that siderophile element abundances in EH3 were the same as those in EH4,5, but that moderately volatile chalcophiles (Mn, Na, K, Se, Zn) were somewhat depleted in EH3 compared with those in EH4,5. Kallemeyn and Wasson (1986) also found variable support for the Weeks-Sears inference of loss of moderately volatile chalcophiles in EH3. They suspect that weathering has reduced the contents of these elements in EH finds. In this study, concentrations of 21 trace elements including 10 REE were determined by radiochemical neutron activation analysis for bulk samples and acid-soluble and insoluble fractions of 4 EH chondrites (Qingzhen (EH3), Yamato-691 (EH3), Abee (EH4), Indarch (EH4)) with the following objectives: (1) compare trace element abundances in EH3 with those in EH4,5; (2) evaluate the possibility that weathering made compositional changes between EH3 and EH4,5; (3) figure how the elemental distribution have changed between EH3 and EH4,5 by metamorphic reheating of the latter.

No significant differences in siderophile elements (Ir, Re, Au, Pd) were confirmed between EH3 and EH4,5 except Indarch, where these siderophiles were found to be enriched by factors of 1.5 - 1.6, suggesting that these four elements were hosted in one or few common mineral phases. Apparent differences were confirmed in the abundances of moderately volatile chalcophile elements, Se and Te, between EH3 and EH4,5: Se and Te are enriched in EH4,5 by factors of 1.4 and 1.8, respectively. Using factor analysis Hertogen et al. (1983) confirmed Se and Te along with Tl, Bi, (Ag) to have strong affinity to troilite and the minor sulfide. Among these elements Tl was on the contrary found to be more depleted in EH4,5 than in EH3. No difference in Ag abundances was found between EH3 and EH4,5. Apparently the weathering is not the cause to make volatile-chalcophile elements depleted in EH3.

In Qingzhen, Cd and Tl, the most volatile elements analyzed in this work, were found to be severely depleted, as much as a factor of 10, compared with those in the other EH chondrites. In the factor analysis of enstatite chondrites (Hertogen et al., 1983), Cd was found to make very compact cluster along with Zn, Br, In, and not be loaded on the same factor as Se, possibly a good tracer for troilite, suggesting that these elements are associated with a minor sulfide component (ZnS?). Though not so

much as for Cd and Tl, Ag also show a slight, but definite depletion in Qingzhen. Since Cd and Tl (+Ag) are possibly present in different mineral phases as inferred from the results of factor analysis, loss of a particular mineral is not the case for depletion of these elements in Qingzhen. The next element to be the most volatile is In, whose abundance in Qingzhen is almost in the same range of those in other EH3 and EH4,5 chondrites. Such a discontinuity in elemental abundances among volatile elements and large depletion of Cd and Tl suggest that the parent body of Qingzhen was accreted at higher temperature than the other EH's.

Reference

Hertogen J., Janssens M.-J., Takahashi H., Norgan J.W. and Anders E. (1983) Geochim. Cosmochim. Acta 47, 2241-2255.
Kellemyn G.W. and Wasson J.T. (1986) Geochim. Cosmochim. Acta 50, 2153-2164.
McKinley S.G., Scott E.R.D. and Keil K. (1884) Proc. Lunar Planet. Sci. Conf. 14th, B567-572.
Prinz M., Nehru C.E., Weisberg M.K. and Delaney J.S. (1984) Lunar and Planet. Sci. XV, 653-654.
Weeks K.S. and Sears D.W. (1985) Geochim. Cosmochim. Acta 49, 1525-1536.

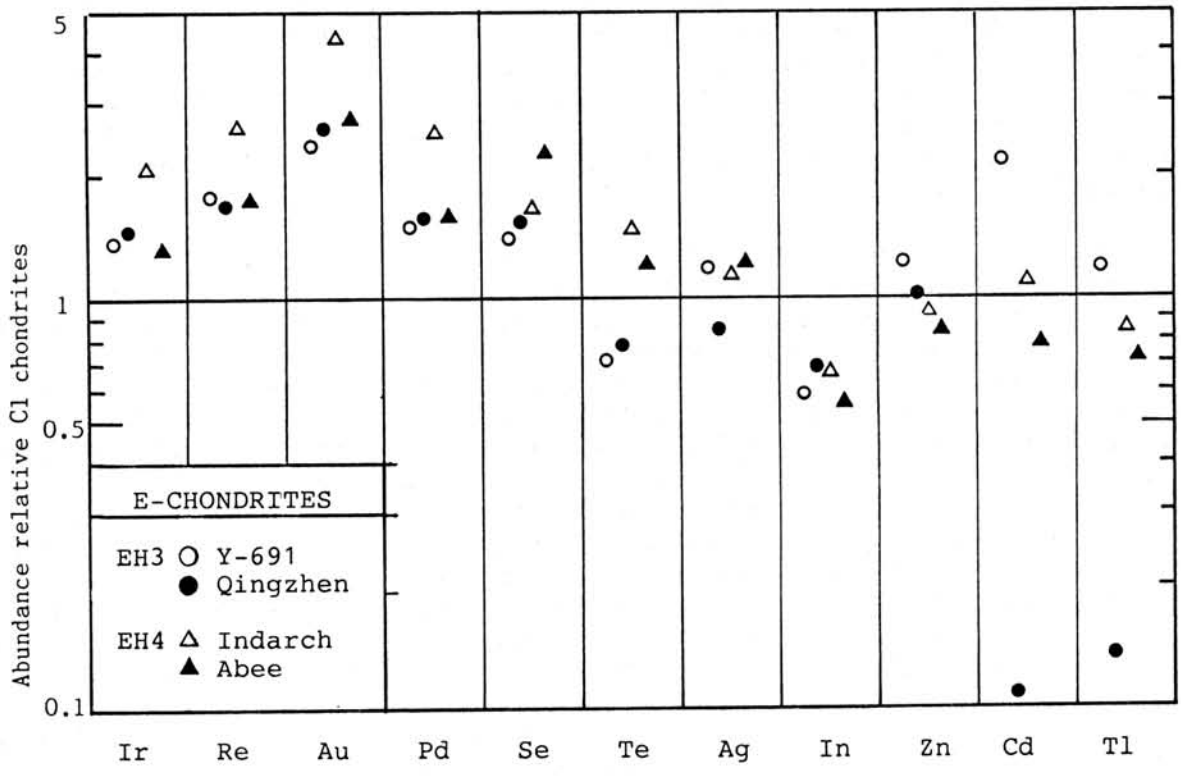

Fig.1 Trace element abundances relative to Cl chondrites.

Ultraviolet spectroscopic measurement of organic extracts from carbonaceous chondrites

S.Yabushita and T.Inagaki
Department of Applied Mathematics & Physics,Kyoto University, Kyoto 606 and
Department of Physics,Osaka Kyciku University,Tennoji, Osaka 543,Osaka

Hoyle and his associates (1979,1985) argued that the well-known peak in the interstellar extinction curve centred at 220 nm is due to absorptions by organic compounds. Hoyle et al.(1985) claimed that their spectrophotometric measurement of microorganisms such as E.coli exhibit absorption peaks at 220 nm.

Motivated by their claim,Yabushita et al.(1986) made spectroscopic investigations of a number of micro-organisms from the infrared to ultraviolet wave regions using conventional and vacuum UV specrometry. The investigation was done in collaboration with the Oak Ridge National Laboratory,U.S.A. All of the microorganisms have absorption peaks at 190 nm, and not at 220nm.

Furthermore, Sakata et al.(1977) made a spectroscopic measurement of organic extract from Murchison chondrite. They used hexafluoroisopropanol as solvent and absorption spectrum was taken with organic extract suspended in the solvent. Their result exhibits a weal absorption peak at 220 nm.

Since we were not able to obtain a peak at 220 nm, it seemed desirable to reinvesigate the problem. It is krown that one sometimes gets a spurious peak near the short wavelength limit of spectrophotometre.Furthermore, it is possible for us to use the vacuum UV spectrometre,which can measure down to 120 nm.

Two samples of carbonaceous chondrites have been loaned to us from the National Institute of Polar Research (8 mg and 10 mg). They were ground and hexafluoroisoproparol was used as solvent. Fig.1 shows absorbance plotted against the wavelength. It is seen that there is a weak absorption at 220 nm.

Next, we made thin films of the organic extracts by letting the solvent evaporate. The solid films were made on CaF_2 plates and transmitted light was then measured. Fig. 2 shows the transmittance plotted against the wavelength. We note that there is no longer an absorption peak near 220 nm.

Since the vacuum UV measurement is now under progress, it is not possible at present to say anything definite as to whether the solid films of the organic extracts exhibit absorption peaks at 190 nm or otherwise. It seems however appropriate to remark that spectroscopic measurement in the UV region of organic compounds contained in carbonaceous chondrites is a subtle problem. We strongly feel that the curve in the wavelength less than 190 nm suggets that there is a peak close to 190 nm in the transmittance of organic compounds casted on CaF_2 plates. If so, the similarity of the peak obtained for microorganisms such as E.coli and that of carbonaceous chondrites should be an extremely interesting topic. from the point of view of the origin of biochemical molecules.

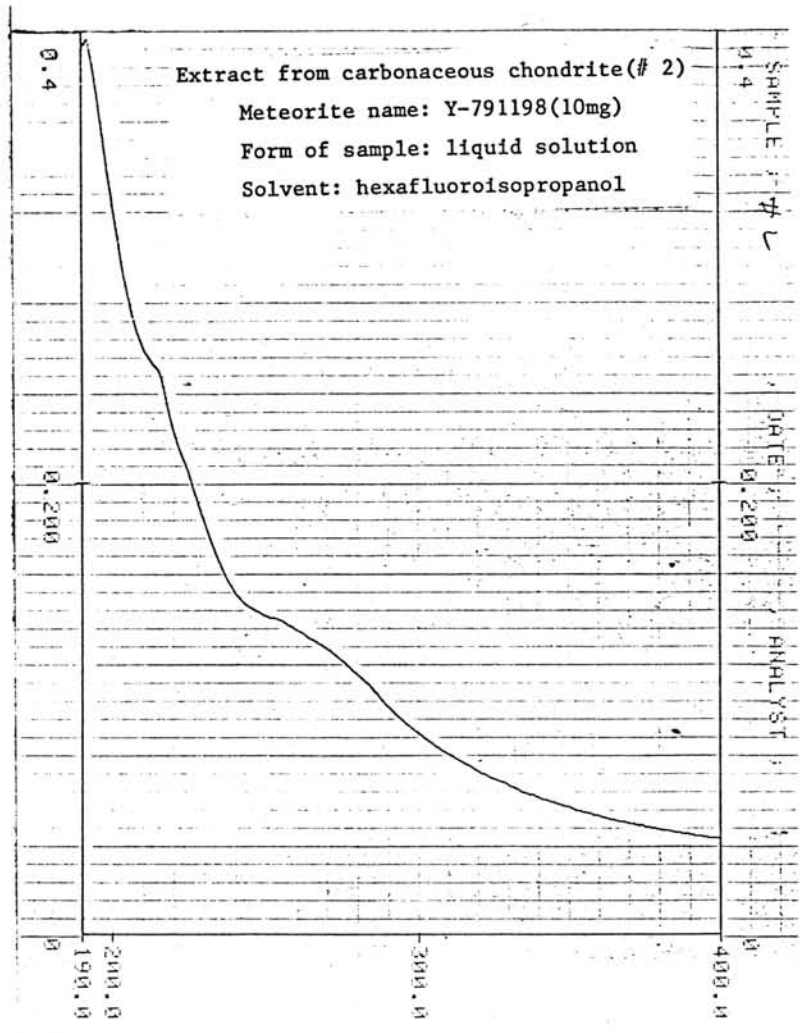

Fig.1

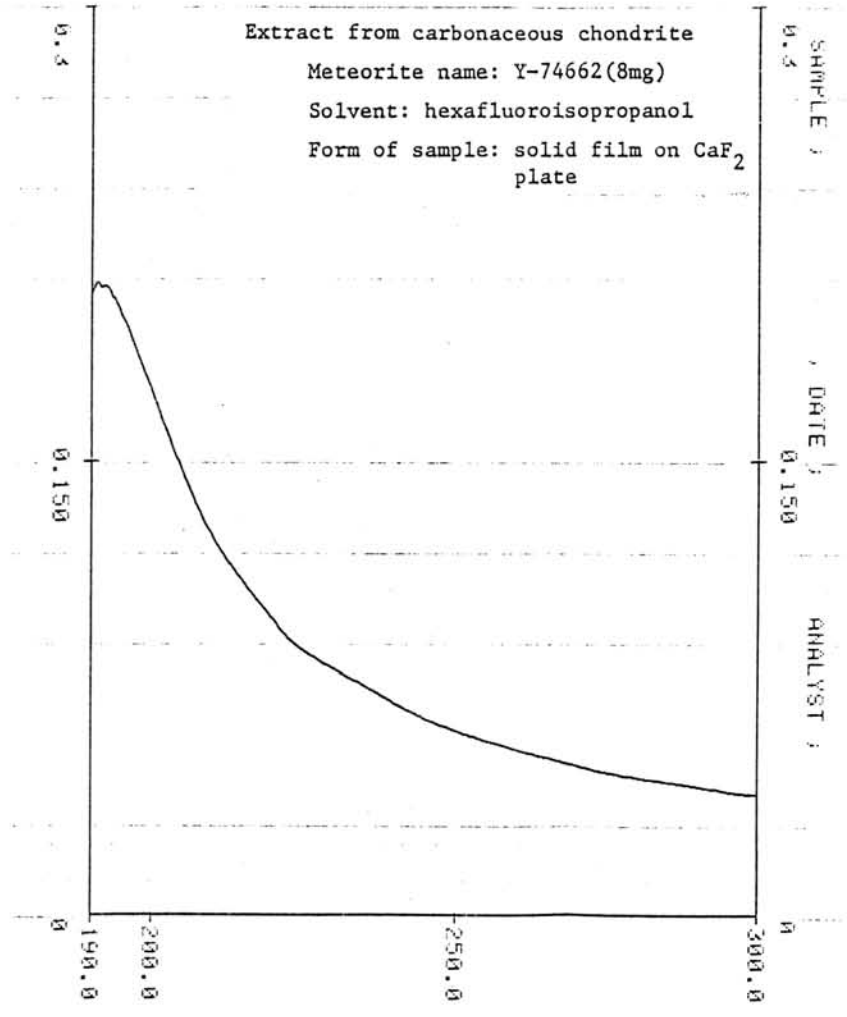

Fig.2

References

Hoyle,F.and Wickramasinghe,N.C.,1979.Astrophys.Space Sci.,66,227.

Hyle,F.,Wickramasinghe,N.C. and Al-Mufti,S.,1985.Astrophys.Space Sci., 111,65.

Sakata,A.,Nakagawa,N,Iguchi,T.,Isobe,S.,Moromoto,M.,Hoyle,F. and Wickramasinghe,N.C.,Nature,1977.Nature,266,24.

Yabushita,S.,Wada,K.,Takai,K.,Inagaki,T.,Young,D. and Arakawa,E.T., 1986.Astrophys. Space Sci.,124,377.

ON THE FORMATION OF MATRIX MATERIALS OF UNEQUILIBRATED ORDINARY CHONDRITES IN TURBULENT SOLAR NEBULA. --- CONSTRAINTS FROM REACTION KINETICS BETWEEN ENSTATITE AND METALLIC IRON:

S. MATSUNAMI: Naruto University of Teacher Education, Naruto, Tokushima 772, Japan.

1. Introduction.

It is widely assumed that the redox state of terrestrial planets and chondritic materials would have been established by a temperature effect in the early solar nebula at the time of the formation through gravitational collapse of a presolar interstellar cloud (Lewis, 1972, 1974; Ringwood, 1975, 1979; Wasson, 1985). In "equilibrium condensation models", primarily presented by Lewis (1972, 1974), the source materials of planets formed along a steady temperature gradient such as adiabatic ones of astrophysical models of Cameron and Pine (1973) and Cameron (1978). Based on "equilibrium condensation", he successfully estimated the temperature gradient ($R \propto T^{-1.1}$) in massive, convectively unstable, turbulent solar nebula. More Recently, Lin and co-workers have developed self-consistent, low-mass models of the solar nebula as a turbulent accretion disk (Lin and Papaloizou, 1980, 1985; Lin, 1981; Lin and Bodenheimer, 1982). In the evolutionary models of turbulent solar nebula, it was theoretically shown that an adiabatic temperature gradient similar to those obtained by Lewis (1972, 1974) would have been maintained during timescale of viscous evolution of the nebula (10^{5-6} years) (Cassen et al. 1985; Morfill et al. 1985; Lin and Papaloizou, 1985). It apparently seems that turbulent solar nebula models well explain compositional variations of terrestrial planets and chondritic materials with combination of equilibrium condensation theory. Nevertheless, some questions remain unanswered.

2. Was equilibrium condensation attained in the low temperature regions of turbulent solar nebula ?

According to equilibrium condensation theory, the oxidation state of terrestrial planets and chondritic materials, as expressed by f value [= FeO/(FeO+MgO) mole ratio], is controlled by a temperature sensitive equilibrium (Larimer, 1968; Grossman, 1972; Ringwood, 1975):

$$MgSiO_3 + Fe + H_2O = (Mg, Fe)SiO_4 + H_2. \quad --- (1)$$

Recently, Saxena and Eriksson (1983) have calculated increasing X_{Fe} of olivine and low-Ca-pyroxene below 700 ^{0}K in detail due to progressive oxidation of metallic Fe to FeO in these magnesian silicates. Since the heterogeneous oxidation reaction (1) is accompanied with both oxidation of metallic Fe to FeO in Mg-silicates and Fe/Mg exchange between olivine and pyroxene through lattice diffusion of Fe^{2+} and Mg^{2+} ions, equilibration process among condensates might have been limited by sluggishness of diffusional transport in olivine and pyroxene at such a low temperature.

Recently Matsunami (1987) experimentally examined reaction rate of the reaction (1) in detail as a function of both

temperature and PO_2 conditions. From his experimental data on reaction kinetics[2] between enstatite and metallic iron and thoretical considerations on reaction mechanisms with use of non-equilibrium thermodynamics, it is shown that rate-determining process of the reaction (1) is the lattice diffusion process of Fe^{2+} ions in Fe-rich olivine (Matsunami, 1987).

In the present paper, applications of these results to the establishment of f values of chondritic materials are discussed from both the detailed observations on matrix materials (especially mode of occurrences of matrix Fe-rich olivine) of UOC and reaction timescales calculated from kinetic data of the reaction (1) in low temperature regions of the turbulent solar nebula models.

Results are illustrated in Figure 1. This figure reveals that in the low temperature regions of turbulent solar nebula models ($R \geq 1$ A.U.; $T \leq 600$ ^{0}K) micron-sized, matrix Fe-rich olivine grains commonly observed in matrix materials of UOC could not have formed through reaction (1) within typical evolution timescale of turbulent solar nebula models ($\sim 10^{6}$ yr). Therefore, it is doubtful that chemical equilibria among condensates such as those of Mg-silicates and metallic Fe-Ni grains would have been attained in these regions. It is suggested that matrix materials in UOC would have formed under higher temperature and more oxidizing conditions than those estimated by means of equilibrium calculations of condensation on solar abundance gas.

References:

Cameron, A.G.W. (1978): Moon and Planets, 18, 5-40./ Cameron, A.G.W. and Pine, M.R. (1973): Icarus, 18, 377-406. / Cassen, P.H., Shu, F.H. and Terebey, S. (1985): In "Protostars and Planets II", ed. D.C. Black & M.S. Matthews, Univ. of Arizona Press, Tucson, pp.448-483. / Grossman, L. (1972): G.C.A., 36,597-619. / Larimer, J.W. (1968): G.C.A., 32,1187-1201./ Lewis, J.S. (1972): E.P.S.L., 15, 286-290. / Lewis, J.S. (1974): Science, 186, 440-443. / Lin, D.N.C. (1981): Astrophys. J., 246, 972-984. / Lin, D.N.C. and Papaloizou, J. (1980): Mon.Not.Roy.Astron.Soc., 191, 37-48. / Lin, D.N.C. and Papaloizou, J. (1985): In "Protostars and Planets II", pp.981-1072. / Lin, D.N.C. and Bodenheimer, P.(1982): Astrophys. J., 262, 768-779. / Matsunami, S. (1987): Kinetics of reaction between Enstatite and Metallic Iron in dust aggregate (in.prep) / Morfill, G.E., Tscharnuter, W. and Völk, H.J. (1985): In "Protostars and Planets II", pp.493-533. / Ringwood, A.E. (1975): Composition and Petrology of the Earth's Mantle. McGraw-Hill, New York, 618pp. / Ringwood, A.E. (1979): Origin of the Earth and Moon. Springer-Verlag, New York, 295pp. / Saxena, S.K. and Eriksson, G. (1983): E.P.S.L., 65, 7-16. / Wasson, J.T. (1985): Meteorites. W.H. Freeman and Company, New York, pp.267.

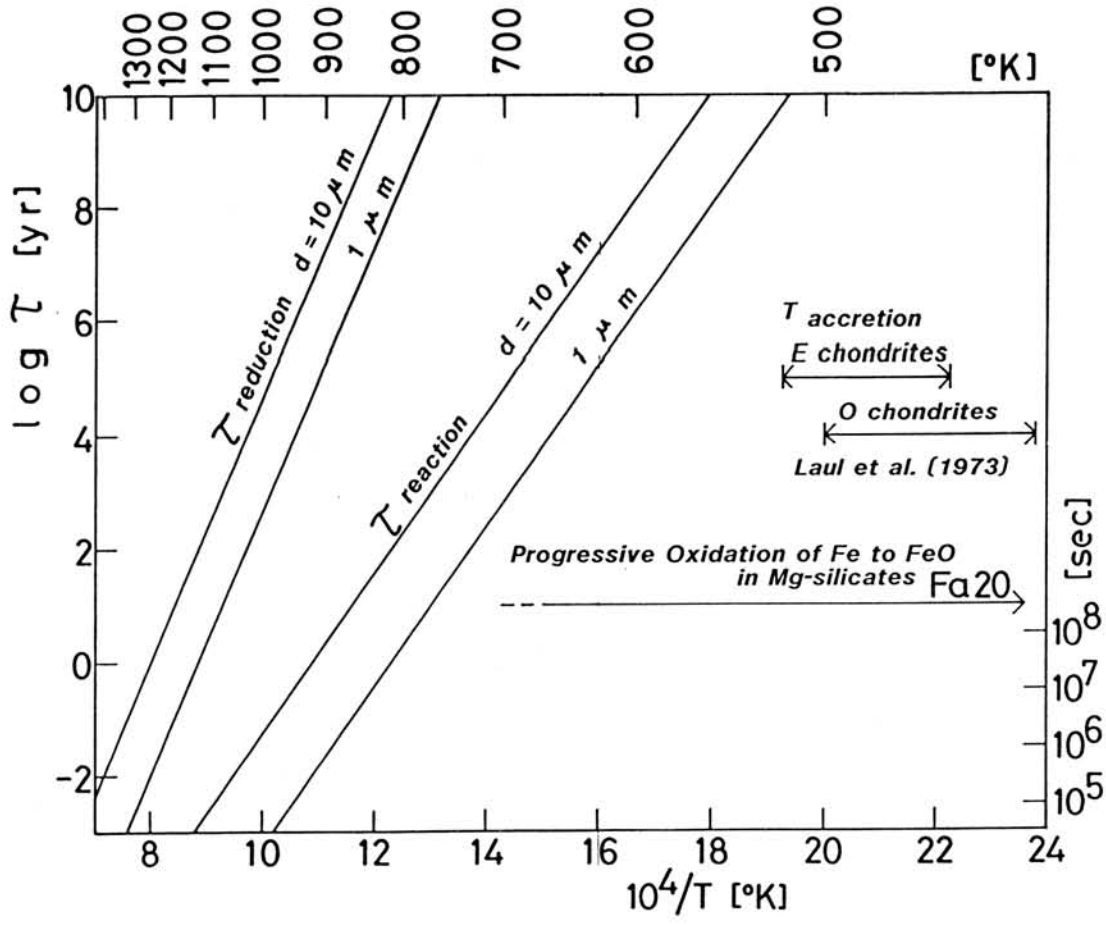

Figure 1. Formation Timescales of matrix Fe-rich olivine grains (d = 1 and 10 micron) as a function of temperature, estimated from reaction kinetics between Enstatite and Metallic Iron (Matsunami, 1987).

MINERALOGICAL STUDY ON THE MATRICES OF YAMATO-790448 AND A FEW CHONDRITES BY TRANSMISSION ELECTRON MICROSCOPE

Sato, H. , Mori, H. and Takeda, H.
Mineralogical Inst., Faculty of Science, University of Tokyo, Hongo, Tokyo 113

We compared the matrices of unequilibrated and equilibrated ordinary chondrites to gain better understanding of the origin of matrices. We selected the Yamato-790448 (LL3) chondrite for the matrix study and the Kokubunji (L6) chondrite (1) for the unweathered sample study.

The matrix of Y-790448 was observed by transmission electron microscope (TEM) using a JEOL 100CX TEM and chemical analyses were performed with a Hitachi H-600 analytical transmission electron microscope (ATEM) with a Kevex X-Ray solid-state detector. The studies of unequilibrated ordinary chondrites have been performed mainly by SEM and EPMA (2,3,4) and the observation by TEM and ATEM has not been performed extensively (4,5).

Representative matrix textures of Y-790448 are as follows.

(1)Aggregate of fine-grained olivine (Fig. 1)

Olivine is the major phase in the matrix of Y-790448. Olivine compositions were determined by ATEM and vary from $Fo_{8.5}$ to $Fo_{54.2}$. Olivines of this kind of occurrence show fine-grained texture and irregular shape. Orientations of the crystals are disordered.

(2)Olivine crystallized from melt (Fig. 2)

Olivines shown in Fig.2 seem to be euhedral crystals. The diffraction patterns indicate that orientation of each crystal is ordered. The interstices between olivine grains are occupied by a Ca-rich pyroxene-like material. This texture suggests that these olivines have been crystallized from melt.

(3)Tiny crystals of Ca-rich pyroxene-like material (Fig. 3)

The materials shown in Fig. 3 are seemingly massive in the TEM image. They show diffraction patterns charactaritic of powder samples and hence they are aggregate of tiny crystals. Their compositions seem to be those of Ca-rich pyroxene.

(4)Othr phases

In addtion to the phases described above, the matrix of Y-790448 contains troilite, Fe-Ni metal, plagioclase and small amount of calcium phosphate.

The areas observed in the TEM study of Y-790448 are very small, but various materials were found in the matrix of Y-790448 as mentioned above. They include a material which shows a texture once molten. If these materials melted after formation of this chondrite, the matrix of entire meteorite should be homogeneous. An evidence that the matrix of this chondrite were very inhomogeneous in large scale but coherent within a certain domain suggests that the events recorded in a restricted area had occurred before the formation of this chondrite and it was not reheated to high temperature after its aggregation.

The Kokubunji chondrite is an equilibrated ordinary chondrite (L6) and clear distinction between chondrules and matrix was not recognized. The compositions of olivine and pyroxene in a little coarser-grained matrix were nearly homogeneous. Fe/(Fe+Mg) of olivine ranges from 23.9% to 24.9%. But plagioclase in the matrix varied from $An_{15}Ab_{87}Or_3$ to $An_{15}Ab_{77}Or_7$. In addition to these phases, whitlockite which contains small amount of Mg and Na was found in the matrix. Glassy phase was not recognized.

We investigated the Kokubunji chondrite in a hope that it will provide us with information of fresh unweathered matrix. The matrix of Kokubunji chondrite turned to be a metamorphosed product of brecciated chondrite matrix and is not an unmodified product of the original matrix. However, as long as the major silicates are concerned, the effect of weathering in Y-790448 is not evident in comparison with the fresh chondrites.

In summary, the events recorded in the matrix of Y-790448 chondrite might have occurred before the formation of this entire chondrite. The supplementary study of Kokubunji chondrite suggests that the effect of weathering is not evident in comparison with the fresh chondrites.

Acknowledgment

We thank National Institute of Polar Research and Dr. N. Sasaki for meteorite samples.

References:

(1) Sasaki, N., Sato, H., Saito, J. and Takeda, H (1987) Abstr. Annual Meet. Mineral. Soc. Japan, Tokyo
(2) Ikeda, Y. (1980) Mem. Natl. Inst. Polar Res. Spec. Issue 17, 50-82
(3) Huss G.R., Keil K. and Taylor G.J. (1981) Geochim. Cosmochim. Acta 45, 33-51
(4) Nagahara, H. (1984) Geochim. Cosmochim. Acta 48, 2581-2595
(5) Ashworth J.R. (1977) Earth Planet. Sci. Lett. 35, 25-34
(6) Ikeda, Y., Kimura, M., Mori, H. and Takeda, H. (1981) Mem. Natl. Inst. Polar Res., Spec. Issue 20, 124-144

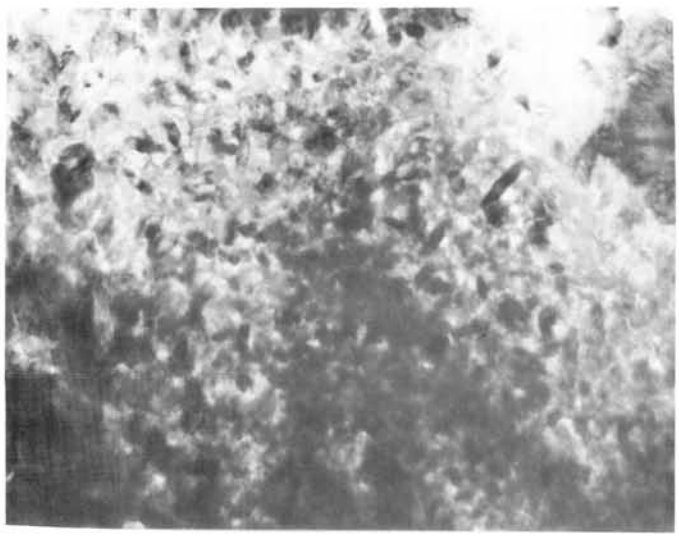

Fig. 1 Aggregate of fine-grained olivine

1 μm

Fig. 2 Olivine crystallized from melt

0.5 μm

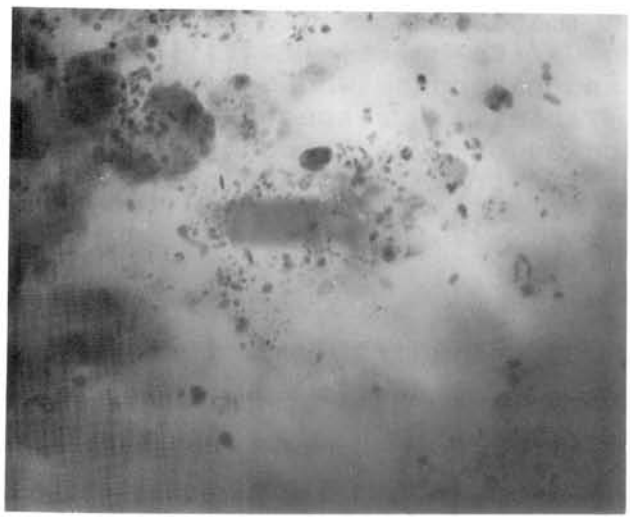

Fig. 3 Tiny crystals of Ca-rich pyroxene-like material

1 μm

A SUBSILICIC ALUMINIAN PYROXENE PAIR IN A FRAGMENT OF Y-82038 (H3)

Seiko WATANABE and Nobuo MORIMOTO
Department of Geology and Mineralogy, Faculty of Science, Kyoto University, Sakyo, Kyoto 606, Japan

A pair of orthopyroxene and augite with anomalously subsilicic aluminian compositions was found in a coarse grained lithic fragment in Y-82038 chondrite (H3).

The fragment (Fig. 1a) consists of olivine (~ 50 vol%), augite (partly pigeonite) (~ 40 vol%), orthopyroxene (~ 10 vol%), metallic iron (~ 2 vol%), spinel (~ 1 vol%), troilite (< 1 vol%), and interstices containing SiO_2, Al_2O_3, Na_2O and K_2O (< 1 vol%). Bulk chemical composition of this fragment and pyroxenes determined by EPMA are shown in Table 1. Although bulk composition predicts appearance of olivine, orthopyroxene, augite and anorthite, anorthite is absent. Instead, orthopyroxene and augite show remarkably high Al_2O_3 contents as MgTs ($MgAl_2SiO_6$) and CaTs ($CaAl_2SiO_6$) components, respectively. Chemical compositions of pyroxenes are plotted in Figure 2. Olivine is in the range from Fo_{81} to Fo_{85}. Spinel occurs in augite. Orthopyroxene and augite show Al_2O_3 content of 25 ~ 31 mol% MgTs and 10 ~ 34 mol% CaTs, respectively.

Occurrence of such subsilicic aluminian pyroxenes, especially orthopyroxene, has never been reported in chondrites, and is quite rare even in the terrestrial rocks. Maximum solubility of Al_2O_3 of pyroxenes in the CaO-MgO-Al_2O_3-SiO_2 (CMAS) system (Gasparik, 1984) is about 5 mol% of MgTs or CaTs components at low pressure, and is even about 20 mol% in higher pressure conditions. Thus, the Al_2O_3 contents of pyroxenes of this fragment far exceed the range of equilibrium solubility of Al_2O_3. The high alumina content is considered to be due to metastable crystallization, although the pyroxenes may have crystallized under some high pressures.

In back scattered electron images, some of augite show irregular-shaped contrast due to Ca/(Ca+Mg+Fe) (Fig. 1b), and probably are mixtures of augite and pigeonite whose compositions are near to AUG-B and AUG-D in Table 1, respectively. This texture is not observed in chondrules of type 3 chondrites, and indicates not a simple history of the fragment before the accumulation to the chondrite.

GASPARIK T. (1984) Contrib. Minerl. Petrol. 87, 87-97.

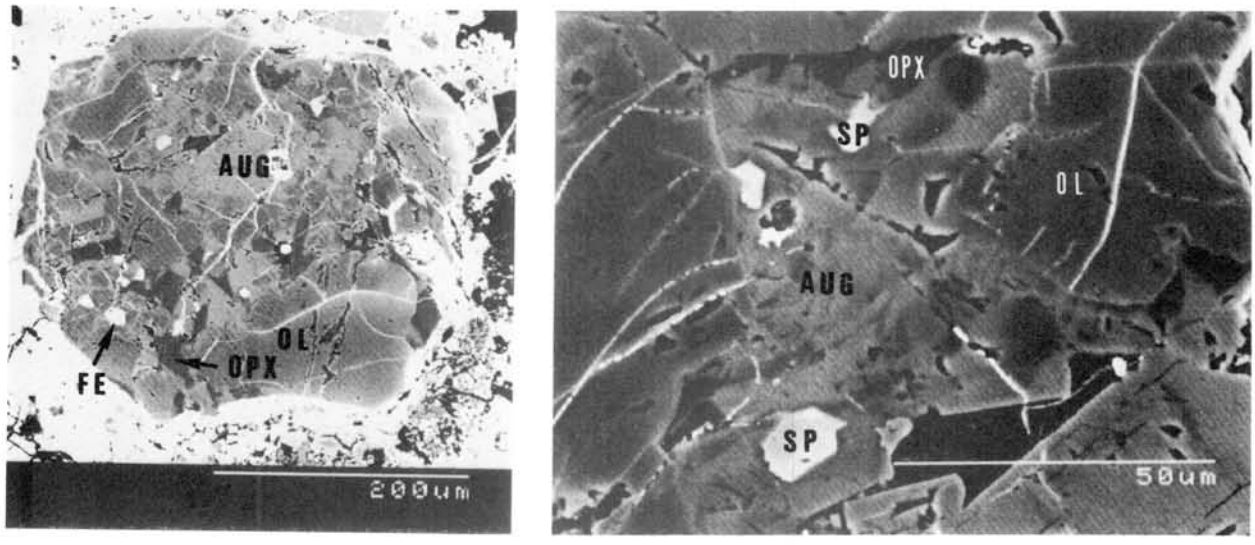

Fig. 1 Back scattered electron images of the fragment (OL= olivine, OPX=orthopyroxene, AUG=augite, SP=spinel, FE= metallic iron).

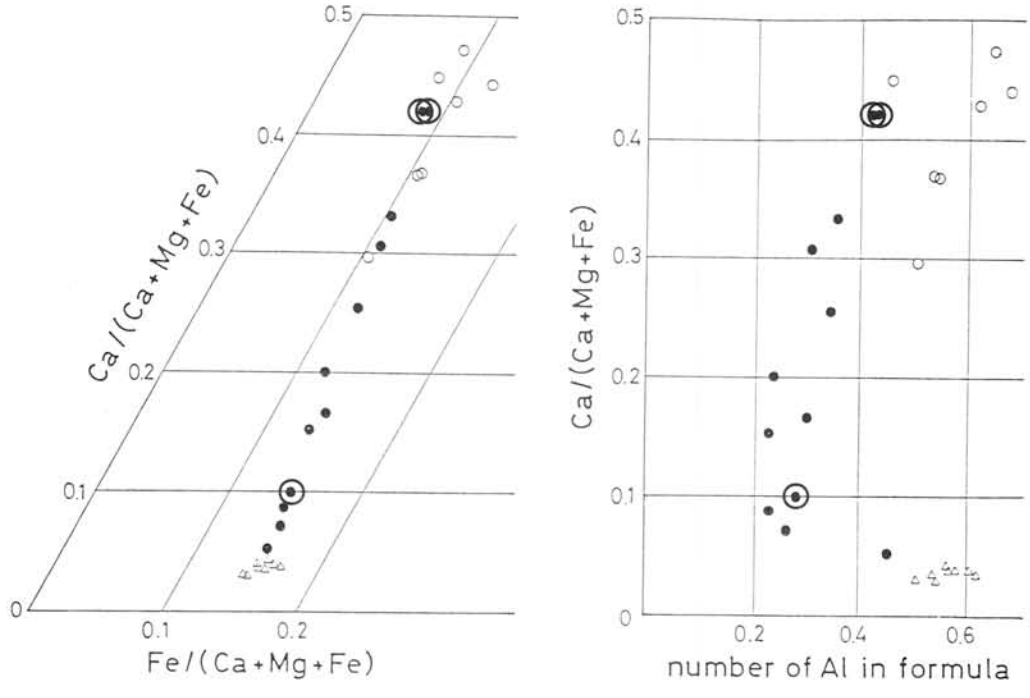

Fig. 2 Chemical composition of pyroxenes (△:orthopyroxene, ○:augite, ●:mixture of pigeonite (◉) and augite (◉) as in Fig. 1b). (a) Atomic ratios of Ca, Mg, and Fe. (b) Atomic ratio of Ca/(Ca+Mg+Fe) and number of Al atoms in formula (O=6).

Table 1 Bulk chemical composition and typical compositions of pyroxenes of the fragment.

	Bulk	OPX	AUG	AUG-B	AUG-D
SiO2	44.2	48.7	45.5	52.3	48.4
TiO2	.3	.4	.9	.2	.9
Al2O3	6.0	13.0	15.1	6.7	10.0
Cr2O3	.8	.7	.3	.9	1.5
FeO	12.3	8.9	4.8	8.9	4.9
MnO	.3	.3	.3	.4	.3
MgO	31.8	26.7	13.3	26.0	15.8
CaO	5.1	1.7	20.0	4.7	18.7
Na2O	.0	.0	.0	.0	.0
K2O	.0	.0	.0	.0	.0
Total	100.8	100.4	100.2	100.1	100.5
Si		1.71	1.66	1.85	1.75
Ti		.01	.02	.07	.03
Al		.54	.65	.28	.43
Cr		.02	.01	.02	.04
Fe		.26	.15	.26	.15
Mn		.01	.01	.01	.01
Mg		1.40	.72	1.37	.85
Ca		.06	.78	.18	.72
Na		.00	.00	.00	.00
K		.00	.00	.00	.00
Total		4.01	4.00	4.04	3.98
		(O=6)	(O=6)	(O=6)	(O=6)
Ca+Mg+Fe		1.66	1.65	1.81	1.72

PETROLOGY OF UNIQUE ANTARCTIC CHONDRITES, Y-74025 AND Y-74063

Kimura M.

Department of Earth Sciences, Ibaraki University, Mito 310

Kojima and Yanai [1] found two unique chondrites from Yamato meteorite collection. The chemical compositions of olivines and pyroxenes in them are intermediate between those of E- and H-chondrites. Recently some unique chondritic meteorites, in which mineral compositions are similar to such chondrites, are found. They are called forsterite chondrites [2], winonaites or primitive achondrites [3], or IAB chondrites [4]. Acapulco, ALH-77081 and Lodranites are also unique chondrites similar to these meteorites. In this paper I will describe Y-74025 and Y-74063 chondrites and discuss the relationships between these meteorites and the other unique meteorites above mentioned.

Y-74025 meteorite shows granoblastic texture and appears unshocked. This consists of a tight assemblage of orthopyroxene, olivine and troilite with minor amount of diopside, plagioclase, Fe-Ni metal (kamacite and taenite), schreibersite and daubreelite. All these minerals except for taenite are homogenous in compositions. Average compositions of orthopyroxene, olivine, diopside and plagioclase are $En_{96}Wo_{1.6}$, Fo_{98}, $En_{53}Wo_{46}$ and $Ab_{77}Or_{2.2}$, respectively. Although Fe-Ni metals contain no Si, troilites contain about 0.4% Cr. The equilibration temperature using Wells [5] pyroxene geothermometer is about 980°C.

Y-74063 meteorite also shows granoblastic texture and appears unshocked. It seems that this contains a chondrule relict. This consists of orthopyroxene, olivine , troilite and Fe-Ni metal with minor amount of diopside, plagioclase and chromite. Trace amounts of apatite, whitlockite and pentlandite are found. They are also homogeneous in compositions. Average compositions of orthopyroxene, olivine, diopside and plagioclase are $En_{87}Wo_{1.6}$, Fo_{89}, $En_{51}Wo_{45}$ and $Ab_{79}Or_{4.4}$, respectively. Troilites hardly contain Cr and Mn. The pyroxene equilibration temperature is 1000°C.

These two meteorites are highly equilibrated and chondritic texture is hardly found. However, the mineral assemblage and modal compositions are similar to those of chondritic meteorites, especially to some unique meteorites as mentioned above. Their textures, equilibration temperatures and cooling rates from Fe-Ni metal resemble those of these unique meteorites. All these features show that Y-74025 belongs to winonaite or related chondrite group and Y-74063 to group of Acapulco [6] and ALH-77081 [7].

[References] [1]Kojima Y. & Yanai K. (1984): Abs. 9th Symp. Antarctic Meteorite, 11. [2]Graham A.L. et al. (1977): Mineral. Mag., 41, 201. [3]Prinz M. et al. (1980): Lunar Planet. Sci., 11, 902. [4]Wasson (1985): Meteorites, 267p. [5]Wells P.R.A. (1977): Contr. Mineral. Petrol., 62, 129. [6]Palme H. et al. (1981): Geochim. Cosmochim. Acta, 45, 727. [7]Takeda H. et al. (1980): Mem. Natl. Inst. Polar Res., 17, 119.

22—1

TEXTURE AND CHEMICAL COMPOSITION OF PYROXENES IN ORDINARY CHONDRITES

Noguchi, T.

Geological Institute, University of Tokyo

For estimating the thermal history of O chondrites, it is important to know the differences of texture and chemical composition of pyroxenes. In this study, I investigated texture and composition of pyroxenes in 13 type 3-6 H chondrites (type 3: Sharps, ALH-77299, Y-74138; type 4: Y-74155, ALH-77208, ALH-77190, Y-74371; type 5: Jilin, ALH-77294, Y-74193, Y-74115; type 6: Y-790142, Y-790417) and those in 6 type 3 L and LL chondrites (Krymka, Semarkona, Chainpur, ALH-77015, Khohar, Hedjaz). Because porphyritic chondrules are most abundant among various chondrule types, pyroxenes in porphyritic chondrules were studied. Pyroxenes were distinguished by their Wo content. Following names are used here as a matter of convenience: low-Ca pyroxene (Wo<3), Ca-poor pyroxene (4<Wo<7), pigeonite (7<Wo<15), Ca-rich pyroxene (25<Wo).

(1) Differences of texture and chemistry of pyroxenes in H chondrites

There are mainly two types of occurrence of pyroxenes in porphyritic chondrules. One is low-Ca pyroxene phenocryst (originally protopyroxene) with Ca-rich pyroxene rim which shows the crystallization sequence (Fig.1). The other is low-Ca pyroxene phenocryst (originally protopyroxene) with Ca-poor pyroxene and Ca-rich pyroxene rims (Fig. 2). The former is much more abundant than the latter. The latter exists in Fe-rich chondrules. The thickness of Ca-rich pyroxene is from 5 to 10 μm thick.

In type 4, occurrence of pyroxenes resembles those in type 3 but the degree of recrystallization of glass in chondrules proceeds. In type 5, both Ca-rich pyroxene in devitrified glass and Ca-rich pyroxene rim of low-Ca pyroxene phenocryst are coarser than those in type 4. Further, in a type 5 chondrite, Y-74115, there are pyroxenes with exsolution lamellae of Ca-rich pyroxene(?) with about 1 μm thick. In type 6, those Ca-rich pyroxenes are well recrystallized.

Fig.3 shows the change of chemical composition of pyroxenes. From this figure, we can see that the CaO content of both low-Ca pyroxene and Ca-rich pyroxene increase with the increase of petrologic type. Increase of the CaO contents of low-Ca pyroxene with petrologic type is consistent with the result by Scott et al. (1986). Further, minor element contents in pyroxenes such as Al_2O_3, TiO_2, Cr_2O_3, and Na_2O, also change with petrologic type. Type 4 to 6 chondrites can be classified by using compositional differences of pyroxenes, because there are differences in homogenity of X_{Mg}, CaO and minor elements in pyroxenes in each petrologic type. In type 3, there is wide variation in X_{Mg} in low-Ca pyroxene. In type 4, there is wide variation in CaO content of Ca-rich pyroxene. In type 5, there is variation in minor element contents in Ca-rich pyroxene. In type 6, the composition of pyroxenes are well homogenized.

Because there is no reliable data of Ca⇌(Mg,Fe) interdiffusion coefficient at the temperature range 800 to 1000 °C, we cannot estimate whether H chondites of higher petrologic type stayed at relatively high temperatures (1000-800°C) for a long duration or they cooled more slowly after crystallization of pyroxenes than chondrites of lower petrologic type.

(2) Differences of texture and composition of pyroxenes in the UOCs

Though the occurrences of low-Ca pyroxene with Ca-poor pyroxene and Ca-rich pyroxene rims shown in Fig. 2 are few in H chondrites, it is rather abundant in L and LL chondrites (Watanabe et al.,1986). There are another differences of texture and chemistry of pyroxenes between H chondrites and L and LL chondrites belonging to higher subtype.

Fig.4 shows pyroxenes in Hedjaz (L 3.7). The light portion has lower X_{Mg} than the dark portion and its X_{Mg} is rather homogeneous throughout the sample. Similar texture is observed in Khohar (L 3.6). Few low-Ca pyroxene phenocrysts having similar texture shown in Fig. 4 have Ca-rich pyroxene rim. I have not observed such pyroxene crystal in H chondrites yet.

Despite of these differences, in type 3 O chondrites of higher subtype, there are some pyroxenes which have similar minor element contents to those in type 4. There are many Ca-rich pyroxenes which have more than 20 weight % CaO and less than 2 weight % Al_2O_3 in type 4. Ca-rich pyroxene crystald with such composition are observed in type 3 O chondrites of higher subtype than 3.6. Chondrules which include these Ca-rich pyroxene crystals may be a kind of the "equilibrated" chondrules discussed in Scott (1984).

References:

Scott, E.R.D. (1984) Smith. Contrib. Earth Sci., 26, 73-94
Scott, E.R.D. et al. (1986) Proc. 17th Lunar Planet. Sci. Conf.,part 1 J. Geophys. Res., 91, E115-123
Watanabe et al. (1986) papers presented to 11th symps. Antarc. Meteor., 74-75

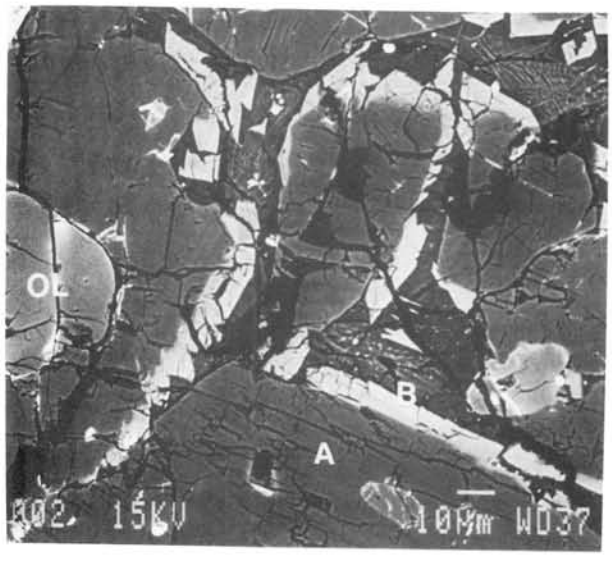

Fig.1 BEI of pyroxenes in chondrule in Sharps. Low-Ca pyroxene phenocryst (A) has Ca-rich pyroxene rim (B).

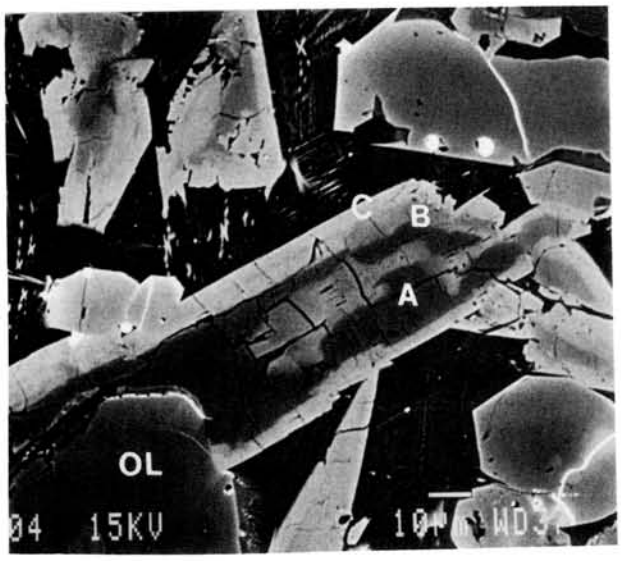

Fig.2 BEI of pyroxenes in chondrule in Sharps. Low-Ca pyroxene pheocryst (A) has Ca-poor (B) and Ca-rich (C) pyroxene rims.

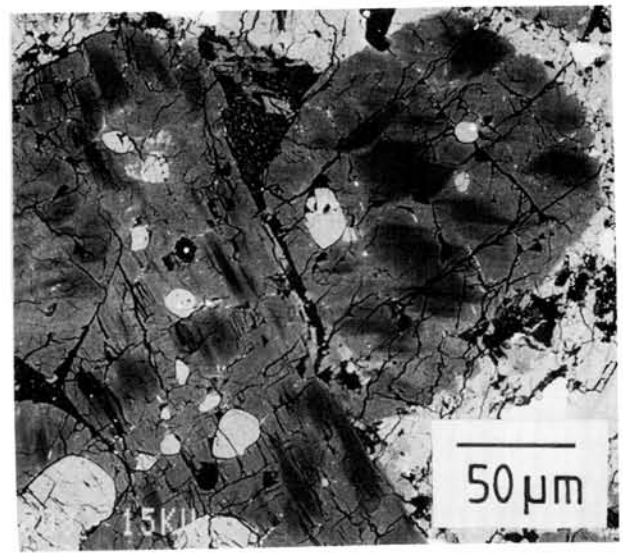

Fig.4 BEI of pyroxenes in Hedjaz. Low-Ca pyroxene phenocrysts show compositional fractuation.

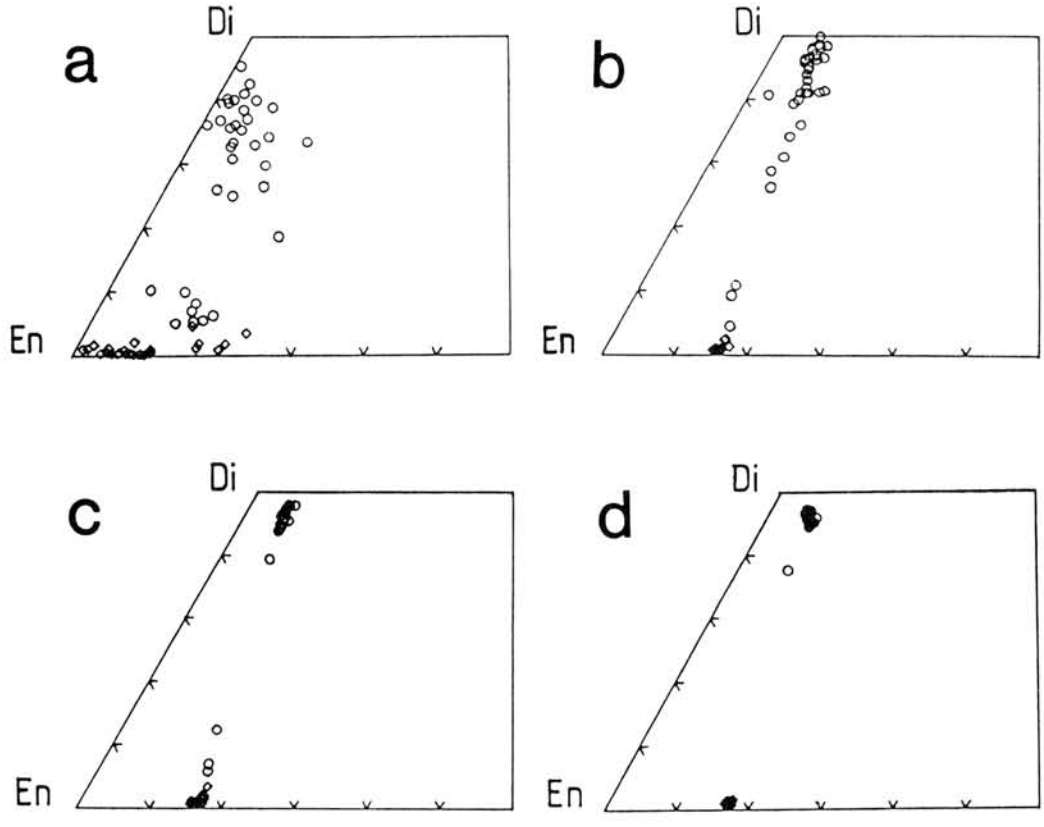

Fig. 3 Chemical composition of pyroxenes in 4 H chondrites. a:type 3 (Sharps), b:type 4 (ALH-77208), c:type 5 (Jilin), d:type6 (Y-790142).

Tuesday, June 9, 1987

0900 - 1605 *Symposium, Auditorium*

1605 - 1705 *Special Lecture*

Dr. Christian Koeberl

(University of Vienna, Austria)

FE-MG HOMOGENIZATION OF PYROXENES IN ORDINARY CHONDRITES.

Tsuchiyama, A., Fujita, T., and Morimoto, N.

Department of Geology and Mineralogy, Kyoto University, Sakyo, Kyoto 606

It has been known that the variations of Fe/Mg ratios of olivine and pyroxene in chondrites become smaller with increasing their petrologic type. In the present study, characteristic Fe/Mg heterogeneity of pyroxenes has been found in ordinary chondrites. This heterogeneity is found in type 3 chondrites with partly transparent matrices (ALH-77304 (LL3) and ALH-78084 (H3); Fig.1b,c), while pyroxene and olivine have the usual Fe-Mg zoning in the typical type 3 chondrites with opaque matrices (eg., Fig.1a). In some type 4 chondrites, weak heterogeneity is still present (ALH-77230 (L4); Fig.1d). The heterogeneity is not detected in the equilibrated chondrites. The above textural change by the petrologic type is considered to be common irrespective of the chemical groups of ordinary chondrites, because the heterogeneity is found in H, L and LL chondrites.

Characteristics of the pyroxene texture observed in the present study are follows; (1) heterogeneity due to Fe/Mg variation is present in Ca-poor pyroxenes (clinoenstatite and orthoenstatite) (Figs.1b,c and 2b,c), (2) the Mg-rich parts are always surrounded by the Fe-rich parts, (3) the Fe/Mg ratios of the most Fe-rich parts are constant among different pyroxene crystals, (4) the Mg-rich parts are elongated to the c-axis, (5) the compositional change at the boundaries between the Mg-rich and Fe-rich parts is gradual in the direction parallel to the c-axis while it is abrupt in the direction normal to the c-axis, and (6) small chromite inclusions are present in the Fe-rich part. All the pyroxenes in chondrules and fragments have such texture throughout the chondrite specimens. Olivine crystals are homogeneous and have the Fe/Mg ratio which is equal or slightly higher than that of the Fe-rich pyroxenes (Fig.2b,c,d).

The fact that the pyroxene texture is spreaded over a whole rock indicates that the texture was formed after chondrite accretion. During metamorphism of chondrites, it is expected that the Fe/Mg homogenization took place by Fe-enrichment of mafic minerals in chondrules and fragments and Mg-enrichment of matrices because the matrices are richer in Fe than the chondrules and fragments in the unequilibrated chondrites (eg., Grossman and Wasson, 1983). Thus the pyroxene heterogeneity is considered to be a transitional texture in the process of the homogenization during metamorphism. In this stage of homogenization, olivine already becomes homogeneous because Fe-Mg diffusion in olivine is much faster than that in pyroxenes. The patterns of the pyroxene heterogeneity suggest that the Fe-enrichment in pyroxene during the homogenization would take

place by diffusion using high diffusivity paths such as cleavages and twin boundaries.

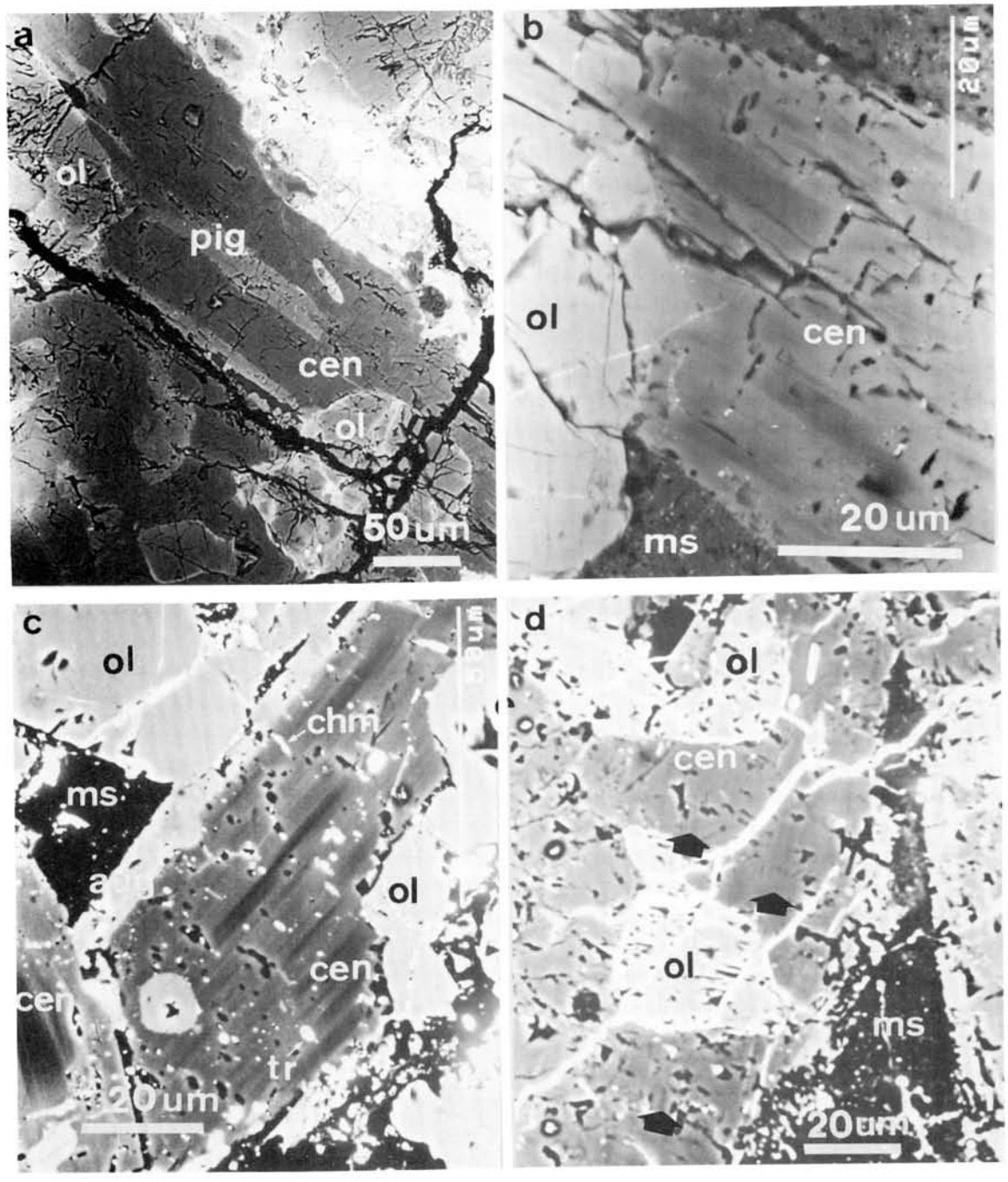

Figure 1. Photomicrographs of back scattered electron images of chondrites. (a) Zoned pyroxene and olivine in ALH-764 (LL3). (b) Fe/Mg heterogeneity of clinoenstatite in ALH-77304 (LL3). (c) Fe-Mg heterogeneity of clinoenstatite in ALH-78084 (H3). (d) Weak Fe/Mg heterogeneity of clinoenstatite (arrows) in ALH-77230 (L4). ol = olivine, cen = clinoenstatite, pig = pigeonite, aug = augite, chm = chromite, tr = troilite, ms = mesostasis.

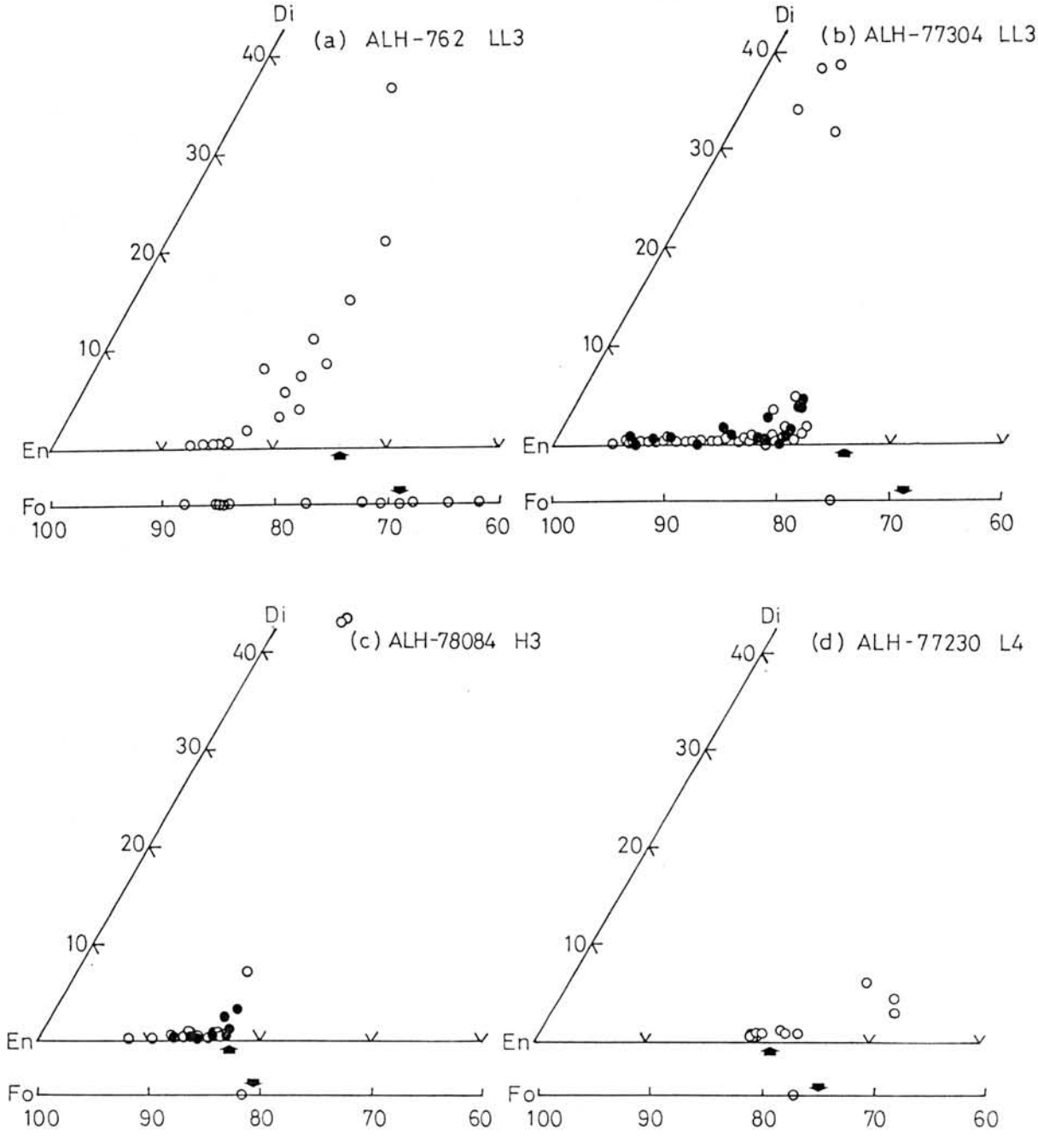

Figure 2. Chemical compositions of pyroxenes and olivines in chondrites. (a) ALH-764 (LL3). (b) ALH-77304 (LL3). (c) ALH-78084 (H3). (d) ALH-77230 (L4). Open and solid circles show the chemical compositions of pyroxenes with clinoenstatite and orthoenstatite cores, respectively. Arrows show the Mg/(Mg+Fe) ratios of orthopyroxene and olivine in the equilibrated chondrites.

COMPOSITIONAL CHARACTERISTICS OF PLAGIOCLASE FELDSPAR IN VARIOUS CHONDRITIC METEORITES

Miúra, Y.

Department of Mineralogical Sciences and Geology, Faculty of Science, Yamaguchi University, Yoshida, Yamaguchi, 753, Japan.

Characteristics of plagioclase feldspar in chondrites are the most difficult problem in meteorite study, mainly because of the tiny grain (10 to 100 um order). The precise discussion should be done from the accurate compositional data by EPMA [1,2].

From computer analysis of plagioclase data, the compositional parameters of ΔTC(crystalline scale), An-content(fractionation scale), mg (differentiation scale) and MgO+FeO (mafic-content) can be discussed and summarized as follows (Figs. 1 to 3; [1-5]):

1. Amorphous composition can be shown as non-stoichiometric value (ΔTC) more than 1 % of deviation from stoichiometric crystal value.

2. Amorphous and crystalline values of plagioclase composition are obtained in all types and groups of chondrites.

3. Relation among petrologic types, crystalline or amorphous state and the compositional parameters is shown in Fig. 1, where characteristics of the amorphous state (more than 1% ΔTC) in H, L and LL groups of types 3 and 6 chondrites are much higher values of mg and ΔTC. Type 6 chondrites have relatively smaller values of the compositional parameters than those of the type 3.

4. The largest changes of An-content and mg value are obtained in LL and L chondrites, whereas the values in H chondrites show relatively little change both in crystalline and amorphous plagioclases, as shown in Fig. 2.

5. Relation among chemical groups, crystalline or amorphous state and the compositional parameters is shown in Fig. 3, where there are regular relations between the groups (H, L and LL) and the compositional parameters (mg, An, MgO and ΔTC) both in crystalline and amorphous plagioclases. The other important result is major break-down or kink between E and H chondrites in the parameter values. This indicates that formation processes of the former (E) and the latter (H, L and LL) chondrites are largely different each others, whereas regular relation between the overall groups and An-content can be obtained in various chondritic meteorites.

6. There are no overall regular relations of formation processes discussed by ΔTC, An-content, mg-value and mafic contents among E, H, L and LL chondrites, though local regular relations are found in some of these chondrites.

7. Diaplectic plagioclases from Manicouagan Impact Crator and Sudbury breccias have higher ΔTC (and An-content) and less mg values as terrestrial impact characteristics, which is fairly similar to amorphous plagioclase of maskelynite in chondritic meteorites [5].

REFERENCES:
[1] Miúra, Y. (1984): Mem. Natl Inst. Polar Res., Spec. Issue, 35, 226-242.
[2] Miúra, Y. et al. (1986): Proc. Symposium on Antarctic Meteorite, pp. 3.
[3] Miúra, Y. et al. (1986): Meteoritics, 460-461.
[4] Miúra, Y.(1987): Lunar and Planetary Science XVIII (Houston), p. 649-650.
[5] Miúra, Y. et al. (1987): 50th Annual Meeting of the Meteoritical Society (submitted).

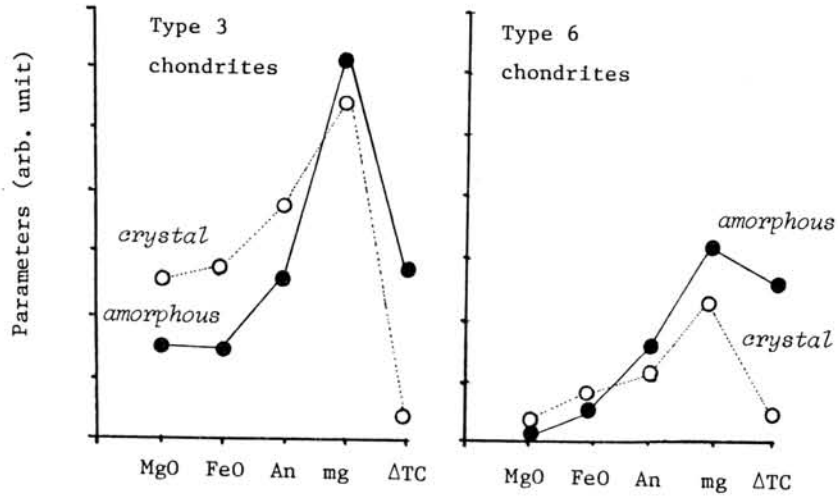

Fig. 1. Relation between petrologic types, crystalline or amorphous state, and the compositional parameters in chondritic meteorites.

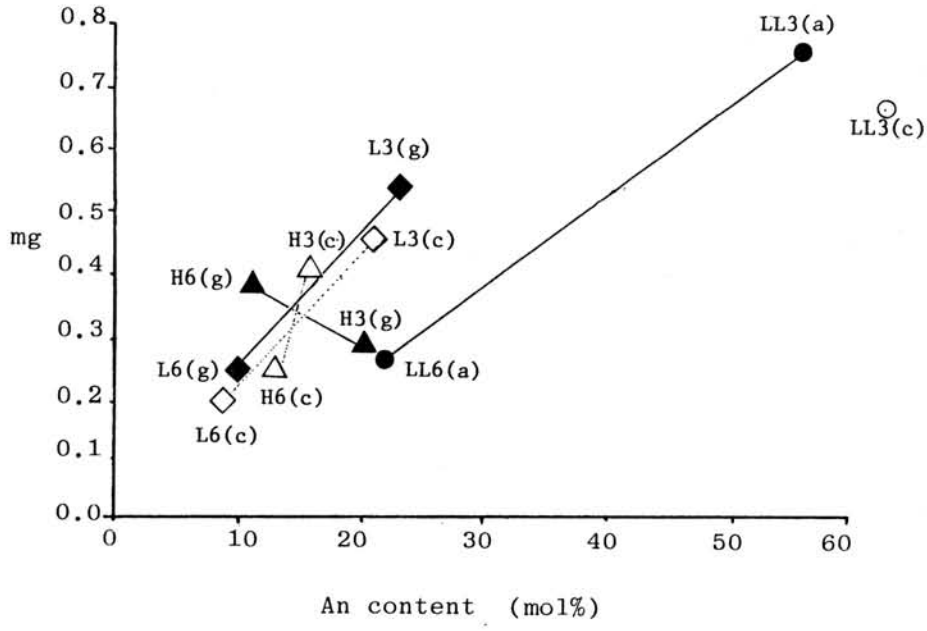

Fig. 2. Diagram of An-content and mg value in E, H, L and LL chondrites of crystalline and amorphous plagioclases.

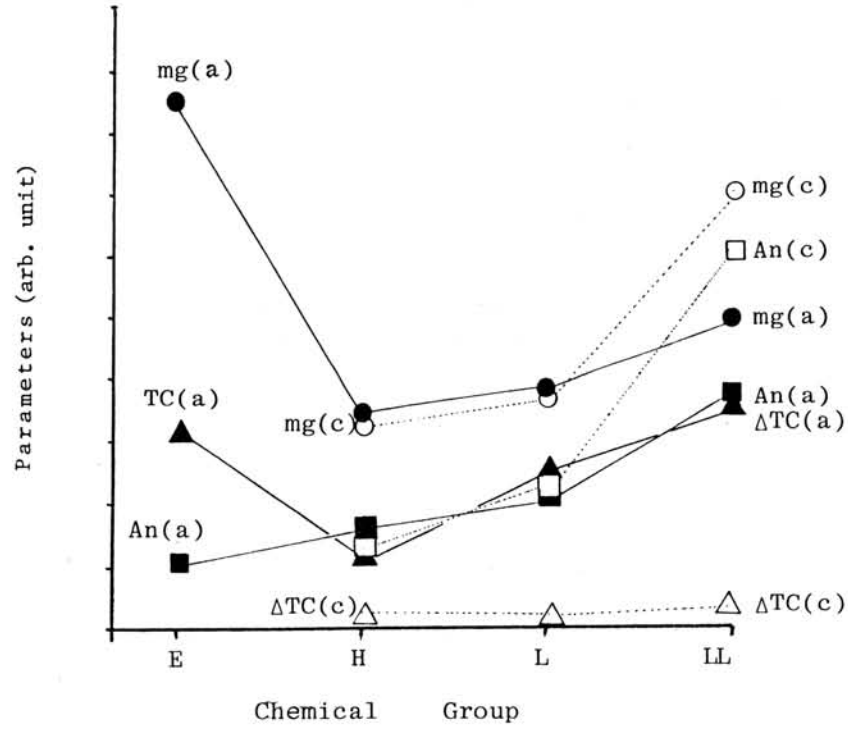

Fig. 3. Relation among chemical groups, crystalline or amorphous state, and the compositional parameters in chondritic meteorites.

THE COMPOSITION OF SPINELS IN THE JULESBURG (L3) METEORITE

A L Graham
Department of Mineralogy, British Museum (Natural History), London, England.

The Julesburg stone is an L3 chondrite which was recovered in 1983 from Sedwick County, Colorado, USA. It contains abundant chondrules and chondrule fragments but very little fine-grained matrix similar to that seen in the Tieschitz stone. The major silicates show some variation in chemistry. Olivine ranges Fa_3 to Fa_{25} but is dominantly Fa_{23} and a frequency plot of olivine compositions is strongly peaked at this value. There is very limited zoning of individual olivine crystals, only rarely more than 2 mole % Fa. The low-Ca pyroxenes show no dominant composition and range from Fs_3 to Fs_{28}. Individual pyroxene crystals show clear zoning, for example Fs_{8-15}.
Against this background of partial equilibration the spinels show a range in chemistry. Spinel group minerals are fairly common in stony meteorites but rarely make up more that 5 modal %. They are generally unzoned but occasionally extensive zoning is seen in individual crystals. The majority of the spinels in this stone are unzoned low-Mg chromites but others present are essentially Cr-free. The stone also contains zoned spinels occurring within olivine-rich inclusions. A similar range in composition has also been reported for the Gobabeb stone (H4), (Fudali and Noonan, 1975), and for Mezo-Madaras (Hoinkes and Kurat, 1974).
The array of points on a 'fe' vs 'cr' diagram seems to be related to the bulk chemistry of the host meteorite. This being the case, the chemistry of each spinel is determined by a complex interplay of the chemistry of the immediate environment and the conditions under which the stone formed and not by any precursor event which formed spinel group minerals independently. The suggestion that the aluminous spinels formed in an event unconnected with the formation of the dominant silicates of these meteorites is not supported by the data.

Fudali, R F and A F Noonan, 1975. Meteoritics, 10, 31-41
Hoinkes, G and G Kurat, 1974. Analyse Extraterr. Mat., W. Kiesl and H. Melissa, eds., Springer Verlag, 265-288.

STUDIES ON METALLIC MINERALS IN ALH-77231 BY X-RAY DIFFRACTION AND S.E.M.

Takashi NISHIDA
College of Arts and Sciences, Chiba University, Chiba 260

ALH-77231 belonging to L6 chondrite contains metallic grains of several millimeters at its maximum diameter and they are distributed separately in the matrix of silicate minerals.

It has been already reported that there are three kinds of large Fe-Ni grains characteristic of their micro textures and chemical compositions.

In this experiment, Laue photographs and micro X-ray powder diffraction patterns were taken to study the orientation of crystalline particles and lattice parameters.

TYPE A : The ranges of Ni content are from 5.7% to 6.5% and it belongs to kamacite. The etched surface is characteristic of a scaly pattern and the direction of etch pits proves that a metallic grain consists of a single crystal, however, diffuse spots of Laue photographs indicate the dispersion of crystallographic direction.

TYPE B : The inner part contains low percentage of Ni from 17.3% to 19.7%, on the other hand, the rim shows high ranges of Ni content from 24.9% to 25.4%. It belongs to taenite. Light etching reveals that inner parts are occupied by sets of lamella oriented in three directions. Laue photographs show diffuse spots with a intense dot at center.

TYPE C : It shows very fine grained intergrowth texture of two phases, which are distinguished by a back scattered image (Fig.1). Ni rich phase comes up to its maximum amounts of 53.8%. Laue photo shows Debye-Scherrer rings with partially intense spots. Micro diffractometry confirms the two phases of fairly perfect crystals and different lattice constant (Fig.2)

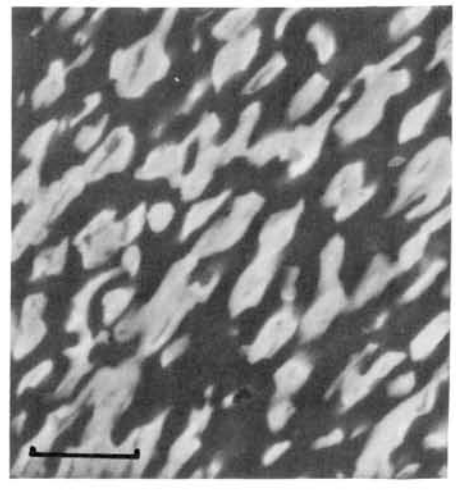

Fig.1-SEM image. scale bar 20m .

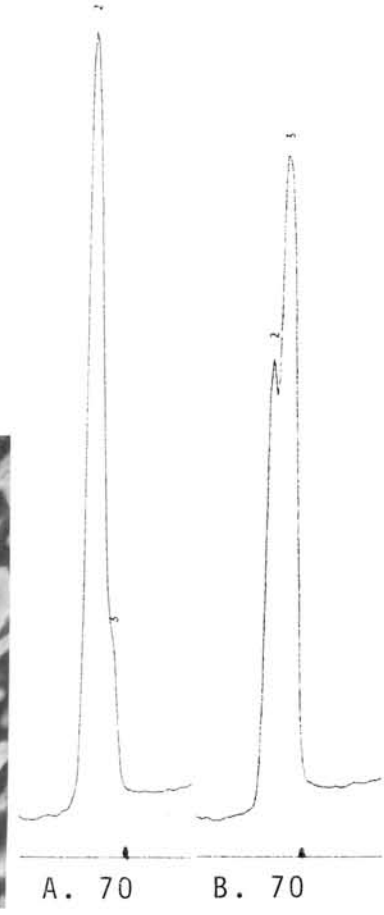

Fig.2-Diffraction tracings.
A; Center
B; Rim

YAMATO-8451; NEWLY IDENTIFIED PYROXENE BEARING PALLASITE

Keizo Yanai and Hideyasu Kojima, National Institute of Polar Research 9-10, Kaga 1-chome, Itabashi-ku, Tokyo 173

Yamato-8451(Y-8451) is a small, thin and elongated fragmental specimen, 54.8 gram partialy covered with shiny black fusion crust. On the exterio surface, this specimen consists of brownish-black weathered Fe-Ni metals and light brownish subhedral silicates which are up to 7mm across. In the thin section this specimen consists mainly of Fe-Ni metal and olivine with low-Ca pyroxene and minor troilite. Olivines and pyroxenes appeared rounded individual grains and aggregates in shape, in which pyroxenes are up to 2mm across. It resembles both silicates set in metal matrix took place as primary for their occurrence. According to the mineral assenblage and texture, this specimen is preliminarily classified as one of pallasite meteorites. But existence of the "primary" pyroxene in Y-8451 differs very remarkedly from those of all known pallasites.

Microprobe analyses show the olivine in Y-8451 has nearly homogeneous composition, ranged from Fo89.2 to Fo91.0 and average is Fo89.7. Pyroxene analyses are given as En89.8 Fs8.9 Wo1.3 in average. Ca content in larger pyroxene grains (up to 2mm across) 1.0-1.1wt%, however smaller grains (about 0.1mm across) have lower Ca-content about 0.3%. The olivine compositions of all known pallasites ranged from Fo80 to Fo88, therefore olivine of Y-8451 is the highest magnesium content in all pallasites.

Buseck (1977) first reported low-Ca pyroxenes bearing pallasites. Buseck (1977) described that pyroxenes in those pallasites were minor phase, few micron in diameter and typically symplectic intergrowith with olivine in their occurrences. Compositionally, low-Ca pyroxenes in known pallasites are grouped as Fs11.7 and Fs16.7 respectively, but both are extremely low Ca-content, 0.04-0.2wt%.

The occurrences and compositionally, Y-8451 pyroxene bearing pallasite differ from those of all pallasites which have been previously identified.

Reference:
Buseck (1977) Geochim. Cosmochim. Acta. 41, 711-740.

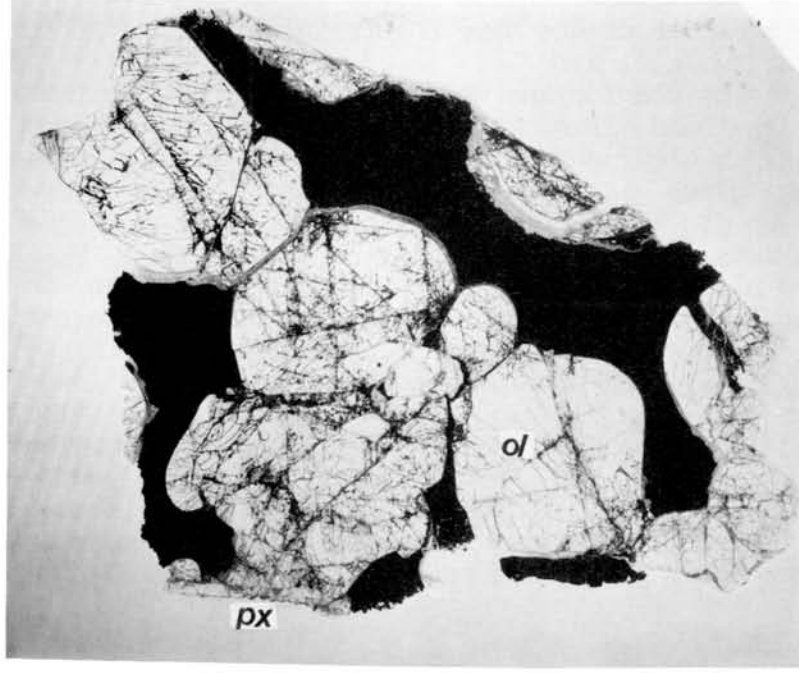

Fig. Photomicrograh of the thin section of Y-8451, with 6.5mm

MINERAL AND LITHIC CLASTS IN THE EET 83309 POLYMICT UREILITE: EVIDENCE FOR PRIMITIVE ORIGINS.

M. Prinz[1], M.K. Weisberg[1,2], C.E. Nehru[1,2], J.S. Delaney[1]
(1)Amer. Museum Nat. Hist., NY, NY 10024; (2)Brooklyn College (CUNY), Brooklyn, NY 11210.

EET 83309 is a 60.8 g Antarctic meteorite which we classified as a polymict ureilite (1). It is the third member of this new group, in addition to North Haig and Nilpena (2). All three meteorites are dominated by a coarse-grained component similar in texture and composition to monomict ureilites. Other components include a wide variety of small, but significant mineral and lithic clasts which differ markedly. These clasts add a great deal of information about the origin and processes operative on the Ureilite Parent Body(ies) (UPB) since the monomict ureilites are dominated by a very limited range of rock types and compositions. There is no evidence that these clasts are foreign to the UPB, and they are considered to be indigenous. They are generally small (usually no larger than 3-4 mm), often fine-grained, and require careful, tedious work to reveal their characteristics. This paper represents a progress report on some of the mineral and lithic clasts found in EET 83309 (hereafter 83309) thus far, and their implications for UPB genesis. This sample is being studied by a consortium led by our group, and including Clayton (stable isotopes), Pillinger (C and N), Palme (trace elements), and Begemann (rare gases).

MINERAL CLASTS

Suessite. The mineral suessite (Fe_3Si) was first found in N. Haig (3), then in Nilpena (2), and now in 83309. Contrary to previous data, it is now reported that suessite does not come from the monomict ureilitic component of the polymict ureilties (which contains 1-5 micron blebs of kamacite) but are present as much larger (up to 100 microns) mineral clasts. The suessite in 83309 ranges from 8.1-23.8% Si, 0.3-4.8% Ni, 70.5-89.7% Fe, with minor Co, Cr and P. One unusual clast has variable composition (based on 17 analyses): 16.2-24.1% Si, 3.9-20.9% Ni, 58.5-79.6% Fe. Some of the suessite clasts have thin margins of attached silicates (forsterite, enstatite, silica).

Plagioclase. Mineral clasts of plagioclase and feldspathic glass, with a wide range of compositions are found (Fig. 1). Most plag ranges from An_{3-52}, some from An_{90-95}, but our survey is not complete as yet. Some K-rich (up to 13% K_2O) plag glass is rarely found. Most grains are small, with the largest up to 3 mm. Plag is also found in some of the small fine-grained lithic clasts.

Pyroxene. Pyroxene data are plotted in Fig. 2. Pigeonite, similar in composition to monomict ureilites, makes up the majority of the pyroxene clasts, and represents at least two populations. One has low Al_2O_3 (0.2-0.5%) and high CaO (3.5-4%), the other higher Al_2O_3 (1-2%) and lower CaO (2-2.5%). Rare FeO-rich (17%) and MnO-rich (1.3%) pigeonite is also found. Low Ca enstatitic pyroxene clasts are present, with FeO ranging from 0.06-2%; some low Ca pyx has 4-10% FeO. High Ca pyx is quite variable (Fig. 2), from diopside to augite. Most cpx contains MnO (0.2-0.6%) and Cr_2O_3 (0.4-1.7%), but some diopside clasts have no detectable MnO or Cr_2O_3; these grains are related to the diopside-rich clasts described below.

LITHIC CLASTS

Black Clasts. 83309 contains numerous angular clasts of dense fine-grained black material. Mineralogically, they consist mainly of Fe-rich olivine, some Fe-rich pyroxene (?), rare feldspathic glass, and minor Fe-Ni sulfides. Additionally, they contain numerous grains of magnetite (5-10 microns), some ilmenite (up to 30-40 microns), and apatite. Their bulk compositions share similarities with the dark carbonaceous chondritic matrix (i.e., they are low in SiO_2, and high in FeO and MgO). These clasts appear to be chondritic matrix which may be petrogenetically related to monomict ureilites.

Diopside-rich Clasts. One clast, 3 mm across, is an aggregate of white MnO- and Cr_2O_3-free diopside, with about 0.5% FeO. This clast appears to be related to mineral clasts of diopside which have similar characteristics. Further data will be available when a thin section is completed.

Orthopyroxene-rich Clasts. Two clasts, less than 1 mm across, were found to consist mainly of MnO- and Cr_2O_3-free opx ($Wo_{4.5}$ $En_{77.6}$). A small amount of forsterite is also associated.

Plagioclase-rich Clast. One clast, about 1.2 mm across, consists almost entirely of plagioclase, An_{41}. This, too, awaits further study of the remaining sample.

Ol-Opx-Cpx-Plag Clasts. Several small clasts consist of the assemblage ol (Fo_{98-99}), opx (Wo_1En_{98-99}), Cpx ($Wo_{37}En_{60}$), and rare plag or feldspathic glass (An_{80}); plag is sometimes absent. Two types of ol are found: a red fluorescent type with Cr_2O_3 (0.3-0.8%), MnO (0.2-0.4%), and FeO (0.6-2%), and a blue fluorescent type with no detectable Cr_2O_3 or MnO, and lower FeO (0.2%).

Ol-Fassaite-Cpx-Spinel Clast. This clast contains one large ol crystal (Fo_{82}), with low Cr_2O_3 (0.2%) and high CaO (0.6%), and smaller ol grains (Fo_{84-86}) with Cr_2O_3 (0.3%) and CaO (0.3%). The pyroxene is $Wo_{46}En_{36}Fs_{18}$, with 18% Al_2O_3, and is fassaitic. The spinel has 40.4% Al_2O_3, 23.7% Cr_2O_3, 17.6% FeO and 1.5% TiO_2, and enriched in the chromite and hercynite molecules. Thus, this clast is Ca- and Al-rich, and probably related to the Fe-gabbroic (ADOR-related) clasts found in N. Haig and Nilpena (2). They may be related to CAI's.

Impact Melt Clasts. There are two clasts (C9 and C11) in 83309,17 which are clearly related, both texturally and mineralogically. Each is dominated by a fine-grained impact melt texture, consisting of small euhedral ol grains (Fo_{96} in C9; Fo_{98-99} in C11), but dominated by plag and plag glass (An_{10-20} in C9; An_{25-30} in C11). C9 contains two relict crystals of ureilitic ol, with cores of Fo_{88} and reduced rims of Fo_{96}. C11 contains a relict ureilitic pigeonite, with 16% FeO. Thus, these two impact melt clasts are basically basaltic in composition, and derived from a plag-rich ureilitic parent rock.

BO-textured Clast. 83309,2 contains an angular clast with a barred-olivine (BO) texture. Modally it contains 59% ol, 13.8% cpx, 26.0% plag glass, and 0.5% troilite. The ol is compositionally ureilitic, and thus this clast is interpreted to be an impact melt derived from a plag-bearing ureilite parent rock.

Other Clasts. There are numerous other small clasts, some of which have not yet been explored.

Conclusions. The 83309 polymict breccia contains a wide variety of minerals and lithic clasts, requiring extensive study in order to determine the full range of materials represented and their implications. Thus far, it is clear that extensive heating, melting and shock processes have occurred on the UPB. The mineral and lithic clasts represent a wide spectrum of rock types, well beyond the dominant ol-pigeonite monomict ureilites. Plag bearing assemblages are quite common. It is not yet clear if these processes represent planetary melting, or local melting on a much smaller scale, or both. The presence of black carbonaceous chondritic matrix clasts provides a strong link with the original parental material. The findings to date tend to support the hypothesis of Takeda (4), that ureilites are samples of primitive carbonaceous chondritic materials, although there is much yet to be learned from the polymict ureilites.

References: (1) Prinz, M. et al. (1987) Lunar Planet. Sci. XVIII, 802-803. (2) Prinz, M. et al. (1986) Lunar Planet. Sci. XVII, 681-682. (3) Keil, K. et al. (1982) Am. Min., 67, 126-131. (4) Takeda, H. (1986/87) EPSL 81, 358-370).

Fig 1.

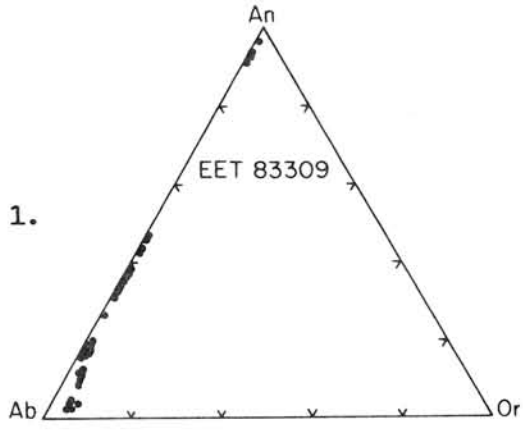

Fig 2.

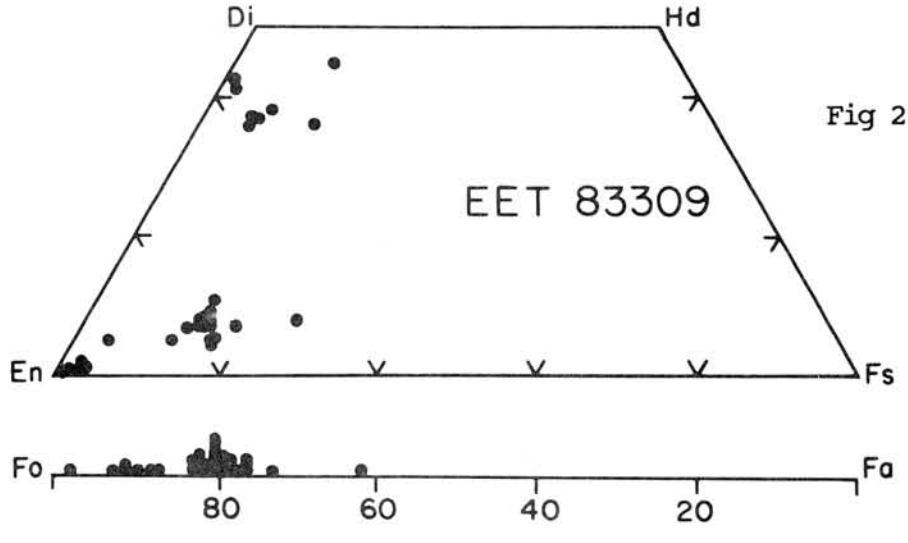

ON THE PAIRING OF ANTARCTIC UREILITES WITH REFERENCE TO THEIR PARENT BODY.

Hiroshi Takeda and Hiromi Ogata

Mineralogical Inst., Faculty of Science, Univ. of Tokyo, Hongo, Tokyo 113.

The significance of differences that exists between Antarctic and non-Antarctic meteorites is beginning to be recognized (1,2). We pointed out that the Antarctic population relative to non-Antarctic falls is overabundant in polymict eucrites, among other HED (howardites, eucrites and diogenites) achondrites, although many specimens of these achondrites may derive from the same fall (2). Ureilites are rare in the non-Antarctic population, but 21 specimens (Table 1) recovered from Antarctica differ chemically or petrologically (3,4). In this study, we compared Y-74123 with Y-82100 and Y-74659 with Y-791538 mineralogically and discuss the problems on the pairing of the Antarctic ureilites by reviewing their literature data.

Y-82100 is a very small stone and the thin section available for our study is also small and rusty. The minerals are finely fractured and pigeonite shows coarse twin band, indicating intermediate shock effects. The modal abundance of olivine and pigeonite is approximately 80:20. The olivine is more abundant in Y-74123 than Y-82100. The Fa contents of olivine range from 19 to 16 with reduced rims. The Y-82100 composition is slightly less Fa-rich than Y-74123. The pigeonite composition of Y-82100, $Ca_9Mg_{76}Fe_{15}$ (Fig. 1) is slightly less Fe-rich and Ca-rich than Y-74123 and is intermediate between Dyalpur (D in Fig. 1) (5) and Y-790981. Y-790981 is characterized by the cloudy appearance of pigeonite and its variable composition. The interstitial rim materials are also present in Y-82100 but they are less abundant than Y-74123. A Ca-rich rim material similar in composition to Y-74123 was found at a pyroxene-pyroxene boundary. The compositions vary from $Ca_{25}Mg_{64}Fe_{11}$ to $Ca_{37}Mg_{57}Fe_6$. In summary, Y-82100 is closest to Y-74123 and ALH83014 but is different from them.

Y-74659 is the most Fe-poor ureilites found among the Yamato ureilites (6). A preliminary study of Y-791538 (Mason, Yanai, Kojima, private communication, 1982) indicates that the Fa content of Y-791538 is almost identical to that of Y-74659 and the possibility of the pairing has been suggested (3). Our mineralogical study of Y-791538 (7) also confirmed their similarity but microscopic observation and the microprobe study indicate that they differ in textures and pyroxene composition. The Y-74659 olivine crystal is less shocked and clear. The Y-791538 olivine is characterized by dusty metal inclusions along the rims and fractures produced by reduction. The Y-791538 olivine crystals show well developed subgrain boundaries with undulatory extinction and the dusty metal particles are deposited along the linear tilt boundaries. The thickness of the carbonaceous veins that reduced the olivine of Y-791538 is thinner than Y-74659. The Y-74659 olivine is difficult to identify by the texture but the Y-791538 olivine can be very easily recognized by this dusty appearance and undulatory extinction.

In the Y-74659 pyroxenes, almost all the grains are pigeonite except for a small round grain of low-Ca pyroxene poikilitically enclosed in olivine. This grain has distinctly low Ca content comparable to that of orthopyroxene (6). In Y-791538, almost exactly the same composition of opx $Ca_5Mg_{88}Fe_7$ has been identified, and this pyroxene has been confirmed to be orthopyroxene by the single crystal X-ray diffraction study (7).

The opx crystals are large discrete grains up to 1 mm in diameter and some crystals are in contact with pigeonite (pig) with distinctly higher Ca content, $Ca_9Mg_{83}Fe_8$. The ratio of pig/opx is approximately 3/2. The opx crystals show fine linear lamellae-like features along (100) but the intensity of the X-ray reflection of augite is weak to be detected. The lamellae may be twinned clinoenstatite produced by shock. The pigeonite crystals are characterized by thick twin bands. The detailed mineralogical study will be given elsewhere (7).

The mineralogical evidence of Y-74659 and Y-791538 suggests that they are very closely related on their parent body, but they are distinct as a meteorite specimen. The higher Ca content of the Y-791538 pig than the Y-74659 pig has been interpreted as an evidence of higher temparature formation of Y-74659 than Y-791538 assuming the same bulk compositions. The dusty rims of the Y-791538 olivine suggest that the reduction after the break up of the parent body is different from Y-74659.

Among other Antarctic ureilites. The pairing of ALH82106 and ALH82130 has been well accepted (4). Because they are the most reduced ureilites among the Antarctic ureilites (6) and because they include augite precipitates in pigeonites produced by complex thermal histories and the primary augite coexisting with them, we have no reason to doubt their pairing.

The pairing of ALHA78019 and ALHA78262 has been proposed on the basis of their unshocked textures and Fe-rich olivine compositions. ALHA78019 has been proposed to preserve a primary igneous features (8), but the deformation microtextures of the ALHA78262 olivine observed by Mori (9) show dislocation recovery during high temperature episodes. Further studies are required to be sure of their pairing. Y-74154 and ALH81101 are heavily shocked and their olivines show granoblastic texture, but no other data exist to support the pairing.

In summary, the pairing of the Antarctic ureilites is well established only for one pair out of 21 specimens. This number is small in comparison with the Antarctic polymict eucrites (2). A common feature between the two achondrite groups is that there are many small-sized specimens and they are easily recognized on the bare ice. The fragmentation to produce such small fragments took place during the entry to the earth's atmosphere for polymict eucrites because of their fragile nature, whereas the small ureilite fragments may have been produced during the break up of the parent body as we have an evidence of rapid cooling after the fragmentation (7). The small parental masses of ureilites may loose their surface portions before the entry to the earth's atmosphere as are indicated by their short cosmic ray exposure ages, but further fragmentation will not take place because of their hardness. Each small specimens of the Antarctic ureilites may represent various portions of the parent body, accumulated during longer time in Antarctica than non-Antarctic ureilites.

We thank NIPR for the meteorite samples.

References

(1) Dennison, J. E., Linger, D. W., and Lipschutz, M. E. (1986) Antarctic and non-Antarctic meteorites from different populations. Nature, 319, 390, 1986.
(2) Takeda, H., Wooden, J. L., Mori, H., Delaney, J. S., Prinz, M., and Nyquist, L. E. (1983) Proc. Lunar Planet. Sci. Conf. 14th, in J. Geophys. Res. 88, B245-B256.
(3) Yanai, K. (1987) Antarctic Meteorites, Sci. in Antarctica No. 6, p.51.
(4) Mason, B. (1985) Antarctic Meteorite Newsletter, 8, No. 2, p. 42.
(5) Berkley, J. L., Taylor, G. J., Keil, K., Harlow, G. E. and Prinz, M.

(1980) Geochim. Cosmochim. Acta. 44, 1579-1597.
(6) Takeda, H. (1987) Earth Planet Sci. Lett. 81, 358-370.
(7) Takeda, H. and Ishii, T. (1987) Abstr. Mineral. Soc. Japan, Tokyo, in press, and 50th Annual. Meet. Meteoritical Soc., Newcastle.
(8) Berkley, J. L., and Jones, J. H. (1982) Proc. Lunar Planet. Sci. Conf. 13th, in J. Geophys. Res. 87, A353-A364.
(9) Mori, H. and Takeda, H. (1983) Lunar and Planetary Science XIV, 519-520, Lunar and Planetary Institute, Houston.

Table 1. Lists of Antarctic Ureilites (3,4)

Sample	Weight(g)	Size(cm)	%Fa	%Fs	%Wo	Pairing
Y-74123	69.9	4.5x3.0	20.7	17.9	6.5	
Y-74130	17.9	3.0x2.7	22.9	13.0	32.5	
Y-74154	2.8	1.7x1.3x0.7				
Y-74659	18.9	4.2x2.7	8.1	8.0	7.2	
Y-790981	213.0	6.3x5.5x4.0	15	18	8	
Y-791538	419.0	8.0x5.3x4.8	8.2	8.1	8.8	
Y-791839	5.8	2.8x2.2x1.2	24	10-16	4-21	
Y-82100	12.3	2.6x2.5x1.2	19	15	9	
Y-84048	53.3	4.8x3.7x1.8				
ALHA77257	1995.7	16x11x9.5	12.9	12.4	6.7	
ALHA78019	30.3	3.0x3.0x2.5	23.2	18.8	9.6	A
ALHA78262	26.2	4.0x2.5x2.0	22	19		A
MET78008	125.5	6x4.5x3.5	22	13	27	
ALHA81101	119.2	7.2x4.5x3	10-22	17-25	3-10	
ALH82106	35.1	4.5x2.5x2.5	3	4.6	9.6	B
ALH82130	44.6	"	3	4		B
ALH83014	44.6	1x0.5x0.5	18	15		
EET83309(p)	60.8	4.0x4.0x2.5	15-23	18-6	5-39	
EET83225	44.0	5x2.5x2.5				
PCA82506	5316.0	22x16x9	21	18	6	

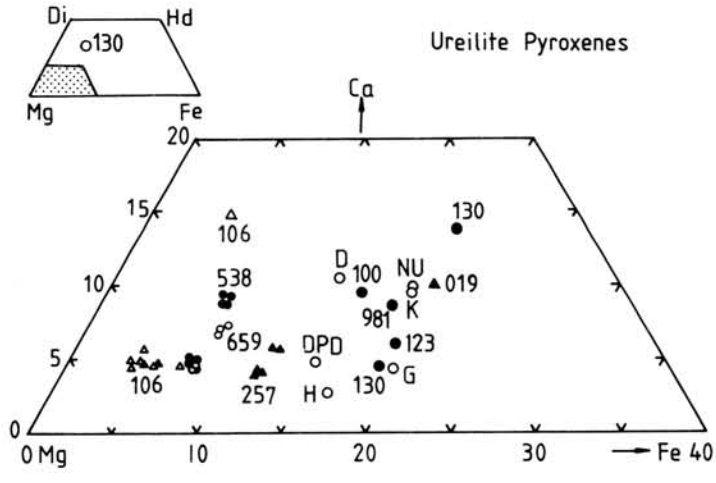

Fig. 1. Enlarged portion of pyroxene quadrilateral for Antarctic and non-Antarctic (open circles) ureilites. Only last three digits of Table 1 are given for the sample numbers (5,6).

MINERALOGY OF YAMATO-79 AND -82 ACHONDRITES AND THEIR PARENT BODY

Aoyama, T. and Takeda, H.
Mineralogical Inst., Faculty of Science, Univ. of Tokyo, Hongo, Tokyo 113

The HED achondrites(howardites, eucrites and diogenites) have been proposed to derive from the same parent body, because of their close petrologic and chemical relationship. During our study of transmittance spectra of the HED meteorites, we found that there is linear relationship between the wavelength of the absorption maximum around 900 nm and the bulk Fe content (1). Yamato(Y-)792769, Y-82082 and Y-82091 show some characteristic features, which are not common in the Yamato HED achondrites. Because Y-82082 and Y-792769 gave longest wavelengths of the absorption maxima, we expected that they are rich in Fe concentration. The bulk wet chemical analysis by H. Haramura also indicates that Y-792769 is very Fe rich. The wavelength of the absorption maximum of Y-82091 is intermediate between howardite and eucrite group. Its bulk chemical composition is rather close to polymict eucrites. This intermediate member has been rare among the Antarctic HED achondrites. We, therefore, investigated polished thin sections (PTS) of these specimens by optical microscope and electron microprobe.

Y-82082 is a polymict eucrite, in view of the fact that it contains a variety of lithic clasts with diverse textures. There are dominant clasts which show ophitic, subophitic and gabbroic textures. Pyroxenes in the ophitic clast is cloudy because of the presence of numerous minute opaque inclusions. The entire PTS of Y-82082 also shows cloudy appearance and grain boundaries of the lithic and mineral clasts are not clear and merge into the matrices. A large pyroxene fragment reveals notable augite lamellae and we can often see such augite lamellae in other pyroxenes. Microprobe analyses show that there is only one chemical trend in pyroxene compositions as is seen in monomict eucrites (Fig. 1). Pyroxenes in any type of clast show the same Mg/Fe ratio. This indicates that Y-82082 has considerably suffered from thermal annealing on the parent body. Y-82082 is a unique achondrite in that it is a polymict eucrite in the clast texture but is monomict eucrite in view of the pyroxene chemical compsitions.

Y-82091 shows textures similar to howardites. Some pale colored large low-Ca pyroxenes up to 2x2.5 mm in size, are dominant in Y-82091, whose compositions are nearly $Wo_{2.0}En_{65.0}Fs_{33.0}$. Because this clast includes minor plagioclases with An 90-80, it mey be fragments of the Y-75032-type achondrites (2). Another type of medium and fine grained pyroxenes can be seen. Microprobe analyses show a wide range in pyroxene composition as is shown in Fig. 2. The diogenitic orthopyroxenes are present as small fragments. Because Y-82091 contains more than 10 % diogenitic component including Y-75032-type clasts, it is classified as a howardite (3), but Y-82091 is not a typical howardite, in that the Mg/(Mg+Fe) ratio of the bulk chemical composition is intermediate between howardites and eucrites or even closer to polymict eucrites as explained previously. The CaO/Al_2O_3 diagram (Fig. 3) shows Y-82091 belongs rather to polymict eucrites than to howardites group. Y-82091 is a howardite closest to polymict eucrites. There have been known polymict eucrites which contain some diogenitic components and locate close to howardites (e.g. Y-791960, ALH-78006) (4). However, the intermediate howardite member like Y-82091 has never been found in the achondrite collections. If polymict eucrites and howardites

are produced on their parent body by cratering process (5), a polymict breccia intermediate between eucrites and howardites should be produced. Y-82091 is a good example of such polymict breccia.

The cut surface of Y-792769 shows compact fine-grained textures with numerous dark veins. The number of lithic and mineral clasts in the matrix is very small. Some clasts show subophitic textures of pigeonite and plagioclase. The Mg/(Mg+Fe) ratios of the pyroxenes of the clasts are constant within one clast but differ from one clast to the others. The abundance of the most Fe-rich eucrite trends is high. Y-792769 may be thermally annealed poymict eucrite and shows fairly homogenized all over feature. However pale colored pyroxene fragments show the Mg-rich composiston. This eucrite is intermediate between the monomict and polymict eucrites.

In summary, Y-82082 and Y-792769 are fairly thermally annealed polymict breccias. According to the geologic setting on the parent body proposed for polymict and monomict eucrites (6), they may have been produced at a region not far from the bottom or wall of a crater where the ejecta were burried deep at high temprature. The mixing of materials was not as extensive as polymict eucrites or howardites. Y-792769 shows the pyroxene chemical trends different from one clast to another, but those in Y-82082 are all the same. This difference may be explained by a model, in which Y-792769 originally contained lithic and pyroxene clasts with various compositions, but a variability of the clasts in Y-82082 was smaller than Y-792769, or the thermal event experienced by Y-82082 might have been more extensive. The intermediate type between howardites and polymict eucrites like Y-82091 has not been found in the HED achondrite collections, but it may not so difficult to visualize a process to form such achondrite. The decision whether Y-82091 is a howardite or polymict eucrite depends largely on the definition of the Y-75032-type achondrites. If we consider this as a diogenite, Y-82091 is a howardite with essentially the bulk composition of eucrites. Y-82091 confirms the expected occurences of brecciated HED achondrites and supports a model for close relationship between howardites and polymict eucrites.

We thank the National Institute of Polar Reseach for the meteorite samples.

References:

(1) Aoyama, T., Hiroi, T., Miyamoto, M. and Takeda, H. (1987) Lunar and Planetary Science XVIII, 27-28, LPI, Houston.
(2) Takeda, H. and Mori, H. (1983) Proc. Lunar Plant. Sci. Conf. 15th, in J. Geophys. Res., 90, 636-648.
(3) Delaney, J. S., Takeda, H., Prinz, M., Nehru, C. E. and Harlow, G. E. (1983) Meteoritics, 18, 103-111.
(4) Takeda, H., Toyoda, H., Delaney, J. S. and Prinz, M. (1986) Meteoritics, 21, 523-524.
(5) Takeda, H. (1979) Icarus, 40, 455-470.
(6) Nyquist, L. E., Takeda, H., Bansal, B. M., Shih, C.-Y., Wiesmann, H. and Wooden, J. L. (1986) J. Geophys. Res., 91, 8137-8150.

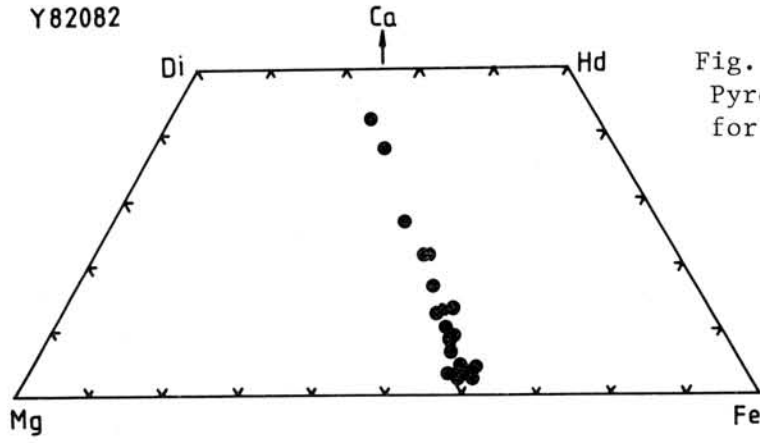

Fig. 1.
Pyroxene quadrilateral diagram for Y-82082

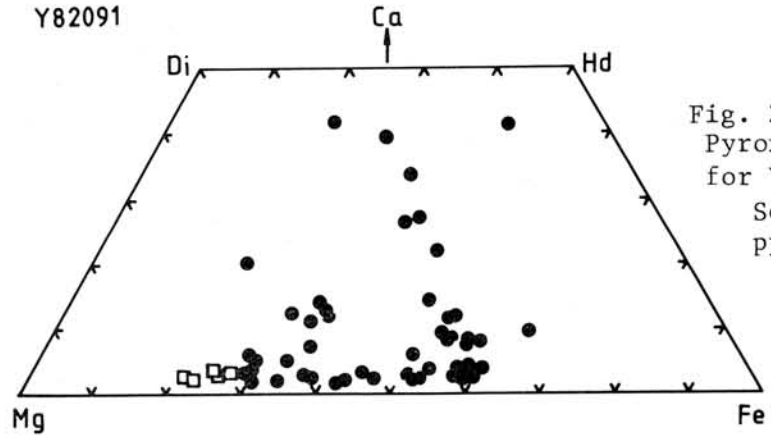

Fig. 2.
Pyroxene quadrilateral diagram for Y-82091
Squares represent diogenitic pyroxenes

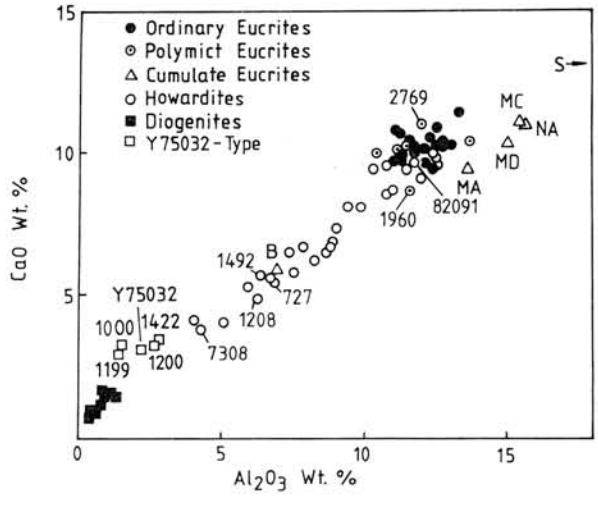

Fig. 3.
$CaO-Al_2O_3$ diagram for the HED achondrites

EXPERIMENTAL STUDIES ON VAPORIZATION AND CONDENSATION IN THE SYSTEM Mg_2SiO_4-SiO_2-H_2 AT LOW PRESSURES: APPLICATION TO THE SOLAR NEBULA PROCESSES

Kushiro, I. and B. O. Mysen
Geological Institute, University of Tokyo, and Geophysical Laboratory of the Carnegie Institution of Washington

Olivine and Ca-poor pyroxene which are two major constituent minerals in chondrites would have been formed in the primitive solar nebula by condensation of gas or crystallization of liquid or recrystallization of precursor solid materials. For understanding the condition and process of formation of these minerals, the system Mg_2SiO_4-SiO_2-H_2 which involves forsterite and enstatite have been studied experimentally in the pressure range 10^{-2}-10^{-10} bar and in the temperature range 1350-1650°C with a high-vacuum, high-temperature apparatus and Knudsen cells. The vaporus curve of forsterite+enstatite assemblage obtained by vapor pressure measurements passes 1.5×10^{-8} bar at 1350°C and 1.0×10^{-6} bar at 1525°C. The vaporous of forsterite is nearly parallel to, but about a factor of 5 lower than that of forsterite+enstatite. The 'triple point' of forsterite+enstatite exists at about 2×10^{-6} bar at 1550°C. In the pressure range of the present experiments, enstatite vaporizes incongruently to forsterite and Si-rich vapor. Natural enstatite (En_{90}) also vaporizes incongruently to almost pure forsterite and vapor enriched in Si and Fe. In consequence, fractional vaporization of solid materials consisting of enstatite with or without forsterite produces redidues enriched in forsterite.

Condensation of enstatite and silica from gas is observed on the Mo wire above the sample container. Enstatite begins to condense at about 1100°C and ceases to condense at relatively high temperatuare, whereas silica condenses from 1100° to 500°C at pressures from 10^{-10} to 10^{-3} bar. The morphology of silica changes from equant through needle or fibrous to platy form with decreasing temperature of condensation.

The results of the experiments suggest that direct condensation of forsterite from gas and formation of enstatite by reaction of forsterite and gas could occur at pressures as high as 10^{-2} bar in the primitive solar nebula where abundance of hydrogen was about 10^4 times greater than that of Mg and Si. Liquid could be formed, however, at pressures well below 10^{-3} bar by metastable melting. The results also support the suggestion that there is a reaction relation between forsterite and vapor to produce enstatite during the condensation process. Fractional condensation of the nebular gas involving this reaction relation may have produced condensates enriched in forsterite and residual Si-rich vapor. Such a fractional condensation process can explain the lower Mg/Si values of ordinary chondrites than those of carbonaceous chondrites and the primitive solar nebula. Enstatite chondrites which have Mg/Si values significantly less than unity might be a product of extreme fractionation by which 'excess silica' can be produced in the nebula. The fine-grained dark matrices of unequilibrated ordinary chondrites may also be products of extensive fractional condensation.

32—1

AN ELECTRON MICROSCOPIC STUDY OF GAS CONDENSATES IN THE SYSTEM Mg-Si-O-H

Tsuchiyama,A.*, Kushiro,I.**, and Morimoto,N.*

* Department of Geology and Mineralogy, Kyoto University, Sakyo, Kyoto 606.
** Geological Institute, University of Tokyo, Hongo, Tokyo 113.

It has been proposed that condensation of minerals played an important role in chemical processes in the primodial solar nebula, and the planets, such as the earth and parent bodies of meteorites were formed by accretion of the condensates. Kushiro and Mysen (1987) experimentally determined the phase relations in the system Mg_2SiO_4-SiO_2-H_2 in the pressure range from 10^{-2} to 10^{-10} bar and in the temperature range from 1350° to 1650°C, and discussed Mg/Si fractionation of the nebular gas. In the experiments, Si-rich vapor was formed by incongruent volatilization of enstatite, and condensation of $MgSiO_3$ and SiO_2 phases took place from the Si-rich vapor. This can be regarded as reproduction experiments of the condensation in the primodial solar nebula, and the condensates were reproduced for the first time under the conditions that mimic the solar nebula as far as the authors know. In the present study, the condensates are investigated mainly by an analytical transmission electron microscope (ATEM) to determine the phases of the condensates which are too small to be observed under an optical microscope and examine their fine textures.

A specimen used in the present study was produced at 1525°C and 4.4×10^{-10} bar for 4 days. Condensation took place on a molybdenum wire for the suspension of a Knudsen cell of molybdenum, a container of the enstatite starting material. The condensates grow at 1.2 cm above the top of the cell and zone of the condensation extends more than 1 cm. The specimen was observed carefully under a scanning electron microscope, HITACHI-S530, before observation under a TEM. A large amount of prismatic, platy, and fibrous SiO_2 and a small amount of prismatic $MgSiO_3$ are present near the highest temperature part of the wire as shown in Fig.1a,b (about 1100°C: the temperature estimated from a thermal gradient measured previously). The products are less than a few um in width, and fibrous SiO_2 is usually more than a few tens of um in length. Near a middle temperature zone (about 1000°C) the $MgSiO_3$ phase disappears and only fibrous SiO_2 is found (Fig.1c,d). With decreasing the temperature to about 600°C, the SiO_2 fibers become thinner. Molybdenum vaporized from the Knudsen cell itself is also found in the condensates (Fig.1b,d). It is known from an EDX study that molybdenum is always found in the SiO_2 phase but not in the $MgSiO_3$ phase.

The condensates are observed under a TEM, HITACHI-H700, with an EDX analytical system, HORIBA-EMAX3000. It is realized

from the observation that the $MgSiO_3$ phase is always low-clinoenstatite elongated to the c-axis with many (100) polysynthetic twins (Fig.2a). This texture indicates that the pyroxene was formed as protoenstatite at a high temperature and inverted to clinoenstatite during cooling in the experiment. The SiO_2 phase is always quartz irrespective of the morphology, and any specific crystallographic orientation is not recognized. Fibrous molybdenum inclusions are always present in the quartz crystals. Especially, a molybdenum fiber is present at the center of a fibrous quartz, which is coated by amorphous SiO_2 concentrically. Usually ball-shaped amorphous SiO_2 is also attached to the fibrous quartz. From the results it is suggested that the quartz crystals nucleated heterogeneously on the fibrous molybdenum which grew first from the vapor. Amorphous silicas are not the products of the VLS mechanism because they are pure. Probably, they are condensation products during cooling.

The protoenstatite-quartz assemblage near the highest temperature part shows that they grew simultaneously. However, this assemblage is inconsistent with the temperature stability fields of the two minerals; protoenstatite is stable at temperatures above 985°C, and quartz below 867°C. The estimated condensation temperature indicates that protoenstatite grew in its stability field and quartz grew metastably on molybdenum fibers. However, we cannot exclude the possibility that metastable and stable growth of protoenstatite and quartz, respectively at a lower temperature because the condensation temperature was not measured directly in the experiments.

Among interplanetary dust particles, clinoenstatite elongated to the a-axis has been found, and it was proposed that they are primary vapor phase condensates which could have formed in the nebula (Bradley et al., 1983). Such pyroxene was not observed in the present study.

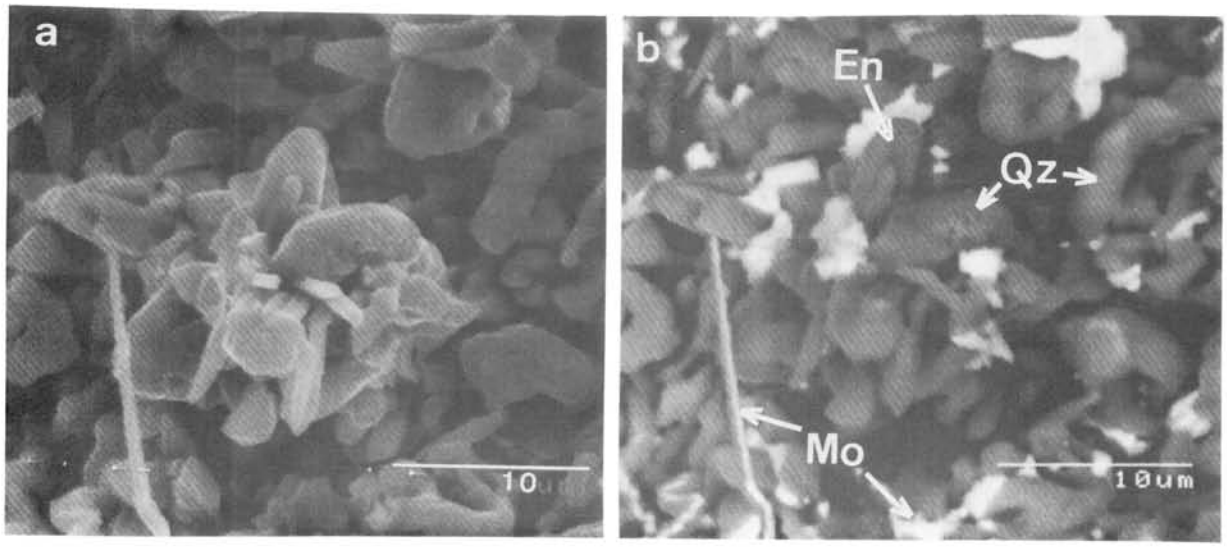

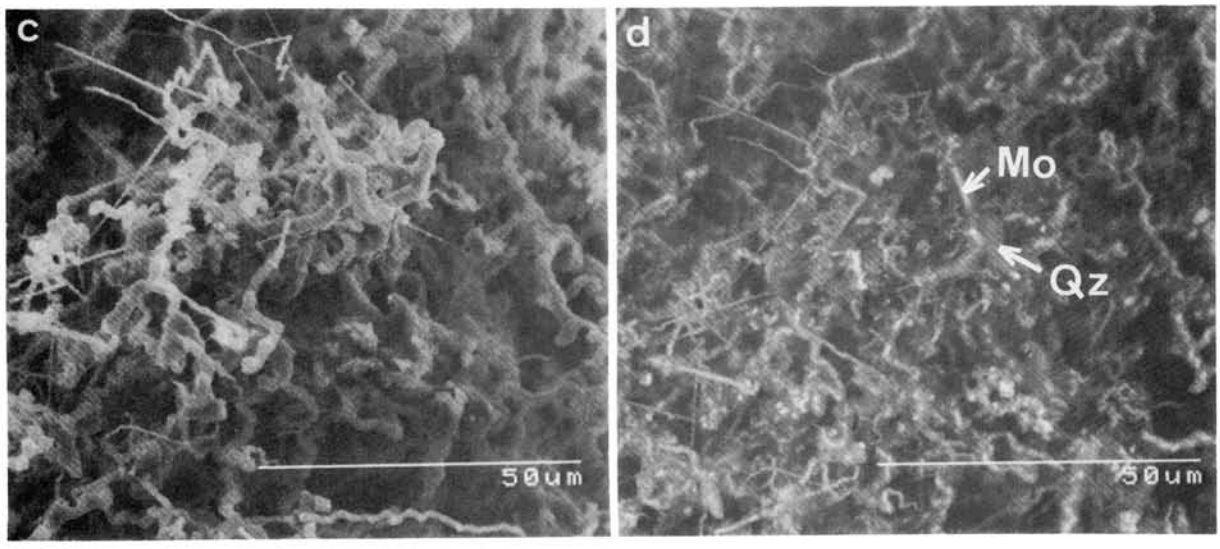

Figure 1. Scanning electron micrographs of the condensates. (a) $MgSiO_3$ (En), SiO_2 (Qz), and molybdenum (Mo) near the highest temperature part (about 1100°C). Secondary electron image. (b) Back scattered electron image of (a). (c) Fibrous SiO_2 (Qz) and molybdenum (Mo) near a middle temperature part (about 1000°C). Secondary electron image. (d) Back scattered electron image of (c).

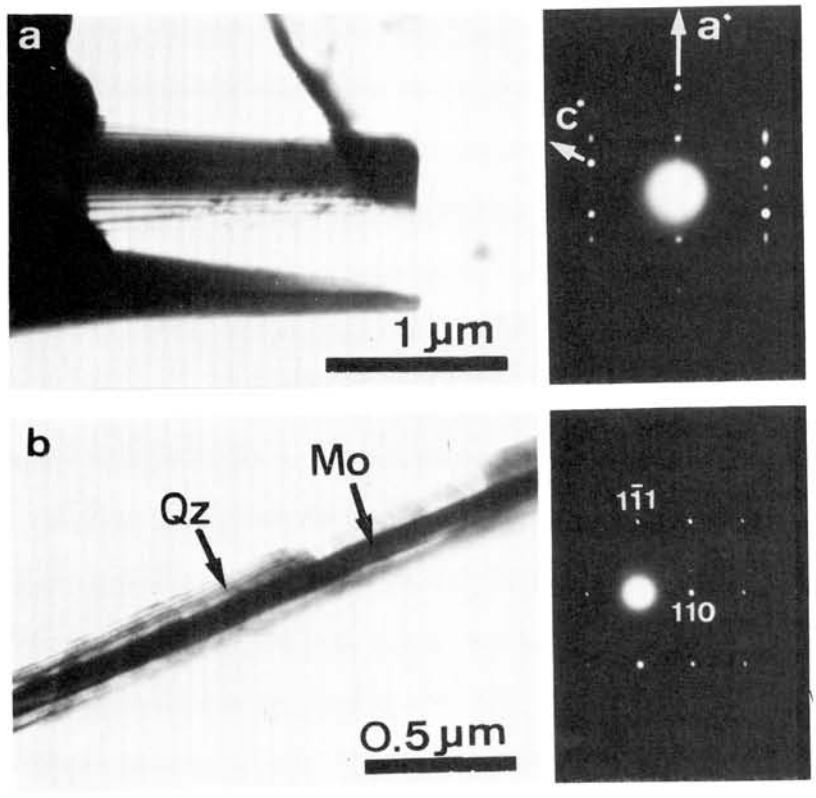

Figure 2. Transmission electron micrographs of the condensates with the diffraction patterns. (a) Low-clinoenstatite elongated to the c-axis. (b) Fibrous quartz (Qz) with a molybdenum core (Mo).

VAPORIZATION AND CONDENSATION EXPERIMENTS ON OLIVINE SOLID SOLUTION SYSTEM

Nagahara, H.[1], Kushiro, I.[1], Mysen, B. O.[2], and Mori, H.[3]
1:Geol. Inst., Univ. Tokyo., Tokyo 113, Japan, 2: Geophy. Lab., Carnegie Inst. Washington, 2801 Upton Street, Washington, D.C. 20008, U. S. A., 3: Mineral. Inst., Univ. Tokyo, Tokyo 113, Japan

Mysen and Kushiro have conducted vaporization experiments in the systems $CaMgSi_2O_6$-H_2 and Mg_2SiO_4-SiO_2-H_2 at low pressure and high temperature conditions [1,2]. For understanding vaporization and condensation processes in the solar system, experiments in the olivine solid solution were carried out. Special interests were paid on the condensates successfully formed on the cool wire above the sample container. The results show that olivine vaporizes congruently and that chemical composition and phases of the condensates greatly vary with temperature.

Detailed experimental techniques are shown in [1]. Three olivines were prepared for starting materials; OL-1 is a homogeneous phenocryst of basalt from Miyakejima volcano (Fo_{84}); OL-2 is a megacryst of basalt from San Carlos, Arizona ($Fo_{91.5}$); OL-3 is a synthetic forsterite. They were ground to 1 to 10 um, kept in sample containers and held in the high vacuum and high temperature apparatus. Total pressure in the apparatus is kept at 10^{-6} bar, where gas is composed mainly of hydrogen. Condensation from the gas takes place on the molybdenum or tungsten wire attached vertically to the sample container of which temperature gradients were previously calibrated. After the runs, both residues and condensates were observed under SEM equipped with EDS and parts of condensates were investigated with TEM.

OL-1: After the runs at 1550°C for 1340 and 2000 min, at 1500°C for 1200 min, and at 1450°C for 900 min, the residues were stoichiometric olivine and no other phase was observed, which suggests that olivine vaporizes congruently. Composition of residual olivine varies with temperature; Fo_{100-98} at 1550°, Fo_{98-95} at 1500°, and Fo_{95-92} at 1450°C. Among these variations, the most magnesian compositions seem to correspond to the solidus of olivine solid solution at each temperature. It is suggested that the gas vaporized should be more iron-rich.

Grain size, composition, and mineral assemblage of the condensates significantly vary with condensation temperature. Condensates at the highest temperature is coarse-grained (10 to 20 um), but those at lower temperatures are fine-grained (0.1 um in average) forming complex aggregates. Compositions obtained by scanning the electron beam over fairly large area (about 70x50 to 20x15 um depending on the grain size of condensates) are shown in Fig. 1. Composition is close to stoichiometric forsterite at the highest temperature (about 1100°C), enriched in Si without Fe enrichment to enstatite composition, enriched in both Si and Fe, Si being highest at about 800°C, depleted in Si and enriched in Fe, reaches closely to Fe-rich olivine (Mg/(Mg+Fe)=0.15-0.20) at 650 to 600°C, and finally again enriched slightly in Si and Mg. The condensates of 1440 and 2000 min runs follow quite similar paths.

TEM investigation revealed that phases condensed are forsterite, enstatite (probably clinoenstatite), silica, Fe-rich olivine, and intermediate pyroxene, without any amorphous materials. Condensates are composed of one or more of these phases. Thus the compositional trends above descrived would be defined by the difference of volatility of condensed phases: forsterite, enstatite, silica, fayalite, intermediate pyroxene would have condensed successively in the order of increasing volatility.

OL-2: The compositional trend of the condensates of OL-2 is similar to that of OL-1, but the final composition is more enriched in Mg and almost of intermediate pyroxene (Mg/(Mg +Fe)=0.5). Though the path is similar to that of OL-1, condensation temperature is systematically lower than that for the case of OL-1, and the grain size of condensates is smaller than that of OL-1 contrary to higher vaporization temperature. The reason of these inconsistencies is now under investigation.

OL-3: Gas vaporized at 1550°C from pure forsterite formed condensates with a compositional path different from those formed from OL-1 and OL-2. It is close to enstatite at the highest temperature (ca. 1360°C), enriched in Si, stays at 0.22 Mg/Si mol ratio from 1200 to 900°C, and finally becomes silica alone below 650°C. Mg/Si ratio of 0.22 is surprisingly very close to the eutectic composition of Mg_2SiO_4-SiO_2 system calculated by [3].

Assuming that the compositions of low temperature condensates of OL-1 and OL-2 close to Fe-rich olivine represent those of gas in equilibrium with residual olivine, binary loop of olivine solid solution can be drawn as shown in Fig. 2. It is essentially similar to liquidus-solidus relationship, but the temperature interval between vaporous and solidus is wide in the Mg end of the loop.

Althoguh the present experiments show many interesting results, they still contain some problems. One is estimation of local total and partial pressures of the gas along the wire which is 3 to 4 cm long and of which temperature varies from the run temperature to below 500°C. In the experiments, total and partial pressures of gas change with increasing height from the sample container. The higher the temperature, that is, the nearer to the container, the higher the partial pressure of gas species containing Mg, Fe, and Si. Furthermore, though the total pressure of the system is kept at 10^{-6} bar, partial pressure of hydrogen along the wire where condensation takes place is not known either. Consequently, the condensation path in the runs is neither of equilibrium nor of fractiontion. Another technical problem is overlapping of Si condensate on the wire. During quenching, Si in the gas condenses on the wire, making the apparent composition of the condensates more Si-rich than the real composition. In Fig. 1, effect of overlapped Si is eliminated by estimating the amount of the overlapped Si along the wire.

In spite of these problems, present experiments show the striking results that gas vaporized from olivine could condense various minerals depending on the temperature. If the chondritic materials, most of which are rich in olivine component, partially vaporized and cooled rapidly in the solar nebula, olivine and pyroxene with varying composition and even silica could have easily condensed. Matrices of chondrites contain various phases different from those in chondrules, such as Fe-rich olivine and silica which cannot be in equilibrium with major constituents, magnesian olivine and pyroxene [4], requiring fractionation of the nebular gas to become saturated in silica [5]. Partial vaporization and rapid condensation would be one of the most probable processes forming such matrix materials.

References: [1] Mysen, B. O. et al. (1985) Earth Planet. Sci. Lett., 75, 139-146. [2] Kushiro, I. and Mysen, B. O. (submitted). [3] Mysen, B. O. and Kushiro, I. (submitted). [4] Nagahara, H. (1984) Geochim. Cosmochim. Acta, 45, 2581-2595. [5] Nagahara, H. and Kushiro, I. (submitted).

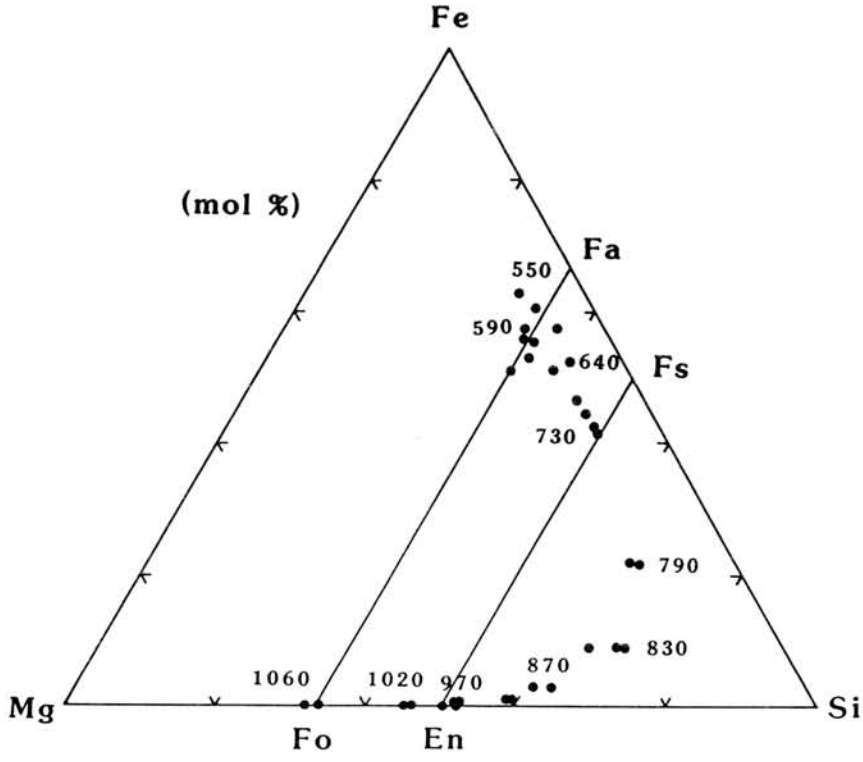

Fig. 1 Compositional variation of the condensates formed in the run on OL-1 at 1550°C for 2000min. Numbers in the figure show the approximate condensation temperature (°C) along the wire.

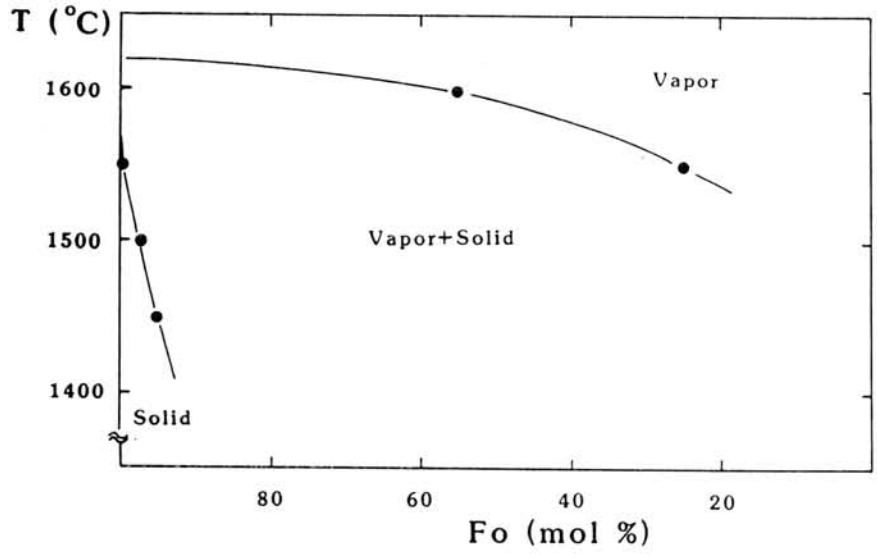

Fig. 2 Hypothetical phase diagram of olivine solid solution assuming that the composition of low temperature condensates close to Fe-rich olivine represents that of gas coexisting with residual olivine.

34—1

Crystal Structure of Perryite

Akihiko Okada[1)], Tetsuzo Ito[1), 2)], Kimiko Kobayashi[1)] and Toshio Sakurai[3)]

1) Institute of Physical and Chemical Research, Wako, Saitama
2) Present address: Ikutoku Technical University, Atsugi, Kanagawa
3) Faculty of Education, Shinshu University, Nagano

Perryite is a nickel silicide mineral containing accessory amounts of iron and phosphorus, and occurs usually as thin rims and lamellae around and within kamacite grains of enstatite chondrites, enstatite achondrites and an unusual iron meteorite. Chemical composition of perryite as determined by electron probe microanalysis is Ni: 75.5-83.7, Fe: 1.7-9.4, Si: 9.7-15.0 and P: 2.4-5.2 wt.% (Fredriksson and Henderson, 1965; Okada, Keil and Taylor, 1987; Reed, 1968; Wai, 1970), and the atomic ratio, (Ni+Fe)/(Si+P), is 2.30-2.78. This mineral has not been well-characterized because of the lack of knowledge about chemical formula and crystallographic property. In this work, synthetic crystals composed of Ni: 82.5, Fe: 2.4, Si: 12.2 and P: 3.7 wt.% were used for X-ray crystallographic study, because natural perryite in meteorite is too small in size, usually less than 20 μm. The synthetic crystals exhibit twinning on (0001) plane of the hexagonal lattice in the same way as perryite in Norton County enstatite achondrite does. 3288 reflections with $2\theta \leq 45°$, $\pm hkl$, were collected, and 221 unique intensity data were used for the structure analysis by the direct method using MULTAN. Least-squares refinement on F converged to R=0.080 and wR=0.049. Perryite has the space group R3c and the hexagonal lattice parameters a=6.640(1), c=37.982(6) A and V=1450.2(4) A^3. The bond lengths of Ni-Ni neighbours and Ni-Si neighbours lie in the range of 2.43-2.57 and 2.24-2.41 A, respectively. The crystal structure of perryite is closely related to that of Pd_8Sb_3 (Wopersnow and Schubert, 1976). The structure is a stacking variant of Ni_5Si_2 or $Ni_{31}Si_{12}$ structure (Saini et al., 1964; Frank and Schubert, 1971). The presence of 96 Ni(Fe) and 36 Si(P) atoms in the unit cell indicates that perryite has a molecular formula $(Ni,Fe)_8(Si,P)_3$.

References

Frank, K. and Schubert, K. (1971): Acta Cryst., B27, 916; Fredriksson, K. and Henderson, E. P. (1965): Trans. Amer. Geophys. Union, 46, 121; Okada, A., Keil, K. and Taylor, G. J. (1987): Chem. Erde (to be published); Reed, S. J. B. (1968): Mineral. Mag., 36, 850; Saini, G. S., Calvert, L. D. and Taylor, J. B. (1964): Can. J. Chem., 42, 1511; Wai, C. M. (1970): Mineral. Mag., 37, 905; Wopersnow, W. and Schubert, K. (1976): J. Less-Common Met., 48, 79.

MELTING OF PERIDOTITE UNDER VERY HIGH PRESSURE-II:
a laboratory simulation for early evolution of the earth

Eiichi TAKAHASHI and Eiji ITO

Institute for Study of the Earth's Interior, Okayama University, Misasa, Tottori-ken 682-02, JAPAN

Accretion of the terrestrial planets from the solar nebula and their subsequent early evolution are one of the most intriguing topics in modern earth and space sciences. Presence or absence of extensive melting stage (magma ocean) in the early history of the earth is a big unknown from which contrasting interpretations on the nature of geophysical and geochemical observations on our planet are originating. Using a uniaxial split-sphere type multi-anvil apparatus (USSA-5000), we have carried out both subsolidus and melting experiments on mantle peridotites and relevant compositions up to pressures equivalent to the lower mantle of the earth.

All the experiments were made with the USSA-5000 apparatus at Okayama University. Run durations are 60min in subsolidus experiments and 10min in hypersolidus experiments. Starting material is a sheared garnet lherzolite xenolith in Lesotho kimberlite (PHN-1611). Both majorite (garnet) and olivine (α-phase) appeared as parallel growth on melt/crystal interface in experimental charges quenched at 15-16GPa (Fig. 1). In experimental charges quenched at 17GPa, majorite becomes the first liquidus phase followed by modified spinel (β-phase).

At 25GPa and under subsolidus conditions (1600-2000°C) the peridotite consists of $MgSiO_3$-perovskite, magnesiowüstite, majorite and a small amount of unquenchable Ca-rich phase of either diopsidic or $CaSiO_3$ composition. In an experiment quenched at about 2500°C and 25GPa, melt and solid are separated almost completely. The higher temperature portion is occupied by quenched liquid consisting of very fine aggregate of perovskite, magnesiowüstite and glass. The lower temperature portion is occupied by crystalline residue which consists almost exclusively of large $MgSiO_3$-perovskite crystals.

Results of the melting experiments at 25GPa (Fig. 1) are summarized as follows: (1) Under the lower mantle conditions (P>24GPa), $MgSiO_3$-perovskite is the principal liquidus phase in the peridotite composition. (2) Small amount of $CaSiO_3$-perovskite may crystallize as the second liquidus phase from the earth building material. (3) At small degrees of partial melting near the solidus, "super-ultramafic" magma (more enriched in MgO+FeO than $(Mg \cdot Fe)_2SiO_4$ stoichiometry) may be produced by eutectic melting of $MgSiO_3$-perovskite and magnesiowüstite. (4) The iron-magnesium partitioning between $MgSiO_3$-perovskite and the ultramafic magma (K_D=0.26-0.31, Table 1) is similar to that between mafic silicates (olivine and pyroxene) and basaltic melts.

It is a common assumption that bulk earth composition has chondritic abundance of elements. Compared with various chondrite rock types (C1, C2, C3, LL, L, H and E), however, the upper mantle peridotites (UMP) are systematically higher in Mg/Si ratio (Fig. 2A,B). Based on systematics in depletion factor of elements in UMP (pyrolite) compared with C1 as a function of volatility, Ringwood (1979) explained the above observation due to volatilization of silicon from the earth building materials prior to or during the accretion stage. Alternatively, Kumazawa (1978) and Ohtani (1983) explained the same observation by assuming chemically stratified mantle (ultramafic upper mantle and silica-rich lower mantle) as a result of perovskite fractionation in the primordial terrestrial magma ocean. Petrogenesis of the ultramafic UMP by extensive melting in the early history of

the earth has been supported by recent high-pressure melting experiments (e.g. Takahashi, 1986). In Figure 2, we have summarized major element ratios (Mg/Si, Ca/Si, Al/Si, and Ca/Al) of upper mantle peridotites (shaded area), estimated primitive upper mantle compositions (MA, R, J, PN), and chondrites (E, L, H, C1). Majorite (open stars) and $MgSiO_3$-perovskite (solid stars) which are the primary liquidus phase at 16-20GPa and >24GPa, respectively, are also plotted in Fig. 2. Because of the high Al/Si ratio of the majorite (0.208, Table 1), it is not plotted in Fig. 2A, C. Binary mixing calculations between the majorite or $MgSiO_3$-perovskite and primitive upper mantle compositions (MA, R, J, PN) were carried out. Only the results for the latter combinations are shown in Fig. 2A-D. Trends of majorite addition are indicated with arrows for the estimated primitive mantle composition PN.

Among the major elements, Ca and Al are most refractory. The significant deviation in Ca/Al ratio of UMPs (1.2-1.4) from chondrites (1.13-1.08) (Fig. 2C,D), therefore, are difficult to explain by selective volatilization. Palme & Nickel (1985) and Ohtani et al. (1985) explained the above deviation by majorite fractionation in the primodial magma ocean. However, any binary mixing of UMPs with majorite cannot satisfy the cosmochemical constraint in Al/Si at given Mg/Si and Ca/Si (see Fig. 2A,C). Thus, majorite fractionation is not compatible with the hypothesis that the bulk silicate earth (BSE) has chondritic element abundances. Because $MgSiO_3$-perovskite has very low Ca content (Table 1), fractionation of this phase from the magma ocean will rapidly increase Ca/Al of the liquid (Fig. 2C,D). Fractionation of 10 to 20 wt% of $MgSiO_3$-perovskite will account for the observed deviation in Ca/Al of UMPs from chondrites (Fig. 2C,D). It is important to note, that a mixture of 90-80 wt% Jagoutz et al.'s mantle (J) and 10-20 wt% $MgSiO_3$-perovskite lies approximately on the cosmochemical array (see Fig. 2A-D). The inferred BSE composition (BSE-M1) is shown in Table 1. Compared with C1, the BSE-M1 is slightly higher in Mg/Si, Ca/Si and Al/Si, possibly due to volatilization of silicon. Because of the small K_D value between $MgSiO_3$-perovskite and liquid (0.26 to 0.30), our BSE estimate is higher in Mg/(Mg+Fe) than those of previous workers.

Table 1 Composition of run products

		20GPa/2200°C				25GPa/2500°C					
	PHN-1611 bulk	maj	B	β	liq	Mg-Pv Av. of 8	Ca-Pv Av. of 7	liq Av. of 3	(liq)* mass balance	BSE-M1 this study	R ref.1
SiO_2	44.54	51.4	32.4	40.2	42.6	54.6 ±0.8	44.3 ±0.1	40.9 ±0.3	(37.8)	46.7	45.1
TiO_2	0.25	0.2	0.0	0.1	0.5	0.25±0.02	0.17±0.01	0.21±0.02	(0.3)	0.23	0.2
Al_2O_3	2.80	9.5	0.7	1.5	1.6	3.2 ±0.2	3.2 ±0.3	3.3 ±0.1	(2.5)	3.9	3.3
FeO*	10.24	4.4	8.5	8.5	15.0	3.6 ±0.6	0.3 ±0.2	10.2 ±0.2	(14.7)	7.0	8.0
MnO	0.13	0.1	0.1	0.1	0.2	-	-	-		0.13	0.15
MgO	37.94	31.0	58.9	48.1	33.2	36.5 ±1.0	1.1 ±0.4	31.9 ±0.6	(38.9)	38.2	38.1
CaO	3.32	2.3	0.0	0.0	5.7	0.42±0.04	41.6 ±1.2	8.9 ±0.3	(5.3)	3.1	3.1
Na_2O	0.34	0.0	0.1	0.0	0.7	0.03±0.01	0.05±0.01	0.12±0.01	(0.5)	0.29	0.4
K_2O	0.14	-	-	-	-	-	-	-	-	0.03	0.03
Cr_2O_3	0.29	1.2	0.6	0.5	0.5	1.4 ±0.3	0.8 ±0.2	2.7 ±0.1	-	0.5	0.4
La_2O_3	-	-	-	-	-	0.00	8.5 ±1.4	1.8 ±0.1	-	-	-
Total	99.99	100.1	101.3	99.0	100.0	100.0	100.0	100.0	(100.0)	100.0	98.8
atomic Mg/(Mg+Fe)	0.868	0.925	0.925	0.910	0.798	0.964	-	0.847	(0.825)	0.91	0.89
$K_D(Fe/Mg)^{sol-liq}$	-	0.31	0.32	0.39	-	0.31(0.26)*	-	-	-	-	-

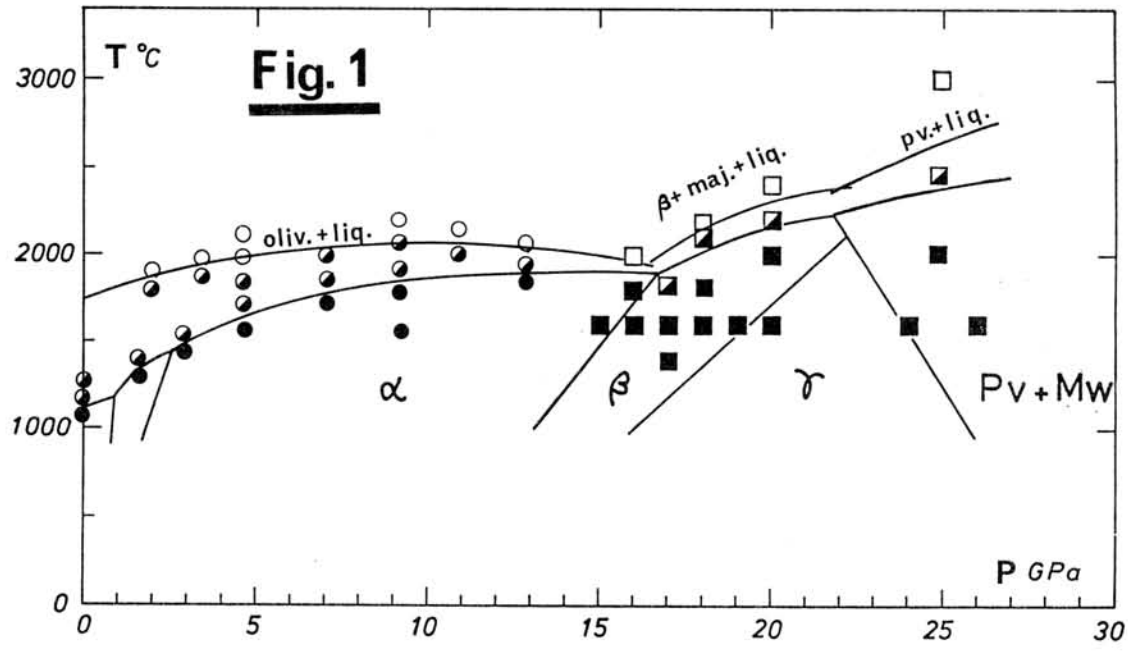

Melting phase relations of a peridotite PHN-1611 up to 25GPa. Circles are experimental data by Scarfe & Takahashi (1986). Open, above liquidus; half solid, subliquidus; solid, subsolidus.

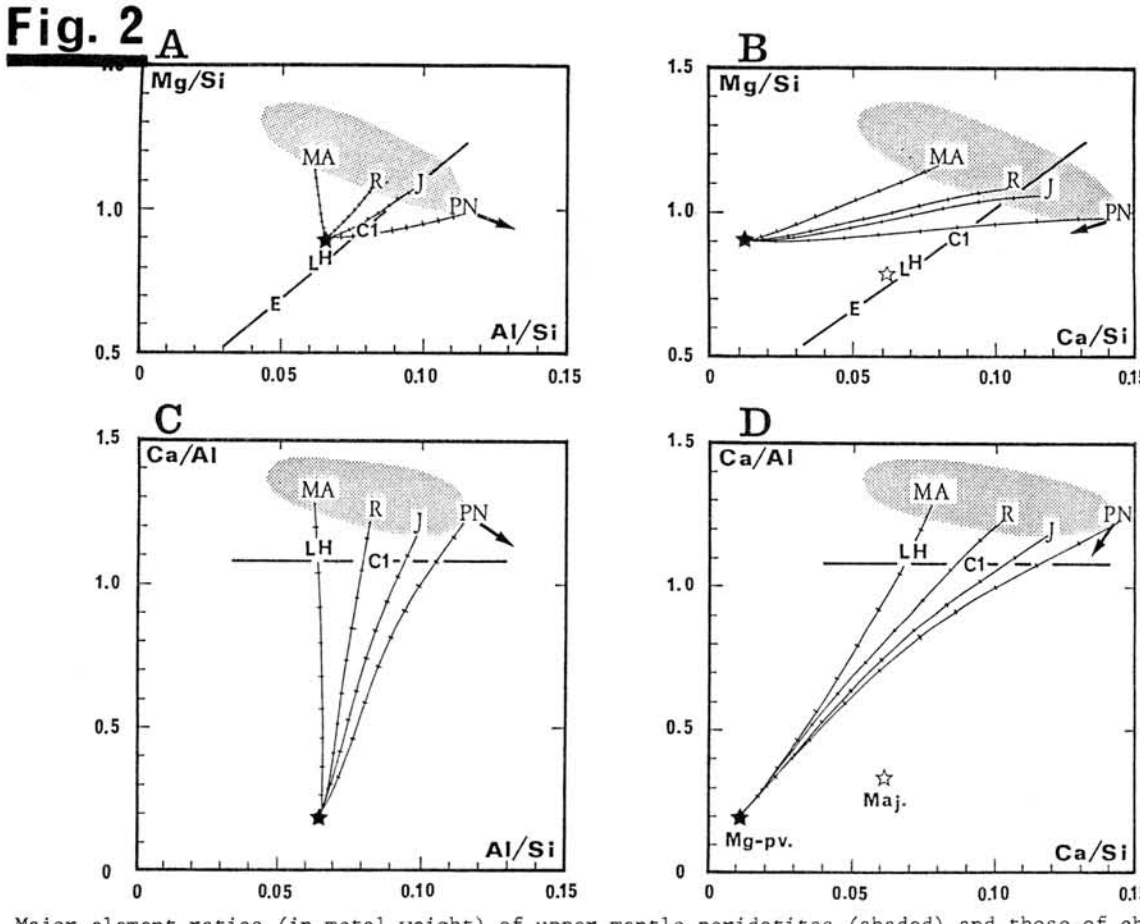

Major element ratios (in metal weight) of upper mantle peridotites (shaded) and those of chondrites (E,H,L, & Cl). Primitive mantle compositions estimated by Maaløe & Aoki (MA), Ringwood (R), Jagoutz (J) and Palme & Nickel (PN) are plotted. Compositions of the Mg-perovskite (★) and majorite (☆), liquidus phase at 25 and 20 GPa, respectively, are shown. In the left diagrams (A & C), however, majorite is not plotted because of its very high Al/Si. A mixture of 15 wt% Mg-perovskite and 85% Jagoutz et al's mantle (J) satisfies the cosmochemical constraint in all the diagrams.

COMPOSITIONAL COMPARISONS OF SOME CO, CV AND METAMORPHOSED CARBONACEOUS CHONDRITES FROM ALLAN HILLS

Gregory W. Kallemeyn
Institute of Geophysics and Planetary Physics, University of California, Los Angeles, CA 90024

Compositional studies by instrumental neutron activation analysis (INAA) were made on several carbonaceous chondrites from the Allan Hills region of Antarctica. The meteorites included two reportedly CV chondrites (Allan Hills A81003, Allan Hills 84028) [1,2], two reportedly CO chondrites (Allan Hills 82101, Allan Hills 83108) [3,4], and one reportedly metamorphosed carbonaceous chondrite (Allan Hills 84038) [5]. Typical sample sizes were 250-300 mg and enough material was available for replicate analyses of all the chondrites except Allan Hills A81003 and Allan Hills 84038.

Despite its small size (10 g) Allan Hills 81003 shows little evidence of weathering. Its interior is black with visible metal grains and numerous white inclusions showing minor oxidation [1]. In contrast, the much larger (0.73 kg) Allan Hills 84028 has a grayish interior showing oxidation haloes and salt deposits [2]. Lithophile element abundance ratios (Mg,CI-normalized) and siderophile/chalcophile element abundance ratios (Ni,CI-normalized) are plotted in Figs. 1(a) and 1(b) for the two chondrites. Also plotted are $\pm 2\sigma$ ranges about group mean CV abundance ratios. Refractory and common element abundances for Allan Hills A81003 fit nicely to CV. Some of the more volatile elements, especially Na and Br, are somewhat enriched, possibly due to contamination from marine air [6] aided by the high surface/volume ratio of this small specimen. Abundance ratios in Allan Hills 84028 are noticeable deviant from CV. The mean concentrations of the normalizing elements Mg and Ni are somewhat higher than mean CV values which could explain most of the deviations except for the refractory lithophiles and Br. A recent CV fall, Ningqiang, also has low refractory lithophile abundances for a CV, probably due to an atypically low abundance of refractory inclusions observed in it petrographically [7]. But a low abundance of refractory inclusions is not noted for Allan Hills 84028. It is petrographically like a typical CV [2].

Allan Hills 82101 and Allan Hills 83108 are both petrographically similar to CO chondrites [3,4]. The abundance data plotted in Figs. 1(c) and 1(d) support the classification, as they both easily fall in the range of mean CO abundances. Allan Hills 82101 shows some low deviations of the Sc and REE abundance ratios relative to the other refractory lithophiles. Except for small deviations between those elements, along with K and Br, both chondrites have nearly identical abundance ratios. Both chondrites show signs of weathering, Allan Hills 82101 is much smaller (29 g) than Allan Hills 83108 (1.5 kg) probably explaining its more noticeable abundance deviations. It was suggested that the two chondrites were paired, based on their similar localities and petrographic characteristics [4], and the compositional data seem to support this.

The Allan Hills 84038 carbonaceous chondrite is classified as petrologic type 4, and possibly paired with the similarly metamorphosed Allan Hills 82135 chondrite [5]. Abundance ratios for both chondrites are plotted in Figs 1(e) and 1(f). They show very similar lithophile abundances, except for a noticeably low value for Sc in ALH 82135. The siderophile/chalcophile abundances for the two chondrites are more deviant, along there would greater agreement if the data were normalized to Fe instead of Ni. Allan Hills 84038 has a fractionated Ni-Co-Fe pattern sometimes observed in other weathered finds, possible reflecting the loss of a Ni-rich metal or sulfide phase. Both chondrites are very small (each 12 g). The Au abundance ratio in Allan Hills 82135 is so high as to suspect contamination. It may be the Au abundance ratio is actually closer to that of Allan Hills 84038. Allan Hills 82135 is similar to Karoonda and is possibly part of a grouplet of along with Pecora Escarpment 82500 [8]. Allan Hills 84038 appears to also belong to this grouplet, and may possibly be paired with Allan Hills 82135.

References: [1] Mason B. (1983) *Ant. Met. Newsl.*, 6(1); [2] MacPherson G. (1985) *Ant. Met. Newsl.*, 8(2); [3] Mason B. (1983) *Ant. Met. Newsl.*, 6(2); [4] Mason B. (1986) *Ant. Met. Newsl.*, 9(1); [5] Mason B. (1986) *Ant. Met. Newsl.*, 9(2); [6] Biswas S., Ngo H.T. and Lipschutz M.E. (1980) *Naturforsch.* 35a, 191-196; [7] Rubin A.E., Wang D., Kallemeyn G.W. and Wasson J.T. (1987)

Geochim. Cosmochim. Acta, submitted; [8] Kallemeyn G.W. (1987) *Mem. Natl. Inst. Polar Res.*, in press.

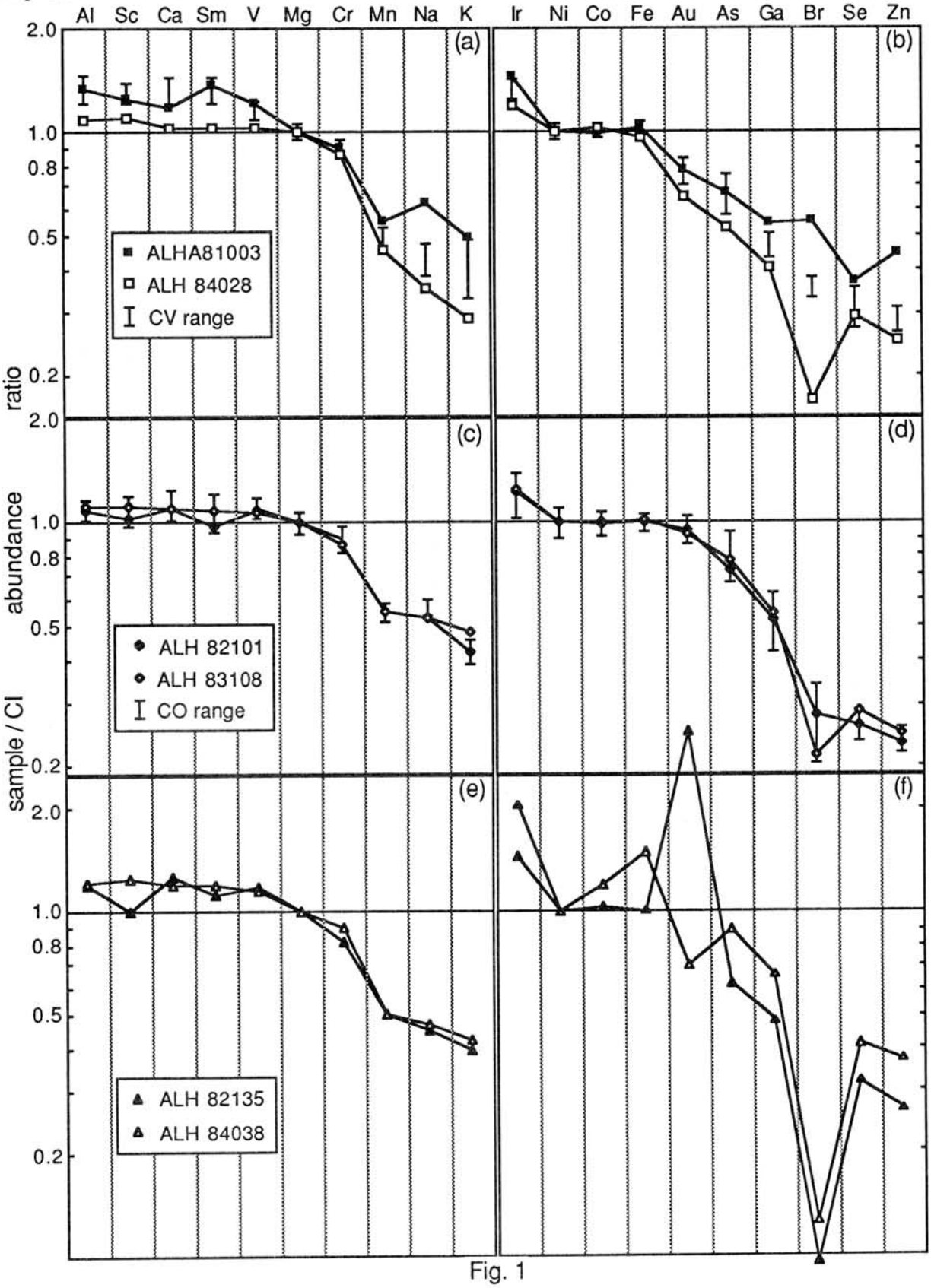

Fig. 1

Chemical Composition of Fusion Crusts on Antarctic Chondrites

Tazawa, Y. (1) and Sasaki, T. (2)
(1) Department of Physics, Kyoto University, Sakyo, Kyoto 606.
(2) Sakuranomiya High School, Miyakojima, Osaka 534.

Fusion crusts of meteorites, the outermost surface layers produced by ablation during atmospheric entry, and samples artificially ablated in laboratories were previously analyzed mostly on major chemical and mineral composition [e.g., 1, 2, 3]. These works presented general information of the nature of alterations produced by the ablation process. In the process large numbers of ablation debris will be released into the atmosphere. Therefore, the information brought about criteria for judgment of whether or no microparticle recovered from Earth's environments and thought, based on other evidence, to be of extraterrestrial origin is the ablation debris, and if it is the case, what kind of meteoroids it was derived from.

To increase the information and criteria, we have studied discrepancies of trace element abundances between fusion crusts and their adjacencies. About 0.3 to 4 mg of comparable samples were taken from four Antarctic chondrites (Y-7304,85(L6); Y-74155,85(H5); Y-790448(LL3); ALH-77272,85(L6)) and non-Antarctic chondrites (Aomori(L6); Allende,#10 and EK-1-34(C3)), by using a diamond file.

Conventional instrumental neutron activation analysis (INAA) were carried out at a neutron flux of 3 x10 n/cm /sec for 240 hours in the JRR-2 reacter, Japan Atomic Energy Research Institute, by installations for Gamma-ray spectrometry (GeLi, LEPS), Gakushuin University. Abundances of rare earth elements (REE), siderophile elements (SPE) and some other elements were determined by using JB-1 and Allende (bulk powder) as standard and control samples.

Thin sections of the crusts were also studied in major chemical and mineral compositions by scanning electron microscopy (SEM) and energy dispersive X-ray spectrometry (EDS).

Preliminary results of INAA indicate that the crust of Aomori considerably decreases abundances of volatile elements (e.g., Na) but does not change those of refractory SPE (e.g., Ir). While, the Antarctic chondrites do not show the considerable discipancies, which may indicate terrestrial weathering for Antarctic meteorites.

References:

(1) Blanchard, M. B. (1972) J. Geophys. Res. 77, 2442.

(2) Fruland, R. M. (1974) Meteoritics, 9, 339.

(3) Brownlee, D. E., Blanchard, M. B., Cunningham, G. C., Beauchamp, R. H., and Fruland, R. M. (1975) J. Geophys. Res. 80, 4917.

38—1

Distribution of trace elements in the rim-core of Tieschitz (H3) chondrules and the matrix

H. Nagamoto[1], N. Nakamura[1,2], Y. Nishikawa[1], K. Misawa[2] and S. Noda[1]

(1) Department of Earth Sciences, Faculty of Science and (2) Department of Material Differentiation, Graduate School of Science and Technology, Kobe University, Nada, Kobe 657, Japan

Elemental abundances of REE, Ba, Sr, Rb, K, Ca and Mg in the individual chondrules from the Tieschitz (H3.6) chondrite were determined by the improved mass spectrometric isotope dilution technique (1) to examine chemical characteristics of chondrule-formation processes and the chondrule-precursors. Chondrule-rim and -core samples, and the matrix materials were also analyzed for the elements. The analytical precisions are estimated to be 3 ~ 5% for most cases.

In Fig. 1, most of the chondrules analyzed in this work have the flat-REE patterns with minor (20-30%) negative Eu anomaly, which confirm the earlier results by the INAA (2). It is pointed out that there are not systematic abundance variations of REE among the different textural types of chondrules and that most chondrules do not show appreciable amounts of the Ce and Yb anomalies. These results are different from those of chondrules from the Allende (CV3) chondrite (1). Generally, Ca and REE are positively correlated, but although Sr abundances are most variable any clear correlation of Sr with REE are not found among Tieschitz chondrules, indicating presence of REE-free refractory precursor materials enriched in Sr.

The moderately-volatile elements, Rb and K, are depleted in the chondrule-cores but relatively enriched in the rims (Fig. 2). Thus, it seems likely that the alkaline element abundances in the bulk chondrule are mainly controlled by the rim. It is worth noting that all the chondrule-materials (bulk, core and rim) analyzed so far, as well as the matrix, have the similar Rb/K ratio close to the CI Rb/K value. Similar results were obtained for the bulk Allende chondrules (1).

The heating experiments for lunar basalts, chondritic meteorites and the synthetic materials (3,4,5) indicate that large elemental fractionations among the alkaline elements occur during the melting-vaporization processes of these materials. Assuming that these experimental results are applicable to chondrule-formation processes, it is considered that vaporization loss of the alkali metals followed by the Rb/K fractionation did not occur during the chondrule formation melting processes, and thus the low Rb and K abundances and the uniform Rb/K distributions found for chondrules were established basically before the melting event.

The matrix materials have lower trace element abundance with the positive Eu anomaly (Fig. 3). The Ca and Mg concentrations in this samples are 0.551% and 4.49%, respectively, suggesting that the matrix materials contained significant amout of non-silicate materials. The trace element pattern of the rim are

quite similar to that of the matrix and particularly the agreement of (non-silicate)-free (Mg-normalized) trace element abundances in the matrix with those in the rim are noteworthy, though it can not be ruled out that the matrix materials are contaminated with the rim materials significantly and the pattern of the marix partly reflect that of the rim. It is possible that the chondrule-rim was formed from the matrix materials by sintering. In addition, in view of the complementary abundance patterns for the cores and the rims (and thus the marix)(Fig. 3), it is considered that precursors of the core and rim (matrix) are related in their previous generation.

From the above results, it is suggested that the main features of trace elements observed for the Tieschitz chondrules were established before the chondrule formation melting; during formation processes of chondrule-precursors and/or accretion of precursor materials.

We thank Dr. R. Hutchison, British Museum, for providing us with the Tieschitz specimens.

References

(1) K. Misawa & N. Nakamura (1987), G.C.A. submitted (2) J.L. Gooding et al. (1980), Earth Planet. Sci. Lett. 50, 171, (3) E.K. Jr. Gibson & N.J. Hubbard (1972), LPSC 3rd, 2003, (4) J.L. Gooding & D.M. Muenow (1976), Geochim. Cosmochim. Acta, 40, 675; Meteoritics 12, 401, (5) M.E. Kreutzberger et al. (1986) Geochim. Cosmochim. Acta 50, 91

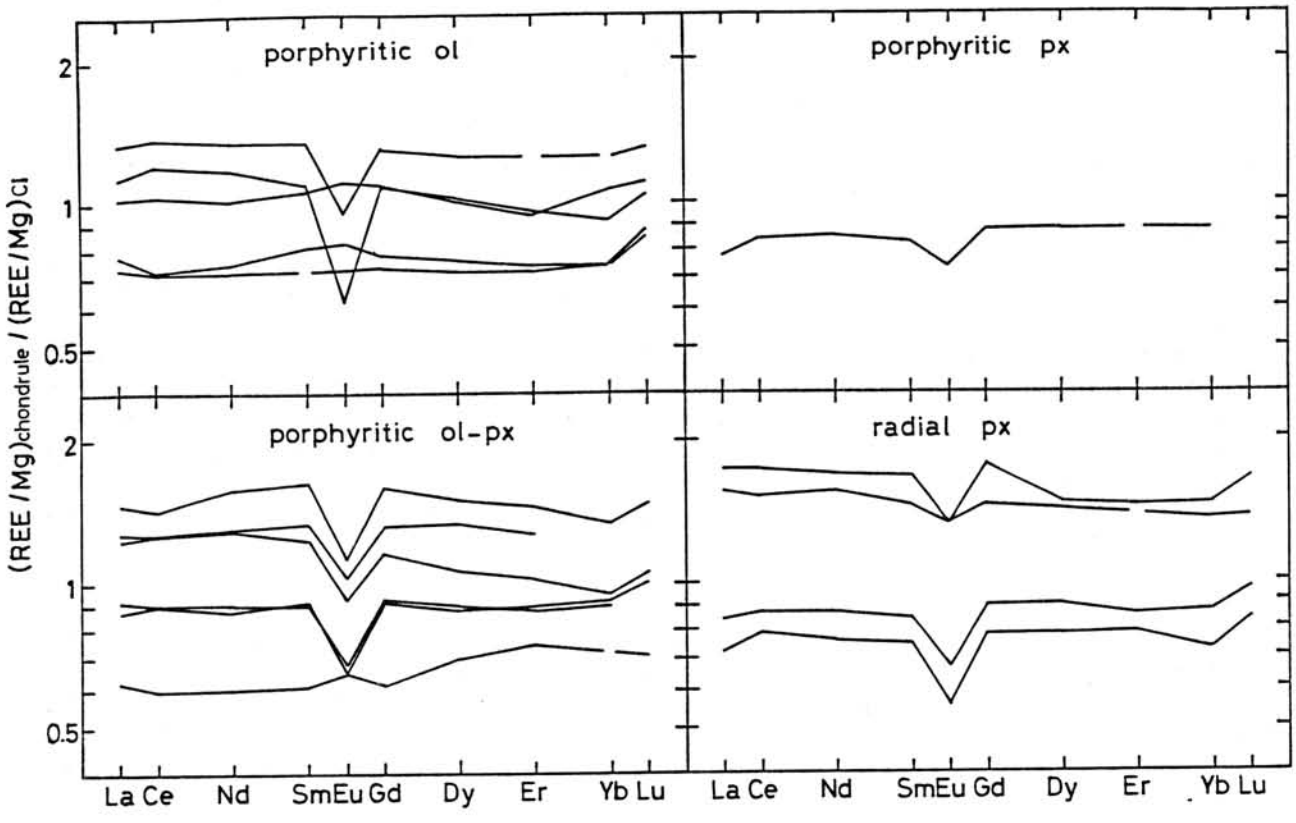

Fig. 1. Trace element abundance patterns for different types of chondrules from the Tieschitz (H3) chondrite.

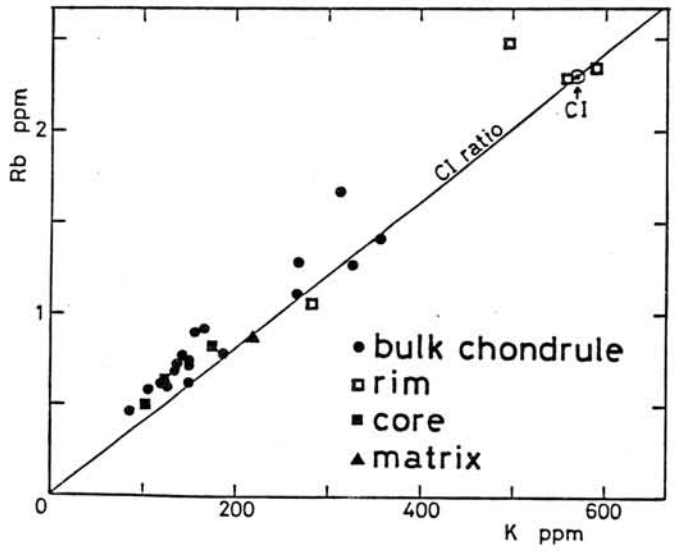

Fig. 2. The K vs Rb plot for the bulk, rim and core samples of chondrules, and the matrix from Tieschitz.

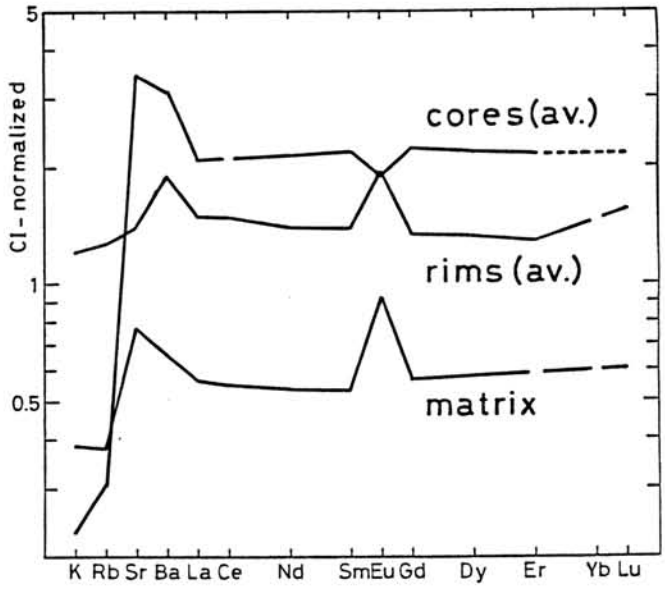

Fig. 3. Trace element abundance patterns for the matrix and averages of cores and rims of 3 chondrules from Tieschitz.

METEORITIC COMPONENTS IN SEDIMENTS COLLECTED FROM IMPACT CRATER, ARIZONA

Fukuoka, T.[1], Tazawa, Y.[2] and Nagasawa, H.[1]

1 Dept. of Chemistry, Gakushuin University, Mejiro, Tokyo 171
2 Dept. of Physics, Kyoto University, Kitashirakawa-oiwake, Kyoto 606

To understand the chemical contamination of terrestrial rocks by meteorite impact and their mechanisms, we analized more than 20 major, minor and trace elements in sedimentary and metalic samples collected from the inside and on the rim of the meteor crater, Arizona by instrumental neutron activation analysis (INAA). The No.1 and 2 samples were separated from the sample like No.7 (metalic) by magnet and hand picking prior to INAA (see Table 1). The No.3, 4 and 5 samples were also separated from the sample like No.9 which consist mostly of iron oxide, (Table 1).

Preliminary analytical results are shown in Table 2 together with the results for standard rocks, JB-1, BHVO-1 and BCR-3 and two Allende powder samples.

Siderophile elements (i.e. Co, Ni, Ir, Au and Os) do not exist in the most terrestrial rocks, although iron meteorite include those elements in high abundances. Sc do not exist in iron meteorite, but it is common in the most terrestrial rocks. The meteor crater was formed by impact of Canyon Diablo iron meteorite. Based on the simple mixing model of two endmember such as Ir and Sc, the mixing rate of iron meteorite component and terrestrial sediment is shown in Fig.1. Although the errors of analytical results are small, the mixing rates show the wide range. Table 3 shows the mixing rate of components of Canyon Diablo in the samples which were calculated based on the chemical abundances of Ir and Ni. Two kind of the rate do not agree completely. These results show the chemical contamination of terrestrial rocks by meteorite impact is not simple, although the results agree with simple mixing model qualitatively.

Table 1. Sample list

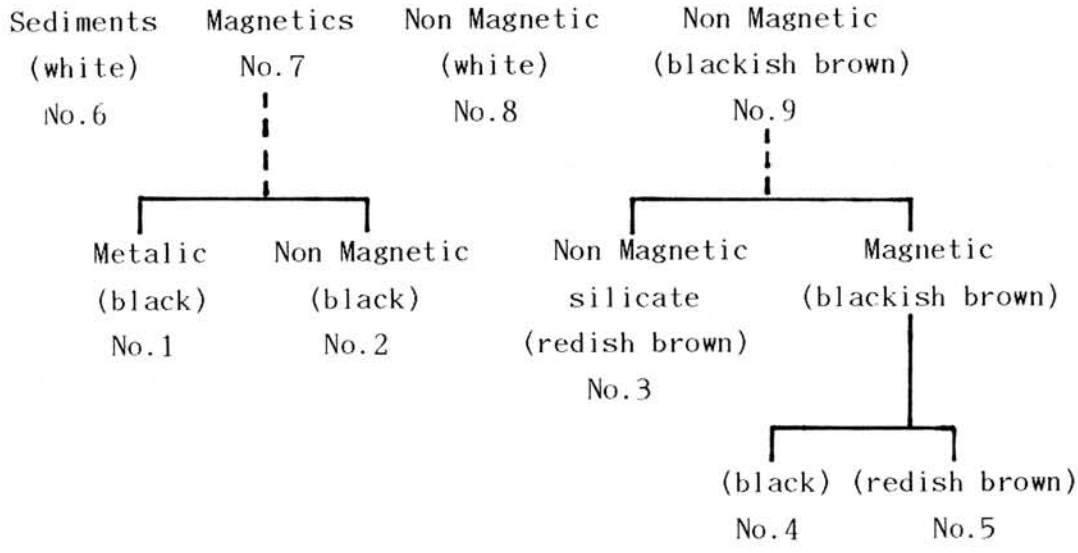

Table 3. The mixing rate of components of Canyon Diablo iron meteorite in the sample

		No.1	No.2	No.3	No.4	No.5	No.6	No.7	No.8	No.9
Ir	%	76	7	0	2	1	0	60	0	98
Ni	%	60	22	5	10	15	0	60	0	75

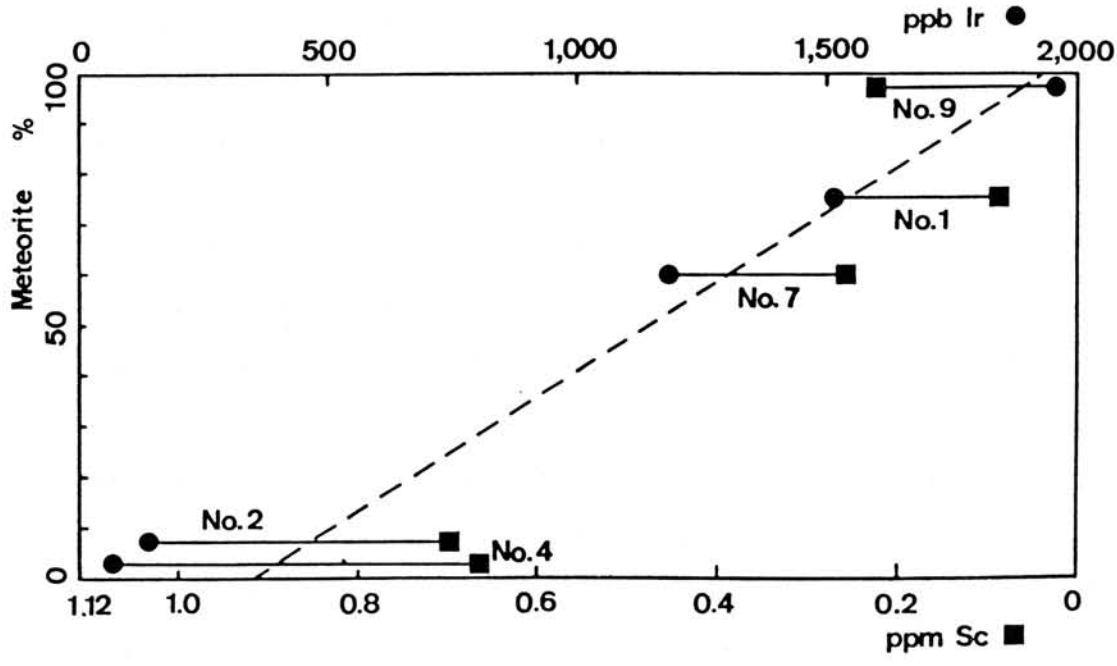

Fig.1. Possible mixing rate of components of iron meteorite and terrestrial sediments.

Table 2. The INAA results.

		No.1	No.2	No.3	No.4	No.5	No.6	No.7	No.8	No.9	JB-1	BHVO-1	BCR-3	Allende A	Allende B	Error (%)
Wt	mg	32.4	14.3	30.6	30.4	43.0	31.5	35.6	23.3	30.6	32.9	26.3	34.1	25.9	30.9	
FeO	%	72.5	58.9	18.6	32.2	45.9	0.014	74.5	17.7	65.1	=8.10	11.0	12.1	31.4	30.9	0.3-2
Cr	ppm	-	49.1	8.3	9.9	82	2.84	-	314	-	=414	229	7.9	2210	2420	0.2-5
Na_2O	%	0.0031	0.0189	0.0084	0.0105	0.0134	0.0050	0.0081	0.0284	0.0064	=2.80	2.24	3.18	0.507	0.461	0.1-2
K_2O	%	0.006	0.057	0.184	0.173	0.246	0.165	0.025	0.64	0.033	=1.44	0.50	1.59	-	-	5-30
Rb	ppm	-	-	7	-	-	3.7	-	19	-	=41.2	7.9	52	-	-	5-8 (1)
Cs	ppm	-	-	0.34	0.33	1.40	0.21	-	0.50	-	=1.1	0.034	0.93	-	-	7-40
Sc	ppm	0.10	0.71	0.64	0.67	0.92	0.46	0.25	1.12	0.22	=28.9	32.75	33.46	12.39	11.14	0.2-10
La	ppm	2.42	6.14	3.45	4.36	3.36	4.18	1.10	4.73	0.64	=38.8	15.44	25.3	0.60	0.53	0.4-5
Ce	ppm	5.9	10.9	6.1	8.8	7.3	5.45	7.2	11.2	6.5	=63	34.8	47.8	1.4	0.8	0.5-7(2)
Nd	ppm	-	5.6	3.3	4.4	2.2	3.1	-	7.8	0.9	28.8	27.4	=30	-	-	3-14 (3)
Sm	ppm	0.051	1.30	0.742	0.902	0.659	0.506	0.176	1.76	0.122	=5.02	6.05	6.44	0.338	0.324	0.2-4
Eu	ppm	-	0.28	0.16	0.25	0.14	0.121	0.07	0.233	-	=1.59	2.11	2.08	0.19	0.17	1-10 (4)
Tb	ppm	-	-	0.031	0.04	-	0.049	-	0.098	-	=0.70	0.81	0.92	0.02	-	3-8 (5)
Yb	ppm	0.20	0.33	0.41	0.40	0.34	0.26	-	0.73	-	=2.4	2.25	3.70	0.35	0.27	2-12 (6)
Lu	ppm	0.024	0.061	0.067	0.058	0.051	0.039	-	0.112	0.010	=0.37	0.35	0.58	0.074	0.066	3-21 (7)
Hf	ppm	-	0.65	1.23	1.19	2.23	1.01	0.35	2.53	0.52	3.44	4.21	=4.70	-	-	1-11
Th	ppm	-	-	1.43	1.41	1.48	0.80	-	0.96	-	9.51	1.18	=6.0	-	-	1-9
U	ppm	0.095	0.76	0.76	0.70	0.89	0.200	0.096	9.15	0.30	1.67	0.096	=1.74	-	-	1-10
Co	ppm	3090	1740	631	923	1400	0.187	2570	13.93	2940	=39.1	46.4	48.2	686	686	0.3-2
Ni	ppm	42500	15900	3810	7250	11000	2.7	42700	45	53400	143	127	13	13400	=14200	0.2-11(8)
Ir	ppb	1520	142	-	43	27	0.8	1190	0.52	1960	-	-	-	930	=780	0.5-7(9)
Au	ppb	777	40	1.4	12.5	14.5	0.29	507	51	662	-	-	-	154	=140	1-5 (10)
Os	ppm	1270	93	-	-	100	-	1000	-	1600	-	-	-	1050	=812	9-40

(1):Except for No.3 (40%). (2):Except for Allende A (14%) and Allende B (25%). (3):Except for No.9 (40%). (4):Except for No.7 (60%).
(5):Except for No.3 (22%), No.4 (30%) and Allende A (50%). (6):Except for No.1 (25%) and Allende B (19%). (7):Except for No.9 (90%).
(8):Except for No.6 (20%) and BCR-3 (46%). (9):Except for No.6 (75%) and No.8 (60%). (10):Except for No.3 (30%) and No.6 (24%).

RARE EARTH ELEMENTS IN CHONDRULES FROM THE FELIX (CO3) CHONDRITE: COMPARISON WITH THE ALLENDE (CV3) CHONDRULES

Keiji MISAWA[1] and Noboru NAKAMURA[1,2]

Department of Science of Material Differentiation, Graduate School of Science and Technology[1] and Department of Earth Sciences, Faculty of Science[2], Kobe University, Nada, Kobe 657, JAPAN

INTRODUCTION: The chondrules and Ca,Al-rich inclusions in the Allende CV3 chondrite have been extensively studied, but little is known about trace element characteristics of chondrules in CO chondrites [1].

In order to study more about the relationship of chondrules in Allende to those in other carbonaceous chondrites, we have determined abundances of trace and major elements (REE, Ba, Sr, Rb, K, Mg and Ca) by precise mass spectrometric isotope dilution technique [2] for individual chondrules from the Felix CO3 chondrite (USNM 235). Ornans-subtype chondrites are characterized by a high density of small (0.2- to 0.5-mm diameter) size-sorted chondrules and inclusions in a fine-grained matrix. Thus, the chondrules analyzed in this study were mainly < 1mg.

RESULTS: Five chondrules with variable Ca contents (1.6-21 wt%) were examined for trace elements. In Fig. 1, CI-normalized REE patterns of Felix chondrules are shown. The Ca-rich chondrule #2 (Ca=23xCI) has a nearly flat REE pattern with enrichment factors of 17-21 relative to CI and large negative Yb anomaly, which may be classified as Group III REE pattern but seems unusual as to the Eu abundance. The negative Yb anomaly is not accompanied by an Eu anomaly of comparable size. Europium is more volatile than Yb in a gas of solar composition [3]. One of the possible explanations of this pattern is that precursor material of chondrule #2 had originally negative Eu and Yb anomalies of equal magnitude (i.e. normal Group III pattern) and later Eu was added but relative abundances of trivalent REE were unaffected. Similar Group III REE patterns with Yb being lower than Eu were observed in meteoritic hibonites especially in Murchison [4]. Chondrule #8 shows a highly fractionated REE pattern (Group II), characterized by the fractionated LREE (7-12xCI) together with a rapid decline in abundance from Gd to Lu and positive Yb (and possibly Tm) anomaly. The abundance of Eu is comparable with that for Yb. The REE pattern with gradual increase from La to Sm and with positive Ce anomaly is first recognized in Allende pyroxene-rich chondrule (Fig. 1 and [2]), and also recently reported for Murchison hibonite MUR-31 and Mokoia CAIs [5]. These Group II patterns with positive Ce anomaly are complement of the REE pattern with negative Ce anomaly of core hibonite in Murchison GR-1 [6]. Under oxidizing condition in the solar nebula Ce exists as tetravalent state and is much more volatile than other REE, and may be partitioned relatively less into hibonite than ambient nebular gas. Thus, it is suggested that refractory precursor material of chondrule #8 was formed from a reservoir remaining after

condensation of ultra-refractory component under oxidizing condition. This simple equilibrium model, however, seems unlikely for explanation of the positive Yb anomaly. Chondrule #3 has a nearly flat pattern with excesses in the volatile REE Ce, Eu and Yb, and LREE enrichment relative to HREE are also appreciable. The light/heavy REE-fractionated pattern with Ce and Yb positive anomalies is similar to those of chondrule #8 and some Allende chondrules (Fig. 1). The common occurrence of both Ce and Yb anomalies in chondrules from Felix and Allende [2] suggests that non-equilibrium processes such as an instantaneous vaporization were involved as one of the important nebular dust fractionations. Chondrule #4 and #7 have flat REE patterns, though chondrule #4 exhibits negative Eu and minor negative Yb anomalies.

In Fig. 2, the elemental abundances normalized to Mg and CI are plotted in the order of increasing volatility expected from the solar nebular gas [7]. As mentioned above, Yb is depleted in Ca-rich chondrule #2 and Ce is enriched in chondrule #8 relative to the lithophile elements with similar volatility. Except for chondrule #2, Mg-normalized abundances of moderately volatile elements (K and Rb) correlate positively with that of refractory lithophile elements, indicating that refractory precursor component of Felix chondrule was alkali-bearing. This is consistent with the results of INAA analysis of Ornans chondrules [1] and also similar to that of Allende chondrules [2].

CONCLUSIONS: The REE abundances are fractionated among individual Felix chondrules. Some chondrules show the LREE/HREE fractionations and/or anomalies of Ce, Eu and Yb, indicating that gas-solid (or liquid) fractionations yielding REE fractionation took place during the formation of refractory lithophile precursors of Felix chondrules. Physico-chemical conditions in a region of the nebula where precursor materials of Felix chondrules were formed seem to resemble to those of Allende chondrules.

ACKNOWLEDGMENTS: We thank Dr. G. J. MacPherson, National Museum of Natural History, Smithsonian Institution for providing us with Felix sample.

REFERENCES: [1] Rubin A.E. and Wasson J.T. (1987) LPS XVIII,866-867. [2] Misawa K. and Nakamura N. (1986) Papers presented to the 11th Symposium on Antarctic Meteorites., 113-115. Misawa K. and Nakamura N. (1987) G.C.A., submitted. [3] Davis A.M. and Grossman L. (1979) G.C.A., 43, 1611-1632. Boynton W.V. and Cunningham C.C (1981) LPS XII, 106-108. Davis A.M. et al. (1982) G.C.A., 46, 1627-1651. [4] Ekambaram V. et al. (1984) G.C.A., 48, 2089-2105. Ekambaram V. et al. (1985) G.C.A., 49, 1293. Hinton R.W. et al. (1985) LPS XVI, 352-353. Fahey A. et al. (1987) G.C.A., 51, 329-350. [5] Liu Y.-G. et al. (1987) LPS XVIII, 562-563. Ireland T. et al. (1986) Meteoritics, 21, 404-405. [6] Hinton R.W. and Davis A.M. (1986) LPS XVII, 344-345. [7] Kornacki A.S and Fegley B. (1986) E.P.S.L., 79, 217-234.

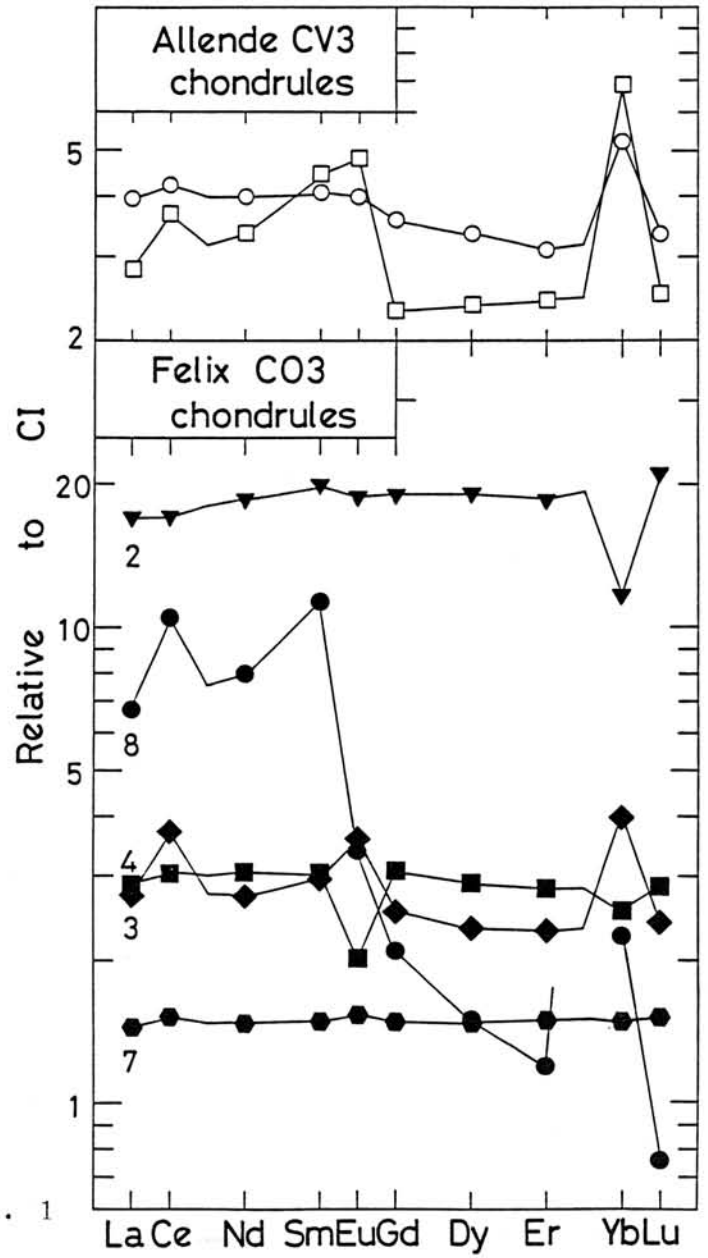

Fig. 1

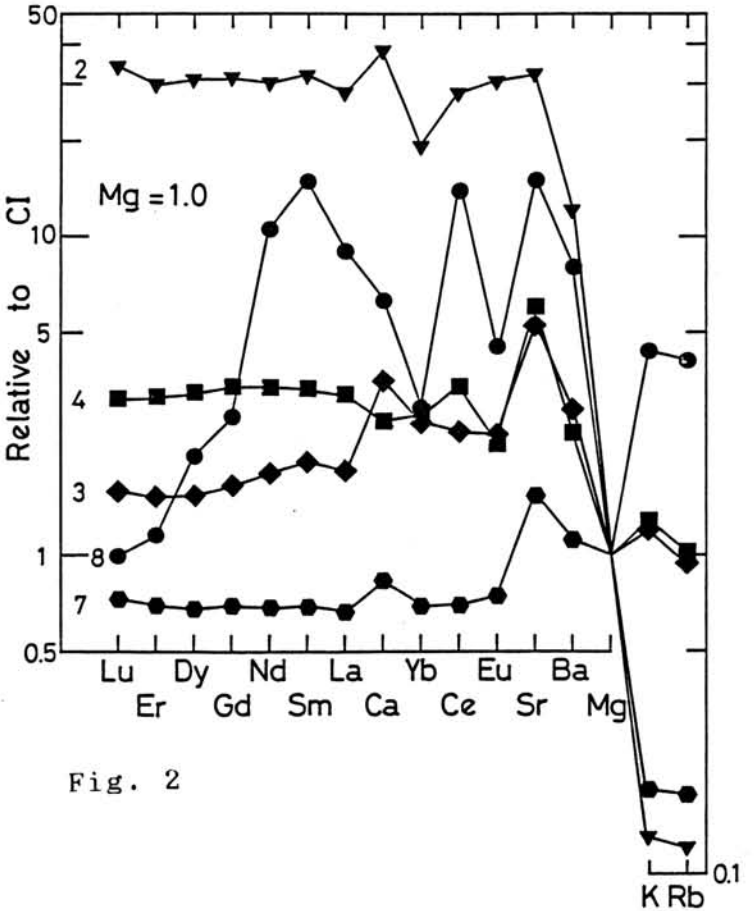

Fig. 2

Fig. 1

CI-normalized REE abundance pattern of individual chondrules from Felix. Light/heavy REE fractionation and anomalies of Ce, Eu and Yb are ubiquitous in CO and CV chondrules.

Fig. 2

CI-normalized abundances of lithophile elements in chondrules from Felix (abundances are normalized to Mg in the sample and then re-normalized to CI). Elements are arranged in the order of increasing volatilities from the left to the right.

THE CORRELATION OF CHONDRULE TEXTURE AND MAGNESIUM ISOTOPE ABUNDUCE

Uyeda Chiaki, Suzuki Mari, Okano Jun

Institute of Geological Science,College of General Education,Osaka University

Previously we reported the excess of ^{24}Mg in a number of Antarctic type 3 chondrites.[1] This isotope anormaly,together with the ^{16}O excess reported by Clayton et al.[2] indicate that the early solar nebula was isotopically inhomogeneous and composed of at least two components. It is suggested from the spacial distribution of ^{24}Mg excess in the meteorites that the anormaly components were injected into each chondrule before or at the time of its formation. So the correlation between chondrule texture and the extent of ^{24}Mg excess in the condrule will give an important key to understand the mechanism of ^{24}Mg injection as well as the formation of chondrules. The ion microprobe mass spectorometer and the polarized microscope are used for the research of this correlation in the following way. A Meteorite sample of about $1cm^3$ is cut by a $\phi 0.12mm$ wire saw. One side of the section is polished into a thin section for texture identification with the polarizing microscope. The other side of the section is attached to the standard sample holder of the ion microprobe mass analyzer in order to study the anomaly of the magnesium isotope abudance on the surface of the section. The section for a single chondrule usually appear in both section with the rate of 15-25 chondrules per $1cm^2$. By the comparison of both sections, the Mg isotope abundunce of a chondrule is measured with its texture identified.

A modified Hitachi IMA-2A ion microprobe mass analyzer was used for this work.[1] The primary ions were 9keV O_2^+ with the beam current of about $1\mu A$. The spot size is $80\text{-}120\mu m$.

Fig.1-4 shows the measured Mg isotope abundunce for each chondrules. In each figure, the horizontal and vertical axes show Δvalues given by the following equation,

$$\Delta(m/25)=\left\{\frac{(^{m}Mg/^{25}Mg)sample}{(^{m}Mg/^{25}Mg)s.t.d.}-1\right\}\times 1000 \qquad m=\begin{cases}24 \text{ for horizontal}\\ 26 \text{ for vertical}\end{cases}$$

Absolute isotope ratios reported by Catansaro et al.[3] are taken as the standard. The solid line with gradient -1 is the normal mass fractionation line (N.M.F.L.). The white circle on N.M.F.L. shows the uncorrected mean value of the laboratory standard forsterite (Ehime perfecture,Japan)which was measured on the bigining of every meteorite measurement.

Fig.1 shows the results of two porphyritic chondrules. For both chondrules,the data show a slight diviation from the laboratory standard (LS) with excess $\Delta(24/25)$ and $\Delta(26/25)$. The maximum amount of deviation is within +13‰ and +10‰ for both direction respectively.

Fig.2 shows the results of two radial pyroxine chondrules. The amount of diviation is similar to that of porphyritic chondrules.

Fig.3 shows the results of four barred orivine chondrules. The diviation amounts to $+10 \pm 7‰$ for $\Delta(24/25)$ and $+1 \pm 5‰$ for $\Delta(26/25)$ with respect to LS. The distribution area of each chondrule on the figure is concentrated within a span of about 10‰.

Fig.4 shows the results of glassy chondrules which shows considerrable positive diviation of $\Delta(24/25)$ comopared to the other chondrule types. It is noted that the spread of data points of glassy chondrule is dominant along the horizontal axis.

From the experimental results shown in Fig. 1-4, it is clear that the diviation of $\Delta(24/25)$ from LS is dominant to that of $\Delta(26/25)$. This indicates that the addition of excess ^{24}Mg-rich component to normal component is the most straightforward explanation for these diviation.

Fig.5 shows the mean isotope abundunce of each chondrule type calculated from the data points of Fig.1-4. It is noted that all the mean value fall on a single linear line with gradient -0.34 (line A). The experimental results can be explained by appling a mixing line hypothesis of normal and anomalous component as is done in the case of oxygen anormaly.[2] The intersection of NMFL and line A is assumed as the Mg isotope abundunce of the primitive solar nebla S before suffering injection of extra-solar component E.

The isotope abundance ratio of E is located somewhere on the extention of line A. The spread of the Mg isotope abundance of each chondrule type is considered to reflect the various mixing ratio of S and E.

It is noted that this sequence of chondrule types on line A coinside with the order of the cooling rate measured from the reproduction experiment.[4] According to the experiment, glassy, barred orivine and radial pyroxine chondrules were reproduced from completely molten liquid with cooling rate of more than 10^4℃/hr, $10^4 \sim 10^2$℃/hr and $10^2 \sim 1$℃/hr, respectively. Further, the isotope sequence also has correlation with the maximum heating temperature. Thus, there exists a possitive correlation between the amount of the ratio of E component to S component and the heating conditions of chondrule formation.

This correlation can be expained in terms of shock wave heating mechanism caused by a injection of extra nebula with E component to the early solar nebula. Details will be discussed elsewhere.

Reference

1) Nishimura,H., Okano,J., Mem.Natl.Inst. Polar Res., Spec.Issue, 25,171(1982) ibid, 30, 332(1983)
Nishimura,H., Okano,J., Meteoritics, 16, 368(1981)
Nishimura,H., Okano,J., Secondary Ion Mass Sectrometry, SIMS IV, ed. A. Benninghoven et al., Springer-Verlag, P475(1984) Okano,J., Uyeda,C. and Nishimura,H., Mass Sectroscopy, 33, 245(1985)
2) Clayton,R. N., Grossman, L, and Mayeda, T. K., Science, 182, 485(1973)
3) Catanzaro, E.J., Murphy,T.J., Garner,E.L. and Shields, W.R., J. Res. Natl. Bureau Stand., 70A, 453(1966)
4) Tsuchiyama, A., Nagahara, H., and Kushiro,i.,Earth Planet Sci. Lett. 48 155(1980)

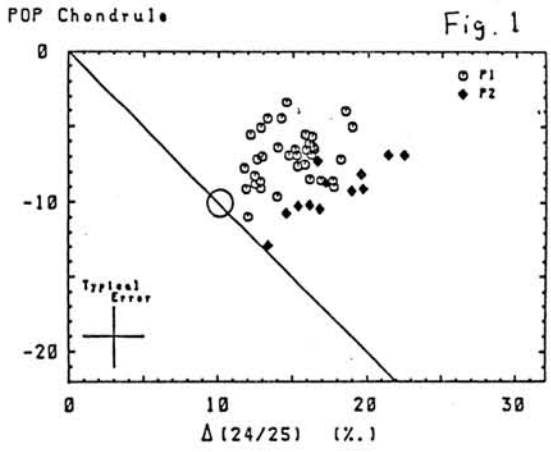

Fig. 1

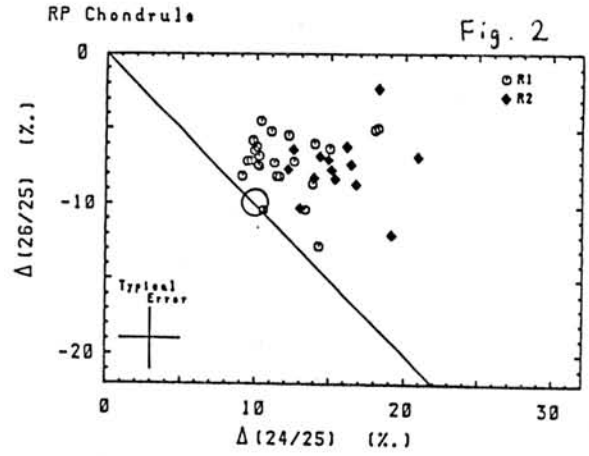

Fig. 2

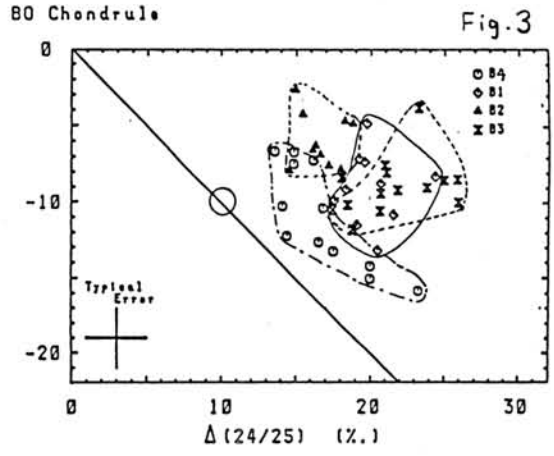

Fig.3

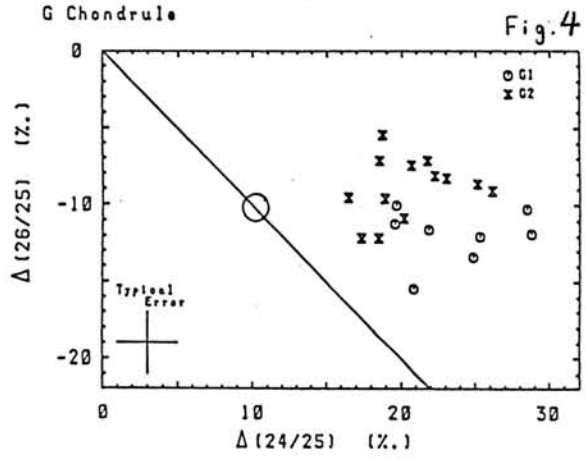

Fig.4

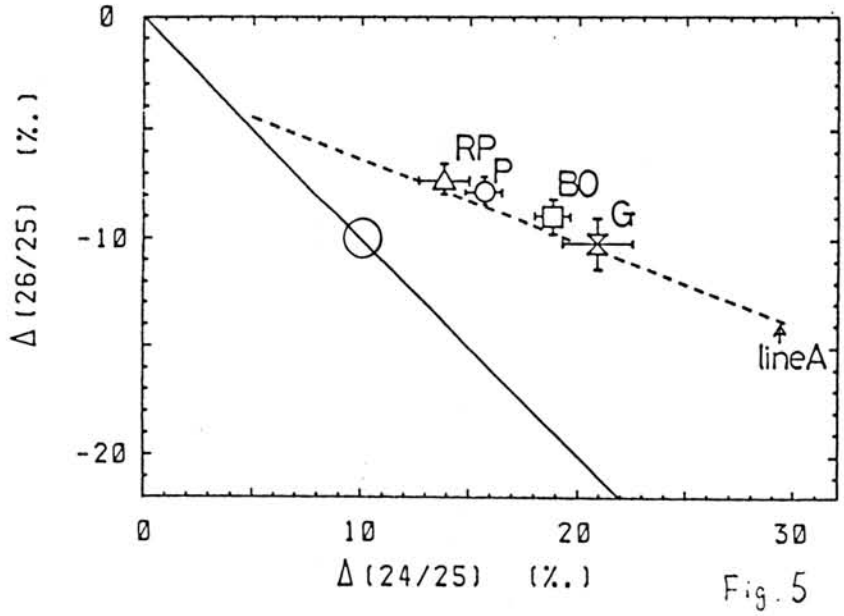

Fig. 5

The Rb-Sr systematics for diogenites

Kazuya Takahashi, Hiroshi Shimizu and Akimasa Masuda
Department of Chemistry, The University of Tokyo

Three types of achondrites, eucrite, howardite and diogenite, have been generally considered to be genetically related. Ages of 4.5-4.6 b.y. for eucrites have been obtained by many workers, using Rb-Sr, Sm-Nd or K-Ar systematics. On the other hand, there have been little chronological studies on diogenites. Since the abundances of Rb, Sr, REE(rare earth elements) and K in diogenites are very low, it has been difficult to measure isotope ratios of these elements precisely. Nakamura et al. (1979) and Kaneoka et al. (1979) carried out chronological studies of Rb-Sr, Sm-Nd and K-Ar systems on several Antarctic diogenites, showing chemical and isotopical disturbance in these diogenites by impact events after the formation of diogenites. Birck and Allegre (1981) reported an age of 4.45±0.18 b.y. for non-Antarctic diogenites.

In this study, analyses of Rb-Sr systematics and REE concentrations have been carried out precisely for five diogenite samples (4 samples from Johnstown and one from Tatahouine) and one pyroxenitic clast in Kapoeta howardite. Furthermore, we obtained an internal isochron for Juvinas eucrite in order to compare the isotopic data of diogenites with those of eucrites.

As shown in Fig. 1, the REE patterns for diogenites can be classified into two groups. One group is characterized by the depletion of light REE and the concave curvature in the light REE span. Another group shows the REE patterns with relatively small Eu anomaly and higher concentrations of REE than those of the first group. These observations suggest a complicated history for the differentiation of diogenite. Fig. 2 shows an internal isochron for Juvinas. The data for Juvinas give an age of 4.52 ±0.15 b.y. with an initial ratio of 0.69896 ±2. These results are consistent with those given by former studies (e.g., Allegre et al., 1975). Fig. 3 is a $^{87}Rb/^{86}Sr$ vs. $^{87}Sr/^{86}Sr$ plot for diogenite samples with the isochron of Juvinas (dotted line). Diogenite samples fall on the distinct positions from the isochron of Juvinas eucrite and these diogenite samples except Kapoeta opx-clast form an isochron, which give a younger age than 4.5 b.y. The data for Kapoeta opx-clast suggest that the Rb-Sr system of this clast had been disturbed by impact and brecciation. The age calculated from the isochron for diogenite samples shown in Fig. 3 is 4.398±0.048 b.y. with an initial ratio of 0.69896±6. Some diogenite samples, such as Tatahouine, cannot be regarded as a breccia, but pyroxenitic rock. Therefore, this younger age is considered to indicate that diogenite was formed at later stage than eucrite. Furthermore, our results would suggest that diogenites were formed through more complex process than eucrite. It is possible that this differentiation process might have no genetic relationship with eucrite formation and it is also possible that inner region of achondrite parent body had kept igneous activity for one or more billion years after the accretion and the formation eucritic layer.

References: Kaneoka et al.(1979):Mem. Natl. Inst. Polar Res. Spec. Issue, 12, 186-206.
Nakamura et al.(1979):Papers presented to the Fifth Symposium on Antarctic Meteorites, Natl Polar Res., 24-25.
Birck and Allegre (1981):Earth and Planetary Science Letters, 55, 116-122.
Allegre et al.(1975):Science,187, 436-438.

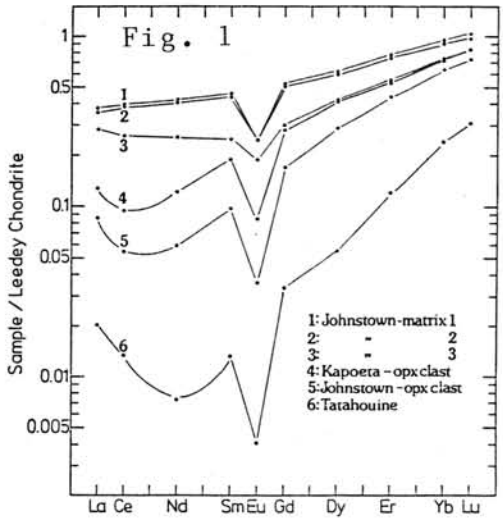

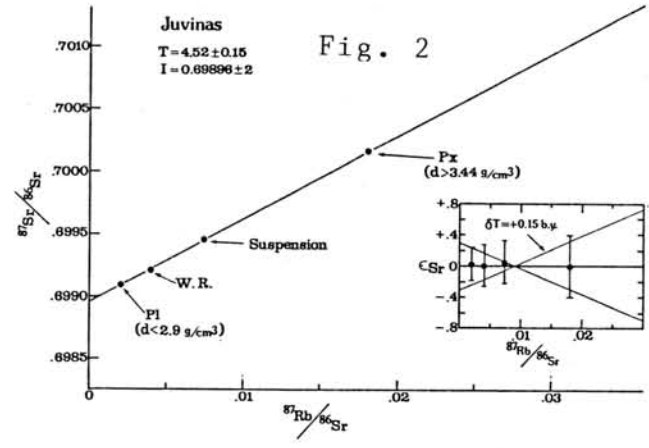

Fig. 1 The REE patterns for five diogenite samples and one opx-clast in Kapoeta.

Fig. 2 An isochron diagram for separated samples from Juvinas.

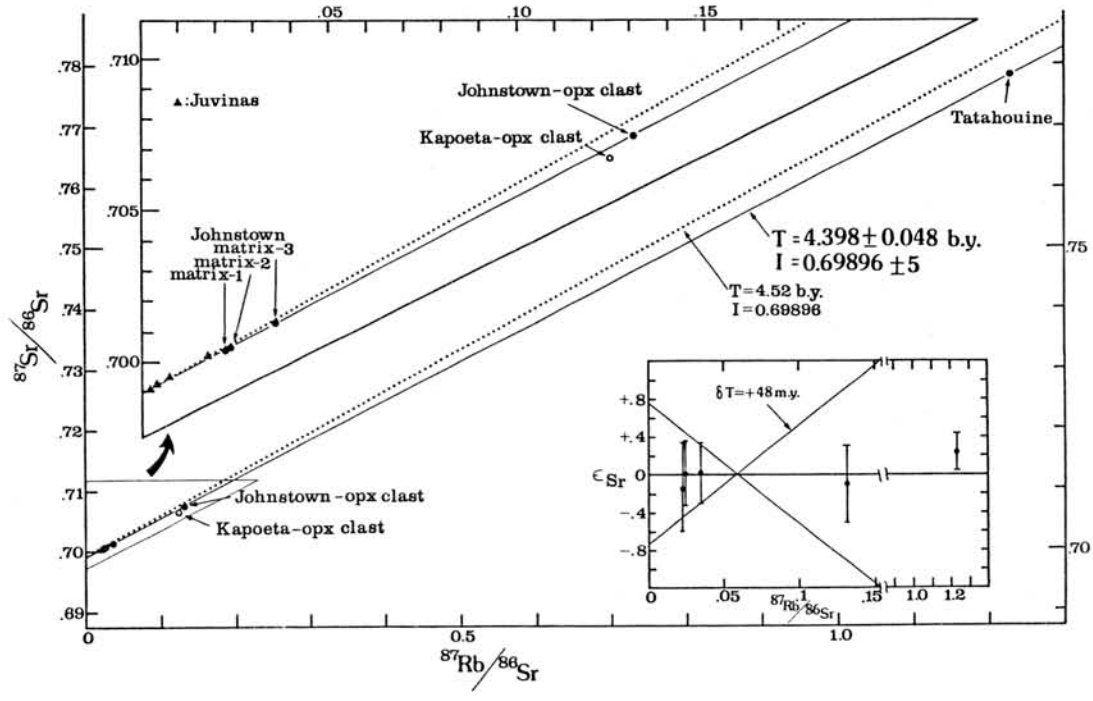

Fig. 3 The Rb-Sr isochron diagram for diogenites.
The data for Kapoeta opx-clast(open circle) were excluded in the age calculation of diogenite.

SCANDIUM 45 IN ANTARCTIC IRON METEORITES.

Honda,M., Nagai,H., Takahashi,M. and Akizawa,S.

College of Humanities and Sciences, Nihon University,Setagaya-ku, Tokyo,156.

As we reported in our previous papers(1), determinations of scandium in iron meteorites are useful to study a cumulative exposure history of cosmic ray effects on the iron meteorites(2). The radiochemical neutron activation method is applied and two gamma rays emitted from ^{46}Sc induced by (n,gamma) reaction. With neutron doses of 10^{17} -10^{19} n/cm^2, this method sensitive enough to detect Sc content as low as 10^{-13} gSc/g, whereas the normal cosmogenic level in irons is 10^{-9} - 10^{-12} gSc/g(Table 1). The lowest figure is for one of the large meteorites, Gibeon, at $5*10^{-12}$ gSc/g. A similar level is observed in DRP78008 but much higher in DRP78007 as their ^{53}Mn contents are indicating(3). Even at this level, Sc seems mostly attributable to cosmic rays.

On the whole,Sc content is best compared with cosmogenic ^4He. This is due to the relation of delta A (dA) values, mass difference between the target and the product, which is 11 for Sc. On the other hand, the effective dA for ^4He has been estimated at 10(5). Therfore the ratio of the two production rates is nearly constant, estimated at 1:20, because the rate for ^4He relative to that for A=46 is estimated at 18.3. So far available sets of data seem to indicate 1:20$\pm$2 for the ratio in a wide range of shieldings. That is, 1ppbSc corresponds to $1000*10^{-8}$ $cc\ ^4He/g$. The highest content in the table is found in Y75031 as indicated by the high noble gas contents, $2600*10^{-8}$ $cc\ ^4He/g$(4). An exception is seen in Braunau(6), where a considerable loss of noble gases is demonstrated.

Our chemical separation scheme for Sc is based on the cation exchange process; REE are also recovered along with the Sc and determined simultaneously. Any terrestrial contamination of Sc in the sample can easily be checked with the REE activities in the gamma spectra of the purified Sc fraction. In fact, REE in Gibeon, DRP78008,and other antarctic irons could not be detected, indicating 10^{-12}g/g or less. For example, chondrites contain about 6 ppmSc in their silicates. The metal fraction separated from Bruderheim contains 25ppbSc which is far higher than the cosmogenic level, 0.1ppbSc, and is attributable to silicates contamination. Besides Sc, REE present also in this sample.

Table 1. Scandium-45 found in Antarctic Iron Meteorites.

SAMPLE	ID	SIZE gr.	SC FOUND ppb	+-	Mn-53 dpm/kg
Antarctic Meteorites:					
DRP78008,IIB		0.09*	0.013	0.001	2.1+-0.2
DRP78007,IIB		0.29	0.25	0.02	144+-6
Y791694,IVB		0.23	0.20	0.02	
Y790517		0.55	0.39	0.20	552+-20
Y790724		0.54	0.20	0.16	518+-18
ALH78100,IIA	71	0.76	0.45	0.03	
PGP77006,IA		0.61	0.83	0.03	569+-23
ALH762,IA	54	0.68	1.06	0.03	556+-21
ALH78252,IVA		0.44	1.18	0.09	376+-14
Y75031,AN		0.29	2.1	0.2	474+-19
Some extreme examples of non-antarctic meteorites:					
GIBEON,IVA,NEW		0.81*	0.005	0.001	
GIBEON,IVA	LJ	0.80*	0.011	0.001	0
ODESSA,IA	H91-2	0.089*	0.12	0.01	20+-3
ODESSA(H91-2)	TROILITE	0.95	0.13	0.02	
ODESSA,IA	H91-3	0.11*	0.91	0.02	190+-25
BRAUNAU,H,IIA		0.11*	0.080	0.011	512+-20
BRUDERHEIM, METAL FRACTION	L6,16-2	0.10	25#		

*: 10^{19} n/cm^2.
#: corresponds to 0.4% of stone in metal;similarly 0.3% and 0.4% based on the Mg and Al contents respectively.

References: (1)Honda,M. et al(1984)This Sympo. the 9th,Mar.22-24,Tokyo,102-3; (1985)The 10th Sympo.,Mar.25-27,174-8. (2) Waenke,H.(1958)Z.f.Naturf.,13a,645;Waenke,H.and Koenig H.(1960) Max Planck Inst.f.Chem.,Mainz,54-57. (3) Nishiizumi, K.(1985-87) Data compilation. (4) Nagao,K. et al(1983)This Sympo. 8th, Mar.,83. (5) Honda,M.(1985)Earth Planet.Sci.Lett.,75,77-80. (6)Hintenberger,H.and Waenke,H.(1964)Z.f.Naturf. 19a,210-218.

Special Lecture

Dr. Christian Koeberl

THE ORIGIN OF TEKTITES: A GEOCHEMICAL DISCUSSION

Christian Koeberl

Institute of Geochemistry, University of Vienna
Dr.-Karl-Lueger-Ring 1, A-1010 Vienna, Austria.

Tektites are naturally occurring glasses, usually black, sometimes brown, grey, or even green. At a first glance they are similar to terrestrial obsidians. Most tektites are homogeneous, sometimes aerodynamically shaped, and up to a few centimeters in length. Forms include spheres, ellipsoids, teardrops, dumbbells, and related shapes. Chemical and morphological studies clearly distinguish them from terrestrial obsidians, so the similiarity is only superficial.

The discussion about the origin of tektites is almost as old as the knowledge of the existence of these objects. At the beginning of our century some extraterrestrial hypotheses flourished. Later arguments like the very low water content of tektites has been cited as an argument against a terrestrial origin. Extensive geochemical studies of tektites led, however, to a strong support of the terrestrial hypothesis, since tektites resemble terrestrial rocks very closely. At that time, about 20-25 years ago, only two sources of origin were left over: terrestrial impact origin, or lunar impact origin, later changed to lunar volcanic origin: Earth vs. Moon. After the first Apollo missions, as analyses of lunar material began to pour in, the pendulum swung completely on the side of the terrestrial impact theory.

Comparing tektites with terrestrial and lunar material leads, from the geochemical point of view, unambigously to the conclusion that tektites originated on Earth. Today, we have a growing database of tektite analyses, now increasingly including trace elements, which holds so many arguments in favor of a terrestrial origin, that it seems virtually impossible to falsify the impact theory. Arguments range from the shape of the rare earth element patterns over trace element ratios to shock-produced inclusions, to name just three.

A crucial point is the connection between tektites and impact glasses. In many cases the investigation of these glasses, which are known to be associated with an impact crater, leads to the same chemical insignia known from tektites. Differences occur, of course. Impact glasses frequently are inhomogeneous, richer in volatile elements, of aspherical shape, and show no indication of aerdynamical reworking. Of special importance is the group of the so-called Muong Nong type tektites. These tektites, which are clearly associated with the Australasian strewn field, show many characteristics of impact glasses, although they are tektites. They do have a much higher volatile content, are often inhomogeneous, and have no indication of aerodynamical effects. From the other side we do have impact craters like the Zhamanshin structure, where a number of different impact glass varieties can be found. Some Si-rich zhamanshinites are very similar to Muong Nong tektites.

Of course, there are a number of open questions: more chemical data are needed for more impact glasses and tektites; the search for craters associated with tektite strewn fields has to continue; more realistic impact models should be used to simulate impact glass and tektite production.....

Reference: Koeberl, C. (1986) Ann. Rev. Earth Planet. Sci., 14, 323-350.

Wednesday, June 10, 1987

0900 - 1410	*Symposium, Auditorium*
1410 - 1510	*Special Lecture*
	Professor James R. Arnold
	(University of California San Diego)

ALUMINUM 26 AND BERYLLIUM 10 IN METEORITIC IRONS.

Nagai,H.[1],Imamura,M.[2],Kobayashi,K.[3],Kobayashi,T.[1] and Honda,M.[1]
1)College of Humanities and Sciences,Nihon Univ. Setagaya,Tokyo.
2)Inst.for Nuclear Study,Univ.Tokyo,Tanashi,Tokyo.
3)Res.Center for Nuclear & Technol.,Univ. Tokyo,Bunkyo-ku,Tokyo.

Some iron meteorites, and metals and silicates of ordinary chondrites were examined for their ^{26}Al(1) and ^{10}Be(2). We applied the AMS method employing a Tandem van de Graaff accelerator at the Univ. of Tokyo(1). The samples were dissolved in nitric acid (HF), and 1-2 mg of Al and Be carriers were added. Both were separated from Fe+Ni, and finally separated each other by the cation exchange. As a monitor a few micrograms of enriched ^{10}B were added in the form of boric acid. For ^{26}Al, Al^- and $^{10}BO^-$, both M/e=26, are injected into the accelerator tube. After the 1st stage acceleration with 2MV, terminal voltage, using an Ar stripper $^{26}Al^{+3}$ and O^{+2} beams are separated by the main magnet. The former is measured by a solid state detector, and the latter is collected by a Faraday cup to monitor the beam of ^{26}Al(1).

For the determinations of high energy cosmogenic products in metal phases of chondrites, a sample preparation is important(3). In this work the grades of 0.1-1% stone in metal were obtained and the measurements could be carried out with minor stone corrections. Some results are tabulated in Table 1. The 1st step is to crush chondrite fragments down to about 100 mesh. The 2nd step is to collect the magnetic fraction using a hand magnet. The 3rd is to remove silicates by attacks using a 50% HF. The 4th is to pulverize further and flattened them by hitting again with a hammer, and stones evolved are removed again by washing and by HF repeatedly. Finally metals are dissolved into a neutral ammonium persulfate solution and insoluble stones and metal are separated by centrifuge. The contamination levels of stones are estimated based on contents of lithophile elements such as Mg, Al and Sc in the solution and in the chondrites.

As shown in the Table 2, the activity ratio of ^{26}Al to ^{10}Be in irons is relatively constant at 0.7-1.2, but varying with the shielding. In general,

$$p(A,Z)=f*k'_1(dA')^{-k'_2}$$

can be applied for the production rate, p(A,Z), where f the fraction of a partial production of the product mass A and Z in the total yield of A, and k's the parameter, the former indicating the level and the latter indicating the shielding; dA'=dA+4 is a corrected dA for smaller dA products. For example, for ^{26}Al in Grant, f=0.3 is estimated. As in the cases of He isotopes(4), dA' for ^{10}Be can be estimated to be near 17 corresponding to A=43. Relatively high ^{26}Al, 6 dpm/kg, in metal of chondrites are understood from that in chondrites, 60 dpm/kg. The main targets are Si and Al, and the effective dA' are close to those of Mn from Fe. Taking the spallation cross-section as proportional to $A_{target}^{2/3}$, we can estimate ^{26}Al in irons at 10% relative to that in chondrites (5).

Table 1. Metal Phase Separation from Chondrites.

Name ID	Sample wt. g.	Crude metal g.	Before dissol. g.	Insol. stone %	Metal in Solution mgMg/g	st. %	mgAl/g	st. %
Bruderheim,L6								
16-2*	10.8	1.17	0.74	--	0.37	0.26	0.04	0.36
B-156	8.9	1.00	0.63	0.06	0.12	0.08	0.0	<0.2
Peace River,L6	12	1.46	0.80	0.09	0.13	0.09	0.01	0.09
Y74192,H5	2.3	0.42	0.36	0.0	0.51	0.35	--	--
Jilin,H4,T-E	18	6.1	2.8	0.8	0.9	0.65	0.04	0.36

*Bruderheim 16-2 was not treated through the 4th step.

Table 2. ^{26}Al and ^{10}Be contents found in Irons by AMS.

Sample Metal	^{26}Al dpm/kg	^{10}Be dpm/kg	$^{26}Al/^{10}Be$ dpm/dpm	$^{53}Mn/^{26}Al$ dpm/dpm
PeaceRiver	5.9±0.5	5.1±1.0	1.2±0.2	68± 6
Bruderheim				
B-156	6.4±1.2	7.2±1.7 6.5±0.5*	0.9±0.3	77±14
16-2	5.4±0.8	4.7±0.3	1.2±0.2	98±15
ALH 762	2.6±0.2	3.8±0.3 3.7±0.6*	0.68±0.08	215±20
Grant				
G-320	2.2±0.3	3.3±0.2	0.67±0.08	164±19
Henbury				
193-488	0.95±0.09	1.43±0.10	0.67±0.08	348±39**
Odessa				
H91-3	0.68±0.08	1.30±0.05	0.52±0.07	279±49

Half life data: ^{26}Al: $7.1*10^5$ y.; ^{10}Be: $1.5*10^6$ y.
Stone corrections (0.1-1% chondrite in metal) are made for metal samples from chondrites, which are 1-10% for ^{26}Al and 0.5-5% for ^{10}Be.
* Ref.2: Due to a calibration error in the ^{10}Be standard, the figures appeared in the table of previous paper(1983) have to be reduced to 75% of the original.
**When we apply a terrestrial age correction to this meteorite, this ratio will be reduced in some extents.
^{53}Mn data are from the compilations by K.Nishiizumi(1985-7).

References: (1)Nagai,H. et al(1987) 4th Sympo. AMS, Niagara, Canada April.(2)Honda,M.and Nagai,H.(1983) Meteoritics, 18,315. (3)Vilcsek,E. and Waenke,H.(1965)Z.f.Naturf. 20a,1282; Begemann, F. et al(1976) Geochim.Cosmochim.Acta 40 353 (4)Honda,M.(1985) Earth and Planet.Sci.Lett. 75,77 (5) Honda,M. to be published.

^{40}Ar-^{39}Ar AGE OF A L7 CLAST-BEARING CHONDRITE Y-75097(L6) AND THE EFFECT OF COLLISION ON DEGASSING

Kaneoka, I.*, Takaoka, N.** and Yanai, K.***
* Earthquake Research Institute, University of Tokyo, Bunkyo-ku, Tokyo 113.
** Department of Earth Sciences, Faculty of Science, Yamagata University, Yamagata 990.
*** National Institute of Polar Research, Itabashi-ku, Tokyo 173.

The Yamato-75097(L6) chondrite has been known to contain unique inclusions (L7 clasts), one of which has been observed to have a fine-grained granular texture (1) and to be similar to that of Brachina meteorite (2). The host rock has a chondritic structure, but chondrules and chondrule fragments show extensive integration with the granular groundmass which consists of olivine and pyroxene as major components (1). Further, the meteorite is observed to have been traversed by thin black veinlets probably produced by shock (1). Hence, it is worthwhile to get some information on the age of such a shock event for this meteorite to compare the time of the event with those observed for many ordinary chondrites (3). For this purpose, the ^{40}Ar-^{39}Ar method was applied to the Yamato-75097, 82.

For ^{40}Ar-^{39}Ar analyses, a chip of this meteorite was irradiated as a bulk sample with neutrons in the JMTR of Tohoku University with the total fast neutron fluence of about 8×10^{18} nvt/cm^2. The hornblende MMhb-I(K-Ar age: 519.5±2.5Ma) (4) was used as the age monitor. Ar gas was extracted and purified after the conventional procedures at the Isotope Center of the University of Tokyo. Ar isotope analyses were performed on a Nier-type mass-spectrometer with a resolving power of about 600 at the Yamagata University. Nine temperature fractions (600-1600°C) were taken for analyses, each of which was kept for 45 minutes for degassing from the meteorite. Blanks and K-derived interfering isotopes were corrected to calculate ages. No Ca-derived interfering isotopes were corrected, because the analyses were made after the irradiaiton of the sample for more than two years. However, it is inferred that the effect is not significant in the calculated ages except for the highest fraction (1600°C). Even for the highest fraction, the effect is estimated to be a few per cent at most in the calculated age.

The result is shown in Fig. 1. As shown in this figure, this meteorite shows a pattern of serious Ar degassing aroud 500Ma or slightly less. No plateau age is observed, but the 800°C fraction shows the youngest age of about 490Ma, which covers about 34% of the total degassed ^{39}Ar. The 900°C fraction shows an age of 505Ma, which covers about 23% of the total degassed ^{39}Ar. The lower and higher temperature fractions show older ages, suggesting that a strong shock effect affected for this meteorite about 490-500Ma or slightly less. The total ^{40}Ar-^{39}Ar age is about 583Ma.

Such a young age has been expected for this meteorite on the basis of noble gas analyses (5). Present result confirms this inference.

The analyses of Ar-degassing patterns for this meteorite indicate that this meteorite shows the "B" type degassing pattern defined by Kaneoka (6), which suggests a typical Ar-degassing pattern of an ordinary chondtite with no weathering effect. This is compatible with an observation that this meteorite appears to be unweathered (1).

If we assume that the meteorite was formed 4550Ma and seriously degassed 490Ma by a shock event, the degassing rate of radiogenic ^{40}Ar from this

meteorite is calculated to be more than 99% at the time of shock event. Since the clasts remained unmelted, the highest temperature reached during the event should not exceed the melting temperatures of the composed minerals. Based on some diffusion parameters observed for this meteorite, it is inferred that the meteorite should have been kept at relatively high temperatures (for example around 1000°C) for at least more than a few hours to degass the radiogenic ^{40}Ar seriously.

References

(1) Yanai, K., Matsumoto, Y. and Kojima, H., Mam. Natl. Inst. Polar Res., Spec. Issue No.30, 29-35, (1983).
(2) Johnson, J.E., Scrymgour, J.M., Jarosewich, E. and Mason, B., Rec. South Austr. Mus. (Adelaide), 17, 309-319, (1977).
(3) Bogard, D.D., Husain, L. and Nyquist, L.E., J. Geophys. Res., 81, 5664-5678, (1976).
(4) Alexander, Jr., E.C., Mickelson, G.M. and Lanphere, M.A., U.S.Geol. Surv. Open-File Rep., 78-701, 6-8, (1978).
(5) Takaoka, N., Saito, K., Ohba, Y. and Nagao, K., Mem. Natl. Inst. Polar Res., Spec. Issue No.20, 264-275, (1981).
(6) Kaneoka, I., Mem. Natl. Inst. Polar Res., Spec. Issue No.35, 272-284, (1984).

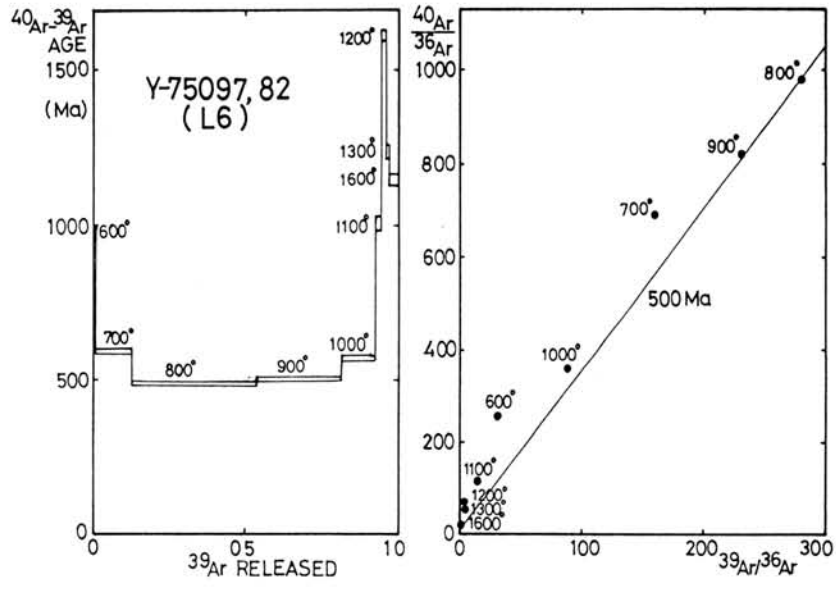

Fig. 1. ^{40}Ar-^{39}Ar age spectrum of the Yamato-75097(L6).

^{14}C AGES OF YAMATO AND ALLAN HILLS METEORITES

Beukens, R.P.[1]), Rucklidge, J.C.[1]) and Miura, Y.[2])
[1]) Isotrace Lab. University of Toronto, Toronto (Ont) M5S 1A7, Canada
[2]) Dept. of Mineralogical Sciences & Geology, Yamaguchi University, Yoshida, Yamaguchi 753

Carbon was extracted from 1 gram samples of ten Antarctic chondrites, using stepwise heating. The evolved CO_2 was collected at 1000°C, melt and remelt. The ^{14}C activities were measured at the Isotrace AMS facility and were compared with the activity of the recently fallen Bruderheim (L6) chondrite. The terrestrial age, thus obtained, for the one Allan Hills meteorite ALH-77231 (L6) confirmed the old ages (>20ka) obtained for these meteorites. The terrestrial ages of the nine Yamato meteorites; Y-74014 (H6), Y-74097 (Dio), Y-74191 (L3), Y-75271 (L5), Y-790448 (LL3), Y-791500 (H3), Y-791630 (L4), Y-791717 (C3) and Y-74647 (H5); show a larger range than measured before from 6ka to over 40ka.

NOBLE GASES IN BELGICA-7904 CARBONACEOUS CHONDRITE

Matsubara, K.[1], Nagao, K.[2] and Matsuda, J.[1]

1. Department of Earth Sciences, Faculty of Science, Kobe University, Nada, Kobe 657.
2. Okayama University of Science, Ridai-cho, Okayama 700.

Carbonaceous chondrites are regarded to be the most primitive ones among the meteorite and, therefore, are very important to study the initial stage of our solar system. Belgica-7904 is C2 carbonaceous chondrite collected by the Japanese team of antarctic research expedition at Belgica Mountains, Antarctica.

The elemental and isotopic compositions of noble gases in Belgica-7904 extracted by stepwise heating tecnique have been reported (1), which showed various components such as primordial Ar, Ne-E and ^{132}Xe excess. These results encouraged us to do physical separation of this meteorite to isolate these components.

We did the stepwise heating measurement for the size-separated samples (>8μ and <8μ) which were prepared by 8μ filter after being applied "freeze-thaw disaggregation" method. Noble gases were enriched in <8μ fraction, whereas those in >8μ fraction showed similar concentration in bulk sample. The cosmogenic components and Ne-E were detected in >8μ fraction, but not observed in <8μ fraction. Thus, size separation was useful to isolate the phase of noble gas component in the meteorite. As a next step, we prepared new nine fractions of size-separated samples. A schematic diagram of separation is shown in Fig.1 and Table 1.

Noble gas concentrations in NB1 was much higher than those in the bulk sample. Although NB2 inclusion rich sample showed gas concentration lower than that of the bulk sample, all other samples had similar concentration to that of the latter. The helium isotopic composition in the lowest temperature fraction of 700°C of almost all samples showed $^{3}He/^{4}He$ ratios in the order of 10^{-2} from the cosmogenic component. $^{3}He/^{4}He$ ratios of 1000 and 1300°C fraction were in the order of 10^{-4}, suggesting the primordial He. Ne isotopic compositions were quite different among samples. Because of a small quantity of NB1 we could not Ne isotopic composition except for 900°C for this sample. The cosmogenic Ne was found for almost all samples except NB1 and NB6. NB6 colloidal sample included primordial Ne components of both Ne-A and Ne-B. Ne-E was observed in 1000-1100°C for samples except NB1, NB2 and NB6, but was not clear like in >8μ sample. Ar isotopic composition showed $^{40}Ar/^{36}Ar$ ratio lower than 1 in 1100-1300°C for almost all samples, suggesting the existence of primordial component. CCF-Xe was not clear in >8μ and <8μ samples, but observed in 900°C fractions for all new samples except NB1. This was clearly shown for NB6. ^{132}Xe-excess which was observed in the bulk sample was only slightly detected in NB4, but was not confirmed in other samples.

According to the noble gas compositions, NB1 and NB2 are

quite different from the bulk sample, but NB3, NB4 and NB5 are similar to the latter. There were no significant differences of noble gas compositions among the samples separated by heavy liquid for NB7. The summary of various noble gas components included in each fraction are shown in Table 2.

References: (1)Nagao, K., Inoue, K. and Ogata, K. (1984) Mem. Natl. Inst. Polar Res. Issue 35,257.

Fig.1

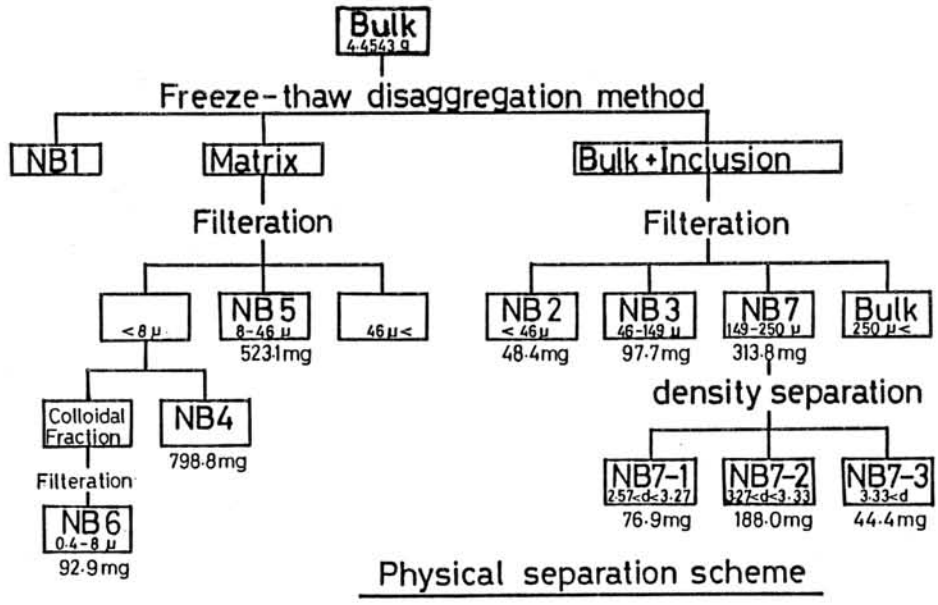

Table 1

SAMPLES FOR NOBLE GAS MEASUREMENT

Sample Name	Weight(mg)	Remarks
NB1	0.317	Floating fraction
NB2	43.9	<46μ,Most inclusion rich
NB3	94.3	46-149μ,inclusion rich
NB4	111.6	<8μ,Non colloidal
NB5	192.8	8-46μ
NB6	64.6	Colloidal
NB7		149-250μ
NB7-1	61.4	2.57<d<3.27
NB7-2	89.4	3.27<d<3.33
NB7-3	26.5	3.33<d * d:density

Table 2

Summary

	gas content	cosmogenic	Ne-E	CCF-Xe	^{132}Xe-excess
Bulk		+	++	++	++
>8μ	=bulk	+	+++	?	+
<8μ	high	-	-	?	+
NB1	high	-	-	-	-
NB2	low	++	-	+	-
NB3	=bulk	++	++	++	-
NB4	=bulk	+	++	++	-
NB5	=bulk	++	++	++	+
NB6	=bulk	-	-	+++	-
NB7-1	=bulk	++	++	++	-
NB7-2	=bulk	++	++	++	-
NB7-3	=bulk	++	++	++	-

RARE GAS ISOTOPIC COMPOSITION OF ACHONDRITES FROM ANTARCTICA

K. NAGAO
Okayama University of Science, Ridai-cho 1-1, Okayama 700

Rare gas isotopic compositions of several achondrites have been measured. The results are listed in Table 1.

Y-74159 eucrite is characterized by the high concentration of cosmogenic rare gases, and the rare gas composition is similar to that for Y-75015 eucrite(Nagao et al.,1983). The concentrations of 36Ar and 40Ar are in good agreement with those reported by Kaneoka(1979). Cosmic-ray exposure age of these eucrites is as long as about 60 m.y. Cosmogenic 81Kr was observed in Y-74159 and Y-790260 eucrites. Rough estimation of terrestrial 81Kr-Kr age for these two eucrites with the method proposed by Schultz(1985) indicates that the terrestrial age for Y-74159 is less than 0.07 m.y. , whereas the age for Y-790260 is about 0.18 m.y. The long exposure age and rare gas concentration for the eucrites, Y-74159 and Y-75015, are identical with those for Y-74450 and Y-790007 eucrites reported by Schultz(1985). The terrestrial age for these eucrites is less than 0.04 m.y. These data strongly suggest that Y-74159, Y-75015, Y-74450 and Y-790007 are paied, which has already been mentioned by Schultz(1985) .

The cosmic-ray exposure age for Y-790260 is (10-20)m.y. which is much shorter than that for the paired eucrites.

ALH-77005 shergottite did not show a clear evidence of the martian atmospheric rare gas composition as found in EETA-79001 glass(Wiens et al., 1986). Two step heating of rare gas extraction indicates that trapped or adsorbed rare gases were released at low temperature(700°C) and that the high temperature fraction was enriched in cosmogenic rare gases. Xe isotopic ratios are the mixtue of trapped, which may be a terrestrial Xe incorporated into the sample, and cosmogenic Xe. Fissiogenic Xe was not found in this meteorite.

The howardite Y-790727 has appreciable amount of trapped gases and the Ar and Kr data are consistent with those reported by Schultz(1985).

References: 1) Nagao,K., Ogata,K., Takaoka, N. and Saito,K.(1983): Mem. Nat l. Inst. Polar Res., Spec. Issue 30, 349-361. 2) Kaneoka,I., Ozima,M. and Y anagisawa,M.(1979): Mem. Natl. Inst. Polar Res., Spec. Issue 12, 186-206. 3) Schultz,L.(1985):Mem. Natl. Inst. Polar Res., Spec. Issue 41,319-327. 4) Wiens,R.C., Becker,R.H. and Pepin,R.O.(1986): Earth Planet. Sci. Lett. 77, 1 49-158.

Table 1. Rare gas isotopic compositions.

Sample	4He*	3He/4He	20Ne*	20Ne/22Ne	21Ne/22Ne	36Ar*	38A/36Ar	40Ar/36Ar	84Kr#	132Xe#
Y-74159(Eu)	5330	0.00915	11.7	0.8051	0.8695	6.64	1.481	416.8	0.81	0.72
	4300	0.01037	8.87	0.8044	0.8181	6.69	1.495	443.2	0.70	0.75
Y-75015(Eu)$	10100	0.00998	14.5	0.8162	0.8609	6.71	1.493	376.6	0.60	0.89
Y-790260(Eu)	——	0.01255	2.86	0.8185	0.8407	1.68	1.463	898.3	0.14	0.18
	1560	0.01249	3.90	0.8122	0.7956	2.18	1.387	830.7	0.27	0.44
ALH-77005(She)	14.7	0.1653	0.820	0.9283	0.7747	0.414	0.499	638.0	1.36	0.50
700°C	2.4	0.1655	0.141	4.738	0.4498	0.158	0.193	302.1	1.96	1.67
1800°C	26.0	0.2091	1.05	0.9231	0.7345	0.851	0.347	437.9	3.62	1.36
Y-790727(How)	336	0.00226	26.5	4.207	0.5937	2.41	0.602	163.1	0.31	0.21
	480	0.00286	33.0	4.037	0.5991	2.94	0.547	142.1	——	——

* 10^{-8}cm^{3}STP/g. # 10^{-10}cm^{3}STP/g. $ Nagao et al.(1983)

Noble Gas Analysis of Yamato-74013(Di)

Nobuo Takaoka

Department of Earth Sciences, Yamagata University, Yamagata 990.

Yamato-74013 diogenite (4.819 g) was heated stepwise at 700, 900, 1100, 1300, 1500, 1700, 1750 and 1800 C for 30 minutes, and gases released at each temperature step were analysed for isotopic and elemental compositions of all five stable noble gases. Spallogenic gases are predominant in He, Ne and Ar except for ^{40}Ar which is mostly radiogenic, while Kr and Xe are dominated by trapped gases.

Fig. 1 shows release patterns of noble gases. More than 50 % of ^{3}He was released at 700 C, indicating extremely low retentivity of He in diogenite, while ^{21}Ne and ^{36}Ar, mostly spallogenic gases, were released at 1500 C. Large parts of ^{40}Ar and ^{132}Xe appeared in the 700 C fraction. ^{40}Ar is a mixture of radiogenic and atmospheric gases, while ^{132}Xe is mostly of atmospheric origin. This indicates that heavy noble gases adsorbed on sample grains were released at 700 C. The release pattern of radiogenic ^{40}Ar is bimodal having small peaks at 700 and 1300 C, in contrast to that most of spallogenic Ar appeared at 1500 C. This suggests that large part of potassium is concentrated in low-temperature accessary minerals. The release of trapped Kr and Xe is also bimodal with smooth peaks at 1100 and 1500 C.

Fig. 2 is a linear correlation plot of $^{38}Ar/^{36}Ar$ vs. $1/^{36}Ar$. Since both ^{36}Ar and ^{38}Ar compose mainly of the spallogenic gas except for the 700 C fraction, the intercept gives the $^{38}Ar/^{36}Ar$ ratio for spallogenic Ar in diogenite. The ratio is 1.544 +/- 0.027 by least-squares fitting. The $^{38}Ar/^{36}Ar$ ratio for total Ar is 1.48, slightly lower than the ratio given above. This is due to exsistence partially of the atmospheric gas at 700 C and partially of the trapped gas released at higher temperatures. The fraction of trapped ^{36}Ar is very low, only 2.4% of total ^{36}Ar except for the 700 C fraction.

The concentration of spallogenic ^{38}Ar is 1.86×10^{-8} cc/g.

This is 40 % more than the previous result (Nagao and Takaoka, 1979). An exposure age is estimated to be 57 m.y. with an elemental production rate of ^{38}Ar (Freundel et al.,1986), and the chemical composition of target elements (Takeda et al., 1979). Comparison with spallogenic gases given by Nagao and Takaoka (1979) indicates that the present sample is greatly depleted in spallogenic He and Ne (Table 1). From the release pattern (Fig. 1), large parts of He and Ne seem to have been lost from low retentivity sites.

Radiogenic ^{40}Ar is 35.3×10^{-8} cc/g with an assumption that ^{36}Ar released at 700 C is atmospheric and ^{40}Ar at higher temperatures is the radiogenic produced by in-situ decay of ^{40}K. This gives 1.3 Ga for the K-Ar age with the K content of 48 ppm (Kaneoka et al.,1979).

Fig. 3 shows an elemental abundance relative to the cosmic rock (Ozima and Podosek, 1983). The relative abundance for Y-74013 falls between lines for Earth and Mars. The relative abundance such as for Y-74013 has been found in terrestrial pyroxene mirerals separated from Hawaiian volcanic rocks (Rison, 1980). This suggests that diogenite crystallised in a geochemical condition for noble gas composition and partial pressure similar to the Hawaiian volcano, or the abundance pattern for Y-74013 may be typical to pyroxene minerals.

References: Freundel et al.,(1986), Geochim. Cosmochim. Acta,50, 2663; Kaneoka et al.,(1979), Mem. Nat. Inst. Polar Res. Spec. Iss. No.12, 186; Nagao and Takaoka (1979), ibid, No.12, 207; Ozima and Podosek (1983), Noble Gas Geochemistry, Cambridge Uni. Press; Rison (1980), Ph. D. Thesis, Uni. California, Berkeley; Takeda et al.,(1979), Mem. Nat. Inst. Polar Res. Spec. Iss. No. 15, 54

Table 1. Noble gases in Y-74013 diogenite.

	^{3}He	^{4}He	^{20}Ne	^{21}Ne	^{22}Ne	^{36}Ar	^{38}Ar	^{40}Ar	^{84}Kr	^{132}Xe
This work	28.8	200	10.6	11.6	12.7	1.27	1.88	43.5	0.240	0.0652
Nagao-Takaoka (1979)	69.0	531	15.6	16.9	18.4	0.90	1.32	32.1	---	---

Concentration in 10^{-8}cc/g for He, Ne and Ar, and in 10^{-10}cc/g for Kr and Xe.

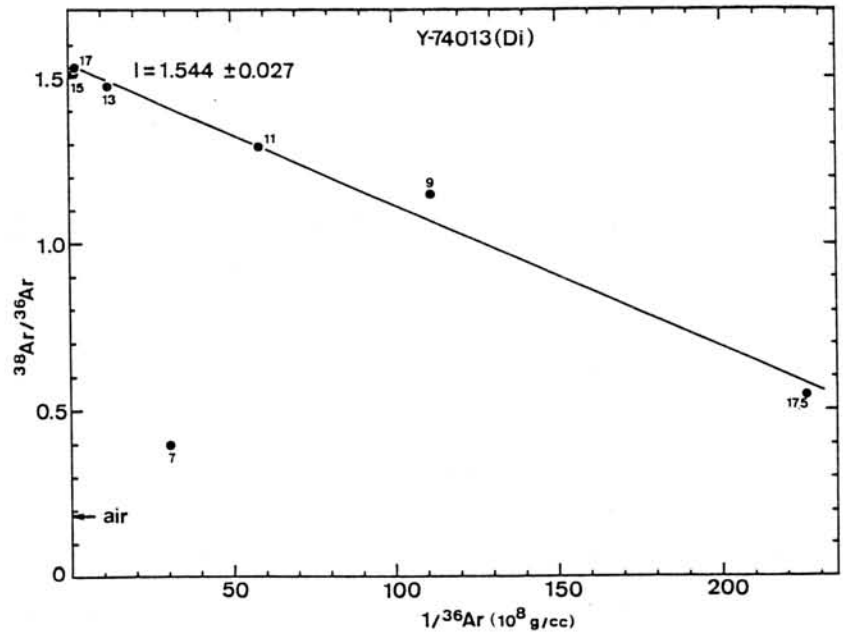

Fig. 2

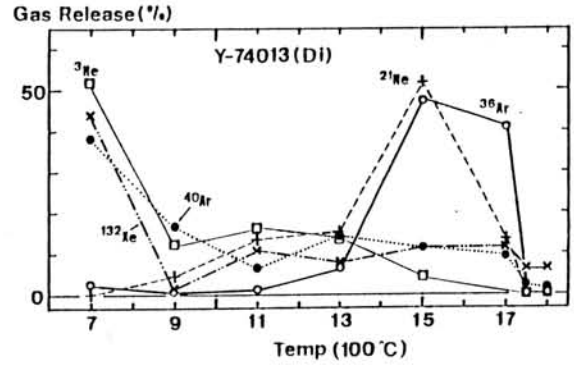

Fig. 1

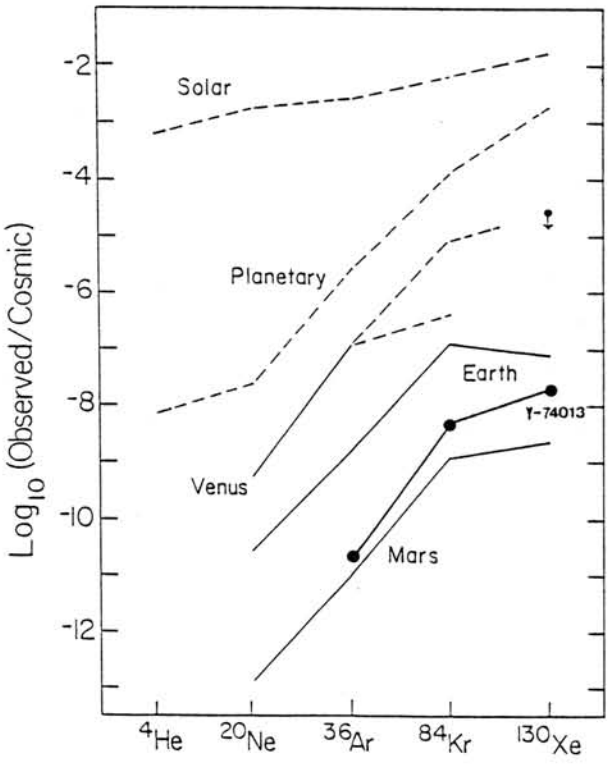

Fig. 3

Comparison between Terrestrial Xe and Xe in Carbonaceous Meteorites; Constraints on the Early History of the Earth

George IGARASHI and Minoru OZIMA

Geophysical Institute, University of Tokyo, Bunkyo-ku Tokyo 113

Components of Xe in carbonaceous meteorites: We compile all published Xe isotope data on carbonaceous meteorites and examine them by a multi-dimensional correlation analysis. We apply "Principal Component Analysis", which is a more refined method of multivariate analyses than those used by previous authers(1, 2). We reestimate compositions of several components of Xe in carbonaceous meteorites such as H-Xe(CCF-Xe), L-Xe and S-Xe and determine the distribution of those Xe isotope data in multi-dimensional space.

Isotopic fractionation of terrestrial Xe: We propose a possible mechanism for isotopic fractionation of terrestrial Xe, that is, mixing of planetesimal-type noble gases(3) which planetesimals have a size distribution. This mechanism can explain the absence of fractionation in terrestrial Kr and Ar.

244Pu-Xe in terrestrial atmospheric Xe and Primitive Xe(U-Xe): Using the results of the multi-dimentional correlation analyses of Xe isotope data on carbonaceous meteorites and fractionation function for terrestrial Xe(mixed planetesimal-type Xe), we examine relation between terrestrial atmospheric Xe and Xe in carbonaceous meteorites. We reestimate the amount of terrestrial atmospheric ^{244}Pu-Xe and composition of primitive Xe(U-Xe) in the solar nebula. Thus estimated fraction of ^{244}Pu-Xe in terrestrial atmospheric ^{136}Xe is 3 ± 1%, which is much smaller than that estimated by Pepin and Phinney(4.65 ± 0.30%).

Constraints on the early history of the Earth: We estimate a lower limit of the formation interval of the Earth relative to the time of formation of primitive meteorites, 70 m.y., by I-Pu-Xe dating. This long formation interval of the Earth may be attributed to significant loss of Xe from the atmosphere due to severe impacts at the late stage of Earth's accretion(4).

References

1. Takaoka N. Mass Spectroscopy, 20, 287-302 (1972)
2. Pepin R. O. and Phinney D., (preprint in 1978)
3. Ozima M. and Nakazawa K., Nature, 284, 313-316 (1980)
4. Cameron A. G. W., Icarus, 56, 195-201 (1983)

NOBLE GAS ENRICHMENT IN VAPOR GROWTH DIAMONDS AND THE ORIGIN OF DIAMONDS IN METEORITES

Fukunaga, K.[1], Matsuda, J.[1], Nagao, K.[2], Miyamoto, M.[3] & Ito, K.[1]

1 Department of Earth Sciences, Faculty of Science, Kobe University, Nada, Kobe 657, Japan
2 Okayama University of Science, Ridai-cho, Okayama 700, Japan
3 College of Arts and Sciences, University of Tokyo, Komaba, Tokyo 153, Japan

Ureilites and some of chondrites are known to have diamonds (1,2). It is conceivable that these diamonds were not shock-induced and directly formed from the solar nebula.

We synthesized diamond and graphite by chemical vapor deposition (C.V.D.) from gaseous mixtures of H_2 and CH_4 including Ar, and examined Ar trapped in carbon by mass spectrometry employing the stepwise heating technique (3). The concentrations of CH_4 were 0.5 , 1 and 5 vol%, respectively and Ar was 4 vol%. According to X-ray diffraction analyses, only diamond or graphite was detected and high CH_4 concentrations seem to favor the growth of graphite. The concentration of ^{36}Ar as great about as $8\times10^{-6}cm^3STP/g$ was extracted at the 2000°C fraction for diamond, while graphite was almost gas-free (3).

In this study, we used similar gaseous mixtures (concentrations of CH_4 1 vol%) including Ar and He (concentrations of Ar and He 1 and 5 vol%, respectively) to examine the fractionation of rare gases. A schematic drawing of the experimental apparatus is shown in Fig.1. Gases were being evacuated by a rotary pump and were fed into a quartz discharge tube to be ionized in a microwave oven for home use. The obtained results are given in Table 1. The $^4He/^{36}Ar$ ratios in the synthesized diamond were nearly equal to that of the gaseous mixture where diamond was synthesized. Therefore, it is concluded from this study that there was no fractionation between He and Ar during the vapor growth of diamond. The released patterns of ^4He and ^{36}Ar were in Fig.2, which shows the major

peaks for these gases at the 2000 ℃ fraction. Those of ^{36}Ar show the small secondary release peak at 1400 ℃, which was also observed in our previous experiment (3). It is not clear whether these small peaks are originated from another carbon phase like amorphous carbon rather than diamond. There was no secondary peak at 1400 ℃ for He. Both concentrations of ^{4}He and ^{36}Ar in the sample #16 was not five times as much as that in the sample #17, although the rare gas concentration of the gaseous mixture to produce sample #16 is five times as much as that for the sample #17. This leads us to consider that the concentration of rare gases trapped in our synthesized diamond have already been saturated by rare gases because the rare gas pressure of the atmosphere was too high. In our previous study (3) we estimated a concentration of ^{36}Ar trapped in diamond synthesized in the solar nebula to be $9.1 \times 10^{-9} cm^3 STP/g$ which is 3 to 4 orders in magnitude smaller than that in the diamonds in ureilites . This was on the assumption that the concentration of ^{36}Ar trapped in diamond by vapor growth is proportional to the partial pressure of ^{36}Ar. From this work it may be concluded that the concentration of ^{36}Ar trapped in diamond in the solar nebula could be much higher than our previous estimate because of saturation.

Ionization could have occurred in the solar nebula due to either lighting, shock wave, or solar wind etc. The major element of the solar nebula was hydrogen. The dominant carbon compound, CO, progressively transforms to CH_4 on cooling by the reaction $CO+3H_2$ CH_4+H_2O (4). About 1% CH_4 or less is enough to produce diamonds. Therefore, the condition of gaseous mixture to form diamonds could have been satisfied in the solar nebula. Vapor-growth diamonds should have been widely observed in the meteorites (2).

References: (1) Vdovykin, G. P. (1970) Sp. Sci. Rev., 10, 483-510. (2) Lewis, R. S., Ming, T., Wacker, J. F., Anders, E. & Steel, E. (1987) Nature, 326, 160-162. (3) Fukunaga, K., Matsuda, J., Nagao, K., Miyamoto, M. & Ito, K. (1987) (Submitted to Nature). (4) Grossman, L. & Larimer, J. W. (1974) Rev. Geophys. Space Phys., 12, 71-101.

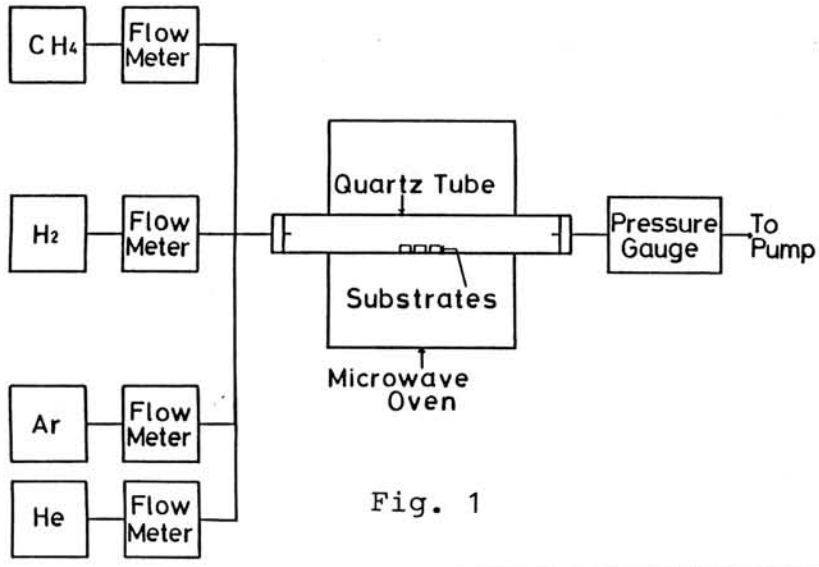

Fig. 1

Sample Number	Temperature (°C)	^{4}He ($\times10^{-6}$cm^{3}STP/g)	^{36}Ar ($\times10^{-8}$cm^{3}STP/g)	(^{4}He/^{36}Ar)diamond / (^{4}He/^{36}Ar)gas	Gas Concentration(%) CH_4	H_2	He	Ar	Total Pressure (Torr)
	800	0.87	1.5						
	1100	4.4	6.7						
	1400	43	28						
#16	1700	120	3.3		1	89	5	5	30
(diamond)	2000	720	170						
	2100	0.38	1.4						
	Total	890	210	2.1					
	800	0.17	1.2						
	1100	5.1	3.9						
	1400	33	29						
#17	1700	39	6.2		1	97	1	1	30
(diamond)	2000	240	110						
	2100	0.60	1.7						
	Total	310	150	0.81					

Table 1

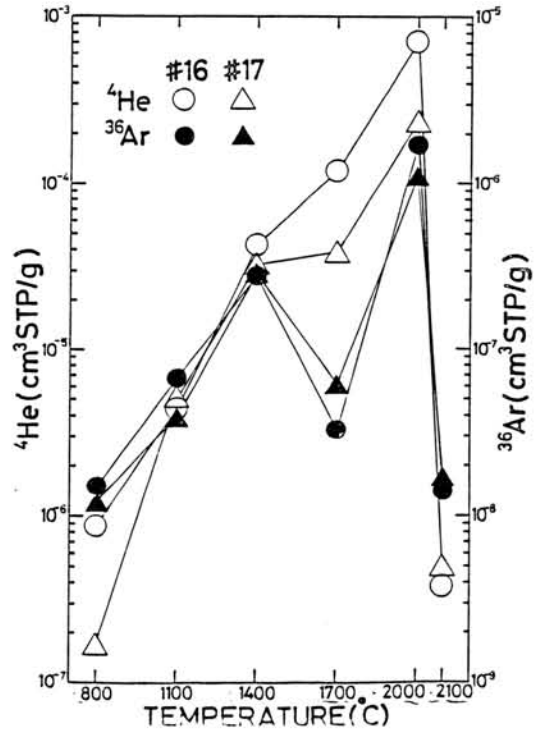

Fig. 2

Solar type He and Ne in diamonds

Ozima, M. and S. Zashu, Geophysical Institute, University of Tokyo, Tokyo 113, JAPAN

Because of the enormous stability against chemicals and high temperature, and also of extreme antiquity of some diamonds, they would offer unique information as to ancient noble gas state in the mantle, which is vital in understanding the origin and evolution of the earth. We have been investigating noble gas elemental and isotopic compositions in more than one-hundred diamonds from various localities. Owing to extremely small amount of noble gases in diamonds, we have so far been successful only in measuring precise isotopic compositions of He and Ne in some diamonds. Within our experimental uncertainties, heavier noble gases (Ar, Kr, Xe) are indistinguishable from atmospheric ones.

In Fig. 1, we compiled all $^3He/^4He$ data analysed in our laboratory. Data also include those obtained by Berkely gourp (1). Other typical terrestrial materials are also compared. $^3He/^4He$ ratio in diamonds extends far above those in the other terrestrial materials and even exceeds He-Ar or planetary helium ($^3He/^4He=1.4X10^{-4}$), being close to a solar helium ($^3He/^4He=4X10^{-4}$). Since there are no likely sources for ^3He production in the mantle except for a primordial one and therefore $^3He/^4He$ ratio only decreases owing to radioactive decay of U, Th, we suggest that primordial helium in the earth was a solar helium. The supposition is further supported by discovery of solar-like neon in one Australian diamond by Berkeley group (1) and in Zaire diamonds by us.

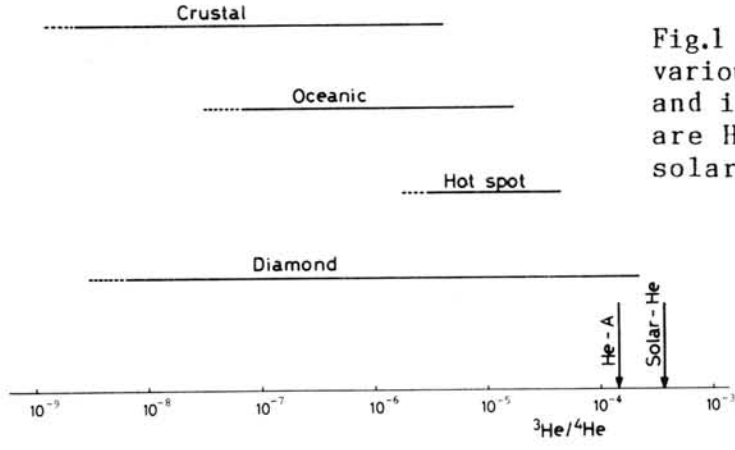

Fig.1 He-3/He-4 ratio in various terrestrial materials and in diamonds. Also shown are He-A or planetary He and solar He.

Fig.2 Shows neon isotope data obtained for Zaire cubic diamonds for which we applied a K-Ar isochron dating (2) . Neons in these diamonds are clearly non-atomospheric, but close to a solar neon. Spread in the isotopic composition displayed in the three isotope plot (Fig.2) is attributable to contamination of varied amount of air neon as demonstrated in Fig.3. Deviation in $^{21}Ne/^{22}Ne$ ratios from a solar Ne ratio is attributable to nuclear reactions $^{18}O\ (\alpha,n)\ ^{21}Ne$ and $^{24}Mg\ (n,\alpha)\ ^{21}Ne$ in the diamonds.

If the earth trapped meaningful amount of solar type noble gases as infered from helium and neon isotopic data in diamonds, this has far-reaching implications on the state of primitive solar nebula. For example, we must consider seriously possibilities that earth accreting materials in comparatively small size ($\lesssim$cm) were once subjected to intense solar wind implantation, or primitive solar nebula had noble gases similar to those observed in the solar wind but not planetary noble gases as generally assumed.

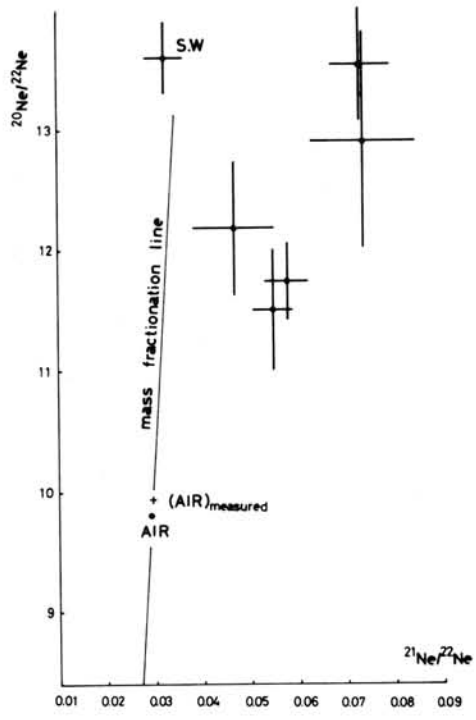

Fig.2 Ne isotopic composition of Zaire diamonds displayed in a three isotope plot. (Air) measured indicates an average measured value of air Ne.

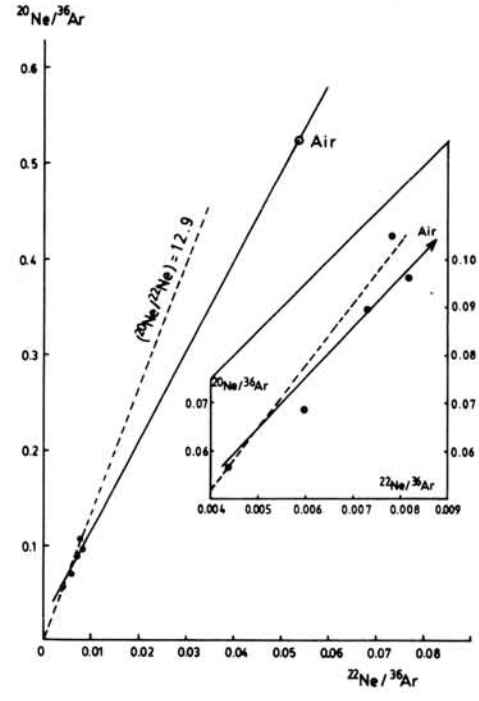

Fig.3 Diamond Ne data lie approximately on a mixing line between air Ne and "diamond Ne"(not shown). Dotted line corresponds to a minimum Ne-20/Ne-22 ratio in "daimond Ne".

(1) Honda, M., J.H. Reynolds, E. Roedder and S. Epstein (1987) Noble gases in diamonds, J. Geophys. Res. (in press).
(2) Zashu, S. and M. Ozima (1986) K-Ar isochron data of Zaire diamonds, Nature, 323, 710-712.

$^3He/^4He$ ratios in a sedimentary rock from K-T boundary, Hokkaido and in Fig Tree shales

Sachiko AMARI[1], Minoru OZIMA[1] and Yozo HAMANO[2]
1) Geophysical Institute, Faculty of Science, University of Tokyo, Bunkyo-ku, Tokyo 113, Japan
2) Earthquake Research Institute, Universitiy of Tokyo, Bunkyo-ku, Tokyo 113, Japan

We studied He isotopic ratios and He contents in a sedimentary rock from K-T boundary in Hokkaido in Japan and Fig Tree shales.

(a) A sedimentary rock from K-T boundary in Hokkaido in Japan

It is well known that many sedimentary rocks from K-T boundary have high Ir content (e.g. ~9ppb for Italian limestones from Gubbio[1]). Whether the enrichment of the siderophile element comes from meteoritic impact debris or from mantle materials erupted from volcanos is not settled yet. Several isotopic investigaions have been done until now. However we still do not have defenite isotopic evidence, by which we can check which of these hypothesis is more likely. Therefore we measured He isotopic ratios and contents of a sedimentary rock from K-T boundary. Besides a bulk sample, we measured acid residue leached by HCl-HF mixtures. In both samples, ^3He content is scarce, so that we could only determine the upper limits of $^3He/^4He$ ratios (6×10^{-6} for bulk sample and 1.4×10^{-5}).

(b) Fig Tree shales

A decade yeas ago, Frick and Chang[2] analysed noble gases of carbon phases (kerogen) in Fig Tree shales. They found high $^3He/^4He$ ratios (up to 1.5×10^{-4}) and elemental abundance patterns which are similar to that of carbonaceous matter in Murray meteorite (C2). They considered that this fact will be a key to understand the trapping mechanism of noble gases in meteorites.

To confirm this results, we studied He of bulk samples of two Fig Tree shales. We found very small amount of ^3He ($\leq 10^{-13}$ cm^3 STP/g) and we could only determine the the upper limits of $^3He/^4He$ ratios (10^{-7} to 10^{-8}). Using carbon content in Fig Tree shales (~1%[3]) and the data by Frick and Chang ($^3He/^4He$ = 1.2×10^{-4}, ^4He ~ 1×10^{-6} cm^3 STP/g), we should expect ^3He content of order of 10^{-11} to 10^{-10} cm^3 STP/g in the bulk samples. However we found that ^3He content is two or three orders of magnitute smaller than that expected from their data. At present, we determine whether this discrepancy is due to sample heterogeneity or to experimental artifact.

REFERENCES

(1) Alvarez, W. L. et al. Science, 208, 1095-1108 (1980)
(2) Frick, U. and Chang, S. Proc. Lunar Sci. Conf. 8th, 263-272 (1977)
(3) Holland, D. H. The chemical evolution of the atmosphere and Oceans. 140 (1984)

55—1

SIGNIFICANCE OF THE GEOSCIENCE IN THE DUOLUN CRATER IMPACT EVENT

Wu Siben[1], Zhang Shuyuan[2]

1. Institute of Mineral Deposits, Chinese Academy of Geological Sciences, Baiwanzhuang Road, Beijing, China
2. Department of Geology, Peking University, Beijing, China

The Duolun impact crater is located in the border between the Hebei province and the Inner-Mongolia, at 42°3'N, 116°15'E, It is a multiple ring structure. The inner ring is a 70km diameter outlined by the Luan river, The Shandian river and their tributaries which form a circle. The outer ring is about 190km diameter, and the middle ring is about 120km diameter. Therefore, the Duolun impact crater has become the largest impact crater in the world.

At the western part of this circle, the Heichengzi middlingsize coal field has been found by drilling and consists of the Lower Cretaceous coal-bearing formation which has no surface expression and has been covered by the Tertiary and Quaternary sediments at this peripheral trough. At the easten part of the circle the Meiyaogou coal deposit also has been found by drilling. According to the drilling data the peripheral trough is more than 600 meters in depth and up to 6km in width.

The target rocks of the crater are: granodiorite-porphyry, shale, siltstone, sandstone, limestone and the Upper Jurassic andesite, etc. The various impact melts are predominantly found at the surface of the crater, but relatively small masses of impact breccia have been identified.

The age of the Duolun crater may be between Jurassic period and Cretaceous period, because one of the target rocks is the Upper Jurassic andesite, and the Lower Cretaceous coal-bearing formation occurs on the peripheral trough in the Duolun crater.

According to potassium-argon age determinations, the impact melting rock of Duolun has an age of 129 ± 2 m.y. It is worthwhile to note that the isotopic age of the Jura-Cretaceous boundary, which value is between 144 m.y. and 130 m.y., has always been an item for debate. It could thought that the age of the melting rocks in the Duolun impact crater could possibly provide a more reasonable answer, at least in the North-eastern Asia.

We have discovered the paleontologic mass extinction during the Juro-Cretaceous boundary, maybe induced by the Duolun impact event.

According to the existing paleontological information 3,4, the extinction rate is 86% in the Bivalvia, 37% in the Sporo-pollen in the Shihebei formation (J_3), also, the new born rate is 92% in the Bivalvia, 50% in the Sporo-pollen in the Chengzihe formation (K_1).

W.Alvarez 5 pointed out, when astroids impact the Earth, several months of darkness and violent changes of temperature could be the cause of death for these lifeforms. Some scientists believe in their papers on Nuclear Winter: the dust and smoke caused by a large scale global nuclear war could yield the fact that the temperature below zero could last for a few months. According to S.L.Thompson 6, the large scale global nuclear war could release energy about 3×10^{20} J. We use the outer ring diameter (190 km) to estimate the energy that was release by the Duolun cratering: 4×10^{23} J. and that is 1000 times of those of the global thermal nuclear war. Therefore, it follows that the Duolun impact event could have caused the large death of the lifeforms at that time.

REFERENCES: (1) Wu Siben (1986) China Geol. News, 10 Oct. (2) Wu Siben (1987) 18th Lunar Planet. Sci. Conf., (3) Li Zishun, Yu Xihan (1982) Bull. Shenyang Inst. Geol. Min. Res., Chinese Acad. Geol. Sci., No. 5, pp. 156-216. (4) Pu Ronggan, Wu Hongzhang (1982) Bull. Shenyang Inst. Geol. Min. Res., Chinese Acad. Geol. Sci., No. 5, pp. 444-478.

(5) W.Alvarez et al. (1982) Geol. Soc. Amer., Special paper 190, pp. 305-315. (6) S.L.Thompson et al. (1984) Nature, 310, pp. 625-626.

The multiple ring structure of Duolun

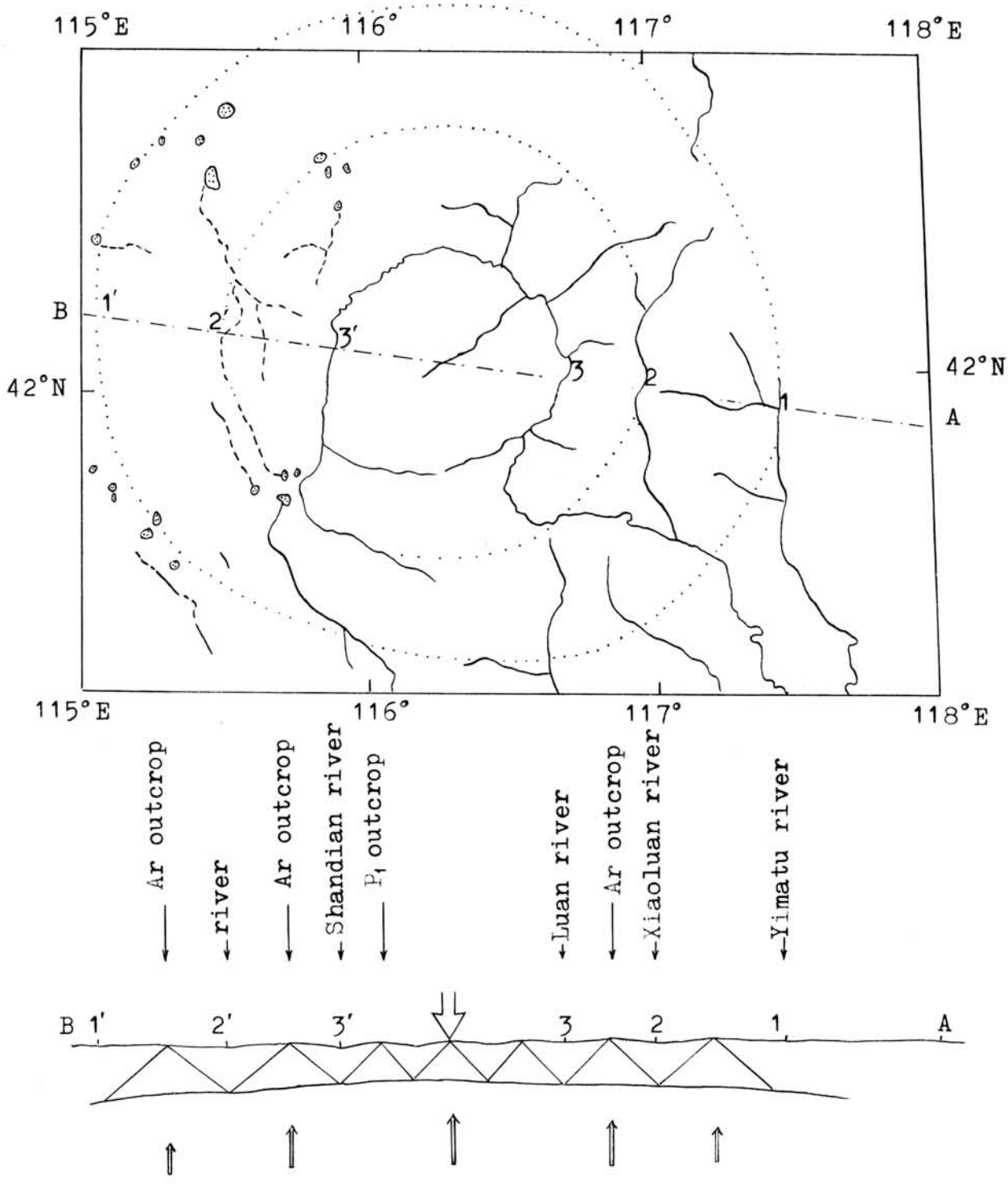

Ar: Archean metamorphic rocks

P_1 : Lower Permian limestone

HYDRATION BANDS AROUND 3 μm AND WEATHERING OF METEORITES

Miyamoto, M.

College of Arts and Sciences, University of Tokyo, Komaba, Tokyo 153

We measured infrared diffuse reflectances (2.5-25 μm) of serpentine-olivine mixtures and some Antarctic meteorites to study the degree of weathering. Absorption bands around the 3 μm wavelength region show evidence of the presence of hydrates or hydroxyle, because the bands are due to the OH streching vibrations. The band strength near 3 μm may be dependent on the degree of weathering (1), because terrestrial weathering produces hydrates.

Measurements were made with a JASCO FT/IR-3 Fourier transform infrared spectrophotometer equipped with a diffuse reflectance attachment. Details of measurements are described in (2). Powder samples (<100 μm in size) of serpentine and olivine (San Carlos) were used to make mixtures. Powder samples of Antarctic meteorites we used were supplied from N.I.P.R. The results of reflectances are shown in Figs. 1 and 2. We define the strength of hydration bands by the shaded area near 3 μm in Fig. 1 to study the degree of weathering. We subtracted the background curve by the polynomial approximation from the reflectance curve to obtain the band strength.

Fig. 3 shows the correlation between the area (strength) of hydration bands near 3 μm and the amounts of serpentine in the serpentine-olivine mixtures. The area is related to the amounts of serpentine. Up to about 10 % of serpentine in the serpentine-olivine mixtures, the area is almost proportional to the amounts of serpentine (Fig. 3). Small amounts of serpentine can be detected by the absorption feature of the 3 μm wavelength region (Fig. 2).

Table 1 shows the results of the band strengths for some Antarctic meteorites and Allende (C3)(fell 1969) and Nuevo Mercurio (H5) (fell 1978) for comparison. These two meteorites show weak band strengths. The Allan Hills meteorites measured show significantly stronger hydration bands than the Yamato meteorites measured. This suggests that the Allan Hills meteorites are more weathered than the Yamato meteorites. Nishiizumi and Elmore (1985)(3) reported that the Allan Hills meteorites clearly show longer terrestrial age than other Antarctic meteorites on the basis of cosmic ray produced nuclide data. Our results are consistent with their results.

The strength of hydration bands around 3 μm has potential for quantifying the degree of weathering. Further studies combined with terrestrial age data are required.

We thank National Institute of Polar Research for the meteorite samples and Dr. K. Ozawa for the serpentine sample.

References: (1) Salisbury J. W. and Hunt G. R. (1974) J. Geophys. Res., 4439-4441. (2) Miyamoto M. (1987) Icarus, (in press). (3) Nishiizumi K. and Elmore D. (1985) Papers presented to the 10th Symposium on Antarctic Meteorites, 108-109. (4) Yanai K. and Kojima H. (1985) Meteorites News, Vol. 4, No. 1.

Table 1. Band strengths near 3 μm of some meteorites.

Meteorites	Band strength	Degree of weathering*
Allende (C3)	22	-
Nuevo Mercurio (H5)	23	-
Yamato-75097 (L6)	31	-
Yamato-74156 (H4)	45	A
Yamato-74647 (H5)	46	A
Yamato-74191 (L3)	64	A
ALH-769,10 (L6)	70	B
ALH-769 (L6)	75	B
ALH-77299 (H3)	85	A
ALH-765 (Euc)	85	A
ALH-77003 (C3)	93	A

* Yanai and Kojima (1985)

Fig. 1. Infrared reflectance curves of some meteorites.

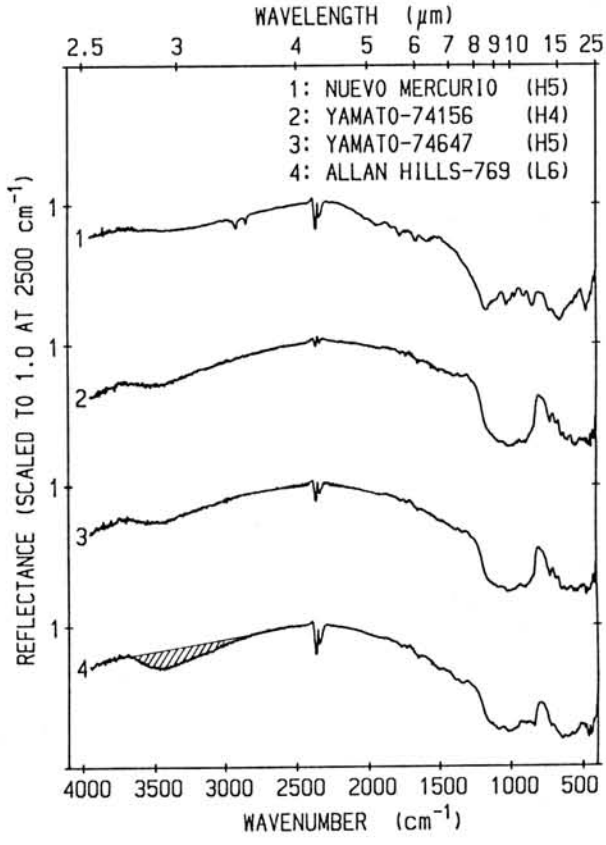

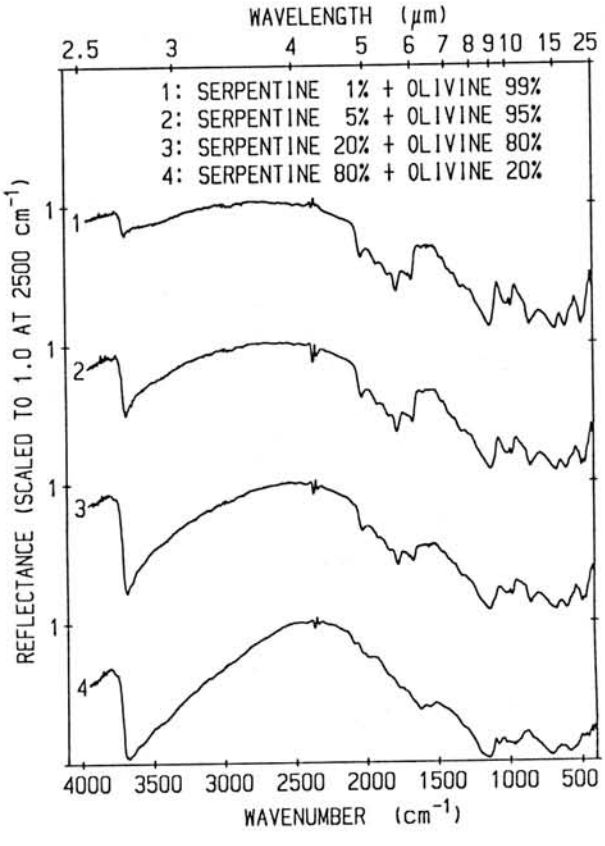

Fig. 2. Infrared reflectance curves of serpentine-olivine mixtures.

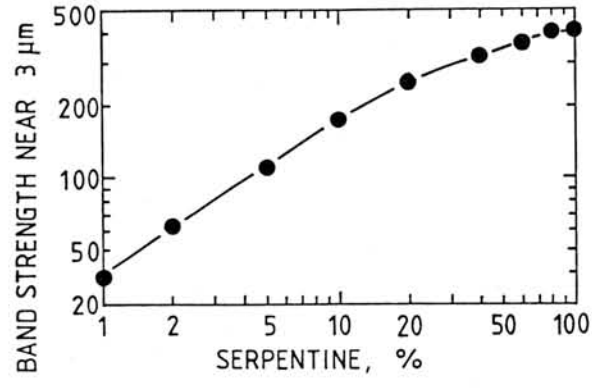

Fig. 3. Correlation between band strengths near 3 μm vs. amounts of serpentine in serpentine-olivine mixtures.

Orbit of the Allende meteorite
-- Is the Allende meteorite an extinct cometary nucleus? --

Takafumi Matsui and Eiichi Tajika
Geophysical Institute, University of Tokyo

Orbit of meteorite is one of the most fundamental informations to consider the origin of meteorite and solar system bodies. However, so far, orbit of meteorite has been succesfully determined for only 3 meteorites based on the analysis of local camera network observation of the fireball phenomena (1). All the meteorites whose orbits were thus determined are ordinary chondrites. There has been no report on orbit of other type of meteorites. This is because fall of meteorite is random and thus it is hard to cover every fall by such a local camera network system.

In this paper we try to infer orbit of meteorite by analysing the space-distribution of individual fragments of a single meteorite shower. We think this sort of analysis is the only possible way to clarify orbital information and atmospheric breakup process of some specific meteorite and is useful even though significant uncertainties are accompanied with this method.

Allende meteorite is one of the most important extraterrestrial materials and also the largest meteorite shower obseved to date. It seems, therefore, appropriate for this sort of analysis. To study the space-distribution of Allende individual fragments we conducted field work studies of the Allende fall area in 1984 and 1985 (2). Through these studies we find that the size of individual fragments decreases with increasing the distance from the point where the largest fragment was found (Figure 1).

Surface of almost all the individual fragments collected during these fieldwork studies is entirely covered by crust, which strongly suggests that the fragmentation occured at upper atmosphere. Since the impact velocity of meteorite into the earth's atmosphere has been reported to be around 15-20 km/sec (1), we can estimate the height of fragmentation if we know the strength of Allende meteorite (3). We are measuring the strength but have not yet completed. However, judging from other physical properties so far measured, we may assume that the strength is around 100 bars.

There is no reason to consider that the fragmentation did not occur once at the same moment. Ejecta velcity is considered to be much smaller than the impact velocity and so the trajectory of individual fragment does no depend on ejecta velocity. We assume the ejects velocity to be zero.

Shape-distribution of the Allende individual fragments indicates that the shape clusters around sphere, which is a remarkable difference from that of Antarctic chondrites and ejecta produced by impact experiments (2). We can thus reasonably assume the shape of the Allende individual fragments to be sphere. Then we can calculate trajectory of the Allende individual fragments.

In Figure 2 we show the numerical results of some typical

cases. By comparison between observation and numerical results (Figure 1), we can determine plausible sets of parameters such as impact velocity and angle. The results are summarized in Table 1.

We can calculate the orbital elements by using the above results. The derived orbital elements are also listed in Table 1. The orbit of model A is shown in Figure 3. Although the semi-major axis varies significantly with impact velocity, high inclination and eccentricity of the Allende meteorite are very close to those of short-period comet. Parent body of the Allende meteorite might be a nucleus of extinct comet.

References

(1) ReVelle, D.O. (1979) J. Atmos. Terres. Phys. 41, 453-473.
(2) Nagasawa, H. et al. (1987) Report on Overseas Scientific Research Project (Nos. 59042011, 60041064, and 61034059).
(3) Passey, Q.R. and H.J. Melosh (1980) Icarus 42, 211-233.

Table 1. Results on impact parameter and orbital element

Model	A	B	C
V(km/s)	20.0	18.0	15.0
H(km)	28.0	26.4	23.7
θ(°)	24.5	23.0	19.5
α(°)	98.58	95.63	86.24
δ(°)	-34.27	-37.20	-44.77
V_∞(km/s)	39.00	37.31	34.61
a(AU)	3.46	2.32	1.56
e	0.72	0.58	0.37
i	21.56	19.57	15.67
ω(°)	26.64	23.61	14.60
Ω(°)	141.79	141.79	141.79
P(year)	6.43	3.54	1.96
q(AU)	0.96	0.97	0.99
q'(AU)	5.96	3.68	2.14

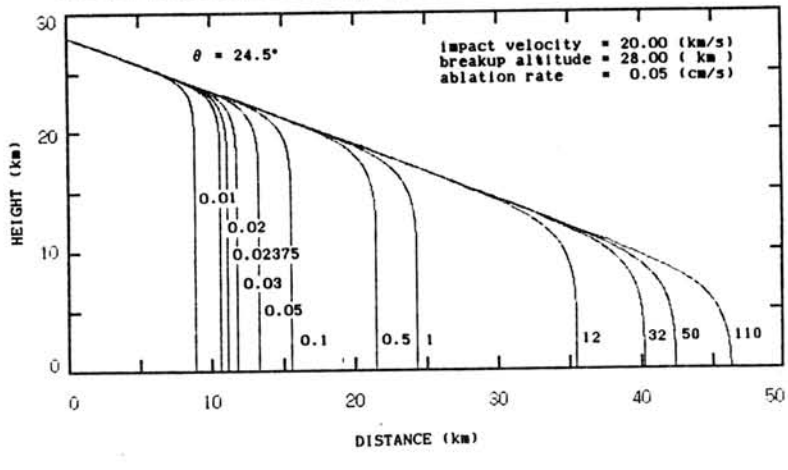

Figure 2

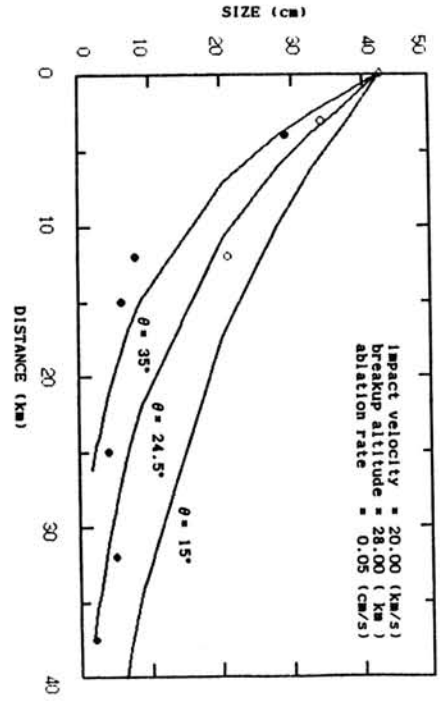

Figure 1

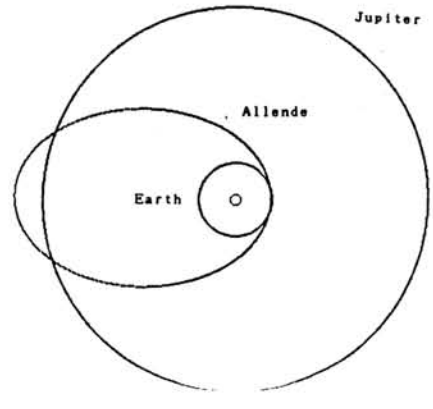

Figure 3

Magnetic susceptibility anisotropy and porosity of chondrites; A review.

N.Sugiura* and D.Sneyd**

*Geophysical Institute, Univ. of Tokyo, Tokyo, JAPAN
**Dept. of Geological Sciences, Univ. of Tennessee, Tennessee, U.S.A.

A fair number of data on magnetic susceptibility anisotropy and porosity of chondrites have been accumulated since the early studies [1,2]. The negative correlation between the anisotropy and the porosity still persists among L+LL chondrites. The anisotropy and porosity are not dependent on the metamorphic grade of chondrites. K-Ar ages of strongly anisotropic chondrites tend to be younger than those of less anisotropic chondrites. These observations suggest that impacts which reset the K-Ar ages produced the anisotropy and reduced the porosity of chondrites.

In the case of H chondrites, however, the relation between the anisotropy and the porosity is obscure. It may be that the H chondrites experienced a different thermal history.

References

[1] Y.Hamano, Proc. 15th ISAS Lunar & Planetary Symposium, (1982) 301.
[2] N.Sugiura and D.W. Strangway, Geophys. Res. Lett. 10 (1983) 83.

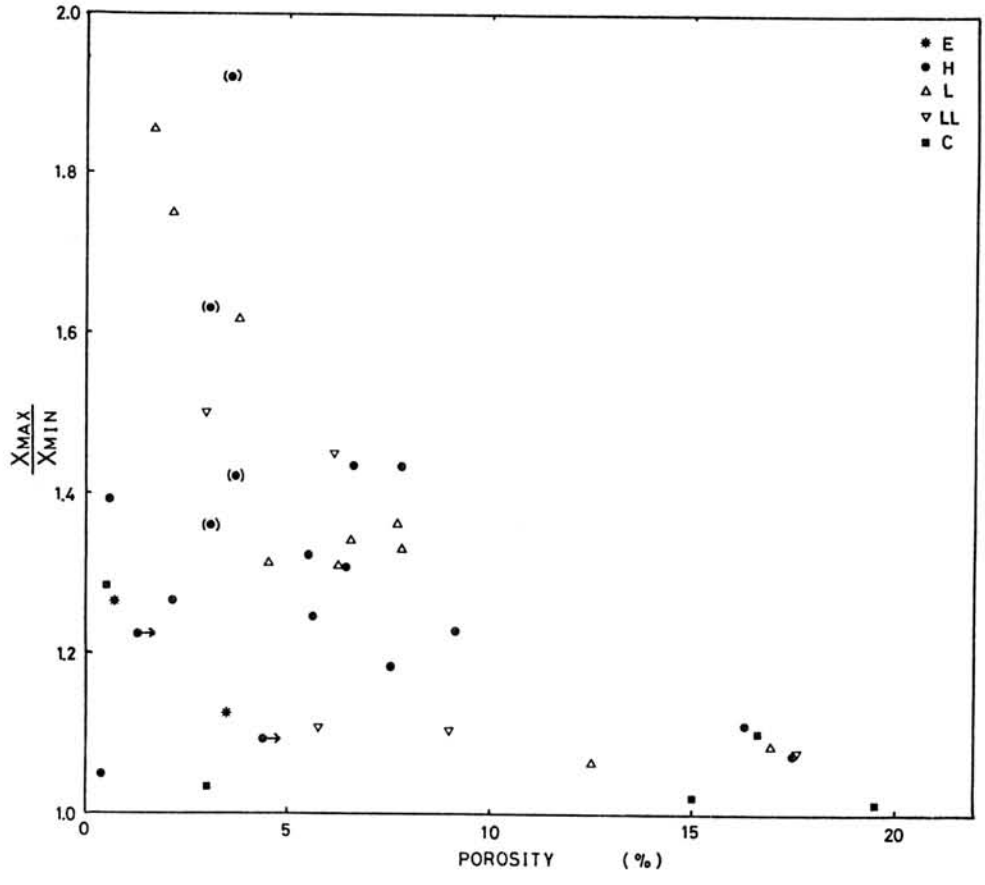

Hysteresis and NRM properties of meteorites

N.Sugiura* and D.W. Strangway**

*Geophysical Institute, Univ. of Tokyo, Tokyo, JAPAN
**University of British Columbia, Vancouver, BC., CANADA

Magnetic properties of various meteorites are reviewed. Natural remanent magnetization vs. saturation remanent magnetization diagrams for carbonaceous chondrites, ordinary and enstatite chondrites, and differentiated meteorites are shown in Figs 1~3, respectively.

The intensity of natural remanent magnetization (NRM) is nearly proportional to the intensity of saturation remanent magnetization (Jrs) in achondrites and carbonaceous chondrites. The NRM in these meteorites is stable against alternating field demagnetization. We consider this NRM to reflect the magnetic field that was present in the early solar system. The correlation between the NRM intensity and the Jrs intensity in ordinary chondrites is weak. Since the coercive force of kamacite in ordinary chondrites is very small, it is possible that the extraterrestrial remanence in many ordinary chondrites is dominated by a soft, spurious remanence.

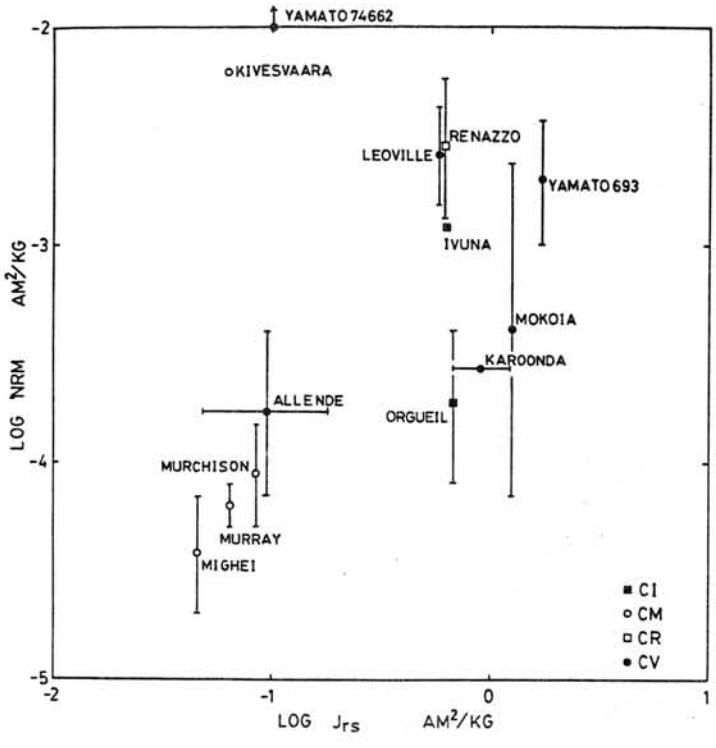

Fig.1
NRM vs. Jrs diagram for carbonaceous chondrites.

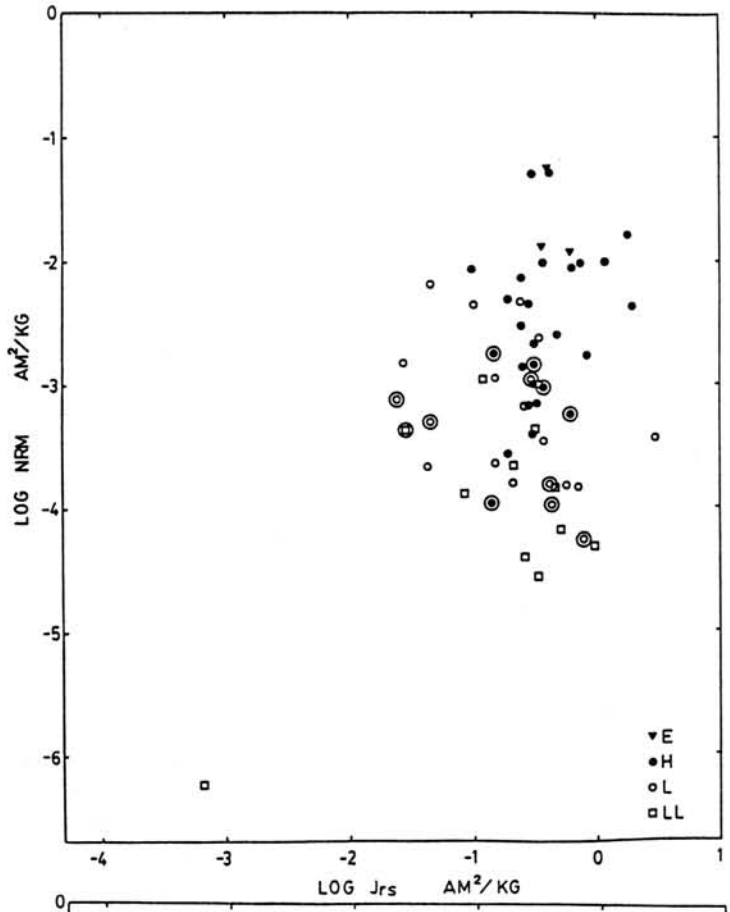

Fig.2
NRM vs. Jrs diagram for ordinary and enstatite chondrites.

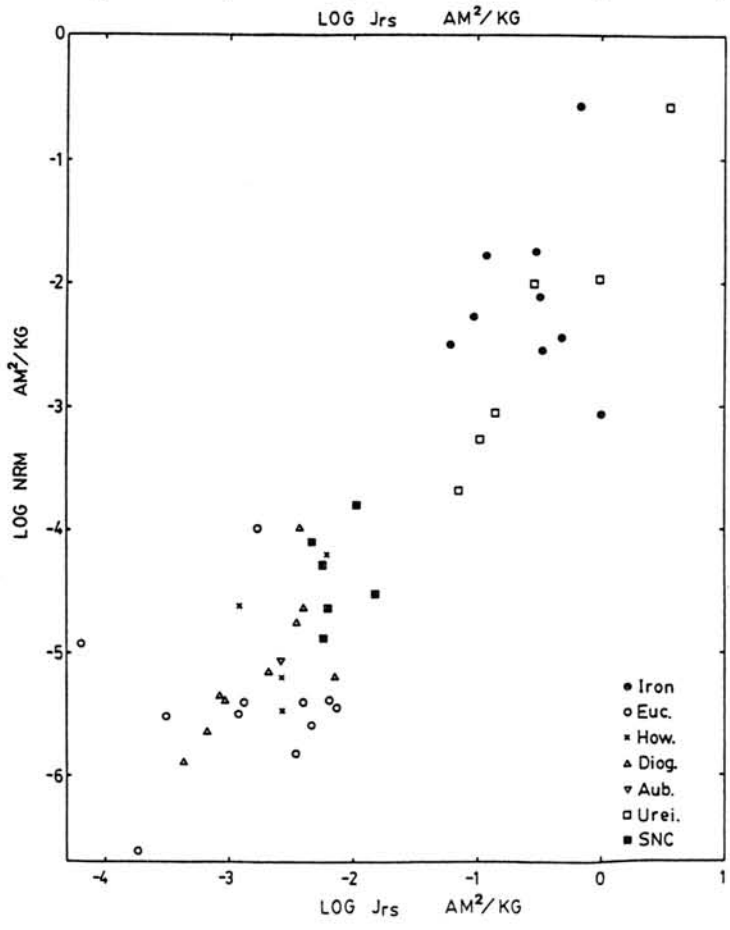

Fig.3
NRM vs. Jrs diagram for differentiated meteorites.

Magnetic and metallographical studies of Bocaiuva iron meteorite

M. Funaki[1], I. Taguchi[2], J. Danon[3] and T. Nagata[1]

1: National Institute of Polar Research, Tokyo
2: National Museum of Japanese History, Sakura City
3: National Observatory, Rio de Janeiro, Brazil

It would be fundamentally significant to clarify the magnetic properties of iron meteorites to understand generally various magnetic behaviours of stony meteorites. It has been recently found that the natural remanent magnetization (NRM) of "Bocaiuva" iron meteorite is extremely stable, though no evidence of presence of tetrataenite phase has been detected. (Araujo et al., 1984). The problem why and how this iron meteorite has acquired the stable NRM is studied in the present work.

The Bocaiuva has a very stable NRM against the AF-demagnetization by more than 500 Oe. The original intensity of NRM ranges widely from 1.1×10^{-1} to 6.0×10^{-3} emu/g. The NRM direction is distributed approximately along a great circle over a hemisphere, as shown in Fig. 1. The intensity and direction of NRM during thermal demagnetization up to 500°C are stable, showing only small changes. The thermal demagnetization characteristics of the Bocaiuva are similar to those of tetrataenite (Funaki et al., 1986).

Thermomagnetic curves of bulk samples of the Bocaiuva indicate kamacite and a small amount of taenite as the main magnetic components, showing no evidence for presence of tetrataenite, magnetite and pyrrhotite. Both coercive force (H_C) and remanence coercive force (H_{RC}) are small, being H_C=40 Oe and H_{RC}=25 Oe in the original pre-heating state. After heating to 850°C, both H_C and H_{RC} values become further smaller.

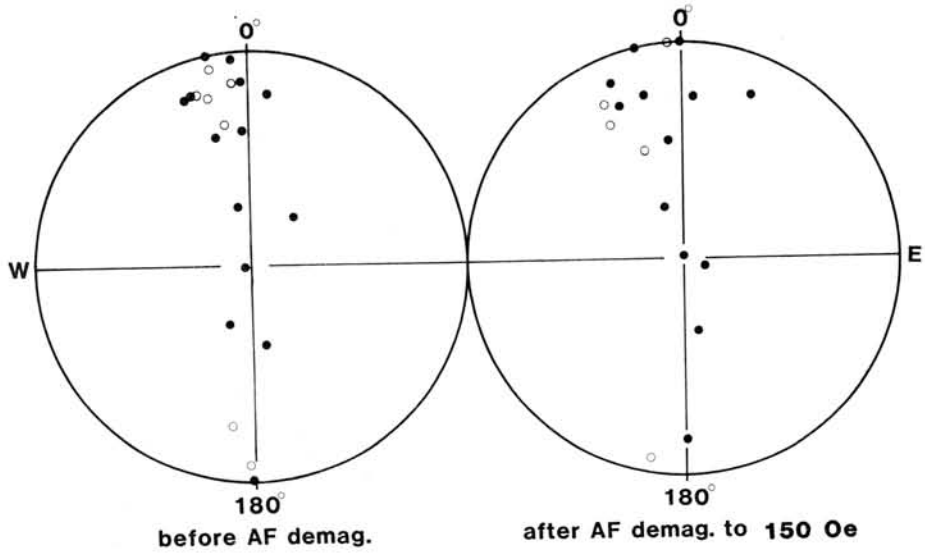

Fig. 1 NRM distributions of Bocaiuva

By microscopical observations and EPMA analyses, opaque minerals are identified as kamacite, taenite, plessite, shcreibersite pyrrhotite and magnetite. Elemental distributions of Fe, Ni, Co and P are examined and mapped by computer-aided microanalyzer. Polished surface of the Bocaiuva is painted by magnetic coloid to see the magnetic minerals. Strong NRM areas, suggesting tetrataenite, are observed to some of taenite lamellae and limbs of isolated small taenite grains in kamacite. The dominant directions of tetrataenite lamellae are observed likely almost parallel to the NRM directions. However, these tetrataenites disappear in the samples heated to 750°C by means of the magnetic coloid method. Furthermore, magnetic multi-domain structures of 5μ in domain-width appear clearly on the surface of kamacite as shown in Fig. 2. The magnetite coloid do not concentrate obviously in the surface of pyrrhotite.

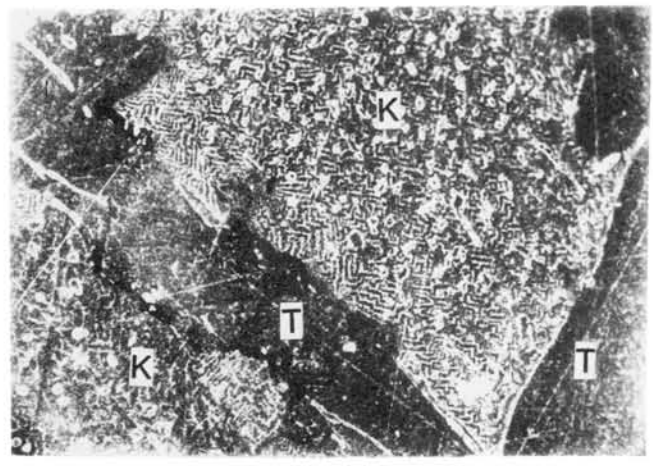

Fig. 2 Magnetic domain structures in kamacite
K: kamacite, T: taenite

From these experimental results, it may be concluded that the tetrataenite exists as the main NRM mineral in the Bocaiuva. This is the main reason why the Bocaiuva has the stable NRM compared with ordinary octahedrites. The influences of kamacite and other magnetic minerls on NRM may be small. The NRM distributions along a great circle may be explained by the dominant direction of tetrataenite lamellae. Since an amount of tetrataenite is so small compared with kamacite, it can not be identified as tetrataenite by Mössbauer spectroscopy, thermomagnetic curves and magnetic hysteresis curves.

References

Araujo, S.I., Danon, J., Scorzelli, R.B. and Azevedo, I.S. (1984). Meteoritics, 18, 261.

Funaki, M., Nagata, T. and Danon, J. (1986), Mem. Natl. Inst. Polar Res., Spec. Issue, 41, 382-293.

Magnetic Analysis of Antarctic Stony Meteorites on the Basis of Magnetic Coercivity

Takesi NAGATA
Nat'l Inst. Polar Research, Tokyo

1. Introduction

The ratio of remanence coercive force (H_{RC}) to coercive force (H_C) of an assemblage of randomly oriented ferromagnetic particles of nearly same composition and structure, which are non-interactively dispersed in non-magnetic matrix, such as natural rocks, generally ranges between 1.2 and 5.0 where H_{RC}/H_C=1.2~1.8 corresponds to the case of uniaxial magnetic anisotropy such as single-domain particles or single crystals of Fe-Ni γ' phase, while H_{RC}/H_C=4~5 corresponds to the case of multi-domain particles having weak magnetic anisotropy. Most terrestrial rocks satisfy the condition of $1.5 \lesssim H_{RC}/H_C \lesssim 5.0$.

As shown in Fig. 1, however, H_{RC}/H_C values of the majority (>71%) of chondrites exceed 8, H_{RC}/H_C values of 20% of the examined chondrites are larger than 32. The observed anomalously large values of H_{RC}/H_C of chondrites may be interpreted as due to the co-existence of a magnetically hard component (a) having large values of H_{RC} and H_C and a magnetically soft component (b) of small values of H_{RC} and H_C in accordance with a theoretical model of a magnetic binary system (Nagata and Carleton, 1987).

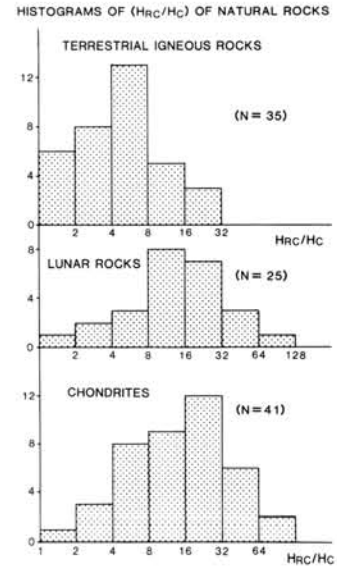

Fig. 1

2. Magnetic binary system model

An outline of the Nagata-Carleton model of a magnetic binary system is as follows. Consider a magnetic binary system, which is composed of 100m% of (a) particles characterized by saturation magnetization=$I_S^{(a)}$, saturated remanent magnetization=$I_R^{(a)}$, $H_C^{(a)}$ and $H_{RC}^{(a)}$ and 100(1-m)% of (b) particles characterized by $I_S^{(b)}$, $I_R^{(b)}$, $H_C^{(b)}$ and $H_{RC}^{(b)}$ where $H_{RC}^{(a)} > H_{RC}^{(b)}$ and $H_C^{(a)} > H_C^{(b)}$.

Approximating the magnetization curve I(H) in the course of magnetizing the member magnetics in H, after magnetizing into the opposite direction up to saturation, by

$$I(H) = I_R \left\{ 1 - \frac{H_C H + H^2}{2H_C^2} \right\}, \qquad (1)$$

which satisfies the necessary conditions for the definition of H_C, and further approximating remanent magntization $I_r(H)$ acquired after magnetizing up to H, by

$$Ir(H) = \frac{1}{2} I_R(H/H_{RC}) \quad \text{for } H \leqq H_{RC},$$
$$Ir(H) = I_R\left\{1-\frac{1}{2}(H_{RC}/H)\right\} \quad \text{for } H \geqq H_{RC}, \tag{2}$$

which satisfies the necessary conditions for the definition of H_{RC}, $\zeta \equiv H_C/H_C^{(a)}$ and $\zeta^* \equiv H_{RC}/H_{RC}^{(a)}$ for the binary system are expressed by

$$\left\{mY + (1-m)\eta^2\right\}\zeta^2 + \left\{mY + (1-m)\eta\right\}\zeta - 2\left\{mY+(1-m)\right\} = 0, \tag{3}$$

$$mY\eta^*(\zeta^*)^2 - \left\{mY-(1-m)\right\}\eta^*\zeta^* - (1-m) = 0, \tag{4}$$

where $Y \equiv I_R^{(a)}/I_R^{(b)}$, $\eta \equiv H_C^{(a)}/H_C^{(b)}$ and $\eta^* \equiv H_{RC}^{(a)}/H_{RC}^{(b)}$. (5)

Fig 2 shows an example of a comparison of the theoretical evaluations of H_{RC} vs m and H_C vs m obtained by the present model with experimental results (Day et al., 1977) for a non-interactive mixture of (a) titanomagnetite single domain particles and titanomagnetite multi-domain particles. The theoretical estimates are in reasonably good agreement with the experimental results.

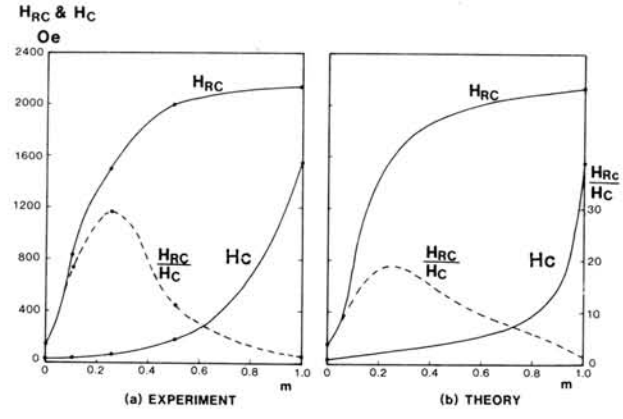

Fig. 2

3. Magnetic analysis of Antarctic stony meteorites based on H_{RC}/H_C

In the case of natural rocks such as meteorites, only the bulk values of I_S, I_R, H_C and H_{RC} are measurable. The Nagata-Carleton model can provide a method to approximately evaluate m, $H_C^{(a)}$, $H_{RC}^{(a)}$, $H_C^{(b)}$ and $H_{RC}^{(b)}$, separately, from the four measured parameters on reasonable assumptions for parameters Y, $H_{RC}^{(a)}/H_C^{(a)}$ and $H_{RC}^{(b)}/H_C^{(b)}$.

(3-1) Evaluation of m

Putting $I_R^{(a)}/I_S^{(a)} \equiv \alpha$ and $I_R^{(b)}/I_S^{(b)} \equiv \beta$, m is given by

$$m = \left[1 + (\alpha - I_R/I_S)I_S^{(a)}/(I_R/I_S - \beta)I_S^{(b)}\right]^{-1}. \tag{6}$$

Experimentally and theoretically, α for a randomly oriented assemblage of uniaxial anisotropy particles is $\alpha \simeq \frac{1}{2}$, and β of multi-domain particles is 0.002~0.003 for Fe-Ni metallic particles in meteorites and lunar rocks (β =0.02~0.04 for titanomagnetites in terrestrial rocks). As $I_S^{(a)}$ and $I_S^{(b)}$ are reasonably well estimated from observed qualification of the magnetic particles concerned, m can be determined by (6).

(3-2) Evaluations of $H_C^{(a)}$, $H_{RC}^{(a)}$ $H_C^{(b)}$ and $H_{RC}^{(b)}$

For stony meteroites, approximately, $\alpha \simeq 0.5$, β=0.002~0.003, $H_{RC}^{(a)}/H_C^{(a)} \simeq 1.5$ and $H_{RC}^{(b)}/H_C^{(b)}$=4.0 on average in general so that Y=127~191, η^*=0.375 and $H_{RC}/H_C = 1.5\zeta^*/\zeta$. Then, η (and

therefore η^*) to satisfy the associated algebraic equations, (3) and (4), for m and the observed value of H_{RC}/H_C can be uniquely determined. Table 1 gives examples of observed values of I_S, I_R, H_C and H_{RC} of Antarctic chondrites having anomalously large values of H_{RC}/H_C. Table 2 gives their m, $H_C^{(a)}$, $H_{RC}^{(a)}$, $H_C^{(b)}$ and $H_{RC}^{(b)}$ evaluated by the present binary system model method, where $\beta=0.003$ is assumed. (No significant change comes out if $\beta=0.002$ is assumed in place of $\beta=0.003$.)

Table 1. Magnetic Hysteresis Parameters of Antarctic Chondrites

		I_S (emu/g)	I_R (emu/g)	I_R/I_S	H_C (Oe)	H_{RC} (Oe)	H_{RC}/H_C
Y-7301	(H4)	15.0	0.14	0.00933	16	1700	106.3
Y-74647	(H4-5)	27.9	0.34	0.01219	14	1080	77.1
Y-74191	(L3)	6.8	0.22	0.03235	30	1330	44.3
Y-74354	(L)	21.8	0.71	0.03257	66	2620	39.7
Y-74362	(L)	8.1	0.27	0.03333	38	1300	34.2
Y-74646	(L5-6)	3.2	0.026	0.00813	20	405	20.3
ALH-77260	(L3)	5.20	0.16	0.03077	86	1150	13.4
ALH-76009(I)	(L6)	8.35	0.52	0.06228	160	2100	13.1
ALH-76009(II)	(L6)	9.80	0.37	0.03776	110	2470	22.5

Table 2. Magnetic Coercivity Parameters in the Binary System.

	m (%)	$H_C^{(a)}$ (Oe)	$H_{RC}^{(a)}$ (Oe)	$H_C^{(b)}$ (Oe)	$H_{RC}^{(b)}$ (Oe)
Y-7301	1.7	2036	3053	7.5	31
Y-74647	2.5	1022	1534	5.5	22
Y-74191	7.6	978	1467	7	28
Y-74354(*)	7.7	1925	2887	15.5	62
Y-74362(*)	7.85	952	1428	9	35
Y-74646	1.35	558	837	10.5	42
ALH-77260(*)	7.2	846	1269	21	84
ALH-76009(I)(*)	15.1	1462	2192	26	103
(II)(*)	9.0	1784	2675	24	95

The (a) component of the chondrites which have an asterisk mark(*) in Table 2 has been thermomagnetically identified with Fe-Ni γ-phase (Tetrataenite). (Nagata and Funaki, 1987). Metallographic aspects of (a) and (b) components are discussed with respect to the Fe-Ni metal phase diagram.

References:

Day, R., Fuller, M. and Schmidt, V.A., Phys. Earth Planet. Inter., 13,260, (1977)

Nagata, T. and Carleton, B.J., J. Geomag. Geoele., (In Press) (1987)

Nagata,T. and Funaki, M., Proc. 11th Symp. Antar. Meteor., Spec. Issue 46, 245-262, (1987)

Special Lecture

Professor James R. Arnold

TERRESTRIAL AGES OF ANTARCTIC METEORITES AND ICE

Arnold, James R.

Dept. of Chemistry, Univ. of California, San Diego, La Jolla, CA 92093,USA

It has been known for some time that the Antarctic meteorites have spent substantial periods on earth since their fall. Measurements of ^{14}C, ^{36}Cl, ^{26}Al, ^{10}Be, and ^{53}Mn have provided much information on this subject. We know also that these ages vary systematically with the collection region. Objects collected in the Allan Hills region are on the average much older than those collected in the Yamato area or elsewhere. The oldest (longest preserved) meteorites so far found are irons recovered on rocky terrain or moraines. The most remarkable example is Lazarev, dated at $\sim 5 \times 10^6$ years.

These data tell us something also about ice movement and history, though the interpretation is not entirely clear. It seems probable that the regions where Lazarev and other "old" irons were recovered have been ice-free over the whole period since fall. The detailed mapping of terrestrial age against location shows that the oldest objects occur only near the east edge of the main Allan Hills field, which glaciologists consider to be downstream, while younger ones occur upstream. A positive correlation of mean terrestrial age with areal density of objects should be observed on some models, but there seems to be no definite result.

Lipschutz has given data and arguments tending to show that the Antarctic finds sample a different population than recorded falls on the other continents. If this is true, it can only be due to a variation in time (within the last million years) or space or some combination. It is very difficult to explain such a phenomenon based on orbital dynamics. Perhaps some statistical considerations may be useful in resolving this puzzle.